Design of granular near-bed structures in waves and currents

MSc thesis

J.P. van den Bos
March, 2006

Delft University of Technology
Faculty of Civil Engineering and Geosciences
Section of Hydraulic Engineering

Royal Boskalis Westminster nv
Hydronamic bv

Design of granular near-bed structures in waves and currents

J.P. van den Bos
Student number 1233424

March, 2006

A dissertation submitted in partial fulfilment of the requirements for the degree of Master of Science in Civil Engineering, specialisation Hydraulic Engineering and Fluid Mechanics

Committee:

prof. dr. ir. M.J.F. Stive
Delft University of Technology, Hydraulic Engineering section

dr. ir. B. Hofland
WL|Delft Hydraulics

ir. J. Olthof
Delft University of Technology, Hydraulic Engineering section
Royal Boskalis Westminster, Hydronamic Engineering Department

dr. ir. W.S.J. Uijttewaal
Delft University of Technology, Environmental Fluid Mechanics section

ir. H.J. Verhagen
Delft University of Technology, Hydraulic Engineering section

TU Delft
Delft University of Technology

Koninklijke Boskalis Westminster nv

hydronamic

Cover picture: ballasting of a fascine mattress at Schelphoek, Schouwen-Duiveland during the restoration works after the 1953 flooding disaster (photographer unknown)

Abstract

This thesis studies the design of near-bed structures, more specifically horizontal bed protections and pipeline covers. The present design methods are all based on the approach developed by Shields (1936), which has three major shortcomings: it is not directly applicable for non-uniform flow (waves and accelerations/decelerations around structures), it assumes a threshold of motion and is therefore not suitable for damage-based design, and it is not based on a complete understanding of the physical processes that destabilise a stone. In literature, many suggestions to overcome these issues have been put forward, especially in the last decade or so. This thesis reviews a selection of these suggestions, and contains a quantitative analysis of the most promising among them against a dataset of scale model tests. The main research goal is to find a design formula, expressing the damage to a near-bed structure as a function of the stability of the individual stones, that can be used for a damage-based design of horizontal bed protections and pipeline covers under a wide range of flow situations (including a combination of current and waves). A secondary goal is to test some elements of the present 'critical stability' design approach against the same datasets and give practical recommendations on their use.

The damage to horizontal bed protections is likely to be related to the transport of the stones that make up the protection; this transport is caused by the current and enhanced by the presence of the waves. Unfortunately nearly all existing (morphological) transport formulas have been developed to predict transport rates of sand, not stones. The transport of stones is essentially different: occasional rolling or sliding along the bed as opposed to bulk transport in suspension. Only the formula by Paintal (1969) was found to be suitable to describe the transport of stones, but it has been developed for currents only. This formula uses the bed shear stress as the governing parameter, so in order to make it work for a combination of waves and a current the combined bed shear stress must be calculated. This is not straightforward as the current and the waves influence each other in a nonlinear way and the resulting bed shear stress can only be calculated

using (sometimes rather complex) wave-current interaction models. Several of these models are described and tested in this thesis. The conclusion is that the Paintal formula can also be used in the case of a combination of waves and a current, provided that the bed shear stress is replaced by the combined shear stress using the wave-current interaction model by Fredsøe (1984). The final step in the design process, the translation from transport to the actual damage to the structure could not be made in this thesis because the dataset that was used did not contain this information. This leaves room for further research.

For pipeline covers no relation between transport and damage could be found at all. The conclusion is that an alternative design approach must be followed, in which the damage to the structure is expressed as a dimensionless erosion area and directly linked to the hydraulic boundary conditions. Several design formulas of this type have been forward in literature, but there is little consensus on which (structural and hydraulic) parameters must be included in such a formula and the overall goodness-of-fit of these formulas on a dataset of scale model tests is low. In this thesis the individual (sometimes conflicting) elements of these formulas are all tested against the dataset using a regression analysis; eventually a new design formula is presented that shows less scatter. This formula can be used for the preliminary design of pipeline covers for waves only, or for waves combined with a relatively weak current. In addition, this thesis presents methods to relate the thus obtained erosion area to practical measures of damage to the structure, both qualitatively (in terms of a description of the expected damage) and quantitatively (in terms of the expected reduction in crest height of the structure).

For the critical stability approach it was found that the recommendations in CIRIA/CUR (1991) could best be followed, also for the combination of waves and a current, and always with a critical Shields parameter of Ψ_{cr} = 0.03. Other methods, like the method used by the software programme BPP, are not recommended. For pipeline covers it was found that the 1%-exceedance wave height in an irregular wave field ($H_{1\%}$) must be used in these calculations, in combination with the peak wave period and the (enhanced) velocity at the crest of the structure. Other combinations were found to underestimate the resulting shear stress.

Finally, two recent alternatives to the shear-stress based Shields approach are discussed: an approach based on velocities and accelerations (Morison approach) and an approach based on turbulence characteristics of the flow. Although these methods provide a better insight in the actual physical processes involved and especially the second method is considered very promising for the future, they are not far enough developed (yet) to be applicable for practical design purposes.

Acknowledgements

The present thesis is the final report of a research project undertaken in order to obtain the degree of Master of Science at the University of Delft. The research was sponsored by Hydronamic, the engineering department of Royal Boskalis Westminster, and was mainly conducted at the Hydronamic office in Papendrecht.

Originally graduated in Civil Technology and Management at the University of Twente a few years ago, I would never have taken up an extra studies in hydraulic engineering if I had not been so enthusiastically introduced to this field during my previous stay at Boskalis and at Hydronamic in 2002-2004. All my old colleagues, but Jelle especially, are greatly acknowledged for this.

Of course, when embarking on an adventure like this, one needs the support and encouragement of family and friends. Thank you, guys, for being there and helping me to bring this to a good end.

I would also like to thank all staff members of the section of Hydraulic Engineering for providing a welcoming and supportive working environment during my stay in Delft.

Last, but nut least, my thanks go to my graduation committee prof. dr. ir. M.J.F. Stive, dr. ir. B. Hofland, ir. J. Olthof, dr. ir. W.S.J. Uijttewaal and ir. H.J. Verhagen for their kind cooperation, enthusiasm and feedback on this research project, and to the people at Hydronamic, old colleagues as well as new ones, for the very pleasant past six months.

Papendrecht, February 2006
Jeroen van den Bos

Contents

Readers' guide

This study breaks down into two parts. The first part (chapters 1 – 4) takes the form of a literature review. It describes the present approach to the design of granular near-bed structures, the problems and shortcomings associated with this approach and the various solutions to these shortcomings that have been put forward in literature; it ends with a qualitative review of these solutions and the identification of the most promising concepts among them. The second part (chapters 5 – 8) is aimed at further quantifying these concepts and see whether they can be used in a practical design formula for near-bed structures; this part takes the form of a data analysis. It ends with recommendations on which parameters should be used in a design formula and a few suggestions on what such a formula should look like.

This report was written for an intended audience of design engineers. Apart from providing practical guidance on which parameters should be used in the design of near-bed structures it is also serves as a reference work for those engineers interested in a general overview of the latest (scientific) developments in this field and the physical backgrounds to most of the methods that are discussed. This latter aspect explains most of the bulkiness of the report: a lot of background information is provided in a reasonable amount of detail.

Those readers who are only interested in the practical guidance aspect of this report should not be put off by this: they are advised to read only the chapters 1 (introduction), 4 (review), 7 (conclusions) and 8 (recommendations). These chapters can be seen as a 'quick tour' through the report; they contain the main story and were written in such a style that they can be read without loss of continuity.

Readers who are interested in the broader picture and the physical backgrounds are encouraged to read the other chapters as well: especially chapter 3, which contains the main part of the literature review, and chapter 6, which contains the main part of the quantitative analysis. Reading this last chapter will not only provide information on the

concepts that work well in a design formula, but also (perhaps equally importantly) on concepts that were tested and were found *not* to work well.

Finally, chapter 2 describes the present (critical stability) design method for near-bed structures and forms the starting point for most of the discussions in this report. It is mainly intended for those readers who are not familiar with this method.

The outline of this thesis is illustrated in the flow chart below. The chapters that make up the 'quick tour' are marked with an asterisk (*).

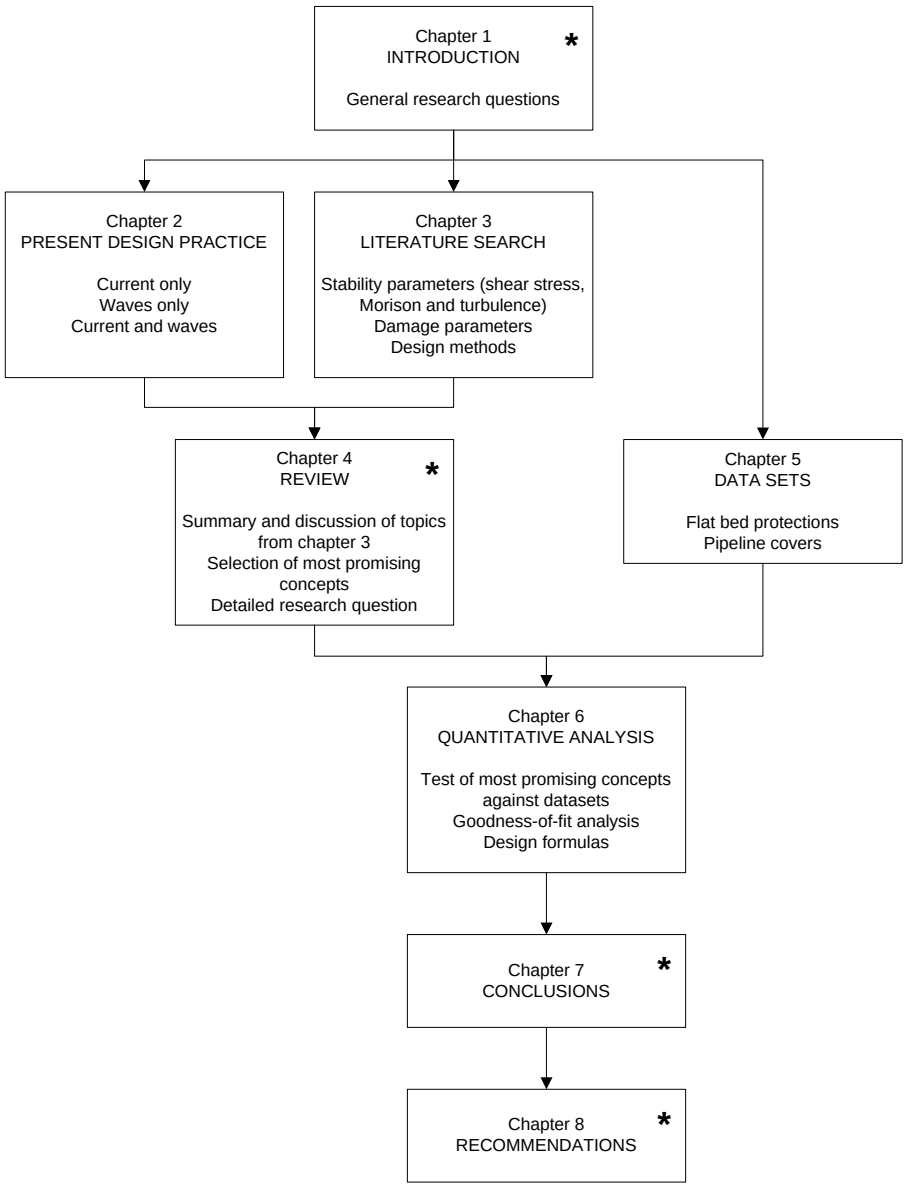

List of figures

Chapter 1 Introduction

Chapter 2 Present design practice

Chapter 3 Literature search

Chapter 4 Review

Chapter 5 Data sets

Chapter 6 Quantitative analysis

Appendix 3 Fredsøe's wave-current interaction load model

Appendix 4 Paintal's bed load model

Appendix 7 Statistical tools

Appendix 8 Calculation results

Appendix 9 Case study: Santander outfall

List of tables

Appendix 5 Data set for horizontal bed protections

Appendix 5 Data set for pipeline covers

Appendix 7 Statistical tools

Appendix 8 Calculation results

Appendix 9 Case study: Santander outfall

List of symbols

Symbol	Parameter	Unit
a	flow acceleration	m/s^2
$\hat{a}_0$	maximum horizontal excursion orbital motion at the bottom	m
A_0	original cross sectional area of a pipeline cover	m^2
A_e	erosion area (area of displaced stones in a cross section)	m^2
B	footprint width of a pipeline cover	m
B_c	crest width of a pipeline cover	m
C	Chézy coefficient	$m^{1/2}/s$
C_B	bulk coefficient, combines effects of C_D and C_L	-
C_D	drag force coefficient	-
C_D	current friction coefficient	-
C_L	lift force coefficient	-
C_M	inertia coefficient	-
d	stone diameter	m
d_*	dimensionless stone diameter, defined as $d_* \equiv d(\Delta g d)^{1/3}$	-
d_{n50}	nominal mean stone diameter, defined as $d_{n50} \equiv \sqrt[3]{\frac{M_{50}}{\rho_s}}$	m
D	duration (of a load)	s
E	entrainment parameter (volume of displaced stones per unit of bed area and time)	m^3/m^2s or m/s
E_n	number entrainment parameter (number of displaced stones per unit of bed area and time)	$1/m^2s$
f_c	current friction factor	-
f_w	wave friction factor	-
F_D	drag force	N
F_L	lift force	N

F_M	inertia force	N
F_R	resultant force (of drag and lift forces)	N
g	acceleration of gravity, g = 9.81 m/s^2	m/s^2
G	gravity force (underwater weight)	N
h	water depth	m
h_c	water depth over crest of pipeline cover	m
H	wave height (in a regular wave field)	m
$H_{1\%}$	wave height that is exceeded by 1% of the waves in an irregular wave field	m
H_s	significant wave height in an irregular wave field	m
i_b	bottom gradient (slope)	-
k	turbulent kinetic energy (per unit of mass)	m^2/s^2 or J/kg
k	wave number, defined as $k \equiv \frac{2\pi}{L}$	rad/m
k_a	apparent roughness height	m
k_s	physical roughness height	m
l_m	mixing length	m
1:m_0	side slope of a pipeline cover	-
1:m_d	side slope of a pipeline cover after damage	-
M_{50}	mean stone weight (mass)	kg
N	number of waves	-
N_s	Hudson number; stability parameter based on wave height, defined as $N_s \equiv \frac{H_s}{\Delta d_{n50}}$	-
q_s	volume transport through a cross section per unit of time and width	m^3/ms or m^2/s
r	turbulence intensity defined as $r \equiv \frac{\sqrt{\overline{u'}}}{\overline{u}} = \frac{\sigma_u}{\mu_u}$	-
Re	flow Reynolds number, defined as $\mathrm{Re} \equiv \frac{\overline{\overline{u}}h}{\nu}$	-
Re_*	particle Reynolds number, defined as $\mathrm{Re}_* \equiv \frac{u_* d}{\nu}$	-
Re_w	wave Reynolds number, defined as $\mathrm{Re}_w \equiv \frac{\hat{u}_0 a_0}{\nu}$	-

S	damage number (dimensionless erosion area) defined as $S \equiv \frac{A_e}{d_{n50}^2}$	-
S*	damage number per unit crest width defined as $S^* \equiv \frac{A_e}{B_c d_{n50}}$	-
Sa	Saers number, defined as $Sa \equiv \frac{z_c m_0}{\hat{a}_0}$	-
t	time	s
T	wave period	s
$\hat{u}_0$	amplitude of horizontal near-bed orbital velocity	m/s
u	flow velocity	m/s
$\overline{\overline{u}}$ or u_{da}	depth-averaged flow velocity defined as $\overline{\overline{u}} \equiv \frac{1}{h}\int_{z=0}^{h} u(z)dz$	m/s
u_*	shear velocity, defined as $u_* \equiv \sqrt{\frac{\tau_0}{\rho}}$	m/s
X	relative current strength defined as $X \equiv \frac{\tau_c}{\tau_c + \hat{\tau}_w}$	-
Y	dimensionless average combined bed shear stress defined as $Y \equiv \frac{\tau_{wc,av}}{\tau_c + \hat{\tau}_w}$	-
z	vertical coordinate, distance from bottom	m
z_0	integration constant, height above bottom where u = 0 in logarithmic velocity profile	m
z_c	crest height of a pipeline cover	m
z_d	crest height of a pipeline cover after damage	m
Z	dimensionless maximum combined bed shear stress defined as $Z \equiv \frac{\tau_{wc,\max}}{\tau_c + \hat{\tau}_w}$	-
Z	dimensionless boundary layer parameter	-
α	slope angle	rad or ^{o}
δ	boundary layer thickness	m

Δ	specific density, defined as $\Delta \equiv \frac{\rho_s - \rho_w}{\rho_w}$	-
ε	dissipation rate of turbulent kinetic energy (per unit of mass)	m^2/s^3 or W/kg
θ	stability parameter based on wave orbital velocity, defined as $\theta \equiv \frac{\hat{u}_0^2}{\Delta g d_{n50}}$	-
Θ	stability parameter based on velocity and acceleration (Morison), defined as $\Theta \equiv \frac{\frac{1}{2} C_B u^2 + C_M a d_{n50}}{g \Delta d_{n50}}$	-
κ	Von Kármán constant, $\kappa \sim 0.4$	-
μ	relative current strength, defined as $\mu \equiv \frac{\tau_c}{\hat{\tau}_w}$	-
ν	kinematic viscosity of the fluid (water)	m/s^2
ν_t	turbulence viscosity (eddy viscosity) of the fluid (water)	m/s^2
ρ or ρ_w	density of the fluid (water)	kg/m^3
ρ_s	density of stone material	kg/m^3
τ	shear stress	Pa
τ_0	bed shear stress	
φ	angle between direction of the current and propagation direction of the waves	rad or ^{o}
Φ_q	dimensionless transport parameter, defined as $\Phi_q \equiv \frac{q_s}{\sqrt{\Delta g d_{n50}^3}}$	-
Φ_{Hall}	dimensionless transport parameter (after Hallermeijer 1982) defined as $\Phi_{Hall} \equiv \frac{q_s}{\omega d_{n50}^2}$	
Φ_E	dimensionless entrainment parameter, defined as $\Phi_E \equiv \frac{E}{\sqrt{\Delta g d_{n50}}}$	-
Φ_{En}	dimensionless number entrainment parameter, defined as $\Phi_{En} \equiv E_n d_{n50}^2 \sqrt{\frac{d_{n50}}{\Delta g}}$	-

Ψ	Shields parameter (stability parameter based on bed shear stress), defined as $\Psi \equiv \frac{\tau_b}{(\rho_s - \rho) g d_{n50}} = \frac{u_*^2}{\Delta g d_{n50}}$	-
Ψ_t	stability parameter based on turbulence parameters of the flow	-
ω	angular wave frequency, defined as $\omega \equiv \frac{2\pi}{T}$	s^{-1} or Hz

Frequently used subscripts:

For bed shear stress:

c	for currents alone
w	for waves alone
wc	waves and currents combined
av	average (of the absolute values)
avx	average (of the projection) in the current direction
T	averaged over full wave period
1/2T	averaged over half wave period
max	maximum value (in full wave period)

In wave parameters

p	based on peak period
m	based on mean period

Other subscripts

cr	critical value
hc	based on enhanced velocity at crest (fig 3.22)
c	based on undisturbed velocity at crest level (fig 3.22)
0	based on undisturbed velocity at bed (fig 3.22)
1%	based on $H_{1\%}$ (and T_p)

Coordinate system

In this thesis a coordinate system is used in which

x = the horizontal coordinate in the direction of the flow
y = the horizontal coordinate perpendicular to the flow
z = the vertical coordinate, positive upwards

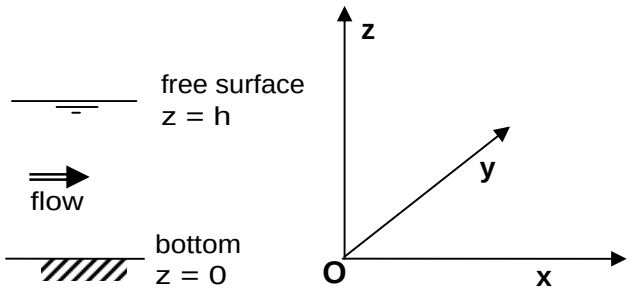

Other notations

f(pars)	an unknown function of the parameters *pars*
$\langle x \rangle_h$	spatial average of x over distance h
$\hat{x}$	amplitude of an oscillatory variable x
$\overline{x}$	ensemble averaged (Reynolds averaged) value of x
x'	(turbulent) fluctuation of x

1 Introduction

1.1 Design of granular near-bed structures: three main problems

Granular near-bed structures are among the more common hydraulic structures. Examples include bottom protections to prevent scour near bridge piers, offshore structures, weirs and sluices and at the toe of bank protections or breakwaters, but also stabilisation/protection covers on offshore pipelines.

The cornerstone of the theory behind the design of these structures was laid by Izbash (1930, cf Schiereck 2001) and, most notably, Shields (1936), who linked the stability of a stone in the near-bed structure to the shear stress exerted on the bottom by a flow. Even today, some 70 years later, the design of near-bed structures is still largely based on Shields's work, despite some apparent shortcomings.

The three most prominent of these shortcomings are:

- Shields based his results on experiments with uniform (gravity driven) flows. This means that his results are not, or not directly, applicable to non-uniform flow situations such as waves and accelerating/decelerating flow around structures. Unfortunately these are quite common situations in hydraulic engineering practice (not in the least place since the existence of such structures is usually the very reason that a near-bed structure is designed).
- Shields postulated that for values of his stability parameter below a certain critical value (the so-called 'threshold of motion') the stones in the bed would not move at all. In reality stones do not exhibit this kind of behaviour; stones have been shown to move at any value of the Shields parameter, also below the 'threshold of motion'. The mobility of the stones does increase with higher values of the Shields parameter, indicating that this is really a mobility parameter rather than a stability parameter.

In practice, this concept has given rise to a rather 'black and white' design approach: a threshold of motion is selected and the size and weight of the stones are chosen such that the Shields parameter does not exceed the critical value. This means that alternative, "dynamically stable" design approaches (in which some movement of stones is allowed in combination with an appropriate maintenance programme) cannot be adopted because the true transport of the bed protection material cannot be predicted and thus the rate of deterioration and the required intensity of the maintenance programme cannot be assessed.

- Shields chose the forces that are proportional to the bottom shear stress as the mechanism that determines stone stability (these include shear, drag and lift forces on the stones). This is an arbitrary choice that left other possible mechanisms such as inertia forces and turbulent flow structures disregarded. There are indications that these mechanisms do play an important role in destabilising stones in a bed protection, which would suggest that the Shields theory is not based on a complete physical understanding of the destabilising mechanisms.

In the present design practice some of these shortcomings have been circumvented: influence factors have been found to account for the effects of non-uniform flow around structures, some researchers have proposed ways to include the effects of waves and attempts have been made to find empirical relationships between the Shields parameter and bed transport.

Still, all this has not lead to a satisfactory design practice. First of all, the issue of limited physical understanding of the actual destabilising mechanisms remains unsolved. Secondly, the use of empirical factors inevitably leads to arbitrary choices and a wide range of possible design outcomes for a given flow situation. There appears to be no real consensus within the engineering community as to which factors to use in which situation. Thirdly, the stability of bed material under a combination of current and waves is not completely understood yet, whereas in hydraulic engineering practice this one of the more common situations. Finally, the few mobility-transport equations that exist (eg Paintal) have not attracted a large following, mainly because of their apparent lack of empirical evidence, limited applicability (flow only, no waves) and potentially large inaccuracies (in the Paintal formula the stability parameter Ψ appears to the 16th power, so a small error in estimating Ψ leads to a large error in the prediction of the bed-load transport).

For these reasons, it can be stated that the engineering community is in search of:

> *"A design formula, based on the true physics of the destabilising mechanisms, that can be used for the preliminary design of near-bed structures under a wide*

range of flow situations, including waves; the formula should enable the assessment of the damage to the structure under design conditions as well as its deterioration over time."

Is such an all-encompassing design formula available at this moment? The answer is almost certainly 'no'. But if that is true, what are the latest theoretical ideas concerning stone stability? Can they be used and combined into a new design method? And to what extent would such a method bring us closer to this 'ultimate' goal? This is the main question this thesis seeks to address.

1.2 Positioning of the subject and limitations

In a broad sense, this thesis is about transport of granular bed material, and in that aspect it follows in a long legacy of theses and publications on that subject. The majority of these publications, however, were written from a morphological point of view and consequently focussed on sand transport. This thesis is about coarse-grained material (rock), which sets it apart from most of the other publications. This focus has a few important implications, including:

- a larger grain size leads to a larger bottom roughness, which is an important scaling parameter for the flow in the bottom boundary layer. This could mean that some of the assumptions on which theoretical flow models are based are no longer valid when they are scaled from sand (for which they were originally derived) to rock.
- sand is transported as bulk transport, partly as bed-load and partly in suspension; consequently sand transport formulas only predict large-scale (bulk) properties. In contrast, the transport of rock is characterised by low mobility and transport rates: there is occasional movement of a stone, rolling or sliding over the bed for a short distance. Design engineers are not interested in bulk properties: the individual movement of a single stone, or a few stones, can determine the functional stability of a structure. This requires a more detailed level of analysis.
- maybe even transport as such, in terms of volume of moving 'particles' per unit of time, may no longer be of primary interest. Designers of near-bed structures are potentially more interested in other indicators of damage to the structure (like pickup rates, entrainment or erosion area). Once a stone has been moved from its position in the bed (ie in the structure), it is of lesser importance to know where it will be transported.

The flow situations that are studied in this thesis are combinations of currents and non-breaking waves. There are no a priori limitations to the relative strength of the current (so both wave dominated situations and current dominated situations will be studied) or to the angle between current and wave propagation.

The term 'near-bed structures' as used in this thesis refers to two types of structure: *bed protections* (a layer of stones on a horizontal bed) and *pipeline covers* (a rubble mound, characterised by a certain crest height, crest width and side slope). The crest height is such that waves do not break over the structure.

Other flow situations like flow after weirs or backward-facing steps, jet flow or breaking waves are not studied; neither are other near-bed structures such as bed protections around gravity-based structures or vertical piles.

1.3 General background: design approaches

Like any mechanical structure, the behaviour of a granular near-bed structure can be described in terms of a response to a certain load. For rubble mound structures it is more common to use the stability as a governing parameter instead of the load, where stability is defined as the ratio of load over strength. When mechanisms like interlocking are neglected, the strength of a rubble mound structure is entirely due to the weight of the individual stones in the structure, so stability can also be defined as the ratio of load over stone weight. When this definition is adopted, it would be appropriate (though not absolutely necessary) to express the load also on the level of an individual stone.

The response of a rubble mound structure can be thought of in terms of a certain degree of damage, expressed for instance as an erosion area or a number of displaced stones. For the time being, the exact way of expressing both load and damage are not of importance yet, and we will only use the general terms.

The relationship between load and response can be depicted graphically in a diagram, for instance the well-known stress-strain diagram (σ-ε diagram) for steel and concrete structures. Given the above considerations, the appropriate analogy for rubble mound structures would be a stability-damage diagram.

In the present design practice a rather crude schematisation of the structure response is made. It is assumed that a certain critical stability level exists, called the threshold of motion, below which the stones do not move (so the response is zero). Above this threshold the stones are assumed to move, which is considered unacceptable. Designing a structure then comes down to selecting a stone size and weight such that this threshold of motion is not exceeded. This is an iterative process because the load parameters are partly influenced by the choice of stone size, too, as will be described in

more detail in Chapter 2. A flow chart describing this process and the corresponding stability-damage diagram are given in Figure 1.1 and Figure 1.3, respectively.

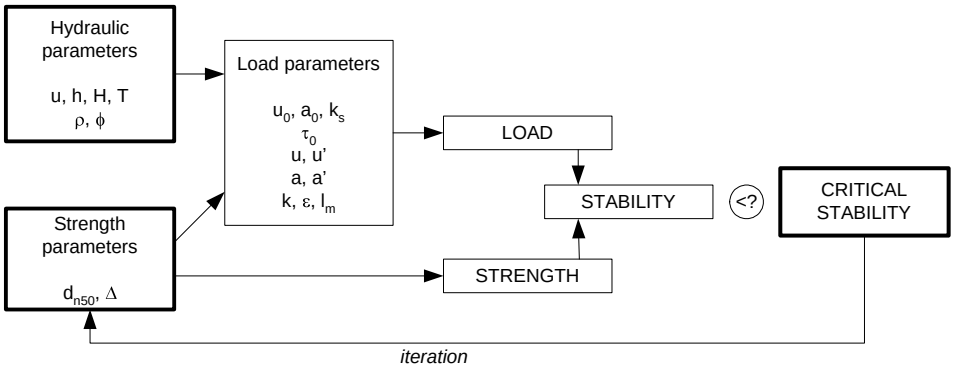

Figure 1.1 – Flow chart 'critical stability' design approach

As mentioned earlier, the threshold of motion concept is too crude an approximation. In reality, stones move at any degree of the stability parameter, also below the critical value, so the damage to the structure is more likely to be a smooth (and rising) function of stability. When this is acknowledged an alternative design approach can be adopted, in which an acceptable degree of damage is set and the stone size and weight are chosen such that this damage is not exceeded. This approach will have some advantages, including:

- when some damage is accepted a smaller stone size can be selected. This could result in the choice of lighter and cheaper construction equipment, leading to substantial construction cost savings. Although allowing for some damage will probably lead to larger construction dimensions (layer thickness) and therefore increased materials cost, this cost increase is likely to be out-weighed by the savings achieved by selecting different construction equipment.
- when the damage can be predicted to a reasonable degree of accuracy, the deterioration of the structure over time can be estimated and the need for maintenance can be assessed beforehand (ie during the design stage). With this knowledge the reduced construction costs for smaller stone sizes can be balanced against the increased maintenance costs and the design can be optimised in terms of total life-cycle costs.

For a successful implementation of this design approach three things are important: the relation between stability and damage (the *design curve*) must be known, the damage must be predicted reasonably accurate, and the damage must be expressed in such a way that the need for maintenance can be easily assessed.

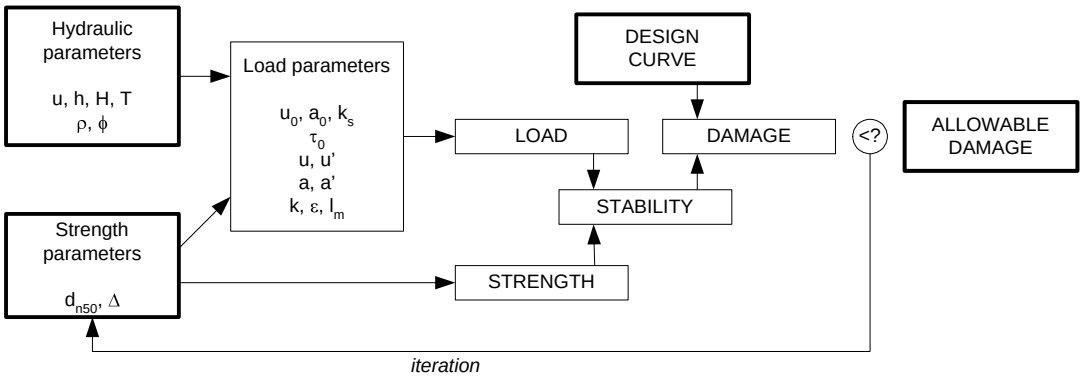

Figure 1.2 – Flow chart 'allowable damage' design approach

This alternative design method is depicted graphically here, in a flow chart (Figure 1.2) and in a stability-damage diagram (Figure 1.3). As Figure 1.3 shows, when the design curve is known, a critical value of the stability parameter can be found by extrapolating the damage to zero. (This is more or less analogous to the way Shields originally found his 'threshold of motion' values).

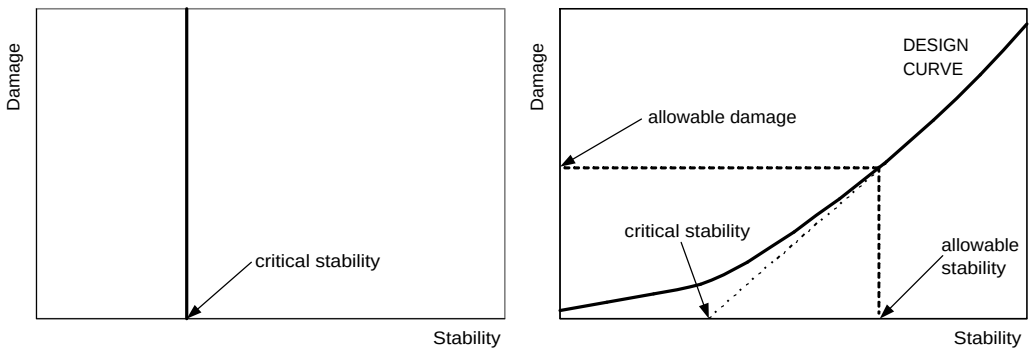

Figure 1.3 – Left: Stability-damage curve 'critical stability' design approach
Right: Stability-damage curve 'allowable damage' design approach

1.4 Research goal and outline of thesis

With this is mind, the research goal of this thesis can be re-phrased as follows:

> *To find a design curve, expressing damage to a near-bed structure as a function of the stability of the individual stones, that can be used for the preliminary design of such structures based on an 'allowable damage' design approach. The stability parameter should be expressed in such a way that it represents the true physics of the destabilising mechanisms and includes a wide range of flow situations, including waves"*

Reaching this goal takes two steps. The first step is to find suitable ways to express the stability and damage parameters; the second step is to try and find a relationship between them. For this reason, this thesis breaks down into two main parts: a literature study (to find expressions for stability and damage) and a quantitative analysis (to find a design curve).

Throughout both parts a practical engineering (designer's) point of view will be adopted. This is a key element in this thesis. All new theoretical ideas will be described against the background of the present design practice, and new concepts will be translated into practical terms as much as possible.

1.4.1 First part: literature review

The first question that needs to be answered is how the stability and damage parameters can be expressed. A lot of scientific research has been carried out to find such expressions, especially in the last decade.

Stability parameters: some researchers have followed in Shields's steps and have sought ways to calculate the bottom shear stresses caused by a combination of currents and waves. Others, including various MSc-students at Delft University have abandoned the shear-stress approach in favour of a 'Morison-type' approach in which fluid velocities and accelerations in the direct vicinity of the stone are the governing load. Recently a PhD thesis by Hofland (2005) introduced a third way: Hofland used state-of-the-art techniques to investigate the real destabilising mechanisms in a flow, found evidence for a large role played by turbulence structures and proposed an alternative stability parameter in which turbulence characteristics are used as direct input. Other researchers have adopted yet a different approach; they do not go into the details of the stability of an individual stone but have suggested formulas that predict the erosion profile of a near-bed structure as a whole, as a direct 'black box' function of the hydraulic load and time. These formulas do not generally apply to all near-bed structures, but are aimed specifically at pipeline covers.

Damage parameters: most of the wave-current interaction research has been carried out to find sand transport formulas in coastal areas. For this reason, the damage is usually expressed in terms of transport rates. Also some of the earlier research specifically aimed at coarse-grained material has followed this approach. However, this may not be the most appropriate choice for granular bed protections, where designers are more interested in 'direct' damage indicators like entrainment or erosion area. In recent years some alternative entrainment/erosion parameters have been proposed.

Chapter 2 will briefly describe the present design practice and the underlying theoretical concepts. This will form the starting point for a description of various stability parameters and damage parameters (in Chapter 3), based on an overview of the scientific research that has been carried out over the years. All four types of stability parameters that were introduced above (wave-current bed shear stress, Morison type, turbulence-based and 'black box') will be explored, and cross-links between concepts will be sought as much as possible. This part of the thesis will be closed with a summary and review of the most promising results, in Chapter 4.

1.4.2 Second part: quantitative evaluation and conclusions

In the second part of the thesis the most promising ideas, including the ones used in the present design practice, will be worked out in a more quantitative way. It will be investigated to what extent these ideas can really be used in the design of near-bed structures; in other words, for each combination of damage parameter and stability parameter it will be investigated how well a design curve can be fitted through data points expressed in these parameters.

For this purpose datasets are needed that are flexible enough to allow both stability and damage parameters to be expressed in various ways, extensive enough to cover the wide range of flow situations (waves and current) that we are interested in and, of course, originating from experiments with coarse-grained material. These datasets were taken from literature sources and previous MSc researches at Delft University. Chapter 5 will describe these datasets in more detail.

The dataset will be expressed in terms of a combination of a stability parameter and a damage parameter. For this combination, a curve will be fitted through the data points (by regression methods) and the goodness-of-fit will be assessed by statistical methods. This is described in Chapter 6.

The results obtained from the quantitative evaluation can be used to answer the research question of which way of expressing the stability and damage parameters is the best way for the design of granular near-bed structures: this is simply the combination that yields the best goodness-of-fit. If this best method yields a design curve that is accurate enough (ie that has a high enough goodness-of-fit), than the 'ultimate' goal has been reached and this design curve can be used for the design of near-bed structures. In any other case the 'ultimate' goal cannot be reached, but at least it can be quantified how far we are still away from this goal, what improvements are needed to bring it any nearer, and, perhaps most importantly, how well the best alternative method performs compared to the present design method. This is described in Chapter 7, after which Chapter 8 will contain some recommendations for further research.

2 Present design practice

2.1 Currents (uniform flow)

2.1.1 Theoretical backgrounds

An important concept in the design of granular structures is the so-called threshold of motion, which can be defined as the load at which the stones first start to move. The first researcher to publish a result in these terms was Izbash (1930, cf Schiereck 2001), who postulated that the threshold of motion could be expressed as a critical velocity u_c given by

$$u_c = 1.2\sqrt{2\Delta g d} \tag{2.1}$$

in which d is the diameter of the stone [m] and $\Delta = (\rho_s - \rho_w)/\rho_w$ is the specific density of the stone [-].

Stones will start to move when the critical velocity is exceeded. The disadvantage of this formula is that it is not clear exactly how and where the velocity should be specified. In general terms, u_c can be thought of as a velocity “in the vicinity of the stone”.

A more thorough investigation into the threshold of motion was conducted by Shields (1936). His work is still one of the cornerstones of any morphological theory, and the design of granular structures is still largely based on his results. Shields reasoned that the destabilising forces on a grain could be represented by

$$F = a\zeta \cdot d^2\left(\frac{1}{2}\rho u_k^2\right) \tag{2.2}$$

where $\frac{1}{2}\rho u_k^2$ is the dynamic pressure related to a local velocity in the vicinity of the stone. The forces that can be represented in this way include drag, shear and lift forces,

so ζ can be thought of as a combined drag/shear/lift coefficient. The constant of proportionality *a* in this formula depends, among other things, on the grain shape.

The velocity u_k is assumed to be the velocity at a level z = c·d, with *c* a constant of order 1. Further assuming a logarithmic velocity profile near the bed, Shields is able to show that

$$u_k = u_* f_1\left(\frac{u_* d}{\nu}\right) = u_* f_1(\mathrm{Re}_*) \tag{2.3}$$

where $u_* = \sqrt{(\tau_0/\rho)}$ [m/s], τ_0 is the bed shear stress [Pa], ν is the dynamic viscosity [m^2/s], $\mathrm{Re}_* = u_* d/\nu$ is the particle Reynolds number and the (unknown) function f_1 depends on the grain shape.

This is a crucial step in Shields's analysis, for it links the destabilising forces to the bed shear stress (which is well-defined and – albeit indirectly – measurable in experiments), rather than to the ill-defined, mysterious 'velocity in the vicinity of the stone' u_k.

In general, the drag/shear/lift coefficient ζ will be a function of the Reynolds number of the flow around the grain:

$$\zeta = f_2\left(\frac{u_k d}{\nu}\right) = f_2\left(\frac{u_* f_1(\mathrm{Re}_*) d}{\nu}\right) = f_3(\mathrm{Re}_*) \tag{2.4}$$

By (2.3) and (2.4) we have shown that all unknown variables in (2.2) are functions of Re_* and the grain shape, so we can write:

$$F = d^2\left(\rho u_*^2\right) f_4(\mathrm{Re}_*) \tag{2.5}$$

The resistance of the grain against movement is caused by its own (under water) weight:

$$G = (\rho_s - \rho) g d^3 \tag{2.6}$$

It is assumed that the threshold of motion is defined by F = G, so in this *critical* situation the destabilising forces are equal to the resistance. Equating (2.5) and (2.6) and writing $\tau_0 = \rho u_*^2$ gives

$$\frac{\tau_{0cr}}{(\rho_s - \rho) g d} = \frac{u_{*cr}^2}{\Delta g d} = f(\mathrm{Re}_*) \tag{2.7}$$

which is the classic Shields formula. The subscript 'critical' (cr) has been applied to denote the critical situation F = G. In Shields's honour the left-hand side of this equation is usually referred to as the Shields parameter Ψ.

Shields conducted a series of measurements in a laboratory flume to find the unknown function *f*. He presented these results in a graph, which is reprinted in Figure 2.1 in its original form (Shields 1936).

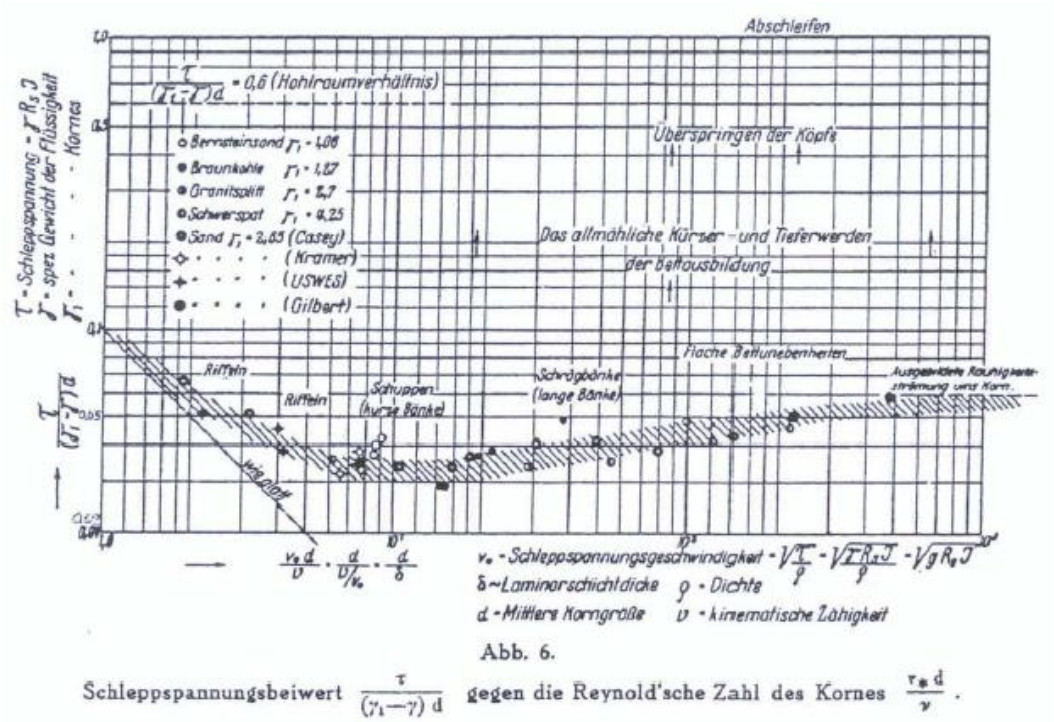

Figure 2.1 – Original presentation of Shields curve (Shields 1936)

The disadvantage of this original presentation is that both u_* and d appear on both axes of the graph, so in practical applications, when a question like 'what is the critical shear stress for a given grain size' must be answered, iteration is necessary. This disadvantage can be circumvented when a dimensionless grain diameter d_* is used:

$$d_* = d\left(\Delta g \nu\right)^{1/3} \tag{2.8}$$

This expression was originally proposed by Van Rijn (cf Schiereck 2001). The Shields graph can now be re-drawn as shown in Figure 2.2 (the values for *d* on the top end of the graph are equivalent to d_* for the 'standard' parameter values $\nu = 1.33*10^{6}$ and ρ_s = 2650 kg/m^3)

An important result for the design of granular bed structures can be seen from this graph: for larger grain sizes, say for d > 10 mm, the Shields parameter becomes a constant with a value of approximately $\Psi_{cr} = 0.055$.

It may be interesting to note that in his original publication (Shields 1936) Shields never *measured* Ψ_c to become constant for large values of Re_*, he only *predicted* it to become constant eventually (from $Re_* \sim 1000$), mainly because both functions f_1 and f_3 in (2.3) and (2.4) tend to become constant for large Reynolds numbers. Shields predicts $\Psi_{cr} \sim 0.06$, but mentions explicitly that this value is obtained "nur durch eine sehr unsichere Extrapolation" (quote from Shields, 1936). This is also illustrated in Figure 2.1, where the horizontal line for large Re_* values does not feature as prominently as in Figure 2.2.

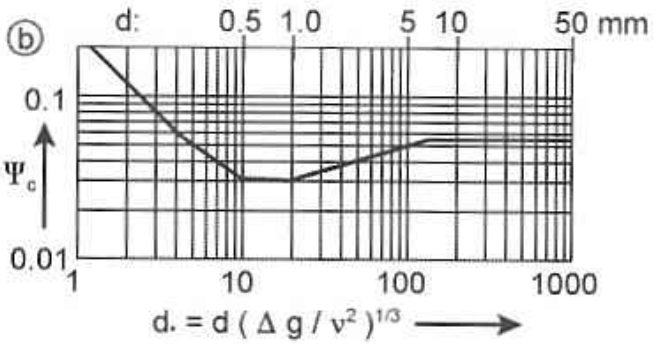

Figure 2.2 –Alternative presentation of Shields curve by Van Rijn (Schiereck 2001)

2.1.2 Design practice

One way to interpret the Shields formula (2.5) is 'for a given type of sediment, represented by d and Δ, there is a certain critical bed shear stress τ_{0c}. When the acting bed shear stress τ_0 is below this critical value, the sediment will not move'.

For design purposes the inverse reasoning is more appropriate: 'for a given acting bed shear stress τ_0 and stone properties a stability parameter Ψ can be defined as:

$$\Psi = \frac{\tau_0}{(\rho_s - \rho)gd} \tag{2.9}$$

When Ψ is lower than the critical value Ψ_{cr} the stones will not move. Therefore the design stone size is the smallest stone size for which $\Psi = \Psi_{cr}$ (being the stone size for which $\Psi = \Psi_{cr}$)'. This means that a design formula can be formulated by re-writing (2.9) as:

$$d = \frac{\tau_0}{(\rho_s - \rho)\Psi_c} \tag{2.10}$$

In uniform, gravity driven flow the bottom shear stress follows from a momentum balance:

$$\tau_0 = \rho g R i_b \tag{2.11}$$

in which R is the hydraulic radius [m] and i_b is the slope of the free surface (or the bottom slope, as these are equal for uniform flow). When a logarithmic velocity profile is assumed over the complete water depth, the Chézy relationship also holds for these types of flow:

$$\overline{\overline{u}} = C\sqrt{R i_b} \tag{2.12}$$

in which C is the Chézy parameter and $\overline{\overline{u}}$ is the depth averaged flow velocity. Combining (2.11) and (2.12) gives two important relationships that will be used frequently throughout this thesis:

$$u_* = \frac{\sqrt{g}}{C}\overline{\overline{u}} \tag{2.13}$$

and

$$\tau_0 = \rho\, u_*^2 = \rho \frac{g}{C^2}\overline{\overline{u}}^2 \tag{2.14}$$

Combined with (2.10) this gives the well-known design formula:

$$d = \frac{\overline{\overline{u}}^2}{\Psi_{cr}\Delta C^2} \tag{2.15}$$

When a design value for Ψ_{cr} is set, equation (2.15) can be used to calculate the required stone size for a structure. It should be noted that this requires an iterative process, since C is dependent on d, as in:

$$C = 18\log\left(\frac{12h}{k_s}\right) \tag{2.16}$$

in which k_s is the bottom roughness [m] (which is proportional to d) and h is the water depth [m].

The use of the Chézy coefficient in (2.14) is common practice in design engineering. In some sources (eg Soulsby 1997) a theoretically more correct, but otherwise completely equivalent alternative is used, in which a current friction coefficient C_D is formally defined as:

$$\tau_c = C_D \rho \overline{\overline{u}}^2 \tag{2.17}$$

and C_D can be calculated (for a logarithmic velocity profile) as:

$$C_D = \left(\frac{0.40}{1 + \ln(z_0/h)} \right)^2 \tag{2.18}$$

With $C_D = g/C^2$ (as follows from a comparison of (2.14) and (2.17)) and $z_0 = k_s/30$ expression 2.16 can be found again, which shows that these two methods are indeed equivalent. (This friction coefficient C_D must not be confused with the drag coefficient C_D introduced in paragraph 3.3; usually the intended meaning will be clear from the context).

A few issues remain to be solved. First of all, Shields conducted his experiments for uniform grains, so he simply used the grain size *d* in his formula. In reality granular near-bed structures are always built with a certain stone grading, in which smaller and larger stones are present. A stone grading is commonly represented by its d_{n50}, which is defined as

$$d_{n50} = \sqrt[3]{\frac{M_{50}}{\rho_s}} \tag{2.19}$$

where M_{50} is the median stone weight [kg], ie exactly 50% (by weight) of all the stones in the grading are lighter than M_{50}. It is commonly assumed that it is justified to simply replace *d* in Shields's formula by d_{n50}.

Another important issue is, of course, the value of the critical stability parameter Ψ_c. From Shields's experiments one could conclude that $\Psi_c = 0.055$, but it should be noted that this is a matter on ongoing debate among researchers and designers. The 'threshold of motion' is not a simple phenomenon that can be objectively and univocally observed, like stones all staying motionless on the bottom at one point, and moving all of

a sudden when the load is increased. In reality, some stones will always move, even for Shields parameters below the threshold of motion. Defining the threshold of motion is really a matter of – arbitrarily - distinguishing between such notions as 'some movement', 'frequent movement', 'continuous movement' and so on, for which various researchers all have their own definitions. It is commonly accepted that the original Shields criterion relates to a situation in which quite a lot of stones are actually moving, so for design purposes it is considered a safe choice to use a lower Ψ_c value. Both Schiereck (2001) and CIRIA/CUR (1995) recommend $\Psi_c = 0.03$.

The fact that the threshold of motion is not a clear, well-defined boundary is further illustrated by Shields's original presentation (Figure 1), which shows the critical stability parameter as a hatched area rather than a sharp line. In most modern representations (eg Figure 2, or CIRIA/CUR 1991 p 297) this feature has been dropped, which could potentially be misleading.

The bottom roughness to be used in design is another much debated issue. Schiereck (2001) recommends $k_s = 2 \cdot d_{n50}$. Other sources may give different values, eg CIRIA/CUR (1995) gives $k_s = (1 \text{ to } 3) \cdot d_{90}$. Lammers (1997) found much higher values based on model tests and proposes $k_s = 6 \cdot d_{n50}$. In morphological research (eg Nielsen 1992) $k_s = 2.5 \cdot d_{n50}$ is a common choice, but even more exotic values like $k_s = 5.1 \cdot d_{84}$ have been proposed.

The value of k_s is not only related to the grain size but also to macroscopic bed forms like ripples or bumps; in practice these 'bed forms' are the result of inaccuracies during construction. These inaccuracies increase the bed roughness and thus the shear stress, leading to lower stability of the stones. However, Lammers (1997) concludes that for design purposes this is not a relevant issue. His model tests showed that the higher shear stress due to the increased bed roughness will move some stones, which will find a more favourable position elsewhere on the bed. This process, called 'ripening', has the tendency to flatten out the bed and increase its strength (or, perhaps more correctly formulated, decrease its initial weakness). Only the situation after ripening is important and the 'flat bed' values for k_s can be used in design.

Schiereck (2001) remarks – not unimportantly - that the choice of k_s and Ψ_c are related. He states that the result of a design process "is not very sensitive to the choice as long as reasonable combination of the two values is used" (quote from Schiereck, 2001). He recommends to use the combination $k_s = 2 \cdot d_{n50}$ and $\Psi_{cr} = 0.03$.

2.1.3 Influence factors

Strictly speaking, the design procedure described above is only valid for the conditions

for which Shields conducted his tests. In practice many situations can be found for which the conditions are different, including:

- non-developed flow, ie the assumption that the logarithmic velocity profile holds for the entire water depth is not valid – this may be the case in tidal flow;
- non-uniform flow, ie the flow accelerates or decelerates, for instance because of the presence of structures;
- there are increased turbulence levels to be expected. for instance in flow behind a backward facing step or flow caused by propeller jets;
- the bed is not flat but sloping.

This paragraph briefly discusses the ways in which designers most commonly account for these deviating circumstances.

Non-developed flow: In open channel flow with limited water depths, like flow in rivers and canals, the flow is usually fully developed. In marine applications, where the dominant flow is tidal flow, the situation may be different. Soulsby (1997) gives the following empirical velocity distribution for tides, based on measurements in the shallow seas around the British Isles:

$$u(z) = \left(\frac{z}{0.32h} \right)^{1/7} \overline{\overline{u}} \qquad \text{for } 0 < z < h/2 \qquad (2.20)$$

$$u(z) = 1.07\overline{\overline{u}} \qquad \text{for } h/2 < z < h$$

When large deviations from the logarithmic profile are expected, the bed shear stress may have to be calculated in a different way, for instance by using the more general expression given in the Coastal Engineering Manual (US Army Corps of Engineers 1995):

$$\tau_0 = \frac{1}{2} \rho \ f_c (u(z_r))^2 \qquad (2.21)$$

in which $u(z_r)$ is the velocity at an arbitrary level z_r above the bed [m/s], which can for instance be obtained from (2.20) or from direct measurements if these are available. The friction factor f_c follows in this case from:

$$\frac{1}{4\sqrt{f_c}} \cong \log\left(\frac{z_r}{z_0}\right) \tag{2.22}$$

where z_0 is the integration constant for the logarithmic profile [m], which is related to the bed roughness and commonly taken as $z_0 = k_s/30$. The 'clean' factor 4 in this formula may be misleading: it is not a theoretical factor, but follows from $\ln(10)/\kappa\sqrt{2} = 4.07\ldots$ This expression provides a more versatile way of calculating the bed shear stress than the classic "Chézy-based" way using the depth-averaged velocity, and has the added advantage that it is does not build on the assumption of a fully developed logarithmic profile, which as we have seen is not always necessarily the case. For $u(z_r) = \overline{\overline{u}}$ and $z_r = 0.37 \cdot h$ the two methods are equivalent.

Another situation in which a logarithmic velocity profile cannot be assumed beforehand is when analysing data from laboratory experiments, especially those conducted in relatively narrow flumes.

Non-uniform flow: In accelerating flow the stability of stones in a bed is no less than in a uniform flow, provided that the local flow velocity is used (Schiereck, 2001). In decelerating flow the situation is different, because the associated loss in kinetic energy causes an increase in turbulence levels. This effect can be accounted for by the multiplying the design flow velocity by an *influence factor* K_v. Note that this influence factor works in the flow velocity, and so the shear stress is increased by K_v *squared*. The value of K_v depends on the type of structure that causes the deceleration (eg a bridge pier or a river groyne) and on the location where the flow velocity *u* is defined. The appropriate K_v values for a given situation can be found in design handbooks, eg Schiereck 2001.

Increased turbulence: Every flow in hydraulic engineering practice is turbulent, including the flows in Shields's experiment, so 'normal' turbulence is already implicitly present in the design rules. Only when the expected turbulence intensities are higher than 'normal' must this be accounted for. The most common way to do this is by describing the flow velocity in terms of turbulent fluctuations around a mean value. The turbulence intensity is then defined as

$$r = \frac{\mu_u}{\sigma_u} \tag{2.23}$$

in which μ_u is the mean flow velocity and σ_u is its standard deviation, expressing the magnitude of the turbulent fluctuations. It is then assumed that an extreme velocity,

defined as the mean plus three standard deviations, is responsible for moving a stone from the bed. This gives a design velocity

$$u = \mu_u + 3\sigma_u = (1+3r)\mu_u \tag{2.24}$$

This means that when the turbulence intensity *r* is increased from r_{normal} to $r_{increased}$ for the same mean velocity μ_u we can define a K_v factor (as introduced above) as:

$$K_v = \frac{1+3r_{increased}}{1+3r_{normal}} \tag{2.25}$$

The 'background' turbulence intensity r_{normal} is directly related to the bottom roughness and can be calculated as a function of C (see appendix 1). As a first estimate r_{normal} = 0.1 is a common choice, so the denominator in (2.25) is usually written as 1.3

Sloping bed: When the stones of a bed protection are situation on a slope rather than on a flat bed their stability decreases. This effect can be accounted for by the use of a slope factor:

$$K_s = \frac{\sin(\phi-\alpha)}{\sin\phi} \qquad \text{for flow up or down the slope} \tag{2.26}$$

$$K_s = \sqrt{1-\frac{\sin^2\alpha}{\sin^2\phi}} \qquad \text{for flow perpendicular to the slope} \tag{2.27}$$

in which α is the slope angle and φ is the angle of internal friction of the bed material (for most situations $\varphi \sim 40^o$). These factors follow from a theoretical analysis of the direction of the forces on the stones on a sloping bed. Please note that these K_s factors must be used on the stone diameter, not on the flow velocity. K_s is always less than one, so the required stone diameter must be calculated as the stone diameter for a flat bed (obtained from the normal design procedure) *divided* by K_s.

2.2 Waves (oscillating flow)

2.2.1 Theoretical backgrounds

Shields's concept of a critical bed shear stress is also used for oscillatory flow situations, even though his original analysis and experiments only considered uniform flow. For very slowly oscillating flows, like tidal flows, the flow is usually considered as quasi-steady

and the procedure described in the previous paragraph is used.

For rapidly oscillating flows like waves a different procedure is followed. The bed shear stress under a wave can be linked to the horizontal orbital velocity close to the bed. This orbital velocity varies over the wave period, and consequently so does the shear stress. This introduces the need to define an 'overall' value for the wave shear; this could either be the maximum value $\hat{\tau}_w$ or the average value $\overline{\tau}_w$.

The maximum shear stress can be expressed as (Jonsson 1966)

$$\hat{\tau}_w = \frac{1}{2}\rho\ f_w \hat{u}_0^{\,2} \tag{2.28}$$

in which f_w is a friction factor [-] and $\hat{u}_0$ is the amplitude of the horizontal near-bed orbital velocity [m/s]. When it is assumed that the orbital velocity varies sinusoidally in time, it follows that $\overline{\tau}_w = ½\,\hat{\tau}_w$ (the average of a sine squared equals ½)

The required horizontal orbital velocity near the bed can be calculated with an appropriate wave theory. In linear wave theory this velocity is given by

$$\hat{u}_0 = \pi \frac{H}{T} \frac{1}{\sinh(kh)} \tag{2.29}$$

in which T is the wave period [s], H is the wave height [m], $k = 2\pi/L$ is the local wave number [rad/m], L is the local wave length [m] and h is the water depth [m]

An empirical relationship for the friction factor f_w was given by Jonsson, and later re-written by Swart (1974, cf CIRIA/CUR 1991) as:

$$f_w = \exp\left(-6.0 + 5.2\left(a_0/k_s\right)^{-0.19}\right) \quad \text{for } a_0/k_s > 1.57 \tag{2.30}$$

$$f_w = 0.3 \qquad \text{for } a_0/k_s \le 1.57$$

in which $a_0 = \hat{u}_0/\omega$ is the maximum horizontal excursion of the water particles near the bed [m] and k_s is the bottom roughness [m]. Many other expressions for f_w exist (see box 2), all of which are functions of the ratio a_0/k_s. Apparently this is an important scaling parameter.

2.2.2 Design practice

Sleath (1978) compared scale measurements from different sources and was able to assemble a 'modified Shields curve' showing the threshold of motion (or critical Ψ_c values) as a function of d_* (using the Van Rijn definition, eq 2.8). This curve, given in Figure 2.3, shows that Ψ_c becomes a constant for larger grain sizes for oscillatory flow, too. This means that once the bed shear stress under the wave load has been calculated a design procedure analogous to the procedure for currents only can be followed, and thus the same choices concerning the values of k_s and Ψ_c must be made.

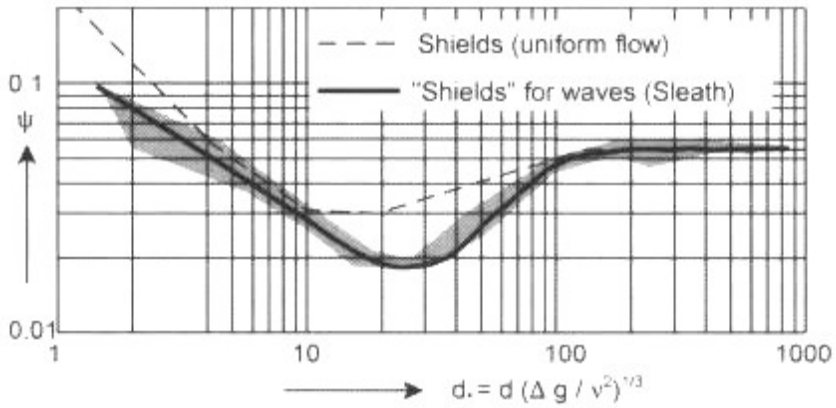

Figure 2.3 – Sleath curve (taken from Schiereck 2001)

From the Sleath curve it seems that $\Psi_c \sim 0.055$; but, keeping in mind the discussion in the previous paragraph, this may not be the right value to use for design purposes. Rance and Warren (1968) were one of the few researchers that conducted laboratory measurements on the stability of (very) coarse material under oscillatory flow. Their results can be used to 'tune' the threshold of motion. Both CIRIA/CUR (1995) and Schiereck (2001) state that when $\hat{\tau}_w$ is evaluated according to Jonsson/Swart, Ψ_c = 0.056 must be used to get good agreement with the results of Rance and Warren.

When the average shear stress $\overline{\tau}_w$ is used, CIRIA/CUR (1995) recommends Ψ_c = 0.03.

2.3 Waves and current combined

2.3.1 Theoretical backgrounds

The most common hydraulic load for near-bed structures, especially in marine environments, is a combination of waves and a current. Unfortunately, this is a

hydrodynamically very complex situation that is still not very well understood. The main problem is that the current and the waves affect each other in a highly nonlinear way, so an approach in which shear stresses for waves and currents are first calculated separately and then simply added, does not yield correct results. The details of wave-current interaction are described in Chapter 3, along with a discussion of a few theories that have been developed to tackle this issue. For the moment, it is convenient to observe that the current bed shear stress is related to $\overline{\overline{u}}$, and the wave shear stress to $\hat{u}_0$. These two velocities occur at different heights in the water column, so that is why the respective shear stresses cannot be added.

The wave-current interaction model that is presently used in design is the model of Bijker (1967). Bijker postulated that the combined shear stress τ_{wc} could be related to a certain combined flow velocity u_r which in turn could be a (vector) addition of the current velocity and the wave orbital velocity, as long as these two velocities were evaluated at the same level above the bed.

The result from Bijker's analysis (which is described in detail in Chapter 3) is that the instantaneous combined bed shear stress can be expressed as (Schiereck, 2001):

$$\tau_{wc}(\omega t) = \rho \kappa^2 u_r(\omega t)^2 \tag{2.31a}$$

where the combined velocity u_r is given by:

$$u_r(\omega t) = \sqrt{\frac{g}{\kappa^2 C^2}\overline{\overline{u}}^2 + \frac{f_w}{2\kappa^2}\hat{u}_0^2 \sin^2(\omega t) + 2\frac{\sqrt{g}}{\kappa C}\overline{\overline{u}}\frac{1}{\kappa}\sqrt{\frac{f_w}{2}}\hat{u}_0 \sin(\omega t)\cos(\phi)} \tag{2.31b}$$

in which κ is Von Kármán's constant (κ = 0.40), ωt is the phase of the wave cycle and φ is the angle between the direction of the current and the propagation direction of the waves. Substituting (2.31b) into (2.31a) and working out using (2.14) and (2.28) gives:

$$\tau_{wc}(\omega t) = \tau_c + \hat{\tau}_w \sin^2(\omega t) + 2\sqrt{\tau_c \hat{\tau}_w}\sin(\omega t)\cos(\phi) \tag{2.32}$$

2.3.2 Design practice

The design practice for a combination of waves and a current is based on the Shields approach, in which the bed shear stress is evaluated according to Bijker (2.31 or 2.32). The same questions as in the pure wave case arise, ie: which measure of τ_0 (maximum or average) should be used, and what is the value of Ψ_c?

The maximum value of τ_0 occurs when $u_r(\omega t)$ is maximum, which is at $\sin(\omega t) = 1$. Substituting this in (2.32) gives

$$\hat{\tau}_0 = \tau_c + \hat{\tau}_w + 2\sqrt{\tau_c \hat{\tau}_w}\cos(\phi) \tag{2.33}$$

The average shear stress can be evaluated in two different ways. When the shear stress is averaged over the full wave period, the second term in (2.32) gets an extra factor ½ (since the average of $\sin^2(\omega t) = ½$) and the third term vanishes (since the average of $\sin(\omega t) = 0$). This leads to

$$\overline{\tau}_0 = \tau_c + \frac{1}{2}\hat{\tau}_w \tag{2.34}$$

When the shear stress is averaged over half a wave period, the second term in (2.32) still gets an extra factor ½ (since the average of $\sin^2(\omega t)$ over half a wave period is ½ as well), but the third term gets an extra factor $2/\pi$, which is the average of $\sin(\omega t)$ over half the period. This gives

$$\overline{\tau}_{0,1/2T} = \tau_c + \frac{1}{2}\hat{\tau}_w + \frac{4}{\pi}\sqrt{\tau_c \hat{\tau}_w}\cos(\phi) \tag{2.35}$$

The recommendations on which measure (maximum or average shear stress) to use in design are not clear. Schiereck (2001) states that the average shear stress is an interesting measure for sediment transport, but the maximum shear stress causes the damage to a structure. This could be interpreted as a recommendation to use eq (2.33) in design. Another important source, CIRIA/CUR (1995) explicitly recommends to use (2.34), along with $\Psi_c = 0.03$. However, this section of the CIRIA/CUR manual is a little obscure. First of all, it states that (2.34) is only valid for waves and currents propagating in the same direction, whereas we have seen that the term containing the angle between waves and currents vanishes completely because of the averaging procedure, so in fact (2.34) is valid for any angle. Secondly, it states that $\Psi_c = 0.03$ should be used when (2.34) is applied “in order to agree with the results of Rance and Warren” (quote from CIRIA/CUR 1991). This is a strange recommendation, as the experiments of Rance and Warren were conducted for waves alone (Rance and Warren 1968) so a formula containing both waves and currents like (2.34) can never be ‘tuned’ to their results.

Finally, a software package that is often used for the design of bed protections called BPP (from WL|Delft Hydraulics) uses the formula

$$\begin{aligned}\tau_0 &= \tau_c + (0.7)^2\hat{\tau}_w + 2(0.7)\sqrt{\tau_c\hat{\tau}_w}\cos(\phi)\\ &= \tau_c + (0.49)\hat{\tau}_w + 1.4\sqrt{\tau_c\hat{\tau}_w}\cos(\phi)\end{aligned} \tag{2.36}$$

in its calculations, as can be (implicitly) made up from the manual accompanying the software package (WL|Delft Hydraulics 1985?). This formula is very close to the Bijker shear stress averaged over half a period, which can be written as (see 2.35)

$$\begin{aligned}\overline{\tau}_{0,1/2T} &= \tau_c + \frac{1}{2}\hat{\tau}_w + \frac{4}{\pi}\sqrt{\tau_c\hat{\tau}_w}\cos(\phi)\\ &= \tau_c + 0.50\hat{\tau}_w + 1.27\sqrt{\tau_c\hat{\tau}_w}\cos(\phi)\end{aligned} \tag{2.37}$$

Apparently BPP uses this method, but the two theoretical values ½ and $4/\pi$ have been replaced by empirical values based on what the manual calls an 'experimental experience value' of 0.7. Regardless of the differences in determining τ_0, BPP still uses $\Psi_c = 0.03$. BPP also uses $k_s = 2 \cdot d_{n50}$.

2.3.3 Irregular waves

The discussion so far has been about regular waves. There appears to be little guidance in literature on which wave height and wave period to use in the case of irregular waves (wind waves). Both Schiereck (2001) and CIRIA/CUR (1995) simply use 'H' and 'T' in their formulas without further specification. BPP uses $H_{1\%}$ and T_p, probably against the background of the idea that the highest waves causes the damage; in deep water the ratio $H_{1\%}/H_s$ is constant, but in shallower water this ratio is dependent on the water depth *h* as the wave height distribution deviates more and more from the theoretical Rayleigh distribution. BPP calculates $H_{1\%}$ from the significant wave height at a given water depth *h* as (WL|Delft Hydraulics 1985?):

$$H_{1\%} = H_s \frac{\sqrt{\frac{1}{2}\ln 100}}{\sqrt[3]{1+\frac{H_s}{h}}} = H_s \frac{1.52}{\sqrt[3]{1+\frac{H_s}{h}}} \tag{2.38}$$

Other, more recent formulas exist to calculate $H_{1\%}$ for a given H_s in shallow water; the method by Battjes and Groenendijk is commonly considered to be the state-of-the-art. This method involves a whole calculation procedure and cannot be written as an explicit formula. Interested readers are referred to literature (Battjes and Groenendijk 2000).

2.4 Conclusion

This chapter has described the present practice regarding the design of near-bed structures under various hydraulic situations: current only, waves only and a combination of these two. The most important theoretical backgrounds to the applied methods have been discussed, and some unresolved issues (such as the definition of the threshold of motion and the appropriate value of Ψ_c, the use of k_s and the way in which currents and waves must be combined) have been mentioned. In the next chapter we will discuss alternative design approaches. First, alternative (more complex) theories regarding the determination of the bed shear stress under waves and currents will be discussed. After that we will introduce completely different design approaches that are no longer based on bed shear stress.

The design method described in this chapter is based on a 'critical stability' approach as defined in the introduction (chapter 1). It will be clear that there is no agreement on the definition of 'critical stability', and there is certainly a lot of debate about the exact value that a critical stability parameter should have. This debate is already prominent in the simple case of a pure current load and becomes even fiercer when a more complex load situation like a combination of waves and a current is considered.

In the next chapters, the step to an 'allowable damage' approach will be taken. Apart from the potential cost savings that can be achieved by this method, an added advantage is that does not use the critical stability concept and therefore avoids much of the discussion involved.

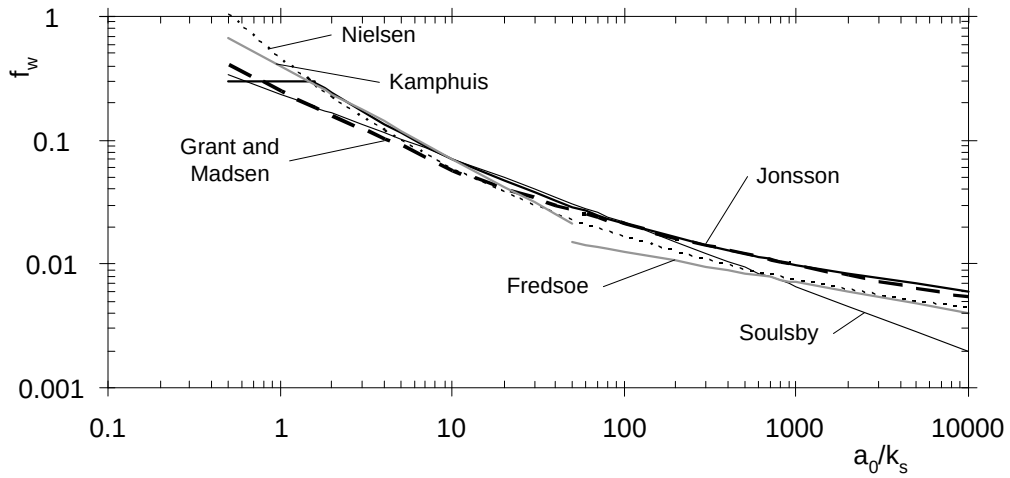

Figure 2.4 – Wave friction factors

Box 2.1 – Wave friction factors

The empirical wave friction factor by Jonsson/Swart (eq 2.18) is the one most commonly used in design, but it is certainly not the only one. Grant and Madsen (1986) have developed a theoretical model for the fluid motion in a wave boundary layer from which they deduced the implicit relationship:

$$\frac{1}{4\sqrt{f_w}} + \log\left(\frac{1}{4\sqrt{f_w}}\right) = \log\left(\frac{a_0}{k_s}\right) - 0.17 + 0.24\left(4\sqrt{f_w}\right)$$

for $a_0/k_s < 100$, this relationship either very slowly converging or no longer valid, and f_w can be read from a graph given in the Coastal Engineering Manual (USACE 1995).

Fredsøe (1984) also developed a theoretical model for the fluid motion which yields a different relationship for f_w. This relationship cannot be expressed analytically, but Fredsøe gives the following approximation of his results:

$$f_w = 0.04\left(a_0/k_s\right)^{-0.25} \qquad \text{for } (a_0/k_s) > 50$$

More information on wave boundary layers and the theories of Grant and Madsen, and Fredsøe can be found in chapter 3.

Other authors have proposed empirical friction factors based on measurements, including:

Kamphuis (1975): $f_w = 0.4\left(a_0/k_s\right)^{-0.75}$ for $(a_0/k_s)<50$ (cf Fredsøe 1992)

Nielsen (1992): $f_w = \exp\left(5.5\left(a_0/k_s\right)^{-0.2} - 6.3\right)$ for all (a_0/k_s) (cf Soulsby 1997)

Soulsby (1992): $f_w = 0.237\left(a_0/k_s\right)^{-0.52}$ for al (a_0/k_s)

All these friction factors are plotted here as functions of a_0/k_s.(See Figure 2.4) It can be seen that all values are in reasonable agreement with each other, except for the Soulsby formula that clearly deviates for large (a_0/k_s). Fredsøe and Nielsen also predict lower values than the other methods at large a_0/k_s. However, for normal waves in coastal areas a_0 is typically in the range 1-3 metres, so for rock structures with *d* (and thus k_s) in the order O(0.1 m) we would expect a_0/k_s to be of the order O(10). Especially in this range the agreement between the various wave friction factors is good. Interestingly, the Jonsson/Swart method is the only method that prescribes a maximum value at $f_w = 0.03$.

From this comparison it can be seen that although many formulations for f_w exist, it does not really matter which one is used, so the widespread use of Jonsson/Swart seems justified

3 Literature search

3.1 Introduction

This chapter describes the various stability parameters and damage parameters that have been put forward in literature. In terms of stability parameters, we can discern three main groups.

First group: the first group of stability parameters is the closest to the present design methods (see chapter 2). These parameters are all based on the bed shear stress as the governing parameter, and are therefore of the form:

$$\Psi = \frac{\tau}{\rho g \Delta d_{n50}} \tag{3.1}$$

In order to be valid for a combination of waves and currents (the area of interest of this research), the shear stress τ must be the combined wave-current shear stress τ_{wc}. Calculating this combined shear stress is not a straightforward task. In paragraph 3.2 we will introduce various calculation models that have been put forward in literature, select a few of them and discuss these selected models in some detail.

Second group: the second group of stability parameters relates directly to the forces that act on the stones. These forces can be linked to the fluid velocities and accelerations in the direct vicinity of the stone. The basic idea behind this method is that not only drag, shear and lift forces (which are proportional to u^2 and d^2) but also inertia forces (which are proportional to *a* and d^3) play a role. In principle the drag and lift forces can be translated to bed shear stresses again (see chapter 2), but the inertia forces and fluid accelerations form a new element in the analysis.

In general, stability parameters of this kind take the form:

$$\Theta = \frac{\frac{1}{2} C_B u^2 + C_M a d_{n50}}{g \Delta d_{n50}} \tag{3.2}$$

in which C_B and C_M are two coefficients that describe the relative influence of the drag and lift forces over the inertia forces. We will use the Greek capital theta (Θ) to denote this type of stability parameters in order to distinguish it from the shear stress-based stability parameters.

This method is inspired by the Morison formula for wave forces on piles (Morison *et al* 1950) which is also a combination of drag forces and inertia forces. For this reason the ideas behind this second group of stability parameters are commonly referred to as the *Morison-type* approach. This second group of stability parameters is discussed in paragraph 3.3.

Third group: the third group of stability parameters is based on the idea that the entrainment of an individual stone is not caused by average parameters like velocity, shear stress or accelerations, but by rare extreme events, like a bypassing eddy, which can in turn be related to the turbulence of the flow. This crucial role played by turbulence must be represented in the stability parameter, which will therefore be of the general form:

$$\Psi_t = \frac{f\left(\overline{u}^2, k, \varepsilon, l_m\right)}{g \Delta d_{n50}} \tag{3.3}$$

in which $\overline{u}$ is the Reynolds-averaged flow velocity and k, ε and l_m are turbulence parameters (see appendix A for a brief introduction to these and other concepts from turbulence theory). Paragraph 3.4 discusses this type of stability parameters in more detail.

The various damage parameters that have been proposed in literature are introduced in paragraph 3.5. Traditionally, damage has been expressed in terms of a transport rate, and a large section of this paragraph will be devoted to a discussion of various transport formulae, after which a short introduction to alternative damage parameters such as entrainment will be given.

This thesis is about the *design* of near-bed structures, so all the concepts introduced above will – somehow – have to be translated to a practical, damage-based design method. Some methods have been proposed in literature, either based on transport or on other damage parameters. These methods will be introduced in paragraph 3.6.

3.2 Shear stress based stability parameters

3.2.1 Adding shear stresses without wave-current interaction

The bed shear stress under a current and the bed shear stress under waves can both be calculated separately using the methods described in Chapter 2. When a structure is loaded by a combination of a current and waves we are interested in the resulting combined bed shear stress. The most straightforward way of calculating this is by a simple addition of the current-only bed shear stress τ_c and the instantaneous wave-only bed shear stress τ_w; when the current and the waves meet at an angle φ we must use a vector addition as in Figure 3.1.

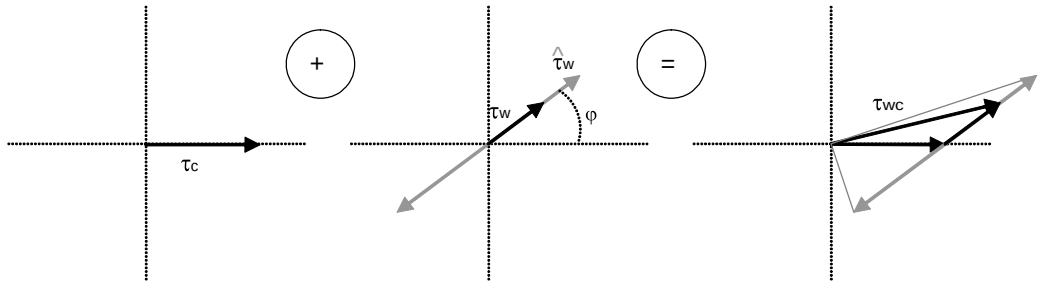

Figure 3.1 – Vector addition of bed shear stresses (without wave-current interaction)

This instantaneous combined bed shear stress τ_{wc} varies over time as sketched in Figure 3.2 (for the case $\varphi = 0^o$; when $\varphi > 0^o$ we must reduce $\hat{\tau}_w$ by a factor $\cos(\varphi)$). For practical design purposes we need to translate this time-variant parameter to one single characteristic value; for this purpose we can either use the maximum value $\tau_{wc,max}$ (indicated in Figure 3.2) or an average value.

Unfortunately 'the' average value is not uniquely defined, but depends on the outcome of two choices:

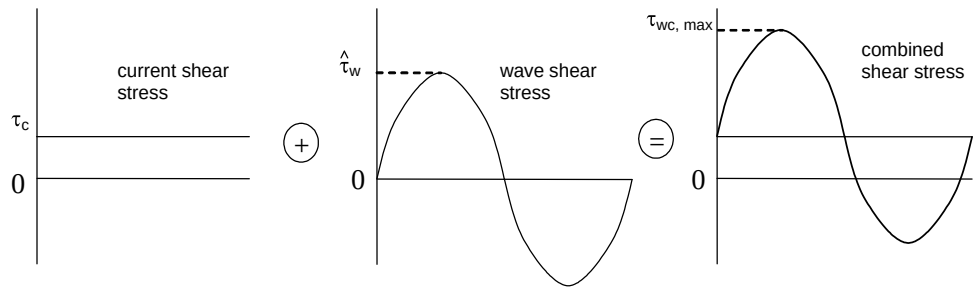

Figure 3.2 –Combined shear stresses (without wave-current interaction) as a function of time

with or without directional information: the shear stress itself is, by definition, a positive quantity; the sign of the shear stresses depicted in Figure 3.2 is purely related to the direction of the stress: a stress against the direction of the current is shown as negative. We can now choose to include this directional information in our averaging procedure, or not. Mathematically this difference comes down to averaging the *projection* of the combined shear stress in the current direction (the x-axis in Figure 3.1), or averaging the *modulus* (absolute value) of the combined shear stress, respectively. Though this is perhaps counter-intuitive, we must realise that when we take a straightforward mathematical average of the combined shear stress, we are effectively doing this last thing: we are averaging the absolute values. When $\varphi > 0^o$ these two procedures will obviously lead to different results, but also in the case $\varphi = 0^o$ there will be a difference. This can be explained as follows: when the waves are dominant (ie $\hat{\tau}_w > \tau_c$) there will be a period during the wave cycle that the combined shear stress is negative (ie against the direction of the current). When we do not disregard the directional information this negative contribution is taken into account in the averaging procedure, and so in general the resulting average shear stress will be lower. Only in the case $\varphi = 0^o$ and current dominance ($\tau_c > \hat{\tau}_w$) there will be no difference between these two methods.

averaging period: we can either average the instantaneous combined shear stress over the full wave cycle or over half the wave cycle. The latter approach is inspired by the fact that the software program BPP uses it (see chapter 2). The combined shear stresses

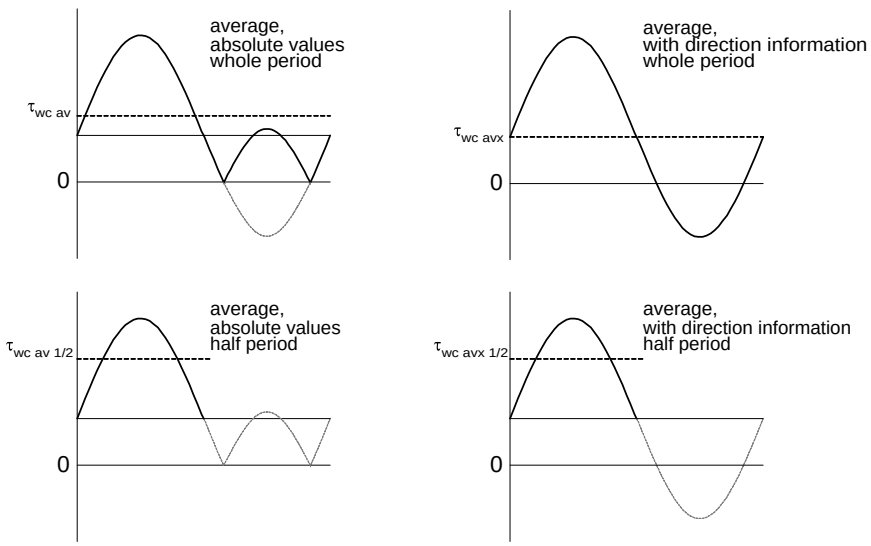

Figure 3.3 –Averaging procedures for the combined bed shear stress

during the first half wave cycle (when the wave shear stress and the current shear stress work in the same direction) will be higher than the combined shear stress during the second half wave cycle (when the two components work in opposite directions). For this reason the averaged shear stress over half the wave cycle will always be higher than the averaged shear stress over the full wave cycle.

These two choices, direction and averaging period, can be combined to give rise to (2x2) = 4 different average shear stresses. These are illustrated in Figure 3.3 (again for φ = 0^o). We see that in this case the 'average absolute shear stress over half the wave cycle' is equal to the 'average shear stress over half the wave cycle with direction information'. In the present research we will always deal with collinear flow ($\varphi = 0^o$), simply because our analysis will be based on scale model tests in which φ has not been varied (see Chapter 5). For this reason there is no further need to distinguish between the two 'half cycle' averaging procedures *within the context of this thesis*.

Also, to avoid long and cumbersome phrases, we will refer to the "average of the absolute values of the shear stress " simply as the "average" shear stress, because it is related to the mathematical average. The "average of the shear stress with direction information" will be called the "average in the direction of the flow" since it is essentially just that: the average of the projection of the combined shear stress in the flow direction.

In short, there are four remaining ways to express 'the' combined shear stress:

- the maximum shear stress $\tau_{wc,max}$. This parameter is used in the analysis because it is suggested by Schiereck (2001) that the maximum shear stress causes the damage to a structure.
- the average shear stress over the whole period $\tau_{wc,av}$ This parameter is used in the present design method recommended by CIRIA/CUR (1995).
- the average shear stress in the direction of the flow $\tau_{wc,\ avx}$. This parameter is often used in morphological research into sand transport under combined wave-current load;
- the average shear stress over half the period $\tau_{wc\ av\ 1/2}$. This parameter is used in the present design method with the software package BPP.

In this thesis we will use all four parameters and investigate which one can best be used in the design of granular near-bed structures.

Mathematically we can work this out a little further. The instantaneous combined bed shear stress follows from a vector addition of τ_c and $\tau_w(\omega t) = \hat{\tau}_w \sin(\omega t)$ using the cosine

rule. Again we see that this is essentially the *modulus* of the combined shear stress:

$$\left|\tau_{wc}(\omega t)\right| = \sqrt{\tau_c^2 + \hat{\tau}_w^2 \sin^2(\omega t) + 2\tau_c \hat{\tau}_w \sin(\omega t)\cos(\phi)} \tag{3.4}$$

The maximum shear stress occurs when sin(ωt) = 1, so

$$\tau_{wc,\max} = \sqrt{\tau_c^2 + \hat{\tau}_w^2 + 2\tau_c \hat{\tau}_w \cos(\phi)} \tag{3.5}$$

For collinear flow cos(φ) = 1 so equation (3.5) reduces to:

$$\tau_{wc,\max} = \sqrt{\tau_c^2 + \hat{\tau}_w^2 + 2\tau_c \hat{\tau}_w} = \sqrt{(\tau_c + \hat{\tau}_w)^2} = \left|\tau_c + \hat{\tau}_w\right| \tag{3.6}$$

which is also intuitively clear.

The average shear stress over the full period and the average shear stress over half the period follow theoretically as:

$$\tau_{wc,av} = \frac{1}{2\pi}\int_0^{2\pi} \sqrt{\tau_c^2 + \hat{\tau}_w^2 \sin^2(\omega t) + 2\tau_c \hat{\tau}_w \sin(\omega t)\cos(\phi)}\, d(\omega t) \tag{3.7}$$

$$\tau_{wc,av,1/2} = \frac{1}{\pi}\int_0^{\pi} \sqrt{\tau_c^2 + \hat{\tau}_w^2 \sin^2(\omega t) + 2\tau_c \hat{\tau}_w \sin(\omega t)\cos(\phi)}\, d(\omega t) \tag{3.8}$$

Neither integral can be solved analytically (because of the presence of the square root) and so the average values must be found with a numerical averaging procedure.

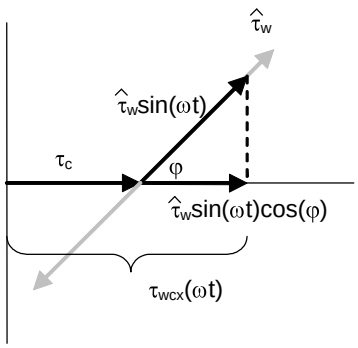

Figure 3.4 – Instantaneous combined shear stress in the direction of the current

Finally, the instantaneous shear stress in the direction of the current can be simplified to (see Figure 3.4):

$$\tau_{wcx}(\omega t) = \tau_c + \hat{\tau}_w \sin(\omega t)\cos(\phi) \tag{3.9}$$

and so the average shear stress in the direction of the current follows from:

$$\tau_{wc,avx} = \frac{1}{2\pi}\int_0^{2\pi}\left(\tau_c + \hat{\tau}_w \sin(\omega t)\cos(\phi)\right)d(\omega t) = \tau_c \tag{3.10}$$

which can also be seen from the graphical representation in Figure 3.2. At the moment the fact that $\tau_{wc,avx} = \tau_c$ may seem trivial and the inclusion of $\tau_{wc,avx}$ in our analysis may appear to make little sense, but we will see later (when we discuss the phenomenon of wave-current interaction) that it *is* an important parameter.

In (3.10) we have used the fact that the average of sin(ωt) over the full wave cycle equals zero. We will use these kind of mathematical averaging procedures throughout this thesis, so for completeness' sake we will introduce the most important basic formulae here:

$$\begin{aligned}
&\frac{1}{\pi}\int_0^{\pi}\sin(\omega t)d(\omega t) = \frac{2}{\pi}\\
&\frac{1}{2\pi}\int_0^{2\pi}\sin(\omega t)d(\omega t) = 0\\
&\frac{1}{\pi}\int_0^{\pi}\sin^2(\omega t)d(\omega t) = \frac{1}{2}\\
&\frac{1}{2\pi}\int_0^{2\pi}\sin^2(\omega t)d(\omega t) = \frac{1}{2}
\end{aligned} \tag{3.11}$$

3.2.2 Wave-current interaction: general remarks

In the previous paragraph we have simply added the bed shear stress caused by the current and the bed shear stress caused by the waves. Physically speaking this is not a correct approach, because the current and the wave influence each other. This effect, in general terms called *wave-current interaction* (WCI) is so strong that its influence must be accounted for.

Soulsby (1997) lists three ways in which the waves and the current interact:

a) modification of the phase speed and wavelength of the waves by the current, leading to refraction of the waves

b) interaction of the wave and current boundary layers, leading to enhancement of both the steady and oscillatory components of the bed shear stress

c) generation of currents by the waves, including longshore currents, undertow and mass transport (streaming) currents

In design practice the current and wave climate are usually given as boundary conditions and are either taken from site measurements or a computer model. In these measurements or calculations the interactions mentioned under a) and c) are already (implicitly) present; with the possible exception of undertow and streaming currents mentioned under c). This effect will be neglected and only the second way of wave-current interaction, the enhancement of the bed shear stress, will be treated in this thesis.

Wave-current interaction is a nonlinear phenomenon: the presence of the current influences the waves (leading to an enhanced wave shear stress), but the presence of the waves also influences the current (leading to an enhanced current shear stress). The details of this phenomenon and its physical background are described in paragraph 3.2.3. Many models to describe this wave-current interaction have been put forward in literature; unfortunately they all differ in their predictions of the enhanced shear stresses and the resulting combined shear stress.

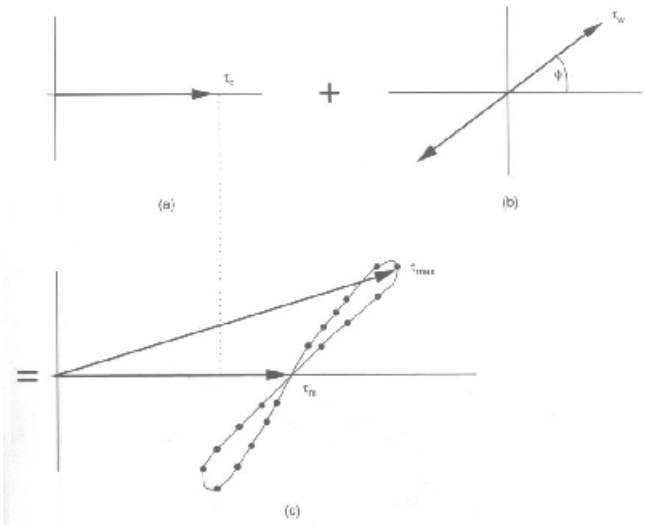

Figure 3.5 - Vector addition of bed shear stresses with wave-current interaction (Souslby et al 1993)

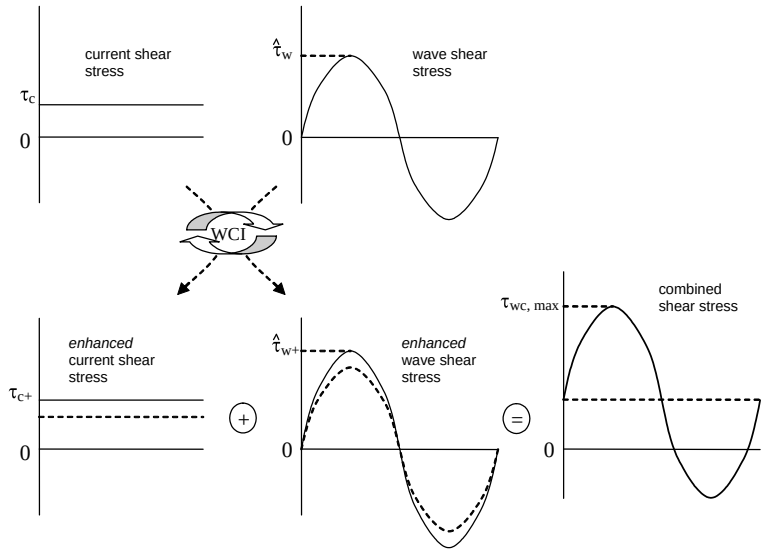

Figure 3.6 –Combined bed shear stresses with wave-current interaction as a function of time

A general illustration of the resulting instantaneous bed shear stress when wave-current interaction is taken into account is given in Figure 3.5 (Soulsby *et al*, 1993) and Figure 3.6. It is illustrative to compare these figures to Figure 3.2 and Figure 3.3, respectively. It must be said that most wave-current models do not follow the explicit steps as sketched in Figure 3.6; this figure must be seen as an idealised illustration of the basic idea behind wave-current interaction.

After the instantaneous combined bed shear stress has been obtained, the same maximum/averaging procedures can be applied as discussed in the previous paragraph. In particular we see now that $\tau_{wc,avx}$ is no longer equal to the pure current shear stress τ_c, but to the *enhanced* current shear stress τ_{c+}. This is why $\tau_{wc,avx}$ is such an important parameter: it shows how the current shear stress (which features in many morphological transport formulae) is enhanced by the presence of the waves.

A useful overview of existing wave-current interaction models is given by Soulsby *et al* (1993). They mention having compiled a list of 21 different models, and explicitly discuss the models of Grant and Madsen (1979), Christofferson and Jonsson (1985), Bijker (1967), Van Kesteren and Bakker (1984), Fredsøe (1984), Myrhaug and Slaattelid (1990), Davies, Soulsby and King (1988) and Hyunh-Thanh and Temperville (1991).

Soulsby *et al* compared these eight models in terms of their prediction of the mean and maximum combined shear stress for the same input parameters (exactly how ‘mean’ is

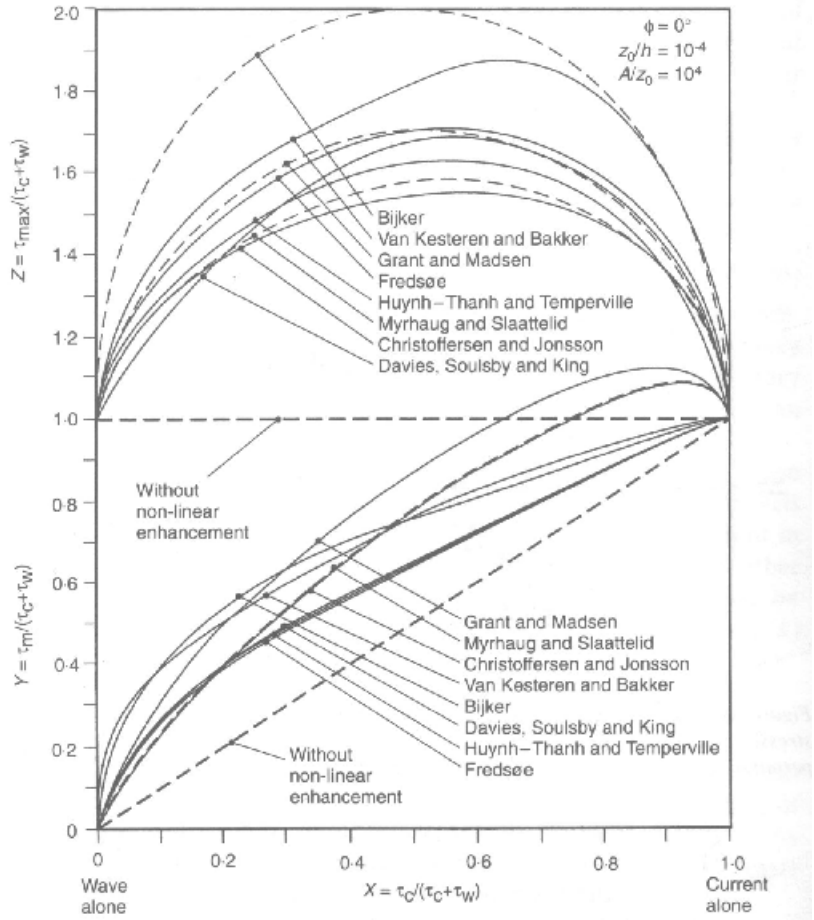

Figure 3.7 - Comparison of eight different wave-current interaction models (Soulsby *et al* 1993)

defined will be discussed later). The input parameters are the same for all models: the relative bottom roughness z_0/h, the relative wave excursion a_0/z_0 and the angle between the current and the wave propagation direction φ. Soulsby *et al* devised a useful dimensionless way of plotting their results that will be used in this thesis as well. They defined a dimensionless input parameter X

$$X = \frac{\tau_c}{\tau_c + \hat{\tau}_w} \tag{3.12}$$

in which τ_c and $\hat{\tau}_w$ are the current-only and maximum wave-only bed shear stresses (for instance calculated with eq 2.14 and 2.21), respectively. This parameter can be seen as a measure for the relative strength of the current and wave components, for X = 0 there are only waves, for X = 1 there is only a current. In this respect this parameter X is more

practical than the other commonly used current strength parameter $\mu = \tau_c / \hat{\tau}_w$ which scales between $\mu = 0$ and $\mu = \infty$.

The average combined shear stress in the direction of the flow is defined in a similar way:

$$Y = \frac{\tau_{wc,avx}}{\tau_c + \hat{\tau}_w} \tag{3.13}$$

and so is the maximum combined shear stress:

$$Z = \frac{\tau_{wc,\max}}{\tau_c + \hat{\tau}_w} \tag{3.14}$$

In their original publication Soulsby *et al* do not use the term $\tau_{wc,\,avx}$. Instead they refer to the 'mean' combined shear stress without explicitly defining what 'mean' means. A comparison of the results from Soulsby *et al* with the results obtained in the present research shows that their $\tau_{wc,mean}$ is equal to our $\tau_{wc,avx}$.

A typical plot from the comparison in Soulsby *et al* is given in Figure 3.7. The dashed lines in this figure are the combined shear stresses without wave-current interaction. Dividing equations (3.6) and (3.10) by $(\tau_c + \hat{\tau}_w)$ shows that in these cases we have Z = 1 and Y = X (note that Figure 3.7 has been obtained for $\varphi = 0^o$). As can be seen from this plot, the predicted combined shear stresses with wave-current interaction differ a lot from the situation without wave-current interaction; in addition, there are quite some differences between the various models.

It appears that, roughly speaking, three groups of models can be discerned (Bijman 2000):

a) the first group, containing Bijker, and Van Kesteren and Bakker, give strikingly larger maximum shear stresses than the other models, and also higher mean stresses than the other models for wave dominated situations (low X values);

b) The second group is formed by Grant and Madsen, Myrhaug and Slaattelid, and Christofferson and Jonsson, who predict higher values than the other models for current dominated situations;

c) Finally, Fredsøe, Davies *et al* and Huynh-Thanh and Temperville predict lower values than the other models for all situations (and their predictions appear the match each other closely). They form the third group.

Another useful result from Soulsby *et al* is a parameterisation of Y and Z as a function of X and the input parameters z_0/h, a/z_0 and φ. With this parameterisation the mean and maximum shear stresses predicted by the various models can be approximated without having to go into the details of the models themselves. A disadvantage of this method is that it only gives $\tau_{wc,max}$ (through Z) and $\tau_{wc,avx}$ (through Y). In order to obtain the other parameters that we are interested in in the present research ($\tau_{wc,av}$ and $\tau_{wc,av,1/2}$), we will have to use the full models. The Soulsby parameterisation will only be used in this thesis as a means of comparison to the values obtained from the 'real' models. Appendix 2 contains some more information on this method.

In another publication (Soulsby 1997) Soulsby reports to have matched the performance of these models against a dataset of laboratory and field measurements. He concludes that no single model gave the best overall performance, but mentions four models that performed well and/or are widely used: Grant and Madsen, Fredsøe, Davies *et al* and Huynh-Thanh and Temperville. This would suggest that we would only include only these four models in our present research, with the addition of the Bijker model (given our knowledge that the present design practice of granular near-bed structures is based on this model, see Chapter 2).

Bijman (2000), who did valuable research on transport of coarse material under combined wave-current flow and whose work can be seen as a precursor to the present research, follows this suggestion. In addition, he uses the broad categorisation of models given above and includes one member from each group (*in casu* Bijker, Grant and Madsen, and Fredsøe) in his research.

Van Rijn also gives an overview of wave-current interaction models (Van Rijn 1993). He mentions more or less the same models as Soulsby *et al*, but includes models by Lundgren (1972) and Smith (1977). Van Rijn does not really compare the performance of all these models, but refers to Soulsby and a research by Visser (1986), who measured velocity profiles for a combination of waves and a current at an angle of 90^0. Based on these two sources Van Rijn states that the Fredsøe model gives reasonable results.

Altogether, given the conclusions of Soulsby (1997), Van Rijn (1993) and Bijman (2000) we decide to use the following five models in our research: Bijker; Grant and Madsen; Fredsøe; Davies, Soulsby and King; and Huynh-Thanh and Temperville. We will support this choice with further arguments based on the physical background of the various models in the next paragraph.

3.2.3 Wave-current interaction: physical background

For a physical explanation as to *why* and *how* the current and the wave motion influence each other, we need to know something about boundary layers and turbulence. A brief introduction to these topics is given below.

Shear stresses in a fluid can either be caused by viscosity or by turbulent mixing; the turbulent shear stresses (so-called Reynolds stresses) are much larger than the viscous stresses. This means that, if we want to understand something about the bed shear stresses caused by a flow, we need to understand the turbulence characteristics of that flow (for a background to the concepts from turbulence theory used in this thesis see appendix A).

Any fluid flowing along a fixed boundary (be it the bottom, or a wall) will develop a *boundary layer* in which the friction with the boundary influences the fluid motion, shear stresses develop and turbulence is generated. This boundary layer needs to grow, and so the boundary layer thickness is time-dependent. For a steady current, the boundary layer extends over the full water depth. For tidal currents this is not necessarily the case because they change direction every six hours or so and the boundary layer does not get enough time to grow all the way. For rapidly oscillating flow, like waves, the boundary layer thickness is only a few centimetres; only inside this wave boundary layer do shear stresses and turbulence play a role. Outside the wave boundary layer the fluid motion can be regarded as frictionless and can be described by potential flow theory (eg linear wave theory). The reverse also holds: when we apply linear wave theory we can only describe the fluid motion outside the wave boundary layer; the orbital velocity “at the bottom” (equation 2.24), is really the orbital velocity at the edge of the wave boundary layer. Inside this layer we need other theories to describe the fluid motion.

The existence of the wave boundary layer, and the extra turbulence it generates, is felt by the current as increased resistance which explains the enhanced current-only bed shear stress. On the other hand, the existence of a steady current influences the growth of the wave boundary layer, so this effect in nonlinear. Also, inside the wave boundary layer, the turbulence generated by the current interacts with the turbulence generated by the waves, which has the effect of enhancing both the current and the wave bed shear stress. This effect is also nonlinear, because turbulence is a nonlinear phenomenon (Soulsby *et al*, 1993).

We have seen that the boundary layers, the dominating length scales and the turbulence characteristics are different for uniform currents and for waves; this is one of the main reasons why simply adding the resulting shear stresses is not a valid approach. A

physically more correct approach would be to:

- assume a combined wave-current wave boundary layer and see the flow inside this layer as a separate flow problem;
- find the correct boundary conditions for this flow problem, given the characteristics of the current and the waves;
- solve the equations of motion (Navier-Stokes equations) inside this layer with these boundary conditions; since the flow in the layer is turbulent this means that a closure scheme for the Reynolds equations must be adopted; and finally,
- deduce the resulting combined bed shear stress from there.

This is exactly what the various wave-current interaction models seek to do. The differences between the models are mainly caused by the way in which they incorporate turbulence inside the boundary layer (ie the way in which they close the Reynolds equations). A general illustration of wave-current interaction is given in Figure 3.8.

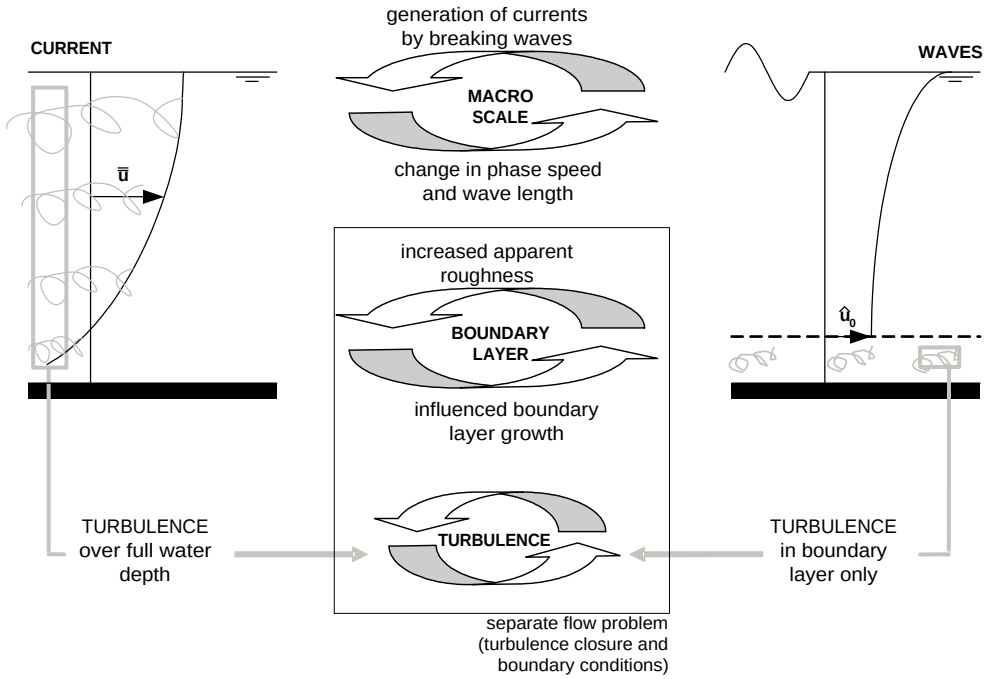

Figure 3.8 - General illustration of wave-current interaction

The fact that the various wave-current interaction models differ by the way in which they incorporate the turbulence in the boundary layer provides us with a way to categorise the wave-current interaction models, which is inspired by the overview of wave-current interaction models by Van Rijn (1993).

All wave-current interaction models discussed in this thesis use the eddy viscosity concept in their turbulence closure. As is described in appendix A, there are four ways to apply this concept which are, in order of increasing complexity:

- assuming a constant eddy viscosity, which is equivalent to using the mixing length hypothesis and assuming that l_m is constant. This leads to a linear velocity profile in the wave boundary layer. This is the basis of the Bijker model.
- using the mixing length hypothesis and assuming that l_m varies with the distance from the bottom, which leads to a logarithmic velocity profile in the boundary layer. Both Grant and Madsen, and Fredsøe use this concept in their models, the main difference being that Grant and Madsen assume the boundary layer thickness and eddy viscosity to be constant in time, while Fredsøe allows these parameters to vary with the wave cycle.
- using a balance equation for the turbulent kinetic energy and an estimated length scale (one-equation model). This approach was adopted by Davies, Soulsby and King.
- using a balance equation for the turbulent kinetic energy and an (assumed) balance equation for the dissipation rate of the turbulent kinetic energy (k-ε closure), as was done by Huynh-Thanh and Temperville.

So we can see that against this background we can further support our choice of five wave-current interaction models: each model represents another turbulence closure method. Also, we can conclude that these five models form a complete set, as each turbulence closure method is represented (at least each method based on the eddy viscosity concept; to our knowledge there are presently no wave-current interaction models based on more advanced turbulence closure methods such as Direct Numerical Simulation or Large Eddy Simulation). Finally, this turbulence-based description gives us the opportunity to apply a ranking in our wave-current interaction models, in order of increasing complexity: Bijker - Grant and Madsen - Fredsøe - Davies, Soulsby and King – Huynh-Thanh and Temperville.

These five models will now be described in more detail in the next paragraphs. In order to illustrate the effects of wave-current interaction we will always compare the results from these models with a situation in which wave-current interaction is *not* taken into account.

3.2.4 Wave-current interaction models: Bijker (1967)

Bijker postulated that the combined shear stress τ_{wc} could be related to a certain combined flow velocity u_r which in turn can be a (vector) addition of the current velocity and the wave orbital velocity, as long as these two velocities were evaluated at the same level above the bed. As described in Appendix 1, an assumption regarding the turbulence in the boundary layer is needed to relate this combined velocity to the bed shear stress. Bijker assumes in this case a constant mixing length l_m, which leads to a linear velocity profile (see Appendix 1):

$$u(z) = \frac{u_*}{l_m} z \tag{3.15}$$

Outside the boundary layer Bijker assumes a classic logarithmic velocity profile

$$u(z) = \frac{u_*}{\kappa} \ln\left(\frac{z}{z_0}\right) \tag{3.16}$$

At some point, this logarithmic profile must turn into the linear profile of equation (3.15), until u = 0 is reached at z = 0. (A definition sketch for the Bijker model is given in Figure 3.9) If we require that both the velocity and the velocity gradient are continuous at the point of intersection, we can show mathematically that these two profiles intersect at $z = ez_0$ (e = 2.718…) and, consequently, that the (constant) mixing length is equal to

$$l_m = \kappa e z_0 \tag{3.17}$$

Bijker chose to evaluate u_r at the level of intersection of the two profiles, so $u_r = u(ez_0)$.

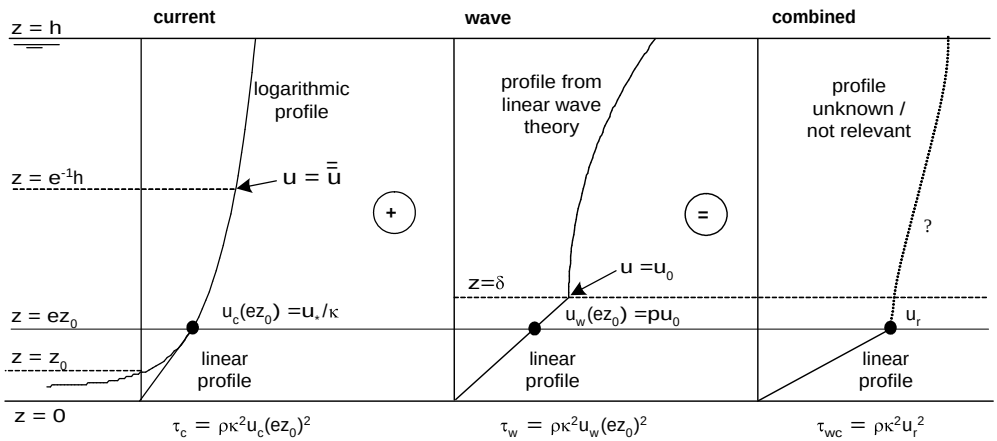

Figure 3.9 – Definition sketch for the Bijker model

The fact that $l_m = \kappa e z_0$ means that, apparently, Bijker assumes the size of the turbulent eddies in the entire boundary layer to be equal to the size they would have had near the top of the boundary layer ($z = ez_o$) if the Von Kármán hypothesis had been used. It is clear that – physically speaking – this is a very crude schematisation.

Substituting $z = ez_0$ and $l_m = \kappa e z_0$ in equation (3.15), and using the definition of the shear stress velocity u_* gives the resulting bed shear stress:

$$\tau_0 = \rho u_*^2 = \rho \kappa^2 u(ez_0)^2 = \rho \kappa^2 u_r^2 \tag{3.18}$$

So, when u_r is a vector addition of the current velocity and the wave velocity, both evaluated at $z = ez_0$, equation (3.18) can be used to find the combined bed shear stress.

From (3.16) it follows that the current component at this level equals

$$u_c(ez_0) = \frac{u_*}{\kappa} = \frac{\sqrt{g}}{\kappa C}\overline{\overline{u}} \tag{3.19}$$

The wave velocity profile is given by linear wave theory throughout the water column, except for the wave boundary layer. At the top of this layer we have the 'near-bed' orbital velocity $\hat{u}_0$. Inside this layer Bijker again assumed a linear profile, from u = 0 at z = 0 to u = u_0 at z = δ. The point ez_0 is within this boundary layer, so the wave-induced component at level $z = e \cdot z_0$ equals

$$u_w(ez_0) = pu_0 \tag{3.20}$$

with *p* a constant < 1. Note that u_0 is the instantaneous orbital velocity, with $u_0 = \hat{u}_0 \sin(\omega t)$.

Entering this wave component in equation (3.18) gives $\tau_0 = \rho\kappa^2 p^2 \hat{u}_0^2$. A comparison with the formulation by Jonsson (2.28) shows that $\frac{1}{2} f_w = \kappa^2 p^2$, so $p = 1/\kappa * \sqrt{(f_w/2)}$, and the wave component of u_r becomes:

$$u_w(ez_0) = \frac{1}{\kappa}\sqrt{\frac{f_w}{2}}u_0 = \frac{1}{\kappa}\sqrt{\frac{f_w}{2}}\hat{u}_0 \sin(\omega t) \tag{3.21}$$

The combined velocity u_r now follows as a vector addition of $u_c(ez_0)$ and $u_w(ez_0)$, as in:

$$u_r = \sqrt{u_c(ez_0)^2 + u_w(ez_0)^2 + 2u_c(ez_0)u_c(ez_0)\cos(\phi)} \tag{3.22}$$

in which φ is the angle between the direction of the current and the propagation direction of the waves.

Inserting equations (3.19) and (3.21) gives (Schiereck, 2001):

$$u_r(\omega t) = \sqrt{\frac{g}{\kappa^2 C^2}\overline{\overline{u}}^2 + \frac{f_w}{2\kappa^2}\hat{u}_0^2 \sin^2(\omega t) + 2\frac{\sqrt{g}}{\kappa C}\overline{\overline{u}}\frac{1}{\kappa}\sqrt{\frac{f_w}{2}}\hat{u}_0 \sin(\omega t)\cos(\phi)} \qquad (3.23)$$

Finally, we can use (3.18) to get the combined bed shear stress:

$$\tau_0(\omega t) = \rho\kappa^2 u_r(\omega t)^2 \qquad (3.24)$$

In chapter 2 is has already been shown that working out these equations (ie substitute (3.23) into (3.24) and use the expressions for the current shear stress (eq 2.14) and wave shear stress (eq 2.28) leads to simplified expressions for the maximum shear stress, the average shear stress over the whole wave period and the average shear stress over half the wave period (eqs 2.33, 2.34 and 2.35; see also table 3.1). For the average shear stress in the direction of the current no simplified expression exists.

The simplicity of equations (2.33), (2.34) and (2.35) suggests that τ_{wc} follows from a straightforward additions of the pure current shear stress τ_c and the pure wave shear stress τ_w, without accounting for wave-current interaction. We emphasise here that this simplicity is deceptive; the Bijker method *does* take wave-current interaction into account. This may be illustrated further by comparing the equations involved (see table 3.1), or by looking at Figure 3.7.

Table 3.1 – Equations for Bijker model and model without wave-current interaction

combined shear stress	**Without wave-current interaction**	**Bijker model**
instantaneous	$\tau_{wc}(\omega t) = \sqrt{\tau_c^2 + \hat{\tau}_w^2 \sin^2(\omega t) + 2\tau_c\hat{\tau}_w \sin(\omega t)\cos(\phi)}$	$\tau_{wc}(\omega t) = \tau_c + \hat{\tau}_w \sin^2(\omega t) + 2\sqrt{\tau_c\hat{\tau}_w} \sin(\omega t)\cos(\phi)$
maximum	$\tau_{wc,\max} = \sqrt{\tau_c^2 + \hat{\tau}_w^2 + 2\tau_c\hat{\tau}_w \cos(\phi)}$	$\tau_{wc,\max} = \tau_c + \hat{\tau}_w + 2\sqrt{\tau_c\hat{\tau}_w} \cos(\phi)$
average	no closed form	$\tau_{wc} = \tau_c + \frac{1}{2}\hat{\tau}_w$
average in current direction	$\tau_{wc,avx} = \tau_c$	no closed form
average over half period	no closed form	$\tau_{wc(1/2T)} = \tau_c + \frac{1}{2}\hat{\tau}_w + \frac{4}{\pi}\sqrt{\tau_c\hat{\tau}_w} \cos(\phi)$

For the present research, the Bijker model was implemented in a simple computer model (in Microsoft Excel). The results can be presented in dimensionless form in the way introduced by Soulsby *et al* (1993). An example of such a plot is given in Figure 3.10. In this plot the same dimensionless input parameters $z_0/h = 10^{-4}$, $a_0/z_0 = 10^4$ and $\varphi = 0^0$ have been used as in the original Soulsby plot (Figure 3.7), so the two plots can be directly compared. In our plot (Figure 3.10) we show the maximum shear stress and the three different ways of averaging the shear stress as described in paragraph 3.2.1. These average values were obtained by calculating $\tau_{wc}(\omega t)$ for various values of ωt and then numerically averaging the results. When an average in the direction of the flow was required the values of $\tau_{wc}(\omega t)$ were multiplied with $\cos(\Phi(\omega t))$, in which $\Phi(\omega t)$ is the instantaneous angle between $\tau_{wc}(\omega t)$ and the direction of the flow.

In addition to the results from the Bijker model we have plotted the results if no wave-current interaction would be taken into account. For the maximum combined shear stress and the average shear stress in the direction of the current we have Z = 1 and Y = X, as follows from equations (3.6) and (3.10), respectively, in combination with the definitions of Z and Y (equations 3.14 and 3.13, respectively). The average combined shear stress over the full period and over half the periods cannot be calculated analytically (as described in paragraph 3.2.1) so these results were obtained from a numerical averaging procedure.

Finally, the results from the CIRIA/CUR method (eq 2.34) and BPP method (eq 2.36), as well as the Soulsby parameterisation for the maximum shear stress (see appendix 2) are also plotted in Figure 3.10.

From a comparison of Figure 3.7 and Figure 3.10 we can see that our results for the combined shear stress in the current direction, averaged over the whole period match the Y-values as plotted by Soulsby. This again confirms our observation that this is the way in which Soulsby defined his ‘mean’ shear stresses. Further, we see that our results for the maximum shear stress match the theoretical curve exactly. Also, our results for the averaged shear stress over the whole period match the results calculated by the CIRIA/CUR method exactly, and our results for the averaged shear stress over half the period match the results calculated by the BPP method reasonably well. This is in line with our conclusion from Chapter 2 that these methods are closely related.

Figure 3.10 clearly illustrates how both the maximum and averaged shear stresses (for all averaging methods) are enhanced compared to the situation when no wave-current interaction is taken into account, except in strongly wave-dominated situations.

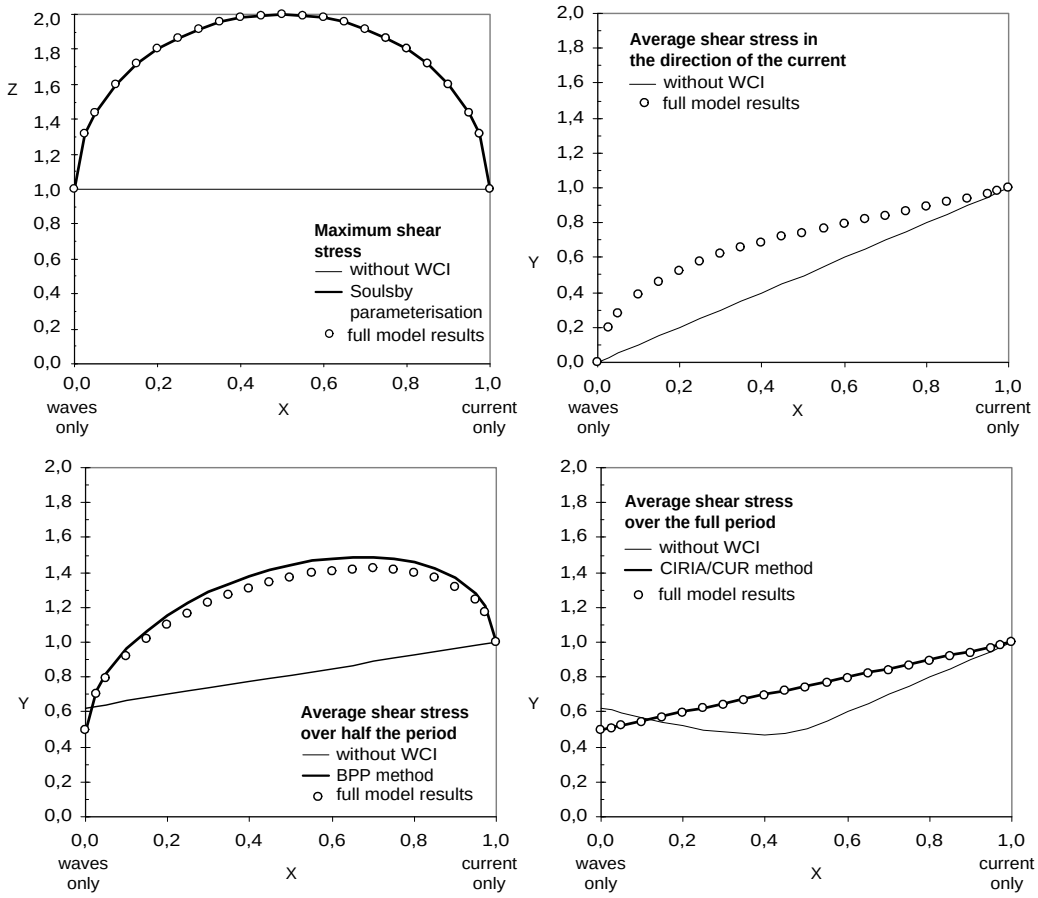

Figure 3.10 – Dimensionless results for the Bijker model, with $z_0/h = 10^{-4}$, $a_0/z_0 = 10^4$ and $\varphi = 0^0$

This last observation can be explained because Bijker adds *velocities*, and the shear stress is proportional to the velocity squared, whereas without wave-current interaction *shear stresses* are added. This means that, in the limit case of pure wave motion (X = 0), the Bijker method contains a factor sin(ωt) *squared*, which when averaged gives Y(0) = ½, and without wave-current interaction we only have sin(ωt) which when averaged gives Y(0) = $2/\pi$ = 0.64.

3.2.5 Wave-current interaction models: Grant and Madsen (1979)

The wave-current interaction model of Grant and Madsen is best described by first looking at their description of wave-only situations, and then adding a current. The Coastal Engineering Manual (USACE1995, chapter III-6) is a very useful source of information on this model, as it describes it in a more practical (and more readable) way than the publications of Grant and Madsen themselves (Grant and Madsen 1979, Grant

and Madsen 1984). The discussion below broadly follows the outline of the CEM.

Grant and Madsen close the Reynolds equations with the eddy viscosity concept, which they assume to vary linearly with the distance from the bed. As discussed in appendix A this leads to a logarithmic velocity profile in the boundary layer. For current only this is a commonly accepted, almost classic approach. For pure wave motion the bed shear stress varies with time, so strictly speaking the eddy viscosity should also be time-dependent. The problem is that this choice would make the analysis a lot more complicated and would lead to a result that cannot be expressed analytically (Grant and Madsen 1979). Grant and Madsen decided to neglect the time dependence of the eddy viscosity and use a time-invariant eddy viscosity based on the maximum bed shear stress under waves. This still gives reasonable results when compared to more complex, time-dependent eddy viscosity closure models (CEM 1995).

When a combination of waves and currents is involved, the basic idea does not change. The eddy viscosity is now based on the shear stress related to the maximum combined shear stress. This is, again, a simplification. As we have seen before, the turbulence in the current boundary layer and the turbulence in the wave boundary layer are dominated by different length scales, so defining a mixing length for the combined case is a little awkward. This is why Grant and Madsen expressed their eddy viscosity in a way that is slightly different from the classic mixing length-based expression used in Appendix A, and do not use the mixing length explicitly. It can be shown that for the current-only case the two expressions are analogous, and it is assumed that this analogy also holds for the combined case (Grant and Madsen 1979).

Grant and Madsen found friction factors for waves only as well as for the combined case, in a way that is, in principle, analogous to the way in which a friction factor for a steady current can be found from the velocity profile (as is explained in many textbooks on open channel flow); only the resulting equations tend to become a little more complex.

For waves only, the friction factor in the Grant and Madsen model is defined similarly to the definition of Jonsson:

$$\hat{\tau}_w = \frac{1}{2}\rho f_w \hat{u}_0^2 \tag{3.25}$$

where $\hat{u}_0$ can be evaluated with linear wave theory. In the case if irregular waves, the CEM recommends to use the root-mean-square wave height ($H_{rms} = H_s/\sqrt{2}$) and the significant wave period ($T_s \tilde{} \ 0.9T_p$), following a later publication by Madsen (1993, cf CEM 1995).

The full theoretical expression for f_w is fairly complicated, but it can be approximated by the following implicit function:

$$\frac{1}{4\sqrt{f_w}} + \log\left(\frac{1}{4\sqrt{f_w}}\right) = \log\left(\frac{a_0}{k_s}\right) - 0.17 + 0.24\left(4\sqrt{f_w}\right) \tag{3.26}$$

This approximation is roughly valid for $(a_0/k_s) < 100$. The exact solution for f_w can be read from the Figure 3.11. A comparison between this friction factor and others can be found in Box 2.1.

For given wave conditions ($\hat{u}_0$, ω and k_s) the problem is now solved and the bed shear stress can be found. In addition, it can be shown that the boundary layer thickness is:

$$\delta = \frac{\kappa u_{*m}}{\omega} \tag{3.27}$$

in which u_{*m} is the shear stress velocity associated with the maximum shear stress and ω

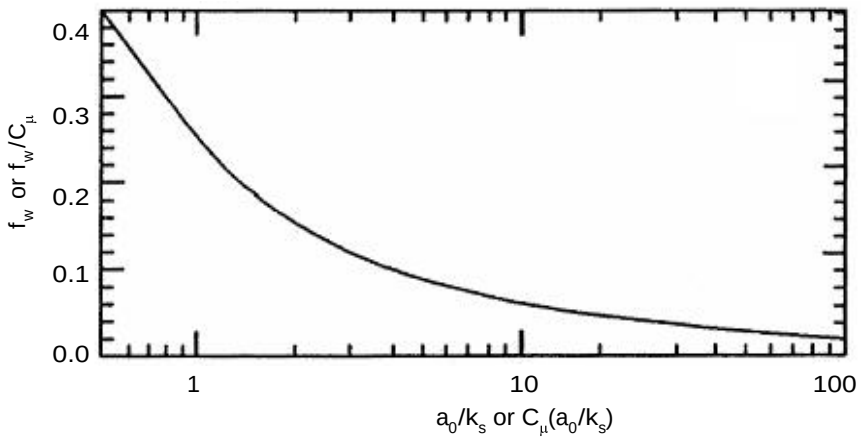

Figure 3.11 - Wave shear stress coefficient for the Grant and Madsen model (adapted from CEM 1995)

is the wave angular frequency ($\omega = 2\pi/T$).

For the combined case, the bed shear stress can be written as a vector addition of the current bed shear stress and the wave bed shear stress:

$$\hat{\tau}_{wc} = \sqrt{\tau_c^2 + \hat{\tau}_w^2 + 2\tau_c\hat{\tau}_w\cos\phi} \tag{3.28}$$

It must be emphasised that in order to account for the wave-current interaction the

enhanced current bed shear stress and the *enhanced* wave bed shear stress must be used here (as in Figure 3.6; as a matter of fact the Grant and Madsen model is the only WCI model that explicitly follows these steps). When we define two parameters μ and C_μ as

$$\mu = \frac{\tau_c}{\hat{\tau}_w} = \frac{u_{*c}^2}{u_{*wm}^2} \tag{3.29a}$$

and

$$C_\mu = \sqrt{1+\mu^2+2\mu\cos\phi} \tag{3.29b}$$

equation (3.28) can be written as

$$\hat{\tau}_{wc} = \hat{\tau}_w C_\mu \tag{3.30}$$

The enhanced wave shear stress can be found using a *combined* friction factor

$$\hat{\tau}_w = \tfrac{1}{2}\rho f_{wc}\hat{u}_0^2 \tag{3.31}$$

where f_{wc} is taken from

$$\frac{1}{4\sqrt{f_w/C_\mu}} + \log\left(\frac{1}{4\sqrt{f_w/C_\mu}}\right) = \log\left(C_\mu\frac{a_0}{k_s}\right) - 0.17 + 0.24\left(4\sqrt{f_w/C_\mu}\right) \tag{3.32}$$

This expression is equivalent to (3.26), so values can be found from Figure 3.11 when the x-axis is replaced by $C_\mu(a_0/k_s)$ and the y-axis by f_w/C_μ.

The (combined) boundary layer thickness is

$$\delta_{wc} = \frac{\kappa u_{*wc}}{\omega} \tag{3.33}$$

where u_{*m} is calculated using the combined shear stress (3.30)[1]

[1] The notation used here (subscripts 'w', 'c' and 'wc') deviates slightly from the original notation by Grant and Madsen; this is done to bring it in line with the notation used elsewhere in this thesis.

$$u_{*wc} = \sqrt{\frac{\hat{\tau}_{wc}}{\rho}} \tag{3.34}$$

The current shear stress can be calculated with the classic Chézy-based equation (2.14), but the CEM recommends to use the more general equation (2.21), where the bed shear stress is related to a (known) velocity $u_c(z_r)$ at a certain reference level z_r. The *enhanced* current bed shear stress can be calculated in the same way, keeping in mind that the effect of the wave boundary layer is felt by the current as an increased bed resistance; so the friction factor is no longer related to the physical bed roughness z_0 (=k_s/30) but to the so-called *apparent* bed roughness, which in turn is related to δ_{wc}.

Altogether, it can be shown that the enhanced current bed shear stress velocity is:

$$u_{*c} = u_{*wc} \frac{\ln \frac{z_r}{\delta_{wc}}}{\ln \frac{\delta_{wc}}{z_0}} \left[-\frac{1}{2} + \sqrt{\frac{1}{4} + \kappa \frac{u_c(z_r)}{u_{*wc}} \frac{\ln \frac{\delta_{wc}}{z_0}}{\left(\ln \frac{z_r}{\delta_{wc}} \right)^2}} \right] \tag{3.35}$$

A derivation of this formula can be found in CEM (1995).

So we see that these equations form a loop: the combination of the enhanced wave and current shear stresses determines μ and C_μ, which determines f_{wc} and thus the enhanced wave shear stress; secondly the enhanced wave shear stress determines δ_{wc} and this in turn determines the enhanced current shear stress. It is clear that iteration is required to solve this loop. This feedback loop, expressing the fact that the waves (by the apparent roughness caused by the wave boundary layer) influence the current is an important improvement of the Grant and Madsen method compared to the Bijker method; in this last method this influence is not accounted for.

The CEM suggests the following procedure to solve this loop:

- start with pure wave conditions, so $\mu = 0$ and $C_\mu = 1$;
- Solve for the wave shear stress (equations 3.31 and 3.32), the combined shear stress (3.30) and for the boundary layer thickness (3.33), and use these values, along with a given $u_c(z_r)$ and z_r to calculate the enhanced current shear stress according to (3.35);
- with the obtained values for the enhanced current and wave bed shear stresses, update μ and C_μ according to (3.29);

- Repeat steps 2-4 until the obtained values for C_μ converge. Then, calculate the combined bed shear stress from (3.30).

In this research we have implemented the Grant and Madsen model in a computer programme. We have chosen to use this approach rather than the Soulsby parameterisation (see appendix 2), because we are interested in the maximum shear stresses as well as the four distinct average shear stresses, which Soulsby does not give. Also, we prefer to work with the 'real' models rather than with the artificial, non-physical parameterisation.

We have used the procedure described above to obtain the maximum shear combined shear stresses. The average shear stresses were obtained by first calculating the enhanced current shear stress τ_c and maximum enhanced wave shear stress $\hat{\tau}_w$ and then assuming that

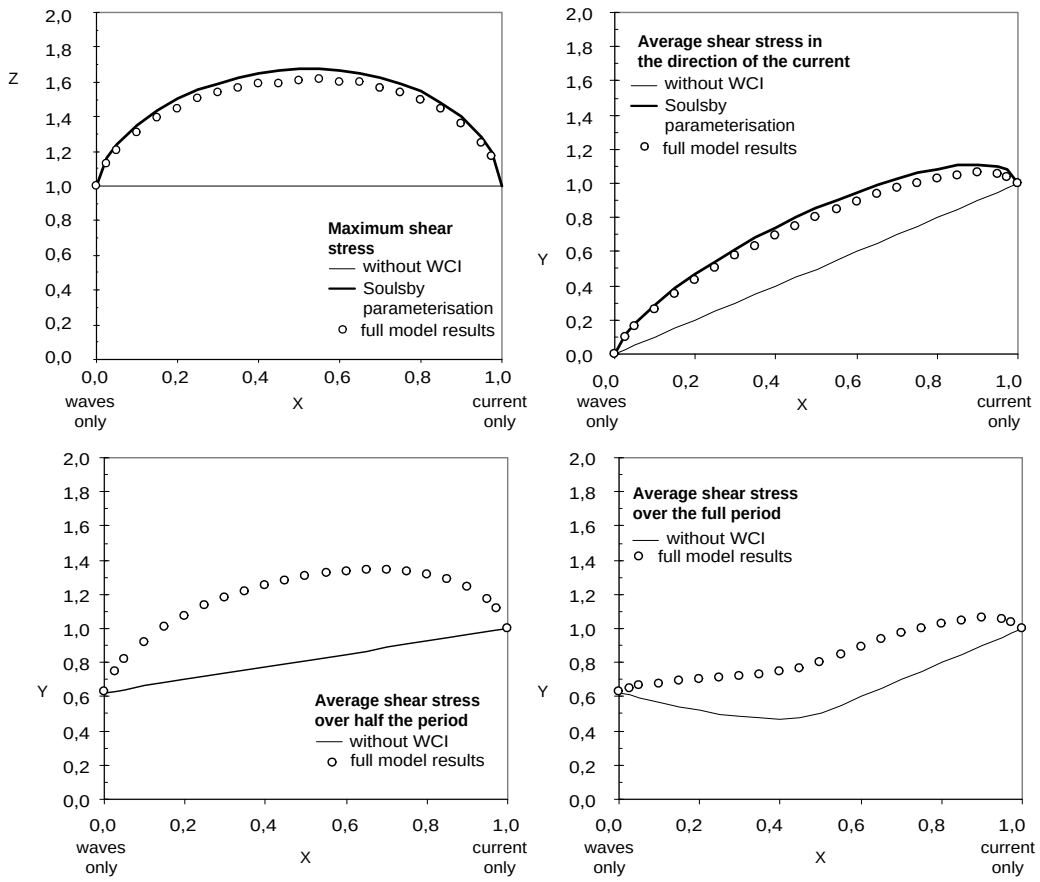

Figure 3.12 - Dimensionless results for the Grant and Madsen model, with $z_0/h = 10^{-4}$, $a_0/z_0 = 10^4$ and $\varphi = 0^o$

$$\tau_{wc}(\omega t) = \sqrt{\tau_c^{\,2} + \hat{\tau}_w^{\,2}\sin^2(\omega t) + 2\tau_c\hat{\tau}_w\sin(\omega t)\cos\phi} \tag{3.36}$$

and

$$\tau_{wcx} = \tau_c + \hat{\tau}_w\sin(\omega t)\cos\phi \tag{3.37}$$

after which the appropriate averaging procedures were followed. Our results are plotted in Figure 3.12, along with the Soulsby parameterisations for the maximum and the 'mean' shear stress. Again, we see that the 'mean' shear stress according to Soulsby corresponds to our 'average over the whole period in the direction of the current'. Also, we see that our values for the maximum shear stress deviate slightly from the Soulsby parameterisation.

Finally, the Grant and Madsen calculation method is summarised in Box 3.2.

3.2.6 Wave-current interaction models: Fredsøe (1984)

As we did for the Grant and Madsen model, we will start the discussion of the Fredsøe model by looking at a wave-only situation and then adding a current. There are two main sources of information on this method: a journal article (Fredsøe 1984) and a book (Fredsøe and Deigaard 1992). Of these two, the book is more readable and explains the theory on a step-by-step basis. The outline below is based on this book; only the most important results and the theoretical ideas behind it will be presented here. Full derivations of the formulae used in the model can be found in the book.

Similarly to Grant and Madsen, Fredsøe assumes that the eddy viscosity varies linearly with the distance from the bottom, but in contrast to Grant and Madsen he does not assume that it is constant in time. The result is a logarithmic profile in the boundary layer in which u_* varies with time:

$$u(t) = \frac{u_*(t)}{\kappa}\ln\left(\frac{z}{z_0}\right) \tag{3.38}$$

At the edge of the boundary layer, which Fredsøe assumes to be at a level $z = z_0 + \delta(t)$, the boundary condition is that this velocity is equal to the bed orbital velocity u_0. Note that u_0 is also a function of time, since $u_0 = \hat{u}_0\sin(\omega t)$, and so is the boundary layer thickness $\delta(t)$.

Fredsøe defines a (time dependent) dimensionless variable Z as

$$Z(t) \equiv \kappa \frac{u_0(t)}{u_*(t)} \tag{3.39}$$

With this definition the boundary condition can be written as:

$$u_0(t) = \frac{u_*(t)}{\kappa} \ln\left(\frac{z_0 + \delta(t)}{z_0}\right) \quad \Rightarrow \quad \delta(t) = z_0\left(e^{Z(t)} - 1\right) \tag{3.40}$$

Having defined these parameters, Fredsøe now proceeds in the following way. The fluid motion inside and outside the boundary layer is governed by the Navier-Stokes equations. In an extremely simplified way these equations read:

$$\rho \frac{\partial u}{\partial t} = -\frac{\partial p}{\partial x} + \frac{\partial \tau}{\partial z} \tag{3.41}$$

Or, in other words: the fluid inertia $\rho(du/dt)$ is balanced by a normal pressure gradient dp/dx and a shear stress gradient $d\tau/dz$. Outside the wave boundary layer $u = u_0$, and the fluid in frictionless so the shear stress term drops out:

$$\rho \frac{\partial u_0}{\partial t} = -\frac{\partial p}{\partial x} \tag{3.42}$$

Inside the wave boundary layer we cannot neglect the friction term, but we can assume that the normal pressure gradient is equal to the normal pressure gradient outside the boundary layer. This means that we can substitute (3.42) into (3.43) to get:

$$\frac{\partial \tau}{\partial z} = -\rho \frac{\partial}{\partial t}\left(u_0 - u\right) \tag{3.43}$$

'The' bed shear stress is now defined as the shear stress according to (3.43) integrated over the whole wave boundary thickness, so:

$$\tau_0 = \rho u_*^2 = -\rho \int_{z_0}^{z_0+\delta} \frac{\partial}{\partial t}\left(u_0 - u\right) dz \tag{3.44}$$

This integral is known as the *momentum integral*, and forms the basis of the Fredsøe method. This integral can be solved analytically; the result is a differential equation for $(u_0 - u)$. With the help of some clever algebra it is possible to write this result as a

differential equation in the previously defined variable Z, as a function of the wave phase (ωt):

$$\frac{dZ}{d(\omega t)} = f\left(Z, \omega t, \frac{a_0}{k_s}\right) \tag{3.45}$$

We will not give the full differential equation for $Z(\omega t)$ here; interested readers are referred to (Fredsøe 1984) or (Fredsøe and Deigaard 1992). It can be shown that for a flow problem (with given $\hat{u}_0$, ω and k_s (or $z_0 = k_s/30$)), the solution of $Z(\omega t)$ depends on (a_0/k_s) only.

The differential equation (3.45) can be solved (unfortunately this has to be done numerically) for any given flow problem to give Z as a function of the wave phase. Now that Z is known, we can also calculate $u_*(\omega t)$ and thus the wave shear stress $\tau(\omega t)$ from the definition of Z (equation 3.39) for any given moment within the wave cycle. This means that we can also find the maximum shear stress or any averaged shear stress at will. Finally, we can obtain a wave friction factor f_w by relating the maximum shear stress to the amplitude of the orbital wave motion like before (equation 3.25).

When we know Z, the boundary layer thickness follows from (3.40). This boundary layer thickness is still a function of time. Fredsøe defines 'the' boundary layer thickness as $\delta_m = \delta(\pi/2)$. In other words: the calculated boundary layer thickness δ_m is defined as the thickness halfway through the first half wave cycle. This is because for pure wave motion the problem is symmetrical: after the first half wave cycle the flow reverses and the boundary layer is destroyed; a new boundary layer starts to grow just like the first one. In other words: only the first half wave cycle has to be calculated.

In principle, for any given flow problem the differential equation (3.45) must be solved. However, Fredsøe has given approximations for the friction factor f_w and the boundary layer thickness δ_m, based on his own results. They are function of a_0/k_s only:

$$f_w = 0.04\left(\frac{a_0}{k_s}\right)^{-0.25} \tag{3.46}$$

$$\frac{\delta_m}{k_s} = 0.09\left(\frac{a_0}{k_s}\right)^{0.82} \tag{3.47}$$

In this approximation the wave shear stress is calculated using (3.25) with the friction

factor according to (3.46).

These approximations are valid for $(a_0/k_s) > 50$. Fredsøe states that for lower values the theory breaks down because the relative size of the grains gets so large that the flow around the individual grains must be modelled in detail; a 'bulk' method like this one is no longer applicable. Interestingly, for rock structures in shallow water values of a_0/k_s are typically in the order of 10 (see also Box 2.1); this indicates that this theory has only limited validity for the purposes of the present research. In fact, this is not just a limitation to this particular theory, but to *all* Shields-based stability parameters because, almost by definition, they are all based on 'bulk' modelling of shear stresses and not on the flow around individual grains.

Just like in the Grant and Madsen method, the basic idea behind the Fredsøe model does not change when a current is added to the situation: it only gets a little more complex. The treatment of this part of the theory in (Fredsøe and Deigaard 1992) is rather difficult; a simplified version is given below.

It is assumed that, just like in the pure wave case, the velocity profile in the combined boundary layer is logarithmic, and all relevant parameters are allowed to vary in time as in equation (3.38). The shear stress velocity in this case is the combined shear stress velocity u_{*wc} The boundary condition in this case is that at the edge of the boundary layer the total velocity $u_{tot}(t)$ is equal to the (vector) addition of the wave orbital velocity $u_0(t)$ and a – still unknown – current velocity u_δ.

$$u_{tot}(\omega t) = \sqrt{u_\delta^2 + \hat{u}_0^2 \sin^2(\omega t) + 2u_\delta \hat{u}_0 \sin(\omega t)\cos\phi} \tag{3.48}$$

Note that u_δ is not a function of time, as the currents is assumed to be steady. The parameter Z is now defined, analogously to the pure wave situation, as

$$Z(t) \equiv \kappa \frac{u_{tot}(t)}{u_{*wc}(t)} \tag{3.49}$$

With these choices the formula for the boundary layer thickness, equation 3.40, does not change.

Again, the equations of motion can be used to obtain a differential equation for $Z(\omega t)$, just like in the pure wave case. In the combined case, the function *f* in (3.45) is a function of both a_0/k_s and the relative current strength $u_\delta/\hat{u}_0$ (and the angle φ).

When the current velocity at the edge of the boundary layer u_δ is known the combined wave-current problem can be solved, in the same way as for a pure wave problem: find $Z(\omega t)$ by solving the differential equation and use (3.49) and (3.40) to find the combined shear stress $\tau_{wc}(\omega t) = \rho(u_{*wc}(\omega t))^2$ and the boundary layer thickness $\delta(\omega t)$. The only difference is that the problem is no longer symmetrical: during one half wave cycle the orbital velocity and the current work in the same direction, in the second half wave cycle they work in opposite directions. This means that the problem must be solved for the complete wave cycle; in this case 'the' boundary layer thickness is defined as the average of the values halfway through both half cycles, so $\delta_m = ½ (\delta(\pi/2)+\delta(3\pi/2))$.

The problem is, of course, that u_δ is *not* known beforehand, so we need to calculate the combined bed shear stress and boundary layer thickness with an assumed value of u_δ, after which we need to take a second step. The velocity profile for the current alone, outside the wave boundary layer, is given by:

$$u_c = \frac{u_{*c}}{\kappa} \ln\left(\frac{z}{z_A}\right) \tag{3.50}$$

in which u_{*c} is the shear stress velocity related to the (combined) bed shear stress *as felt by the current* and z_A is the *apparent* bed roughness (expressing the fact that the existence of the wave boundary layer is felt by the current as an increased roughness height).

The bed shear stress as felt by the current can be calculated from the previous results; it is the averaged bed shear stress *in the direction of the current* $\tau_{wc\ avx}$, so

$$u_{*c} = \sqrt{\frac{\tau_{wc\ avx}}{\rho}} \tag{3.51}$$

where $\tau_{wc\ avx}$ is calculated as the average over the whole wave period of

$$\begin{aligned} \tau_{wcx}(\omega t) &= \tau_{wc}(\omega t)\cos\Phi(\omega t) \\ \cos\Phi(\omega t) &= \frac{u_\delta + \hat{u}_0 \sin(\omega t)\cos\phi}{u_{tot}(\omega t)} \end{aligned} \tag{3.52}$$

in which $\Phi(\omega t)$ is the angle between the instantaneous direction of the combined shear stress and the current direction. This angle can be found from the geometry of the situation (see appendix 3).

The apparent bed roughness z_A can now be found by matching the profile (3.50) with the assumed value of u_δ at the edge of the boundary layer:

$$u_\delta = \frac{u_{*c}}{\kappa}\ln\left(\frac{z_0+\delta_m}{z_A}\right) \quad \Rightarrow \quad z_A = \left(z_0+\delta_m\right)e^{-\frac{\kappa u_\delta}{u_{*c}}} \tag{3.53}$$

In equation (3.53) z_A is now the only unknown variable and can be calculated. Now that z_A and u_{*c} are known the current velocity profile outside the boundary layer is solved; we can for instance calculate the depth-averaged current velocity:

$$\overline{\overline{u}} = \frac{u_{*c}}{\kappa}\left(\ln\left(\frac{h}{z_A}\right)-1\right) \tag{3.54}$$

Usually, a flow problem is characterised by a given depth-averaged flow velocity. In that case, the value resulting from (3.54) can be compared to a given value. When they are not the same, the *whole* procedure, ie assume a new u_δ, solve for $Z(\omega t)$, find τ_{wc} and $\tau_{wc\ avx}$, find the velocity profile outside the boundary layer and find $\overline{\overline{u}}$ must be repeated (iterated) until the right value of $\overline{\overline{u}}$ has been obtained.

So, we see that working with the Fredsøe model is quite laborious: for every flow problem we need to iterate to find the right solution, and *within* that iteration we need to (numerically) solve a – rather complicated – differential equation. In addition, we must always calculate the average bed shear stress in the direction of the flow $\tau_{wc\ avx}$, even when we are not interested in this parameter for our design (but, for instance, in the maximum shear stress). This means that this method is not very useful in practical design.

Like for the Bijker and Grant and Madsen methods we have implemented the Fredsøe method in a computer programme, which we prefer to using the Soulsby parameterisation as explained before. Our results are plotted in figure 3.13. Again we see a very reasonable comparison between our results and Soulsby's. Our results tend to be a little unstable/inaccurate for very low X values (wave dominated situations).

It is noted that this computer programme is based in the full Fredsøe method (Fredsøe and Deigaard 1992), and not on the simplified version given above. Unfortunately there appear to be a few typing errors in the formulae as they are given in Fredsøe and Deigaard (1992), which we have corrected. The structure of the computer programme used in this research, and the way it deviates from the description given by Fredsøe and Deigaard, is explained in appendix 3.

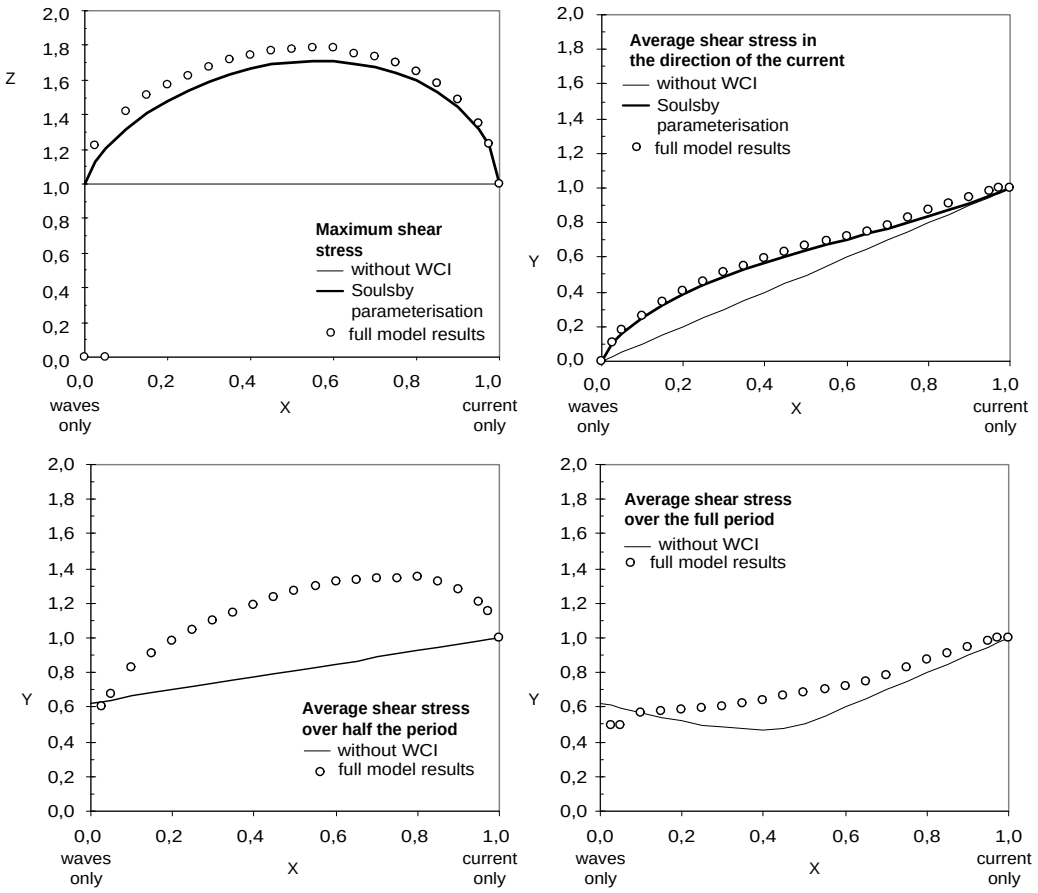

Figure 3.13 - Dimensionless results for the Fredsøe model, with $z_0/h = 10^{-4}$, $a_0/z_0 = 10^4$ and $\varphi = 0^o$

In our programme, the differential equation that features in the method is solved with the simplest possible numerical scheme: Euler explicit. It is understood that some accuracy could be gained with a more advanced numerical scheme, but given the already quite reasonable results that were obtained with Euler explicit (see figure 3.13) this has not been implemented.

3.2.7 Wave-current interaction models: advanced turbulence closures

Both Davies, Soulsby and King (1988) and Huynh-Thanh and Temperville (1991) have presented a wave-current interaction model based on more advanced turbulence closures (but still based on the eddy viscosity concept). Davies, Soulsby and King have used the one-equation model (k-model); Huynh-Thanh and Temperville have gone one step further; they have used the k-ε closure model (for detail on these turbulence closure models see appendix A). Both these wave-current interaction models are purely

numerical; there is no physical background to explain so the treatment of these models in this thesis will be brief. We have not used these models in their full form in a computer programme, as we did for the previous three models, because of their numerical character. We will have to rely on the Soulsby parameterisation to get predictions of the combined shear stress.

When we look at Figure 3.7 it appears that the maximum and mean shear stresses predicted by these two models are very similar to the predictions given by the Fredsøe model, so little is gained when these more sophisticated models are used. Calculations of our own, based on Soulsby parameterisation for various input parameters z_0/h, a_0/z_0 and φ, have confirmed this (see also the graphs in chapter 4). Fredsøe and Deigaard (1992) draw a similar conclusion when they compare the wave friction factors obtained from their own model with those obtained from more complex models (without explicitly mentioning which models; they talk in general terms of 'one equation models' and 'two equation models').

3.2.8 Wave-current interaction models: conclusions

When a combination of waves and a current is considered, the resulting combined shear stress can not be calculated as a simple (vector) addition of the shear stress caused by the waves and the current separately. The waves and the current influence each other in a non-linear way, which results in an enhancement of the resulting shear stresses. For this wave-current interaction various models have been proposed in literature; five of these have been found to be of interest to this research. We have shown how these models can be ranked in increasing order of complexity in terms of the turbulence closure schemes they apply: Bijker (1967) – Grant and Madsen (1979) – Fredsøe (1984) – Davies, Soulsby and King (1988)– Huynh-Thanh and Temperville (1991).

The first three models have a physical background, and we have used this to implement them in a computer programme that calculates the resulting combined shear stress for a given flow problem. The results from this programme closely match similar results obtained by Soulsby (1997).

This programme will be used to analyse the datasets in a later stage of this research

The last two models are purely numerical and have no physical basis (other than the physics behind the assumed turbulence closure scheme). They have not been implemented in a computer programme. However, results obtained from a parameterisation of these models given by Soulsby (1997) indicate that they models predict results that are very close to those predicted by the Fredsøe model. We conclude

that, because these models are more complex and require a lot of computer capacity, but their results are indistinguishable from simpler models, they are of little practical use. For this reason only the models of Bijker, Grant and Madsen, and Fredsøe will be used in the remainder of this thesis.

The Bijker model, Grant and Madsen model and simplified Fredsøe model are summarised in the boxes on the next pages for convenience. A summary of the full Fredsøe model is not easily given. The way in which the Fredsøe model is used in this research is described in appendix 3.

Box 3.1 Summary of the Bijker model

Input:	$\bar{\bar{u}}$	depth averaged current velocity [m/s]
	h	water depth [m]
	$\hat{u}_0$	amplitude of the horizontal orbital velocity near the bed [m/s]
	ω	wave angular frequency ($\omega=2\pi/T$) [rad/s]
	a_0	maximum excursion of the wave orbital motion ($a_0 = \hat{u}_0/\omega$)
	k_s	bottom roughness [m] or $z_0 = k_s/30$ [m]
	φ	angle between directions of current and wave propagation [deg or rad]
	ρ	fluid density [kg/m^3]

Current friction: $C = 18\log\left(\frac{12h}{k_s}\right)$ or $C_D = \left(\frac{0.40}{1+\ln(z_0/h)}\right)^2$

Current shear stress: $\tau_c = \rho\frac{g}{C^2}\bar{\bar{u}}^2$ or $\tau_c = \rho C_D \bar{\bar{u}}^2$

Wave friction: $f_w = \exp\left(-6.0 + 5.2\left(a_0/k_s\right)^{-0.19}\right)$ for $a_0/k_s > 1.57$

$f_w = 0.3$ for $a_0/k_s = 1.57$

Wave shear stress: $\hat{\tau}_w = \frac{1}{2}\rho\ f_w \hat{u}_0^{\ 2}$

Combined shear stress: $\tau_{wc}(\omega t) = \tau_c + \hat{\tau}_w \sin^2(\omega t) + 2\sqrt{\tau_c \hat{\tau}_w}\sin(\omega t)\cos(\phi)$

Box 3.2 Summary of the Grant and Madsen model

Input:

$u_c(z_r)$	flow velocity at reference height [m/s]
z_r	reference height [m]
$\hat{u}_0$	amplitude of the horizontal orbital velocity near the bed [m/s]
ω	wave angular frequency ($\omega=2\pi/T$) [rad/s]
a_0	maximum excursion of the wave orbital motion ($a_0 = \hat{u}_0/\omega$)
k_s	bottom roughness [m]
φ	angle between directions of current and wave propagation [deg or rad]
ρ	fluid density [kg/m^3]

Start iteration assuming pure wave conditions: $\mu = 0$ and $C_\mu = 1$

Iteration

Wave friction factor:

$$\frac{1}{4\sqrt{f_w/C_\mu}} + \log\left(\frac{1}{4\sqrt{f_w/C_\mu}}\right) = \log\left(C_\mu \frac{a_0}{k_s}\right) - 0.17 + 0.24\left(4\sqrt{f_w/C_\mu}\right)$$

(solve by iteration or read from Figure 3.5)

Enhanced wave shear stress (velocity): $\hat{\tau}_w = \frac{1}{2}\rho f_{wc}\hat{u}_0^2 \qquad u_{*w} = \sqrt{\frac{\hat{\tau}_w}{\rho}}$

Maximum combined shear stress (velocity): $\hat{\tau}_{wc} = \hat{\tau}_w C_\mu \qquad u_{*wc} = \sqrt{\frac{\hat{\tau}_{wc}}{\rho}}$

Boundary layer thickness: $\delta_{wc} = \frac{\kappa u_{*wc}}{\omega}$

Enhanced current shear stress (velocity):

$$u_{*c} = u_{*wc}\frac{\ln\frac{z_r}{\delta_{wc}}}{\ln\frac{\delta_{wc}}{z_0}}\left[-\frac{1}{2} + \sqrt{\frac{1}{4} + \kappa\frac{u_c(z_r)}{u_{*wc}}\frac{\ln\frac{\delta_{wc}}{z_0}}{\left(\ln\frac{z_r}{\delta_{wc}}\right)^2}}\right] \qquad \hat{\tau}_c = \rho u_{*c}^2$$

Update relative current strength factors: $\mu = \frac{\tau_c}{\hat{\tau}_w} = \frac{u_{*c}^2}{u_{*wm}^2}$

$$C_\mu = \sqrt{1 + \mu^2 + 2\mu\cos\phi}$$

Instantaneous combined shear stress: $\tau_{wc}(\omega t) = \sqrt{\tau_c^{\,2} + \hat{\tau}_w^{\,2}\sin^2(\omega t) + 2\tau_c\hat{\tau}_w\sin(\omega t)\cos\phi}$

Box 3.3 Summary of the (simplified) Fredsøe model

Input:

	$\bar{\bar{u}}$	depth-averaged flow velocity [m/s]
	h	water depth [m]
	$\hat{u}_0$	amplitude of the horizontal orbital velocity near the bed [m/s]
	ω	wave angular frequency ($\omega=2\pi/T$) [rad/s]
	a_0	maximum excursion of the wave orbital motion ($a_0 = \hat{u}_0/\omega$)
	k_s	bottom roughness [m]
	φ	angle between directions of current and wave propagation [deg or rad]
	ρ	fluid density [kg/m^3]

Start iteration assuming a current velocity at the edge of the combined boundary layer u_δ

Iteration

Calculate instantaneous values for $\omega t \in [0,2\pi]$ of:

Combined velocity: $$u_{tot}(\omega t) = \sqrt{u_\delta^2 + \hat{u}_0^2 \sin^2(\omega t) + 2u_\delta \hat{u}_0 \sin(\omega t)\cos\phi}$$

Boundary layer parameter: (see appendix 3 for full expression) solve $$\frac{dZ}{d(\omega t)} = f\left(\frac{a_0}{k_s}, \frac{u_\delta}{\hat{u}_0}, \phi\right)$$

Combined shear stress velocity: $$u_{*wc}(\omega t) = \kappa \frac{u_{tot}(\omega t)}{Z(\omega t)}$$

Boundary layer thickness: $$\delta(\omega t) = z_0\left(e^{Z(\omega t)} - 1\right)$$

Angle between combined shear stress and current direction: $$\cos\Phi(\omega t) = \frac{u_\delta + \hat{u}_0 \sin(\omega t)\cos\phi}{u_{tot}(\omega t)}$$

Enhanced current shear stress: $$\tau_{wcx}(\omega t) = \rho u_{*wc}^2(\omega t)\cos\Phi(\omega t)$$

Then calculate average properties:

Enhanced current shear stress: $$\tau_{wc\ avx} = \frac{1}{2\pi}\int_0^{2\pi} \tau_{avx}(\omega t)\, d(\omega t)$$

$$u_{*c} = \sqrt{\frac{\tau_{wc\ avx}}{\rho}}$$

Combined boundary layer thickness: $$\delta_m = \frac{1}{2}\left(\delta\left(\frac{\pi}{2}\right) + \delta\left(\frac{3\pi}{2}\right)\right)$$

Apparent roughness: $$z_A = (z_0 + \delta_m)e^{-\frac{\kappa u_\delta}{u_{*c}}}$$

Depth-averaged flow velocity: $$\bar{\bar{u}} = \frac{u_{*c}}{\kappa}\left(\ln\left(\frac{h}{z_A}\right) - 1\right)$$

iterate (choose new u_δ) until the calculated depth-averaged flow velocity matches the given value

3.3 Morison-type stability parameters

3.3.1 Introduction

In the previous paragraphs we have introduced stability parameters that use the bed shear stress to represent the load on the bed material. Physically speaking this is not a (completely) correct approach: shear stresses do not set a particle into motion, *forces* do. In addition, the theory behind shear-stressed based stability is only valid when the flow is steady and uniform, in other words: when there are no accelerations in the flow.

In this paragraph we will study a stability parameter that is directly based on an analysis of the (stabilising and destabilising) forces on an individual bed particle, and that does take the acceleration of the flow into account. Because of these features this approach is commonly referred to as the Morison approach, after the theory for wave forces on piles (Morison *et al* 1950). Recently this approach has attained some attention in hydraulic engineering research, in an attempt to overcome some of the limitations of the shear-stress based approach and find a design formula that is also valid in accelerated flow. Three MSc students devoted their theses to this subject: Dessens (2004) who investigated the stability of stones in accelerated flow through a contraction, and Tromp (2004) and Terrile (2004) who studied the stability of stones under shoaling waves. The following paragraph is mainly based on their work.

Both Tromp and Terrile found that the threshold of motion of stones under pure wave attack could be described with a Morison-type stability equation in which both velocities and accelerations were included; their experiments show that for situations with the same velocities, but different accelerations, the behaviour of the stones is distinctively different. Unfortunately neither Tromp nor Terrile compares this approach to a more classic approach based on shear stresses, so we cannot conclude whether the Morison approach works *better* than a shear stress based approach, or not.

Dessens drew a similar conclusion for accelerated flow through a contraction. Dessens *did* also use a shear-stress based approach, and plotted Ψ (using the local velocity and disregarding the accelerations) against transport (defined as a percentage of stones moved from a cross section). The result is given in Figure 3.14. It appears that Ψ_{cr} = 0.025 - 0.030 is a reasonable measure to describe the threshold of motion, which is considerably lower than the Shields value for uniform flow (Ψ_{cr} = 0.055). This result appears to contradict Schiereck (2001) who states that the stability in an accelerated flow is no less than the stability in uniform flow.

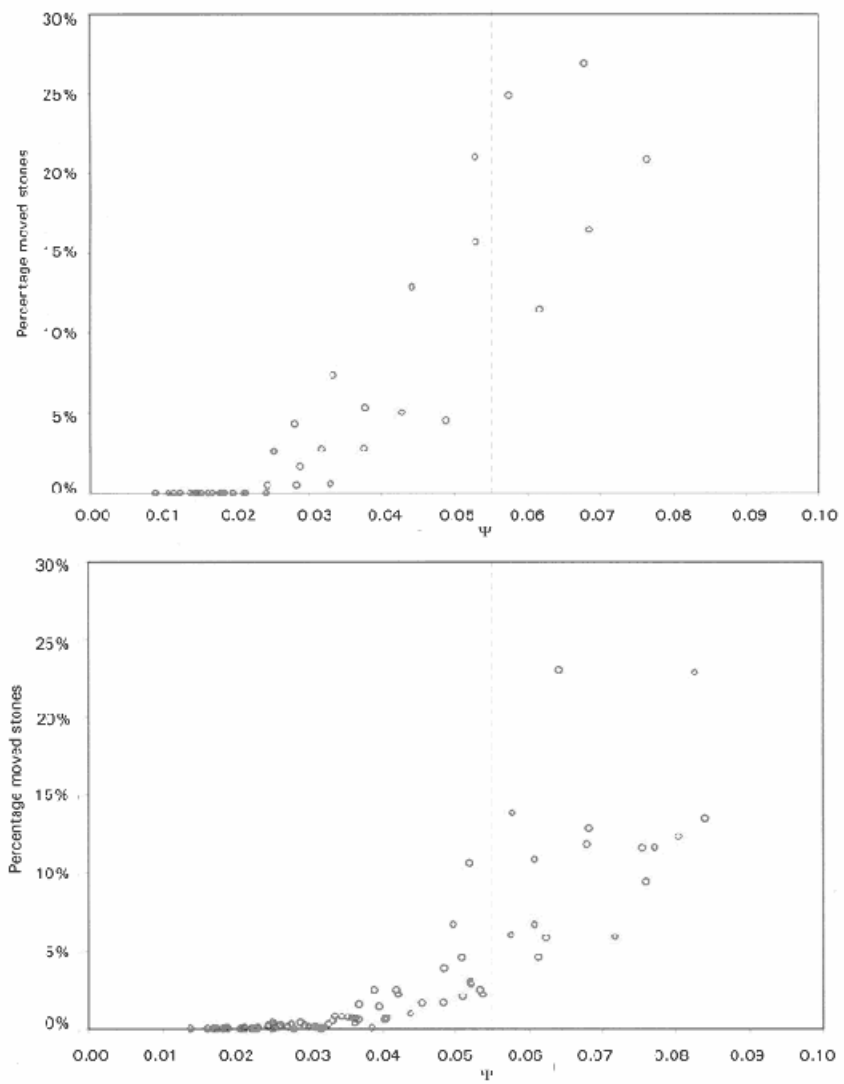

Figure 3.14 – Pick-up rate against Ψ for accelerating flow (from Dessens 2004).
Top: small stones. Bottom: large stones

3.3.2 Forces on a single stone

Figure 3.15 illustrates the forces that act on a bed material particle that is subjected to a passing flow. We can distinguish four different forces:

Gravity: G. The first force on the stone is its own (underwater) weight G:

$$G = (\rho_s - \rho) g V \tag{3.55}$$

in which V is the volume of the stone.

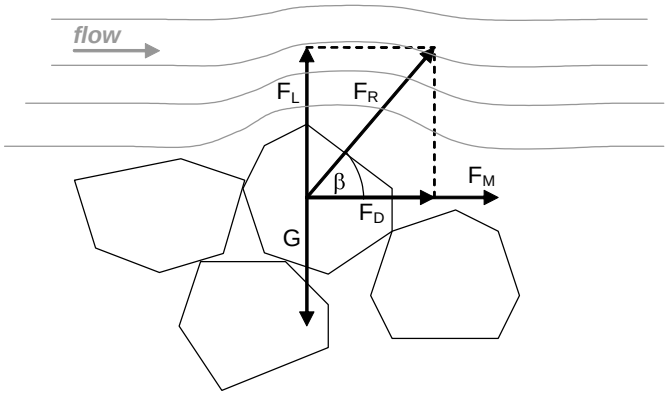

Figure 3.15 – Forces on a bed particle

Drag force: F_D. Any body that is subjected to a flow will experience a drag force in the direction of the flow. In general this force can be calculated as:

$$F_D = \frac{1}{2}\rho C_D u^2 A_1 \tag{3.56}$$

in which C_D is an (empirical) drag coefficient that depends on the shape of the object, u is the local flow velocity and A_1 is the cross sectional area of the object in the direction of the flow. It is immediately clear that using (3.56) for stones in a near-bed structure is not straightforward, since the shape of the stones will be irregular (which gives difficulties in determining C_D), the 'local' velocity is not clearly defined (because the flow velocity will not be uniform over the water depth but follow some kind of velocity profile) and the cross sectional area A_1 is not easily determined (stones will be partly embedded in the structure, partly shielded by other particles and partly protruding into the flow).

Lift force: F_L. When the flow passes the stone the presence of the stone will deflect the streamlines, as illustrated in Figure 3.15. This streamline contraction results in locally higher velocities on top of the stone and consequently a reduction in pressure (Bernoulli-effect). The net result is a lift force perpendicular to the direction of the flow, calculated as:

$$F_L = \frac{1}{2}\rho C_L u^2 A_2 \tag{3.57}$$

In this case C_L is the lift coefficient and A_2 is the cross sectional area of the stone perpendicular to the stone. Calculating the lift force on a stone in the bed protection is

just as difficult as calculating the drag force, for the same reasons. Because of the similarity in (3.57) and (3.58) it is common practice to combine F_L and F_D into one resultant force F_R:

$$F_R = \frac{1}{2}\rho C_B u^2 A \tag{3.58}$$

in which the bulk coefficient C_B combines the effect of the lift and drag forces, and it has been (implicitly) assumed that $A_1 = A_2$. In figure 3.15 we can see that $F_R = \sqrt{(F_L^2 + F_D^2)}$, so we have $C_B = \sqrt{(C_L^2 + C_D^2)}$. The resultant force acts at an angle β to the horizontal. The magnitude of β depends on the relative contributions of the drag and lift forces.

Inertia force: F_M. When the flow accelerates there will be a pressure gradient over the stone (again: Bernoulli-effect) that causes an extra force in the direction of the flow. Theoretically this force is equal to:

$$F_M = \iiint \frac{dp}{dx} dxdydz = V\frac{dp}{dx} \tag{3.59}$$

In (3.59) it is assumed that dp/dx is constant (over a stone diameter), which seems a fair approximation as long as the size of the stone is small compared to the spatial length scale of the pressure fluctuation.

From the simplified equations of motion (1-D Euler equation) we know:

$$\frac{dp}{dx} = -\rho\frac{Du}{Dt} = -\rho\left(\frac{\partial u}{\partial t} + u\frac{\partial u}{\partial x}\right) \tag{3.60}$$

Note that we have to use the *material derivative* Du/Dt here, in other words: the acceleration that causes the inertia force can be due to a *temporal* acceleration $\partial u/\partial t$ (non-steady flow, for instance waves – this is what Tromp measured) or a *spatial* acceleration $u(\partial u/\partial x)$ (non-uniform flow, for instance flow over a contraction – this is what Dessens measured).

In practice stones will not behave exactly according to equation (3.59), because the stones are partly embedded and partly protruding so not the full volume V will be active; secondly it is not just the stones that will be accelerated but also a certain volume of water 'hanging onto' the stone, the so-called *added mass*. These two effects require the introduction of an empirical *added mass coefficient* C_M. Using this coefficient, and substituting (3.60) into (3.59) gives for the inertia force:

$$F_M = C_M \rho V \frac{Du}{Dt} \tag{3.61}$$

Final remark: In this analysis the shear force (caused by the skin friction on the stones) is not included – it is not mentioned in any of the sources that we used for this overview (Dessens 2004, Tromp 2004, Terrile 2004). We assume that the shear force has been implicitly included in the drag force F_D (since it is also proportional to u^2 and also works in the horizontal direction).

3.3.3 Stability

The stability of an individual stone can now be assessed with the help of Figure 3.16, in which we have grouped F_D and F_L into F_R for convenience.

The stone will move about the support point S. It is assumed that the stone will start to move at a certain angle to the horizontal, called the *escape angle* φ. The magnitude of φ is determined by the position of the stone in question and the stone immediately next to it; the more exposed the stone is, the smaller φ will be. In general φ is found to be in the range 30^o – 45^o (Kirchner 1990, cf Dessens 2004, Tromp 2004).

The stability of the stone can be found from a force balance in the direction of motion (Dessens 2004, Tromp 2004):

$$F_R \cos(\beta - \varphi) + F_M \cos\varphi = G \sin\varphi \tag{3.62}$$

so we can define a stability parameter Θ:

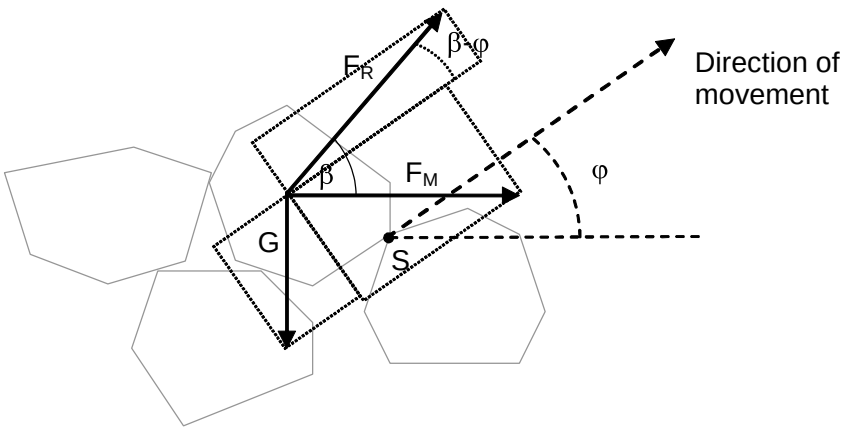

Figure 3.16 – Stability of a bed particle (after Dessens 2004)

$$\Theta \equiv \frac{F}{G} = \frac{F_R \dfrac{\cos(\beta - \varphi)}{\sin \varphi} + F_M \dfrac{\cos \varphi}{\sin \varphi}}{G} \tag{3.63}$$

Substituting (3.55), (3.58) and (3.61), and letting $A = (d_{n50})^2$ and $V = (d_{n50})^3$ gives:

$$\Theta = \frac{\frac{1}{2} C_B \dfrac{\cos(\beta - \varphi)}{\sin \varphi} u^2 + C_M \dfrac{\cos \varphi}{\sin \varphi} \dfrac{Du}{Dt} d_{n50}}{\Delta g d_{n50}} \tag{3.64}$$

Usually the effects of β and φ are implicitly included in the coefficients C_B and C_M (Dessens 2004, Tromp 2004) to give:

$$\Theta = \frac{\frac{1}{2} C_B u^2 + C_M \dfrac{Du}{Dt} d_{n50}}{\Delta g d_{n50}} \tag{3.65}$$

which is also the form that we will use in this thesis. It must be borne in mind that including the effects of β and φ in C_M and C_B again emphasises that these parameters are a function of the position of the stone in the bed. In other words: C_M and C_B are related to the *bed* and not to an individual *stone*. This means that they cannot be found by laboratory measurements on a single stone (as for instance the drag coefficient on a cylinder can be experimentally determined).

3.3.4 Magnitude of coefficients C_B and C_M

The applicability of the Morison approach depends to a large extent on the accuracy with which we can determine the coefficients C_B and C_M. Dessens (2004) notes in his thesis that there is not a lot of literature to be found on this subject. The only coefficients that have been investigated extensively by others are the drag and lift coefficients C_D and C_L. Tromp (2004) gives the following ranges: $C_L = 0.15 – 0.22$ and $C_D = 0.25 – 0.35$. Since $C_B = \sqrt{(C_L^2 + C_D^2)}$ we would expect a range for $C_B = 0.30 – 0.40$.

For C_M there is even less information. The only source that both Dessens and Tromp refer to is Dean and Dalrymple (1991) who give a theoretical added mass coefficient for a cylinder with an ellipsoidal cross section:

$$C_M = 1 + k_M \tag{3.66}$$

in which $k_M = b/a$ is (the inverse of) the length over width ratio of the ellipsoid. See also figure 3.17.

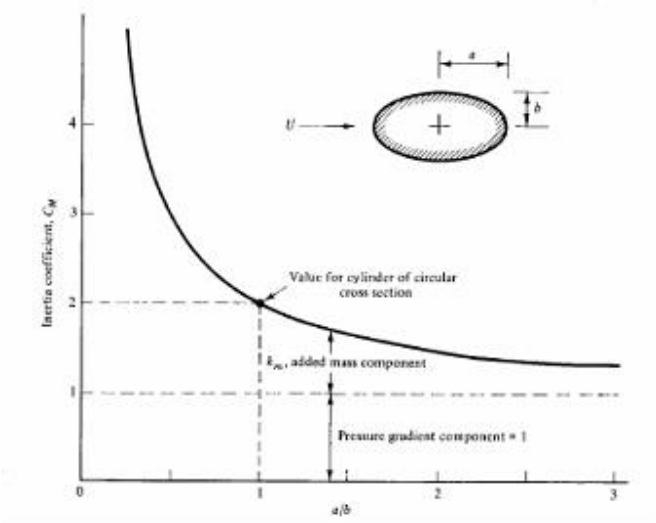

Figure 3.17 – Theoretical inertia coefficient C_M for cylinders of ellipsoidal cross section (from Dean and Dalrymple 1991)

Figure 3.17 shows that the value of C_M is quite sensitive to the orientation of the stone. A normal L/B ratio for stones in a bed protection is roughly L/B = 2 – 3. If the stone has a 'flat' orientation we have k_M = 1/2 - 1/3 (see definition of a and b in figure 3.17) and C_M = 1.33 - 1.50; when the stone is standing upright we get k_M = 2 – 3 and C_M = 3 – 4. So, a different orientation easily leads to a change in C_M by a factor 3.

There are a few reasons why the 'real' value of C_M may deviate from this theoretical value. Firstly, the real value will include an angle factor depending on the escape angle φ. Secondly, equation (3.67) is assumes flow on both sides of the object. This is not the case for a partly embedded stone in a bed protection. For this reason Tromp (2004) proposes to use only half the value of k_M. In that case we would expect k_M to be roughly 0.16 – 1.50, depending on the orientation of the stone. It is not clear why exactly we should take half the value, but in any case it is evident that k_M may be reduced a little. Finally, (3.67) is a theoretical expression that assumes potential (inviscid) flow around the object; in other words that the development of boundary layers and a wake behind the object will not occur. In reality these viscous effects can not be neglected which leads to different k_M-values. For circular pile sections in a real fluid Dean and Agaard (1970, cf Dean and Dalrymple 1991) measured k_M = 0.33 (instead of k_M = 1 as would follow for potential flow). So we see that k_M can be reduced even further.

All things considered, the best estimate for C_M we can expect for theoretical reasons is somewhere in the range 1.2 – 3. Given the reasons for reduction of k_M discussed above, and the empirical knowledge that stones in a bed protection are more likely to have a flat

orientation we expect the lower end of this range to be more probable.

Both Dessens and Tromp measured C_M and C_B in their experiments. Tromp placed stones on a gently sloping bed (1:30) in a laboratory flume and let (regular) waves run up the slope. The idea behind this set-up is that the sloping bed allows measurements at various water depths, and thus various combinations of velocities and accelerations, to be made in the same experiment without having to adapt the generated wave height and wave period. The disadvantage is of course that the stability of the stones is influenced by the slope; this effect is not mentioned explicitly in Tromp (2004). However, given the gentle slope (1:30 $\Rightarrow \alpha = 2^o$) this effect will be limited.

Tromp used video observations to study the threshold of motion of the stones at two different locations and simultaneously measured the 'near-bed' velocities (in fact velocities at some 4 cm above the bed) with an Electromagnetic Flow Sensor (EMS). The accelerations were obtained by differentiation of the velocity signal. In this way the exact values of the velocity and accelerations at the moment the stone starts to move can be determined and the force balance (3.63) can be made up. In principle this leaves two equations (the force balances at the two measurement locations) and four unknowns (β,φ, C_B and C_M). It is assumed that $\beta \approx \varphi$ (which seems reasonable) so $\cos(\beta - \varphi) \approx 1$. This eliminates the influence of β. Solving these equations gives the sought values for C_B and C_M, depending on an estimate of the escape angle φ. For $\varphi = 30^o$, Tromp found $C_B = 0.4$ and $C_M = 2.7$; for $\varphi = 45^o$ the values were $C_B = 0.55$ and $C_M = 3.75$. So we see that the exact values of C_B and C_M cannot be accurately measured but require an estimate of the escape angle. In any case, we observe that for both escape angles the ratio $C_M/C_B = 6.8$.

Dessens (2004) performed similar experiments; he used the classic 'coloured strips' experimental set-up and defined the threshold of motion as a certain percentage of stones moving from a strip. Applying a similar technique as Tromp (ie directly solving the force balance at two locations) Dessens found $C_B = 0.10$ and $C_M = 3.92$ for $\varphi = 30^o$ ($C_M/C_B = 39.2$) and $C_B = 0.4$ and $C_M = 5.55$ for $\varphi = 45^o$ ($C_M/C_B = 13.8$). We see that both the absolute values of the parameters and the ratio C_M/C_B differ greatly from the results by Tromp. It is not clear how this difference in parameter values comes about; this may be a subject for further research. At the moment, all we can say is that the values reported by Tromp are more within the expected ranges.

3.3.5 Concluding remarks

It is interesting to note that because Tromp used a sloping bed his waves were asymmetrical (shoaling). Because of this asymmetry the wave velocity and the wave

acceleration are not 90^o out of phase as they would be if we apply linear wave theory; instead there is a moment in the wave cycle (just before the passage of the wave crest) in which the velocity and the acceleration are both large. It is at this point that the stones start to move (Tromp 2004). A similar analysis, with similar results, was later performed by Terrile (2004). Terrile proposes a way to include this asymmetry in the Morison parameter, unfortunately this method requires knowledge of the variation of the acceleration in time (during the wave cycle). We do not have this information in the data sets that we will use in this present thesis, so we can not use this method. Theoretically we could obtain this temporal information by using a higher-order wave theory, but Terrile has not given any validation of his asymmetry parameter against such theoretical results (his proposal is solely based on his own velocity and acceleration measurements). Therefore we will consider this method outside the scope of our present research, and we will only use linear wave theory in our analysis (and thus necessarily neglect the effects of wave asymmetry). Interested readers are referred to Terrile (2004) or Terrile *et al* (2006) for more information on this topic.

Finally, we remark that in the previous discussions it has been (implicitly) assumed that C_B and C_M are constants. There is no reason to believe that this is necessarily the case. In fact, in the design of vertical piles under wave action (the field of origin of the Morison approach) the values of these coefficients are functions of the fluid motion and the size of the object, expressed in parameters like the relative orbital excursion a_0/d or the Keulegan-Carpenter number ($KC = \hat{u}_0 T/d$). This is also suggested by Terrile *et al* (2006).

3.4 Turbulence-based stability parameters

3.4.1 Introduction

Turbulence is an important phenomenon in the design of hydraulic structures. Intuitively it will be clear that in a more turbulent flow the water motion is more ‘violent’ and the damage to a structure will be larger. In the present design practice this phenomenon is not neglected; increased turbulence levels can be accounted for by the use of a K_V factor (see chapter 2 and appendix 1). For many types of structure the increased turbulence levels (in terms of the turbulence intensity *r*) can be calculated, for instance with the formula of Hoffmans for flow after a weir or backward-facing step (see Schiereck 2001).

This approach has one major disadvantage: the K_V factor acts as a multiplier to the current velocity *u*, so when u = 0 the resulting stability parameter will also be zero, indicating that there can be no damage. Physically, this is not true. The classic example in this case is the reattachment point in the complex flow pattern after a weir or a

backward-facing step, where we know from experience that severe damage to the bed protection occurs even though theoretically the mean flow velocity is zero.

This insight has led researchers to believe that it could be a sensible approach to find a stability parameter that explicitly incorporates the turbulence characteristics of a flow. This paragraph will briefly introduce the most recent advances that have been made in this field. Most of the theoretical concepts in turbulence theory, that the reader may not be familiar with, are explained in appendix 1.

3.4.2 Turbulence forces

Hofland (2005) describes two different sources of turbulent forces: quasi-steady forces (QSF) and turbulence wall pressures (TWP). These will be discussed next.

Quasi-steady forces: In a turbulent flow the instantaneous flow velocity can be described as a fluctuation around a mean value: u = u + u'. Since the dominant forces (drag force and lift force) are related to the flow velocity these, too, will have a mean and a fluctuating part. This means that the forces on a stone are not constant, even when the mean velocity u is constant; instead the magnitude of the forces will have a certain probability distribution. It is assumed that rare events with high forces are responsible for the damage to a structure. (This is also the main idea behind the present use of K_V-factors).

These fluctuations are not *random* (even though they are often described as such); instead, they are related to certain *coherent structures* in the flow (ie vortices). When we look at the definition of turbulent shear stresses:

$$\tau = -\rho u'v' \tag{3.67}$$

we see that we must have both a fluctuation in the horizontal velocity (u') and a fluctuation in the vertical velocity (v') occurring at the same instant (strictly speaking turbulence is essentially a three-dimensional phenomenon; however we will only discuss two dimensions here). In addition u' and v' must have an opposite sign in order for τ to be positive. In other words: we must either have a fluid package with a higher velocity than the surrounding fluid moving down, or a package with a lower velocity moving up. The first phenomenon is called a *sweep*, the second phenomenon an *ejection*. Hofland (2005) states that sweeps are more important for the stability of stones in a bed protection than ejections are. This provides us with a good mental picture of what causes quasi-steady forces: an instability in the flow makes fluid from higher up in the water column, where the velocities are higher, come 'crashing down' onto the bed. This also

means that the origin of the quasi-steady forces are to be found in the entire water column, outside the immediate influence of the bed itself.

Turbulence wall pressures: when a turbulent velocity fluctuation occurs, anywhere in the fluid, it causes a fluctuation in pressure (Bernoulli effect). These pressure fluctuations are propagated through the water column and eventually reach the bed, causing a fluctuating force on the stones. This phenomenon is not related to the bed at all, even for a completely smooth wall TWP can occur. The pressure forces work on the entire volume of the stone and are thus related to the inertia forces that were discussed in the previous paragraphs. In other words, TWP relate to fluctuating *accelerations* (a') whereas QSF relate to fluctuating velocities (u').

Hofland (2005) studied these phenomena and found that both QSF and TWP were responsible for the motion of stones in a bed protection: the former have the capacity to actually transport a stone over some distance, the latter have a much shorter duration and only seem to make a stone rock. However, this rocking motion caused by TWP makes a stone more vulnerable to flow attack (by QSF) because its exposed area (A) is increased and its escape angle (φ) reduced. Hofland suggests that stones are entrained in the (exceptional) case that the two forces occur simultaneously – the turbulence wall pressures give a stone an initial push, after which the quasi-steady forces carry it away: "rock and roll".

3.4.3 Stability parameters

With these two new phenomena we can write a theoretical, all-encompassing stability parameter that includes all of the previously described theory (Hofland, 2005)

$$\Psi = \frac{C_B\left(u+u'\right)^2 + C_M\, d\,(a+a')}{\Delta g d} \tag{3.68}$$

This parameter must be seen as a theoretical end-goal of the currently ongoing research in this field. Before we can use this expression in practice a lot of questions need to be answered, most notably:

- how must we define u, u', a and a' and how must we calculate these parameters for a given flow problem? Can we use analytical expressions or do we need to refer to numerical modelling techniques?
- What should the value of the coefficients CB and CM be? (in this aspect it is interesting to note the absence of the factor ½ in front of CB in equation 3.68)

At the moment the research in this field is still ongoing; it has not advanced far enough to answer these questions completely. It will take a few more years before a stability parameter like (3.68) can be used for design.

Despite all that, a few researchers have proposed parameters that include turbulence characteristics. In these parameters the acceleration part of (3.68) is omitted (and implicitly included in the velocity part). In other words: these parameters only model quasi-steady forces, not turbulent wall pressures.

All parameters are based on numerical models of the flow. In these models the turbulence parameters (like l_m, k, ε and so on, see appendix 1) can be calculated anywhere in the flow. The two formulas that we will introduce here are both based on the output of a k-ε model; they differ only in the way in which they incorporate the output of such a model in a stability parameter. This immediately reveals a clear disadvantage of these methods: they require a numerical fluid model to be run for each designed structure. Building and running such a model is no easy task and requires some skill and experience (and of course specialist computer software). This may be another reason why it is expected that it will take a while before these methods will be fully accepted for design purposes.

The first stability parameter was proposed by Jongeling *et al* (2003):

$$\Psi = \frac{\left\langle (\overline{u} + \alpha\sqrt{k})^2 \right\rangle_{h_m}}{\Delta g d} \tag{3.69}$$

in which k is the turbulent kinetic energy calculated from the k-ε model and the brackets denote that $(u + \alpha\sqrt{k})^2$ must be averaged over an influence height h_m. In this case k is a function of the height above the bed and follows immediately from the output of the k-ε model. Appendix 1 shows that $\sqrt{k} \sim \frac{1}{2}\sigma_u$, so the term $(u + \alpha\sqrt{k})$ effectively means "add $\frac{1}{2}\cdot\alpha$ times the standard deviation to u".

Jongeling *et al* propose to use $\alpha = 6$ and $h_m = 5d + 0.2h$ (in which *d* is the stone diameter and *h* is the water depth). Both these proposals follow from a curve fitting procedure and do not seem to have any physical meaning. The use of $\alpha = 6$ is not surprising, this means that the forces responsible for the motion of the stones are roughly three standard deviations larger than the mean value. This is the same assumption as in the presently used theory behind the use of K_V factors.

Hofland (2004, 2005) proposes another stability parameter:

$$\Psi_{lm} = \frac{\max_{z<h}\left[\left\langle \overline{u} + \alpha\sqrt{k}\right\rangle_{l_m} \frac{l_m}{z}\right]^2}{\Delta g d} \tag{3.70}$$

This parameter also has the term (u + $\alpha\sqrt{k}$), again with α = 6. The main difference with Jongeling's parameter is the use of the mixing length l_m (remember that l_m is a measure of the size of a turbulent eddy – see appendix 1). Here l_m is understood to be a function of the level above the bed: $l_m = l_m(z)$. So, the 'recipe' expressed in the numerator of (3.70) is: at any height *z*, take the local increased velocity (u + $\alpha\sqrt{k}$) and average that over the local mixing length (from z - ½·l_m to z + ½·l_m). This gives an average velocity over the whole eddy that occurs at the level *z*, in other words the Hofland formula explicitly accounts for the fact that the entrainment of the stones in the bed protection is related to coherent structures and not to individual velocity fluctuations. The result is then weighed with a factor l_m/z, so larger eddies are given more influence than smaller ones, and eddies that are further away from the bed are given less influence than eddies that are close to the bed. After this has been done for all *z* (so for the entire water column) it is assumed that the *maximum* of the thus obtained velocities (squared) is responsible for the entrainment of the stones and this value is used in the stability parameter.

The factor *k* in (3.70) is a function of *z*, and follows immediately from the k-ε model as before. The only remaining problem in (3.70) is the determination of the mixing length l_m. The most obvious way to do this is to let l_m follow from the output of the k-ε model as well:

$$l_m(z) \sim \frac{k(z)^{3/2}}{\varepsilon(z)} \tag{3.71}$$

If we would use this relationship we would have a measure of the mixing length that corresponds to the actual flow pattern around the structure that we have modelled. Unfortunately, Hofland reports that a mixing length calculated in this way does not fit his data well; instead he proposes to use the standard Bakhmetev distribution:

$$l_m(z) = \kappa z\sqrt{1 - \frac{z}{h}} \tag{3.72}$$

However, we must realise that the Bakhmetev mixing length distribution is related to fully developed turbulent flows with a logarithmic velocity profile; this is not necessarily the case in the flow around the structure that we are trying to model – in fact, it is an

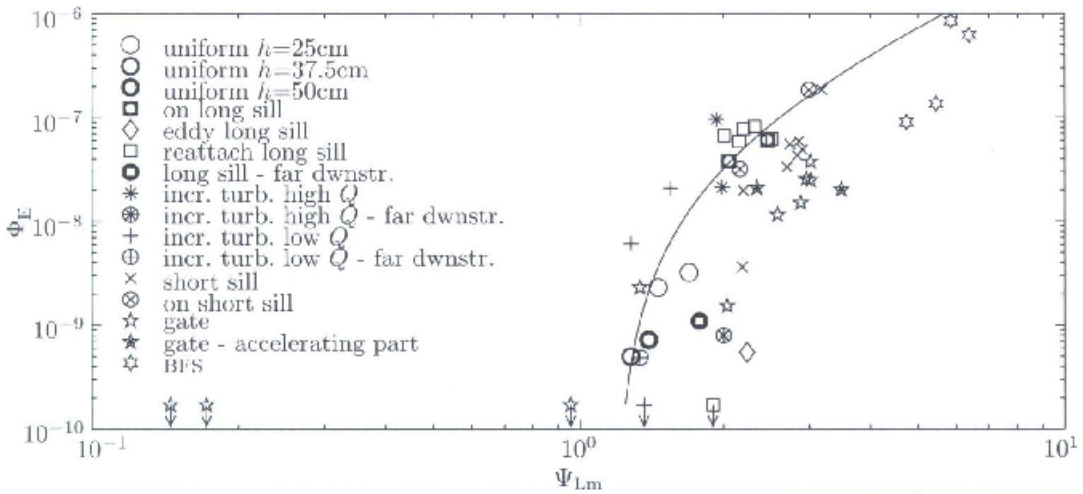

Figure 3.18 – Dimensionless entrainment against Ψ_{lm} (from Hofland, 2005)

assumption that we want to drop, which is why we set out to do complicated turbulence modelling in the first place. This is a possible weak point in this model. Hofland (2005) even goes as far as to state that this is a shortcoming of the k-ε model as such: apparently k is predicted reasonably well, but ε (and consequently l_m) is not.

Hofland (2004, 2005) presents a relation between his stability parameter and the entrainment rate of stones from a bed protection Φ_E (see paragraph 3.5.5) as the (conservative) result of a curve fitting procedure on experimental data for a wide range of non-uniform flow situations like long sills, short sills, gates and backward-facing steps:

$$\Phi_E = 5 \cdot 10^{-8} \left(\Psi_{lm} - \Psi_{lm,cr} \right)^2 \tag{3.73}$$

in which the critical value of Ψ_{lm} is equal to $\Psi_{lm,cr}$ = 1.2. A plot of equation (3.73) along with the data on which it is based, are given in figure 3.18. As can be seen, the scatter is still large.

3.5 Damage parameters

3.5.1 Transport

One way to look at damage to near-bed structures is to acknowledge the broad similarity between movement of stones and sand transport as studied by the adjacent field of morphology, and to see to which extent morphological sand transport formulas can be used to predict stone movement. Transport is then defined as a certain volume of material moving through a cross section per unit width and unit time, denoted q_s (units m^3/m^2s or m^2/s). In dimensionless form transport is expressed as a parameter Φ_q defined

as

$$\Phi_q = \frac{q_s}{\sqrt{g\Delta d_{n50}^3}} \tag{3.74}$$

This dimensionless transport can be linked to the (also dimensionless) bed shear stress Ψ by a variety of transport formulas. It is important to realise that in morphology a distinction is made between bed-load transport (rolling and/or sliding movement of bed material along the bottom) and suspended transport (movement of particles higher up in the water column); these two phenomena are usually described by different formulae. Of course, only bed-load transport is of interest to us here, and we should only seek to apply morphological bed-load formulas.

When applying these formulas, it must be borne in mind that they were originally derived, and tested, for applications in river morphology. This means the translation to our purposes leads to four problems:

- the diameters of stones in a granular near-bed structure is well outside the range of validity of these formulas
- stones in near-bed structures are more angular than river sand grains, so these formulas may under-predict their stability and thus over-predict transport rates. This is probably not a very large effect given Shields's original conclusion that the grain shape did not influence stability much (Shields 1936).
- most formulas were derived for currents only; there are only a few that incorporate the effects of waves.
- all formulas assume, explicitly or implicitly, that there is a threshold of motion and are all based on data with Ψ-values above this threshold. As we have seen before, when we are designing near-bed structures we want to reject the assumption of a threshold of motion, and we are interested in transport rates at low Ψ-values. This problem, though perhaps the least obvious of the four, could be the main reason why morphological transport formulas are not directly applicable to our purposes.

3.5.2 Transport by currents: Paintal

Important research in this field was conducted by A.S. Paintal in the late 1960s (Paintal 1969). Paintal was one of the first to recognise the importance of rejecting the assumed existence of a threshold of motion, or in his own words:

> *"There does not appear to be any limit below which there is no movement. At very, very low shear values one has to wait for a longer time to see the movement, as the probability of movement becomes very small. But this probability of movement is never zero except in still water"* (quotation from Paintal 1969).

He set out to analyse and measure transport rates at low hydraulic loads (ie low Ψ-values). As an added advantage, he conducted his experiments on relatively coarse-grained and angular material, thus solving the first, second and last of the problems mentioned above; only the influence of waves remained un-investigated.

Paintal recognized that the movement of stones at low Ψ-values is essentially stochastic in nature; stones move in discrete 'steps', rolling and sliding a short distance along the bottom before being re-deposited again. The distribution of these steps is random in time and space, and there is no general ongoing movement. In the first part of his PhD thesis Paintal sets up a theoretical, probabilistic model describing this type of movement, from which he was able to show that the dimensionless transport rate Φ is a function of Ψ only. For more details about Paintal's model and the assumptions behind it, see appendix 4.

After completing this model, Paintal conducted laboratory experiments to find empirical values for the remaining unknowns is his model. The result is the following transport formula:

$$\Phi_q = 6.56 \cdot 10^{18} \cdot \Psi^{16} \quad \text{for } \Psi < 0.05 \tag{3.75a}$$

$$\Phi_q = 13 \cdot \Psi^{2.5} \quad \text{for } \Psi > 0.05 \tag{3.75b}$$

The first formula is based on Paintal's own research, the second formula is based on data sets from other researchers (Paintal 1969).

This formula was later corrected by WL|Delft Hydraulics for temperature effects and the apparently false assumption of a hydraulically rough bottom by Paintal in one of his test series. The corrected formula yields:

$$\Phi_q = 1.64 \cdot 10^{10} \cdot \Psi^{11} \quad \text{for } \Psi < 0.085 \tag{3.76a}$$

$$\Phi_q = 13 \cdot \Psi^{2.5} \quad \text{for } \Psi > 0.085 \tag{3.76b}$$

So the second formula remains unaltered, only the transition point (Ψ = 0.085) has moved to ensure a correct transition between the two formulas.

Perhaps confusingly, the Paintal formula was corrected a *second time* by Mosselman and Akkermans (1998, cf Hofland 2005), also -mainly- for the effects of the bed not being hydraulically rough. This second correction yields the following formula:

$$\Phi_q = 3 \cdot 10^7 \cdot \Psi^{8.9} \qquad \text{for } \Psi < 0.05 \tag{3.77}$$

In this thesis we will accept this last version of the Paintal formula as the 'correct' one.

Promising as they may seem, these formulas have not yet been very commonly applied in engineering practice. Looking at the exponent of Ψ in these formulas (and especially the original Paintal formula) may explain why: the transport rate varies with the 16th power of the shear stress, and since $\tau \sim u^2$, it varies with the 32nd power of the velocity. Apart from the strange, perhaps unfamiliar and 'suspicious' magnitude of this exponent (more classic morphological formulas, for higher Ψ-values, predict transport rates varying with the 5th power or so to the velocity) this also means that a small inaccuracy in the estimate of the velocity results in large deviations of the predicted transport. Paintal himself seems to be aware of this consequence of his formula when he writes that

> *"the 16th power correlation […] stipulates that a small increase in shear stress causes a noticeable change in bed load transport"* (quotation from Paintal, 1969)

Because Paintal's formula is potentially still very useful in engineering, these matters have been investigated further. De Boer (1998) also conducted transport measurements for low hydraulic loads and found much lower values than Paintal did. His formula is (De Boer 1998):

$$\Phi_q = 7800 \cdot \Psi^{7.5} \qquad \text{for } \Psi < 0.1 \tag{3.78}$$

The differences between Paintal and De Boer have, at least partly, been explained by Forschelen (1999), who found that they could to a large extent be attributed to a different definition of bottom roughness by the two researchers (again indicating how important this parameter can be, see also Chapter 2), and to an underestimation of friction effects caused by the side walls of the flume in De Boer's experiments. Forschelen also did some transport measurements of his own, which seem to be more in line with Paintal's original findings. Unfortunately Forschelen's data set is too small to fit a transport formula to.

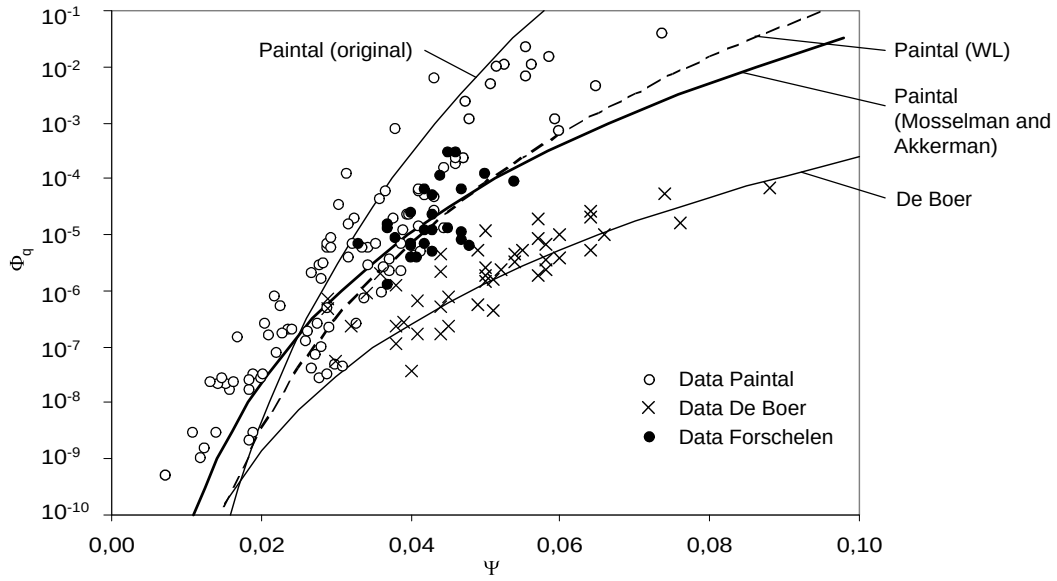

Figure 3.19 - Transport formulas and the data on which they are based

All transport formulas discussed above, and the datasets they are based on, are given in Figure 3.19. Datasets were obtained from Paintal (1969) and Forschelen (1999).

Paintal, de Boer and Forschelen conducted their respective researches for currents only. The combined effect of a combination of a current and waves was studied by Bijman (2000). He did transport measurements in a laboratory flume and concluded that, for his experiments, the transport rate could best be expressed as a Paintal-type formula in which Ψ is calculated using the mean combined wave-current shear stress according to Grant and Madsen (see paragraph 3.2):

$$\Phi_q = 1.54 \cdot \Psi_{GM}^{\ 4.49} \tag{3.79}$$

Bijman also studied other wave-current interaction models and found that the Bijker model did not fit his data very well, whereas there was hardly any difference between the models of Fredsøe and Grant and Madsen. Bijman based his analysis on Soulsby parameterisation only, he did not use the complete models as described in paragraph 3.2.

3.5.3 Transport by waves

Bijman's extension to Paintal's work appears to be the only source of information on transport by waves and currents for low Ψ-values. In coastal morphology literature we

can find some formulations for transport by waves, or waves and currents combined, but they all assume – either implicitly or explicitly – the existence of a threshold of motion and are only tested for Ψ-values above this threshold. For completeness we will briefly introduce the best-known (and most commonly applied) of these transport formulas below.

When waves are symmetrical they will cause no net transport in the wave propagation direction; they will only move the bed material back and forth. The amount of material that is moved during half a wave cycle $q_{w1/2}$ can be estimated, for instance with the formula given by Madsen and Grant (1976, cf Soulsby 1997):

$$\frac{q_{w1/2}}{w_s d_{n50}} = 12.5\Psi^3$$
$$\Psi = \frac{\hat{\tau}_w}{\rho g \Delta d_{n50}} \qquad (3.80)$$

in which w_s is the particle fall velocity and $\hat{\tau}_w$ is the maximum wave-related bed shear stress (eg calculated with Jonsson's equation (2.23). When waves are not symmetrical this formula can be used to estimate the net transport as the difference between $q_{1/2}$ under the wave crest and $q_{1/2}$ under the wave trough.

Van Rijn (1993) gives the following validity ranges for this formula: 300 μm $\leq d_{n50} \leq$ 2800 μm and 1 s $\leq T \leq$ 6 s (without further specifying how T is defined – as T_m or T_s or otherwise). This means that its applicability for design of granular near-bed structures is limited, both in terms of grain size as in terms of load parameter (common design waves have periods that are far larger than six seconds).

Another formula that can be used for this purpose is Hallermeier (1982, cf Levit 1996)

$$\frac{q_{w1/2}}{\omega d_{n50}^2} = (0.1\theta)^{1.5}$$
$$\theta = \frac{\hat{u}_0^2}{g \Delta d_{n50}} \qquad (3.81)$$

in which ω is the wave angular frequency and $\hat{u}_0$ is the maximum orbital velocity at the bed. The ranges of validity are given by Van Rijn (1993) as 150 μm $\leq d_{n50} \leq$ 4200 μm and 1 s $\leq T \leq$ 9 s. These ranges are a little closer to what we need for design purposes, but still not close enough; especially in terms of grain size. In addition, Van Rijn warns that this formula tends to over-predict transport rates for θ < 30 – which is unfortunate for

our purposes, since we are mainly interested in low-mobility transport.

Hallermeier uses a stability parameter that is not based on the shear stress τ but directly on the near-bed velocity $\hat{u}_0$. We will see this type of stability parameter again when we discuss erosion profiles for near-bed structures in paragraph 3.6. In order to avoid confusion we will denote this type of stability parameter with the Greek symbol theta (θ) in this thesis; we will reserve the symbol Ψ exclusively for shear-stress based stability parameters. Since we know that $\tau_w = \frac{1}{2} f_w \hat{u}_0^2$ we see that the only difference between this parameter and a (wave) shear stress based parameter is the absence of the wave friction factor f_w. This friction factor is only dependent on $k_s/a_0 = 2d_{n50}/(\hat{u}_0/\omega))$ and so the only 'missing' parameter in this formulation is the angular frequency ω. In this light it is not surprising that ω appears separately in Hallermeijer's formula.

Despite the fact that these two equations use two different dimensionless transport parameters and two different dimensionless stability parameters, we do see that they are both of the form (transport) = a·(stability)^b, which is similar to Paintal's formulation.

The 'Madsen and Grant'-type transport parameter uses the particle fall velocity and therefore looks different from the way we previously defined dimensionless transport (see equation 3.75). However, when we realise that for coarse particles the fall velocity can be written as (Van Rijn (1984), cf Soulsby 1997)

$$\begin{aligned} w_s &= \frac{1.1\nu D_*^{1.5}}{d_{n50}} \\ D_* &= \left(\frac{g\Delta}{\nu^2}\right)^{1/3} d_{n50} \end{aligned} \tag{3.82}$$

we can write the transport parameter as

$$\frac{q_{w1/2}}{w_s d_{n50}} = \frac{q_{w1/2}}{1.1\nu D_*^{1.5}} = \frac{q_{w1/2}}{1.1\nu\left(\frac{g\Delta}{\nu^2}\right)^{1/2} d_{n50}^{1.5}} = \frac{q_{w1/2}}{1.1\sqrt{g\Delta d_{n50}^3}} \tag{3.83}$$

so the difference comes down to a factor 1.1 which is of no practical interest (and will implicitly be present in the fit parameter *a* in $\Phi = a\Psi^b$, anyway)

3.5.4 Transport by currents and waves

Perhaps the best-know bed-load transport formula for a combination of waves and currents is Bijker (1971, cf Van Rijn 1993):

$$q_s = bu_* d_{n50} \exp\left(-0.27\frac{1}{\mu\Psi}\right) \tag{3.84a}$$

in which $\mu = (C/C_{90})^{1.5}$ is the ripple factor, C is the Chézy coefficient, $C_{90} = 18\log(12h/d_{90})$ is a 'Chézy coefficient' based on d_{90}, and Ψ and u_* are defined in the 'standard' way as $\Psi = \tau_{wc}/(\rho g \Delta d_{n50})$ and $u_* = \sqrt{(\tau_c/\rho)}$. The value of the fit parameter depends on the circumstances, commonly used values are *b* = 5 for breaking waves and *b* = 1 for non-breaking waves. We can write equation (3.85a) in dimensionless form by dividing by $(g\Delta d^3)^{1/2}$:

$$\Phi_q = b\sqrt{\Psi_c}\exp\left(-0.27\frac{1}{\mu\Psi_{wc}}\right) \tag{3.84b}$$

which brings the formula in line with other formulations (eg the Paintal formula).

Van Rijn (1993) notes that Bijker based this formula on earlier work by Kalinske (1947), who developed a theoretical expression for the bed load based on a probabilistic analysis of the flow characteristics, and Frijlink (1952) who fitted Kalinske's formula to experimental data. The factor $(b\sqrt{\Psi})$ is commonly called the "transport part", while the exponential part on the right hand side of the equation is called the "stirring up part". Note that the first part of the equation is based on the current shear stress alone, while the second part is based on the combined shear stress. This leads to the often-quoted dictum "the waves stir up the sediment while the current transport it".

3.5.5 Entrainment

In more recent reports like the MSc theses of Tromp (2004), Dessens (2004) and Terrile (2004), and the PhD thesis of Hofland (2005), damage is not expressed in terms of transport at all, but in terms of the *entrainment* E. This parameter is defined as the volume of displaced stones per unit of bed area and time and has the units m^3/m^2s or m/s; alternatively it can be defined as the *number* of displaced stones per unit of bed area and time: this is called *number entrainment* E_n and has the units $1/m^2s$.

Compared to transport, entrainment can be seen as a more direct measure of damage: in simple terms it measures the 'hole that is left behind' after the stones have moved. Exactly how far the stones move and where they end up is not of interest. It can be argued that, for this reason, entrainment is a more useful damage indicator than transport for design purposes.

Both entrainment and number entrainment can be made dimensionless, in the following

ways:

$$\Phi_E = \frac{E}{\sqrt{g\Delta d_{n50}}} \tag{3.85}$$

and

$$\Phi_{En} = E_n d_{n50}^2 \sqrt{\frac{d_{n50}}{\Delta g}} \tag{3.86}$$

In classic transport measurements (such as the ones conducted by De Boer, Forschelen and Bijman) transport is defined as the product of *pickup* and a *displacement length*. Entrainment is related to the first of these two, and can be calculated from these experiments even when the original results were presented in terms of transport. A way to do this, based on an assumed displacement length distribution, is given by Hofland (2004, 2005). Hofland derived this method for currents only, the validity of this method for experiments with waves and currents (ie Bijman) has not been shown; it can be expected that the displacement length distribution under waves deviates strongly from the assumed displacement length distribution under currents.

3.5.6 Erosion area

A third way to express damage takes its inspiration from the design of breakwaters and revetments, where the damage is expressed in terms of the dimensionless erosion area S (eg in the Van der Meer formulas, cf Schiereck 2001).

The erosion area A_e is measured from experiments and is defined as the area of 'missing' material in a cross section after the load has been applied. The parameter S is then defined as:

$$S = \frac{A_e}{d_{n50}^2} \tag{3.87}$$

Time is no longer present in this parameter. When a measure of time is also needed in the damage indicator, the most common way is to divide by the square root of the number of waves *N* instead of some absolute measure of time. This already indicates that this parameter strongly related to wave-dominated situations. It is not clear beforehand how this parameter can be used in the combined case of waves and a current.

The advantage of using this stability parameter is that it links the design of near-bed structures to the related field of breakwaters and revetments.

3.6 Design methods

3.6.1 Critical scour method (De Groot *et al* 1988)

Many authors have brought forward theoretical concepts and ideas related to the design of granular near-bed structures; only a few have proposed practical design methods based on these concepts. One interesting exception is a publication by De Groot *et al* (1988), who propose a design method based on transport.

De Groot *et al* reason that the most important parameter in the design of near-bed structures is a *layer thickness* (eg the thickness of the armour layer of a bed protection, or the effective cover thickness on top of an offshore pipeline), and so damage can best be expressed as the reduction (over time) of this layer thickness. The core of their design method is that this reduction can be related to a *gradient* in the transport capacity along a structure. This gradient can be estimated by realising that the transport (of stones!) is zero in front of the structure and rises to some maximum value which can be calculated by a suitable transport formula, eg Paintal. The length over which the transport rises from zero to the maximum value, called the *scour length* L_s, must be estimated. De Groot *et al* give a few examples of scour length estimates in common situations, depending on the type of structure; see figure 3.20.

The scour velocity (SV), describing the rate at which the layer thickness decreases, can now be defined as:

$$SV = \frac{dq_s}{dx} \approx \frac{q_{s,\max}}{L_s} \tag{3.88}$$

Note: even though De Groot *et al* do not mention this in their publication, this formula is a direct analogy of the basic morphological balance equation ?z/?t + ?S/?x = 0.

The total scour SC now follows as the scour velocity multiplied by the period of interest (often the lifetime of the structure); or, assuming that the load and thus the scour velocity is time-dependent, as the integral

$$SC = \int_{lifetime} SV dt \tag{3.89}$$

When we assume that the damage occurs gradually during a storm with duration D equation (3.89) reduces to SC = SV·D.

The structure must be designed in such a way that this total scour is less than a certain critical value; this is why De Groot *et al* refer to their method as the critical scour method. This critical scour can for instance be taken equal to the thickness of the armour layer.

De Groot *et al* report to have used this method in a probabilistic calculation, in other words they have evaluated that probability that the total scour is less than a critical scour depth *D*. (In common probabilistic design terms this means evaluating the limit state function Z = D – SC). In this way they have evaluated the stability of a rubble mound sill in a tidal area (*in casu* the Eastern Scheldt Storm Surge Barrier), using a time-dependent load based on a probability distribution of tidal differences and the Paintal formula to calculate transport.

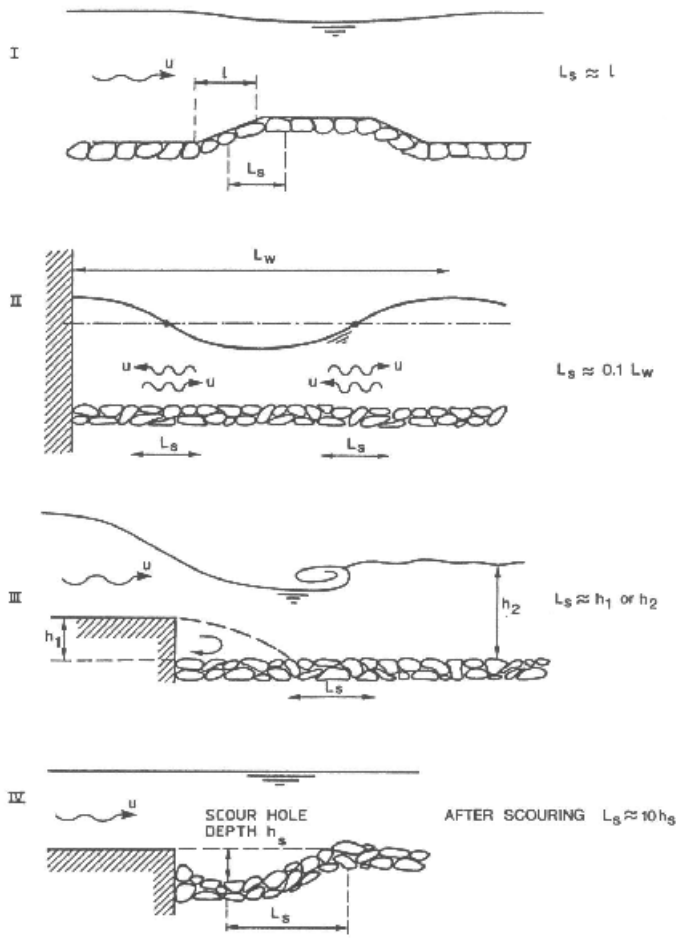

Figure 3.20 - Scour length L_s in various circumstances (taken from De Groot *et al* 1988)

Their calculation is done with a Monte Carlo analysis (level III), in which all relevant parameters were varied, also the fit parameters in the Paintal formula. Their results are somewhat surprising: the uncertainty in the final result was mainly dominated by the uncertainty in the current velocities and by the uncertainty in the bottom roughness. The fit parameters of the Paintal formula were varied with a factor 100 in this analysis, in line with the large uncertainty surrounding these values as discussed in the previous paragraph; still, the final result did not depend much on a variation of these parameters. This is a promising result, which means that this design method can be applied even though its 'main engine', the transport formula, is not completely understood. Also the uncertainty in the estimate of the scour length was found to be of little influence, so the – at fist glance rather rough – estimates obtained from figure 3.20 can be used without much trouble.

The greatest advantages of the design method proposed by De Groot *et al* are:

- it uses damage as a design criterion instead of a critical load
- it predicts the damage to a structure in a understandable and practical way, and enables the evaluation of the development of this damage over time
- it relates to known concepts from morphology
- it is suitable for probabilistic analysis, which seems to be the only appropriate design approach given the large uncertainties surrounding the governing parameters

For these reasons, this method is a potentially very powerful design method for near-bed structures. Its main disadvantage is that it cannot be performed easily by hand but needs a computer program to do the analysis. Secondly, it is dependent on the limitations of the transport formula it uses, which means that it is at present not suitable for a combination of waves and currents.

3.6.2 Damage profile design methods

In offshore engineering, various researchers have studied the stability of rubble mound covers for submerged pipelines, and they have put forward some engineering methods for the design of these structures. These will be discussed next. A definition sketch of the parameters that appear in these methods is given in figure 3.21.

Lomónaco and Klomp (1997) give the following stability formula for the damage after 1000 waves, based on scale model tests with a combination of irregular waves (JONSWAP spectrum) and a steady current:

$$S_{1000} = 21.4 \tan(\alpha)\theta^{2.25}$$
$$\theta = \frac{\hat{u}_0^2}{g\Delta d_{n50}} \tag{3.90}$$

in which S is defined as in equation (3.87) and $\tan(\alpha)=1/m_0$ is the side slope of the structure. Lomónaco and Klomp also give additional formulas that express the time dependence, ie damage after another number of waves than N = 1000, but these are surprisingly complicated.

Lomónaco and Klomp use a stability parameter based on the velocity only, not on shear stresses or a combination of velocity and accelerations; as discussed before we will use the Greek symbol theta (θ) to denote this type of parameter. Because, as they state, the damage to the pipeline cover starts at the top of the structure, the disturbed water depth h_c must be taken as the governing water depth (Lomónaco and Klomp 1997) and all parameters (including $\hat{u}$) must be evaluated as if the water depth were equal to h_c everywhere. In this thesis we will use the subscript 'h_c' for parameters defined in this way. Lomónaco and Klomp report that this parameter appears to fit their data better than other stability parameters.

Levit (1996, Levit *et al* 1997) reports something similar: he tried to explain his measured damage profiles in terms of existing transport formulae but could not find a good match. He also concludes, surprisingly, that structures under a combination of waves and a current were more stable than structures under waves alone. This could be due to a reduction in near-bed velocities at the top of the structure because of a – yet not very well understood – wave-current interaction phenomena. It is not known if this phenomenon applies in general or is just a 'freak' feature of the model layout used by Levit in his tests.

Vidal *et al* (1998) performed a small series of scale model tests for regular waves only (no current). In contrast to Lomónaco and Klomp, Vidal *et al* suggest that a shear stress

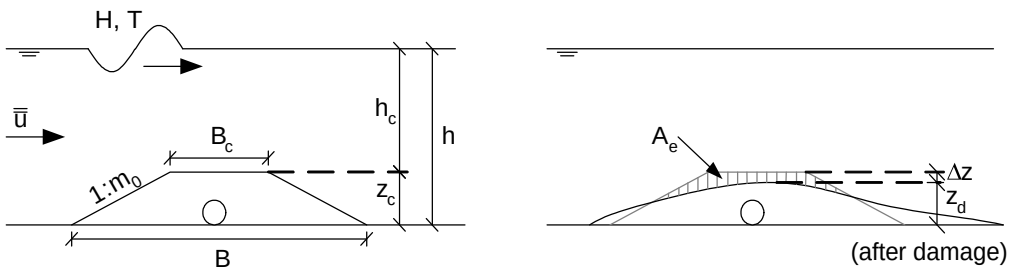

Figure 3.21 - General definition sketch of damage profiles for pipeline covers

based stability parameter *can* be used to predict the damage to the structure. They propose a stability parameter based on the classic wave shear stress according to Jonsson/Bijker (equation 2.28), with the roughness taken as $k_s = 2 \cdot d_{n90}$ and the wave velocity evaluated in the undisturbed profile, at the level of the crest of the structure (see Figure 3.22; we will call this velocity $\hat{u}_c$).

In a second article, this approach was compared with the results from prototype tests at a sewer outfall on the north coast of Spain, off Santander (Vidal *et al* 2002). In this second article it is suggested to use the average of the 50 highest waves as the design load. This last recommendation makes the method less suitable for practical design, because in practice a designer usually only knows H_s, from which it is difficult to find the '50 highest waves' (this would a Monte Carlo simulation of the wave climate).

Van Gent and Wallast (2001, Wallast and Van Gent 2002) did scale model tests on a combination of waves and a current, and again found that a velocity parameter better explained their data than Shields or Morison parameters (very interesting in the light of our present research, but it appears Van Gent and Wallast only tried Shields parameters of the form $\tau = \tau_c + \frac{1}{2}\tau_w$, so there may be room for improvement of this conclusion when we try more sophisticated wave-current interaction models). Another important, and perhaps surprising conclusion is that a stability parameter based on the waves did not perform worse than a stability parameter in which the effect of the current was incorporated, too; so, in other words, the current could be left out of the equation. In this respect it must be noted that Van Gent and Wallast only tested for wave-dominated situations.

Van Gent and Wallast give the following stability formula:

$$\frac{S}{\sqrt{N}} = 0.2\theta^3$$
$$\theta = \frac{\hat{u}^2}{g\Delta d_{n50}} \qquad (3.91)$$

Again we see the use of θ, and this time $\hat{u}$ is defined as $\hat{u}_{hc}$, so similar to the way Lomónaco and Klomp defined it. The influence of the slope has disappeared in comparison to Lomónaco and Klomp.

Saers (2005) conducted scale model tests for irregular waves (JONSWAP spectrum), without a steady current, in the fluid mechanics laboratory of Delft University. He found that the Van Gent and Wallast formula (3.91) generally over-predicted his measured

data. Saers suggests that the influence of time (ie the number of waves) could better be expressed with a logarithmic function instead of the square root function used by Van Gent and Wallast. His design formula is:

$$S = 0.8\theta^{2.5}\log(N)$$
$$\theta = \frac{\hat{u}^2}{g\Delta d_{n50}} \tag{3.92}$$

in which û is defined in the same way as Lomónaco and Klomp, and Van Gent and Wallast did.

A second interesting contribution by Saers is the hypothesis that the main cause of damage to a near-bed structure can be related to what he called *streamline contraction*, ie the acceleration of the orbital velocities from a lower value at the bed to a higher value at the crest of the structure. He proposes a parameter to account for this effect, defined as the ratio of the structure slope length ($z_d \cdot m_0$) over the excursion of the wave orbital motion (so for steep slopes and high structures the streamline contraction is larger), and suggests that damage to a structure occurs when a critical ('threshold') value of this parameter is exceeded. In this thesis we will call this parameter the *Saers number* Sa:

$$Sa = \frac{z_c m_0}{\hat{a}_0} \tag{3.93}$$

In his thesis, Saers does not work out this concept any further.

3.6.3 Conclusion

The deformation of near-bed structures in marine conditions has attracted some attention among scientists lately; various researchers have conducted scale model tests for a variety of flow conditions and structure dimensions. Unfortunately this has not yet led to one commonly accepted engineering method for the design of this type of structures. Instead, it appears that every researcher has put forward his or her own design formula. A first quick comparison of these formulae shows that there does not even appear to be consensus on which parameters play a role and how these should be defined. The most prominent differences are:

- Lomónaco and Klomp include the slope of the structure, others do not;
- Van Gent and Wallast suggest a time dependency described by √N, Saers insists on log(N) and Lomónaco and Klomp do not include N at all;

- Vidal *et al* propose a stability parameter based on shear stress, all others prefer a stability parameter based on the wave velocity;
- The three velocity-based methods differ in the exact way in which they define the governing velocity. This is illustrated in Figure 3.22. Vidal *et al* use the undisturbed velocity at the level of the crest of the structure ($\hat{u}_c$) and Lomónaco and Klomp, Van Gent and Wallast, and Saers use the orbital velocity at the crest of the structure as if the water depth were equal to h_c everywhere ($\hat{u}_{hc}$). Lomónaco *et al* (2005) compared both $\hat{u}_c$ and $\hat{u}_{hc}$ against measurements at the Santander sewer outfall and report that $\hat{u}_{hc}$ matches the measured velocities better.

Despite these differences, all researchers in this field appear to draw the conclusion that it is not a fruitful approach to try and predict transport rates for these type of structures under waves and currents. Instead, they opt for a more direct 'black box' approach in which the damage to the structure is directly expressed in terms of S and related to very basic fluid properties like $\hat{u}_0$. Another general conclusion is that the damage to these structures appears to stop after some time; the waves have reworked the structure into a more stable form. We can see broad similarities with berm breakwater design. In any case it is clear that this wave-dominated design approach is completely different from the current-only approach proposed by De Groot *et al*.

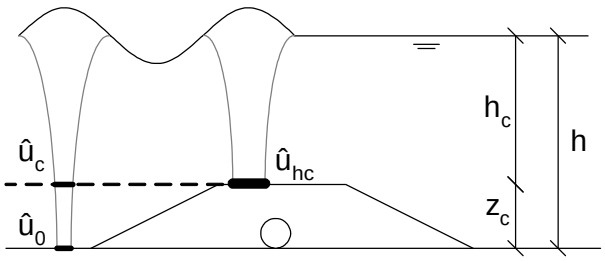

Figure 3.22 – Various definitions of wave orbital velocities used in proposed design methods for near-bed structures

4 Review

4.1 Introduction

In Chapter 1 we described how this thesis would focus on finding a design formula that can be used for the damage-based design of near-bed structures under combined wave and current attack. The previous chapter described many, mainly theoretical concepts and ideas that could potentially be elements of such a design formula. In this present chapter we will briefly review and summarise these, and select a few concepts that will be carried on into the next phase of this research. Finally, we will use these results to present an outline of the second phase of this research.

4.2 Stability parameters

In literature we can find four different groups of stability parameters:

- Shields-type stability parameters, based on the bed shear stress;
- Morison-type stability parameters, based on the velocities and accelerations in the vicinity of the stone;
- Turbulence-based stability parameters that explicitly incorporate the effects of the turbulence characteristics of the flow;
- Other parameters that express the load on the structure in terms of direct wave and current parameters such as u, H, and T.

These will be discussed in the next paragraphs.

4.2.1 Shields-type stability parameters

Shields-type stability parameters use the bed shear stress as the governing load and have been developed for use in uniform flow. In this thesis we study non-uniform flow

(mainly a combination of waves and a current), so we must find ways to extend the use of these parameters for these circumstances. The resulting combined bed shear stress is not easily determined. In general we have two reasons for this:

- The bed shear stress is no longer constant in time[2], as it would be for uniform flow, but varies with the wave cycle. This means that we will have to translate the time-dependent shear stress into one single characteristic value that we can use for design (ie we have to use the maximum or some kind of average value). There is no consensus in literature on the best way to do this.
- The combined bed shear stress can not be calculated as the (vector) summation of the current-only shear stress and the wave-only shear stress. Instead, the current and the waves influence each other in a non-linear way, leading to an enhancement of the shear stresses. This effect *(wave-current interaction* or *WCI)* must be taken into account. Again, there is no consensus in literature on how to do this; in fact, more than 20 WCI models (Soulsby 1997) have been put forward.

In chapter 3 we have explored various averaging procedures and WCI models. A brief summary is given next.

Averaging procedures: The most straightforward way to obtain a characteristic value from a time-dependent variable is to use the maximum value. This could be a reasonable choice for the design of near-bed structures since we could argue that the maximum shear stress is responsible for causing the damage. However, this is not certain *a priori*, since we can also argue that the maximum shear stress has a too short duration for the stone to react to, because of its inertia. In that case an average value of the shear stress could be a better parameter to describe the load on the stones.

There are various ways in which we can average the time-dependent shear stress. Firstly, we can decide to average over the whole wave period, or over half the wave period. The second case can be seen as ‘middle ground’ between using an average value and using the maximum value: we recognise that the first half wave period (when the shear stresses are larger because the wave velocity and the current velocity work in the same direction) is essentially different from the second half wave cycle (when the two velocities are opposite) and assume that the first half wave cycle causes the damage. Then, recognising that inertia plays a role, we average over this half cycle. In any case it is clear that averaging over half the period results in a higher predicted shear stress than averaging over the full period.

[2] We mean the Reynolds averaged shear stress here, so turbulent fluctuations in time are not included

Secondly, we can decide to average the absolute value of the combined shear stress (disregarding any directional information), or we can average only the component of the combined shear stress in the direction of the flow. When the current and the waves meet at an angle φ the differences between these two methods will be obvious, but even in the case of collinear flow ($\varphi = 0^o$) there is a subtle difference: if we look in the direction of the flow, we will see any combined shear stress that is directed against the flow direction as a *negative* contribution, and consequently the resulting average shear stress will be lower than if we take the absolute values. This situation ('negative' combined shear stresses) occurs for some time during the wave cycle if we have a wave dominated situation ($\hat{\tau}_w > \tau_c$).

The two choices give rise to (2x2) = 4 different combinations. These are illustrated in Figure 3.3 (not repeated here). In the datasets that we will use in the present research we always have collinear flow, in which case it can be shown that the 'average in the direction of the current over half the period' is always equal to the 'average of the absolute value over half the period' – so in this thesis it is of no use to maintain this difference. For that reason we will drop the 'average in the direction of the current over half the period' from our analyses.

Wave-current interaction: As for the second difficulty in determining the combined shear stress under currents and waves, wave-current interaction, we have seen that many theories to describe this phenomenon have been put forward in literature. Eventually, we have selected five of them based on their widespread use and/or positive reviews by various authors (see paragraph 3.2.2). On a more theoretical level we have seen that there are three basic levels at which wave-current interaction occurs (illustrated in Figure 3.8):

- macro-scale: a current influences the wavelength and direction of a wave, and obliquely incident breaking waves cause a longshore current. This phenomenon is not studied in this thesis.
- boundary layer: the presence of a oscillating boundary layer (caused by the waves) is felt by the current as increased bed resistance; and the presence of the current influences the growth of the wave boundary layer.
- turbulence: the combined shear stress is directly related to the turbulence in the wave-current boundary layer, which in turn is a function of the (isotropic, small-scale) wave-induced turbulence and (anisotropic, large-scale) current-induced turbulence.

We have seen that, in order to account for wave-current interaction correctly, we should

treat the flow in the combined wave-current boundary layer as a separate flow problem with the appropriate boundary conditions and turbulence closure model.

This is mainly what the various wave-current interaction models seek to do. The main difference between them can be described in terms of the way in which they model the turbulence (paragraph 3.2.3) in the wave-current boundary layer. More particularly, we can use this insight to rank the five selected models in increasing order of complexity:

- Bijker (1967) – uses a constant eddy viscosity (linear velocity profile in the boundary layer).
- Grant and Madsen (1979) – uses a mixing length model (logarithmic velocity profile in the boundary layer) in which the properties are kept constant in time.
- Fredsøe (1984) – uses a mixing length model (logarithmic velocity profile in the boundary layer) in which the properties are allowed to vary with the wave cycle.
- Davies, Soulsby and King (1988) – uses a one-equation numerical model.
- Huynh-Thanh and Temperville (1991) – uses a k-ε numerical model.

In addition, we have seen that the Bijker model is the only model that does not describe the second type of wave-current interaction (boundary layer interaction), which also sets it apart as the simplest of all models.

The first three models have a physical basis and can be expressed in analytical formulas, the last two models are purely numerical. From earlier work by Soulsby et al (1993) we can see that the last two, most complicated, models predict results that are almost indistinguishable from the results predicted by the simpler Fredsøe model. Therefore, we conclude that these two models are of little practical use, and we will only use the first three models in the second phase of this research. In addition, we will also test a design method is which no wave-current interaction is taken in to account, even though we have seen in Chapter 3 that this it is physically incorrect to neglect this phenomenon; this represents a ‘base case’ against which the performance of the various wave-current interaction models can be judged.

All in all, we will use the following four ways to translate the time-dependent combined shear stress into one characteristic value:

- the maximum shear stress during the wave cycle
- the average shear stress over the whole wave cycle

- the shear stress in the direction of the current (averaged over the whole wave cycle)
- the average shear stress over half the wave cycle

and we can combine these with four WCI-models:

- Bijker (1967)
- Grant and Madsen (1979)
- Fredsøe (1984)
- No WCI (base case)

This gives us a total of 4*4 = 16 different Shields-type stability parameters to be tested. It is stressed that these sixteen parameters include the two parameters used in the present design practice, being:

- the average shear stress over the whole wave cycle according to Bijker (method recommended by CIRIA/CUR 1991)
- the average shear stress over half the wave cycle according to Bijker (method used by the software package BPP)

as shown in Chapter 2. This gives us the opportunity to compare all new methods to the present design practice.

In addition to the above, a few conclusions from our theoretical analysis of wave-current interaction are worth mentioning here:

- the effect of wave-current interaction can be quite large and this effect cannot be ignored, especially when the maximum shear stress is used
- the resulting shear stresses are always the largest for $\varphi = 0^o$, in other words collinear flow is the governing situation. This effect is particularly strong for the maximum shear stress and the average shear stress over half the period (remember that this last parameter is used by BPP), it is less pronounced for the average shear stress over the whole period, either in the direction of the current or not. For design practice this means that the stones sizes may be reduced when the waves and the current meet at an angle, but this reduction should only be applied when the designer has a solid reason to assume that the flow will never be collinear.
- In line with the previous remark: when the waves and the current propagate at an angle, the wave-current interaction becomes less pronounced; at $\varphi = 90^o$ there is

not so much difference between the predictions with or without wave-current interaction, or between the various wave-current interaction models.

- The wave-current interaction models can be made more easily accessible by a parameterisation of these models given by Soulsby (1993). This parameterisation approximates the model predictions without having to know the details of the respective models. We have shown in chapter 3 that our own calculations, based on the full models themselves, match Soulsby's results closely. In the second stage of this research we will only use our own calculations rather than Soulsby's parameterisation, firstly because Soulsby's parameterisation does not provide any insight into the (physical) details of the respective models, and secondly because Soulsby only gives the maximum and the 'mean' shear stresses (that we have found to be equal to our 'average shear stress in the direction of the current')
- The theories behind bed shear stresses are based on a 'bulk' approach: 'the' bed shear stress is in fact an average value over the many individual particles that make up a bed. (In that aspect the name *bed* shear stress is very appropriate, it is not a *particle* shear stress). Fredsøe (1984) warns explicitly that for a relatively large bed roughness ($a_0/k_s < 50$) this 'bulk' approach may no longer be valid, because the flow around an individual grain becomes dominant and may have to be modelled in detail. Fredsøe makes this warning within the context of his own WCI-model, but there is no reason to believe why this should not apply for the other models as well. For rock structures in relatively shallow water we can expect a_o/k_s-values of the order 10, so we are outside the range of validity of the 'bulk' bed shear stress approach as indicated by Fredsøe. This means that we must be careful when applying shear-stress based parameters.

4.2.2 Morison-type stability parameters

The stability of an individual stone is related to the balance of forces that act on it. The Shields-type stability parameters discussed above are based on the assumption that all forces on a stone can be related to the shear stress (and are therefore proportional to the flow velocity u (squared) and the surface area of the stone d^2). We have seen in paragraph 3.3.2 that this is no longer true when the flow is accelerated: accelerations give rise to pressure differences that cause an *inertia force* proportional to the volume of the stone (d^3). In recent years some researchers have studied the idea that these accelerations, and the forces they cause, can be a major contributor to (in)stability of the stones and must be taken into account explicitly. The resulting stability parameter is a combination of a contribution by the velocities and a contribution by the accelerations,

weighed with the empirical model parameters C_B and C_M, respectively. In general terms this approach is called the *Morison* approach, after the design method for wave forces on vertical piles (Morison *et al* 1950).

In flowing water there can be two sources of accelerations:

- temporal accelerations (du/dt), also called local accelerations or unsteady flow. The most obvious example in this class is oscillatory flow (waves). This phenomenon was studied by Tromp (2005) who found that the threshold of motion for bed material under waves could be described with a Morison-type stability parameter with $C_B/C_M \tilde{} 7$.

  However, in the previous paragraph we have seen that waves can also be included in a stability parameter through the bed shear stress that they cause. To our knowledge the performance of these two alternative methods has not been directly compared yet.

- spatial accelerations (u·du/dx), also called convective accelerations or non-uniform flow. This occurs for instance near flow contractions and around structures and was studied by Dessens (2005). In the current design practice it is often assumed that the stability of bed material in accelerated flow is no less than the stability in uniform flow (Schiereck 2001); the measurements by Dessens appear to contradict this. This would indicate that the application of a Morison approach is useful here, too.

  For *de*celerating flow the stability of bed material is also different from the stability in uniform flow (ie the stability is lower, Schiereck 2001), but this is more related to the associated increased turbulence levels (a decelerating flow loses energy, which is dissipated through turbulence) than to inertia forces. Moreover, if we draw a force balance for decelerating flow the inertia force would be oriented against the drag force (see eg Figure 3.15, but with F_M pointing to the left) which would have a *stabilising* effect on the stones which – by itself – is clearly incorrect. To our knowledge there are no studies into the applicability of the Morison approach in decelerating flows yet; based on the above, we conclude here that this will not be very useful anyway (unless, perhaps, if it is combined with a study into increased turbulence levels).

The Morison approach is a very recent development in this field of research. In general terms we can say that the physical basis behind the approach is sound and appears to make more sense than the physical basis of the currently applied methods (based on shear stresses) – in that aspect the development of the Morison approach has to be

encouraged. The physical correctness of the method can be illustrated by looking at the theoretical ratio of inertia forces over drag forces on an object under wave load: (Dean and Dalrymple 1991)

$$\frac{F_M}{F_D} = \pi^2 \frac{C_M}{C_D} \frac{1}{KC} \tag{4.1}$$

in which KC is the Keulegan-Carpenter number (KC = $\hat{u}_0 T/d$). Note that this formula is derived for vertical piles and therefore does not include lift forces (these cancel because of the symmetrical load in that case), hence the use of C_D instead of C_B. Anyway, we have C_M/C_D = O(1) (Dean and Dalrymple 1991, but this also follows from Tromp 2005) and for stones (d ~ 0.2 m, $\hat{u}_0$ ~ 1.5 m/s, T ~ 10 s) we can estimate that KC ~ O(10), so we get F_M/F_D = O(1); in other words the drag force and the inertia force are of the same order of magnitude. By contrast, if we do the same estimation for sand (with d ~ 200 μm) we get KC = O(10^4) and consequently $F_D >> F_M$. Therefore it seems necessary to include both drag (/ lift) and inertia forces in a stability parameter for stones; a Shields-type approach in which the inertia forces are disregarded seems more appropriate for sand.

However, there are a three important limitations to a successful application of the method in practical engineering:

- the method requires a measure of 'the' velocity and 'the' acceleration in the vicinity of the stone. This measure is not clearly defined and not easily obtained from main flow properties like u, H, T and so on. In fact, this dilemma can be seen as the very reason why shear-stress based methods (that can be expressed in main flow properties) have been developed in the first place. This dilemma is not solved yet.
- This dilemma is even more pronounced in the combination of waves and a current; it is not clear how the Morison approach should be applied in that case. A suggestion could be to replace the drag-and-lift part of the Morison equation by the bed shear stress (for which we *can* find a combined value in the case of waves and currents, see previous paragraph) and keep the accelerations as they are. This step is further explored in paragraph 4.2.3. To our knowledge such a hybrid parameter has not been suggested in literature yet.
- the method requires a reasonable estimate of the value of the coefficients C_B and C_M. As we have seen in paragraph 3.3.4 there are only a few sources of information on these values, and they seem to contradict one another to quite a large extent. We have seen that the value of these parameters is not easily measured and may depend on things like the orientation of the stones and the

roughness of the bed. There is also no reason to assume that these parameters are constants, they may well depend on flow parameters like a_0/d or the Keulegan-Carpenter number.

In the present thesis we will use an adapted form of the Morison parameter in order to reduce this problem somewhat. If we divide the Morison parameter (see equation 3.2) by C_B we get:

$$\Theta' = \frac{\Theta}{C_B} = \frac{\frac{1}{2}u^2 + \frac{C_M}{C_B} a d_{n50}}{g \Delta d_{n50}} \tag{4.2}$$

We now only have one unknown parameter: the ratio C_M/C_B (for which we will use the value $C_M/C_B = 6.8$ found by Tromp). This simplification means that we will not find the absolute values of C_M and C_B in our analysis: this is not considered a major problem since our prime interest is to test the applicability of a Morison stability parameter in eg a transport formula – in that case the value of C_B will be implicitly present in the fit parameter of our model. In our notation we will usually omit the apostrophe in Θ‘ and simply write Θ. Please note that strictly speaking this simplification is only valid if we assume that C_B and C_M are indeed constants.

In the remainder of this thesis we will only study the Morison approach in combination with temporal accelerations caused by the waves, in an attempt to make the comparison between this method and a shear-stress based method. We will use the orbital velocity at the bed $\hat{u}_0$ as the governing velocity in the Morison equation; the governing acceleration then follows from

$$\begin{aligned} a(t) &= \frac{du}{dt} = \frac{d}{dt}\left(\hat{u}_0 \sin(\omega t)\right) = \omega \hat{u}_0 \cos(\omega t) \\ \Rightarrow \hat{a}_0 &= \omega \hat{u}_0 \end{aligned} \tag{4.3}$$

Spatial accelerations will not be included in the present analysis, even though we study pipeline covers where we can expect spatial accelerations to occur. The main argument for this is dimensional: for normal wave conditions with, say, T = 10 s and $\hat{u}_0$ = 1.5 m/s we have $\hat{a}_0 \sim 1$ m/s^2 (equation 4.3). The order of magnitude of the spatial accelerations around a near-bed structure can be estimated as $u \cdot (du/dx) \sim u \cdot (\Delta u/\Delta x)$, with Δu the difference between the velocity at the crest and the velocity in front of the structure, and Δx equal to the slope length of the structure:

$$
\begin{aligned}
&u \approx \hat{u}_0 \\
&\Delta u = (u_{crest} - u_{bottom}) \approx \left(\frac{h}{h_c}\right)\hat{u}_0 - \hat{u}_0 = \left(\frac{h_c - h}{h_c}\right)\hat{u}_0 = \frac{z_c}{h_c}\hat{u}_0 \\
&\Delta x \approx z_c m_0 \\
&\Rightarrow a \approx u\frac{\Delta u}{\Delta x} = \frac{\hat{u}_0^2}{h_c m_0}
\end{aligned}
\tag{4.4}
$$

(see Figure 3.21 for definitions). With h_c = 10 m and m_0 = 2 we get a ~ 0.1 m/s^2. This rough estimate shows that the spatial acceleration is about one order of magnitude smaller than the temporal acceleration; this is another reason to disregard it.

Instead of incorporating the spatial accelerations explicitly in a Morison-type stability parameter we will investigate the performance of a dimensionless structure parameter that includes the accelerations implicitly: the Saers parameter (Saers 2005), see equation 3.93.

Finally it is noted that both studies into the use of a Morison-type parameter in waves (Tromp 2004, Terrile 2004) have explicitly linked the effect of the acceleration to *wave asymmetry*. This asymmetry causes a moment during the wave cycle, just before the passage of the wave crest, in which both the velocity and the acceleration are large. Both Terrile and Tromp note that the entrainment of stones occurs at this point. Terrile (2004, Terrile *et al* 2006) proposes a way to account for this asymmetry in a Morison-type parameter, but in our view it is not yet possible to apply his method in practice because it requires a measured time series of accelerations during the wave cycle; this information is not known in the datasets that we intend to use in our analysis (nor, for that matter, will it be available to design engineers in practice). It would be more practical if Terrile's acceleration parameter could be linked to large-scale wave parameters such as H, T and h (probably in combination with a higher-order wave theory). There is some room for further research here.

We hypothesise here that asymmetric waves may well be (or become) the main area of application of the Morison approach; for (approximately) symmetric waves we can also apply shear-stress based methods and it is not expected that the Morison approach will add a lot of information there. In the present thesis, for lack of other options, we have to rely on linear wave theory only in our analysis. This means that any asymmetry effect is completely ignored. This may seriously bias our results for the Morison method.

4.2.3 Comparison of Shields and Morison stability parameters

In Chapter 2 we have seen that the simplest stability theory assumes that all destabilising forces on a stone are proportional to u^2, and so this is the only flow parameter that should feature in a stability parameter; this is the Izbash approach. The disadvantage of this method is that it is not certain where *u* must be measured (somewhere 'in the vicinity of the stone'), so we can not simply calculate the stability parameter from macroscopic flow properties (such as *h* and u_{da}). This can be seen as the main reason why an alternative approach was introduced by Shields. In this approach we do not calculate the velocity but the bed shear stress, which has the advantage that it *can* be calculated from macroscopic flow properties. In addition, as we have seen in Chapter 3, this allows us to combine the effect of waves and currents. The disadvantage of this method is that it is based on certain simplifications that limit its applicability: we can only use this method in uniform flow and (approximately) symmetric waves.

		FORCES	SHEAR STRESSES
	advantage	closer to true physics	calculable from macroscopic properties; combination of waves and current possible
	disadvantage	not calculable from macroscopic properties; combination of waves and current difficult	simplification of true physics

	advantage	disadvantage		
NO ACCELARATIONS	simple model	only applicable for uniform flow and (approximately) symmetric waves	IZBASH	SHIELDS
ACCELARATIONS	In principle generally applicable (except in the case of decelerations?)	introduction of extra (unknown) model parameters C_B and C_M; correct representation of wave asymmetry (yet) unknown	MORISON	SHIELDS - PLUS?

Figure 4.1 – Overview of stability parameters

In non-uniform flow and asymmetric waves the associated accelerations in the flow must be taken into account – we can do this with the Morison approach. However, in the light of the above discussion this effectively brings us back to the 'Izbash' starting point with the associated difficulties. It would be an interesting step to try to overcome these by taking a similar step as from 'Izbash' to 'Shields' – in other words to develop a shear-stress based stability parameter in which the accelerations are explicitly present. Such a 'Shields-plus' stability parameter would in fact fill the remaining gap in a (2x2) matrix that can be used to categorise the stability parameters that we discussed so far – see figure 4.1.

The general form of such a Shields-plus stability parameter could be obtained by replacing u^2 in the 'drag-and-lift' part of the Morison parameter by u_*^2, giving:

$$\Psi^+ = \frac{\frac{1}{2} C_B u_*^{\,2} + C_M a d_{n50}}{g \Delta d_{n50}} = \frac{\frac{1}{2} C_B \tau + \rho C_M a d_{n50}}{\rho g \Delta d_{n50}} = \frac{1}{2} C_B \Psi + C_M \frac{a}{g\Delta} \qquad (4.5)$$

This new parameter is a very interesting thought, but it leads to a few complications, including:

- The values of the model parameters C_B and C_M are no longer related to the original values (for velocities instead of shear stresses), since the change from u^2 to u_*^2 has introduced a new scaling (typically u_* is one or two orders of magnitude smaller than u) – in fact the ratio u_*^2/u^2 is mainly governed by a friction parameter (see eg equation 2.21 or 2.28). This friction parameter is not a constant, and especially in the combined case of waves and currents it is dependent on the situation at hand (eg the relative current strength). This introduces yet another complication into the – already quite troublesome – determination of the correct values for C_B and C_M.
- A major reason to develop a Shields-plus parameter is the possibility to use this parameter in the combined case of waves and currents; in that case τ in equation 4.5 would be τ_{wc}. However, we must keep in mind that the Morison approach (and thus this new Shields-plus approach) is strongly associated with asymmetric waves and/or accelerating currents. It is uncertain (in fact: rather doubtful) whether the wave-current interaction models that we can use to calculate τ_{wc} are still valid in those cases.

For these reasons, we will not use the 'Shields-plus' parameter in the remainder of this thesis; we introduce this parameter here only as a suggestion for further research.

4.2.4 Turbulence-based stability parameters

A second recent development is the study of stability parameters that directly include the effects of turbulence. The turbulence in a flow has two effects on the stability of stones:

Quasi-steady forces: turbulence causes the velocities near the bed and the related forces on the stones to fluctuate. This means that there can be rare occasions in which the forces become exceptionally large; these events are thought to be responsible for the entrainment of the stones. These fluctuations are not random; they can be thought of as vortices, originating higher up the fluid column, that come crashing down onto the bed: so-called *sweeps*.

Turbulence wall pressures: turbulence-induced velocity fluctuations elsewhere in the flow that do not reach the bed themselves can still have an influence on the stones in the bed because of the pressure fluctuations they cause (by the Bernoulli effect: increased velocities cause reductions in pressure). These pressure fluctuations are propagated through the fluid and eventually reach the bed causing a (fluctuating) inertia force. This means that these forces are related to the acceleration of the fluid.

Research by Hofland (2005) has shown that these fluctuations are the main cause for the entrainment of stones, especially when they work together. A suitable flow structure (eg a vortex) can cause turbulence wall pressures that make a stone rock and give it a less favourable (more exposed) position, after which the quasi-steady forces associated with the same vortex attack the stone and transport it: “rock and roll”

Again, the physical basis behind these ideas is very sound: not only do these forces provide some insight into the actual mechanisms that make a stone move, they also describe the ‘random’ nature of the threshold of motion. Stability parameters based on these turbulence characteristics could well be the most promising design concept for the future. However, before this type of stability parameters can be applied successfully in engineering practice, a number of issues must be resolved first:

- The calculation of turbulence characteristics requires the detailed modelling of the flow around a structure, for instance with a k-ε numerical modelling. This makes application in practice laborious and cumbersome.
- There is no consensus yet in literature on how the output of such models must be used in a stability parameter, although a few suggestions have been made.
- A turbulence-based stability parameter may have to include an estimate of the length scale of the turbulence (the mixing length l_m). The most common

numerical model for turbulent flow, the k-ε model, appears to be unsuitable to predict this length scale correctly (Hofland 2005). This means that more advanced modelling (eg with Large Eddy Simulation, see appendix 1) may be required.

- The turbulence forces can be split into a part related to velocities (the quasi-steady forces) and a part related to accelerations (turbulence wall pressures). This means that a complete stability parameter will be a combination of these two, which gives us the same problem that we saw in the discussion of the Morison approach: what should the value of the weighing factors C_M and C_B be? The stability parameters that have been proposed so far only include quasi-steady forces, the turbulence wall pressures are included implicitly.
- The turbulence under waves has, to our knowledge, not been investigated yet.

In the context of the present research we see the turbulence-based stability parameters as a promising concept for the future; however, we will not include them in our analysis any further. The main reason for this is the need to model the flow situation around a structure explicitly: an analysis of the datasets that we will use in the remainder of this research would require that we build a numerical flow model for each and every individual model test: this is considered too laborious.

4.2.5 Other stability parameters

In our literature survey we have found some stability parameters that do not fit any of the main groups described above. The first of these stability parameters is based on the maximum wave orbital velocity:

$$\theta = \frac{\hat{u}_0^2}{g\Delta d_{n50}} \tag{4.6}$$

This parameter is used in the transport formula of Hallermeijer (paragraph 3.5.3) and by most studies into the stability of pipeline covers (paragraph 3.6.2). Theoretically we could see this as a “Morison parameter without accelerations”, and thus categorise it in the second main group, but we will treat it separately because we prefer to reserve the term ‘Morison-type parameter’ for those parameters that *do* include accelerations. In fact, (4.6) can be seen as an Izbash-type parameter.

However, the relationship between the two parameters is made clear in our choice of symbols: a small theta (θ) for the direct stability parameter, a capital theta (Θ) for a Morison-type parameter. In this thesis we will refer to θ as the *velocity* parameter.

The second and stability parameter has not been mentioned explicitly in chapter 3, but its performance has been investigated by some researchers (eg Van Gent and Wallast 2001, Vidal *et al* 1998). It is the Hudson number:

$$N_s = \frac{H_s}{\Delta d_{n50}} \tag{4.7}$$

This parameter is used extensively in the design of revetments and breakwaters, in other words in the design of structures that cross the water line; perhaps this parameter can also be used in the design of near-bed structures. However, there is one important limitation in the use of N_s: it does not depend on the water depth. We would expect (by intuition) that a near-bed structure in deeper water experiences less damage than a similar structure in shallow water, and we would require a stability parameter to account for that effect. For this reason it is our opinion that the Hudson number as such can never be used in the design of near-bed structures; we will not include this parameter in our further analysis.

4.2.6 Stability parameters: conclusions

Our literature search has yielded a large number of possible stability parameters that can be used in a design formula for near-bed structures. After some discussion we have narrowed these down to:

- Sixteen Shields-type stability parameters, consisting of all combinations of four wave-current interaction models and four averaging procedures;
- One Morison-type stability parameter, which will include temporal accelerations only. Given the uncertainty with respect to the values of C_B and C_M we will leave these as free parameters in our analysis (their value will follow as a result from the curve fitting procedure). We only have to prescribe the ratio C_M/C_B in order to keep the mathematics of the fitting procedure simple; we will use the value found by Tromp (1995): $C_M/C_B = 6.8$;
- One velocity parameter: the dimensionless orbital velocity θ.

When we study pipeline covers the situation is a little more complicated, because we can use three different definitions for the governing wave orbital velocity: the undisturbed velocity at the bed ($\hat{u}_0$), the undisturbed velocity at the level of the crest of the structure ($\hat{u}_c$) and the velocity at the crest of the structure, calculated as if the water depth is equal to h_c everywhere ($\hat{u}_{hc}$). At present, there is no consensus among researchers as to which definition can best be used, nor is there a clear physical reason to prefer one over the

others. Therefore we will use all three definitions in our analysis and compare the results, in an attempt to shed some light on these matters and investigate which definition can best be used.

4.3 Damage parameters and design methods

Our literature search has yielded three different ways of expressing the damage to a structure:

- as transport, quantifying the amount of material that is washed away from the structure;
- as entrainment or number entrainment, quantifying the volume (or number) of stones moved away from their original positions;
- as erosion area, quantifying the "size of the hole that is left behind" after the load has stopped. This parameter is conceptually related to the entrainment parameter, but is perhaps easier to understand and closer related to intuitive notions about damage to a structure. It also has the added advantage that is relates to the design of breakwaters and revetments, a terrain not unfamiliar to many designers of near-bed structures.

Because the present research is about practical applications in design, these damage parameters cannot be seen separately but must be studied in conjunction with a corresponding design method. From our literature survey it appears that there are two different ways of calculating the damage to a structure for a given load:

- by first linking the load to transport of material, and then using this transport rate to calculate the reduction in layer thickness (transport-based method);
- by linking the load directly to the damage expressed as a (dimensionless) erosion area (damage profile method).

The first method uses transport as an (indirect) damage indicator, the second method uses the erosion area. This means that only these two damage parameters will be studied in the second phase of this research, and the second parameter (entrainment) will be dropped.

Apart from the difference in the use of damage indicators there is a second, more fundamental difference between these two design approaches. Transport of bed material is essentially a current-related phenomenon; the presence of waves will increase the

transport rates but in the absence of a current the (net) transport will always be zero[3].

Waves, by their own right, have a second effect on bed material: a oscillating motion, backwards and forwards under each consecutive half wave period. In terms of damage to a structure, this wave-induced oscillating motion causes a redistribution of the material and a flattening of the structure, as opposed to current-induced transport which causes a net loss of material. This essential difference is illustrated in Figure 4.2

These different mechanisms that cause the damage call for different design methods. In essence, the first (transport-based) method introduced above focuses on the first mechanism, the second method (damage profile) is related to the second mechanism. Both methods can be seen as alternatives to the present design methods that are based on the critical stability concept; they are discussed in the next paragraphs.

4.3.1 The transport-based method

The first method requires two ingredients: a transport formula linking load to transport and a design philosophy linking transport to damage.

Starting with this last point: once we have found a transport formula, we can use the 'critical scour' design philosophy put forward by De Groot *et al* (1988) to calculate the

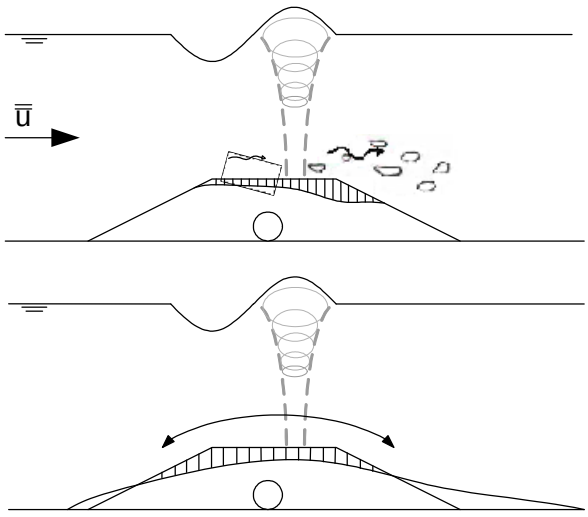

Figure 4.2– two different mechanisms that cause damage to a structure. Top: current induced (and wave-enhanced) transport and loss of material. Bottom: wave-induced redistribution of material

[3] That is, if we assume that the waves are symmetrical. In practice this is never the case: the velocities under the wave crest are higher than those under the trough and consequently there will always be a net transport in the propagation direction of the waves.

resulting damage to the structure (expressed as a reduction of the layer thickness). This is an interesting and potentially very powerful design method that is based on sound and proven concepts from morphology, that predicts the development of the damage over time and that is suitable for a probabilistic analysis (See paragraph 3.6.1). The probabilistic character of the method means that we not only need to find the best values for the fit parameters in our transport formula, but also the confidence bounds around these values.

Alternatively, we can link the transport rate to an erosion area (A_e or S) by assuming that all transported material is washed away from the structure, and therefore $A_e = q_s \cdot D$ with *D* the total duration of the load. This method has two disadvantages when compared to the critical scour method: it does not allow for holes caused by the entrainment of stones to be filled up by material transported from upstream, and the end result (A_e) is less practical than a reduction in layer thickness. Still, this method can be useful in the case of pipeline covers where we can safely assume that the structure (crest) is so short that all material that is entrained from the crest *will* be transported away from it (and deposited at the base of the structure). We will refer to this method as the 'simple transport method'.

The remaining problem – in either case – is of course to find an appropriate transport formula. Transport formulas can be found in abundance in the literature on morphology. To make these formulas applicable to our purposes they have to obey certain criteria. The first criterion is obvious:

- A transport formula must be suitable to include the combined effects of waves and currents.

In addition it must be realised that most, if not all, morphological transport formulas have been derived for prediction of sand transport rates and not for rock. This gives rise to three more criteria:

- A transport formula must express a type of movement that is consistent with the type of movement expected for granular near-bed structures, ie rolling or sliding transport rather than suspended transport. This means that only bed-load transport formulas can be used;
- its range of validity must include the typical size and shapes of the stones used in near-bed structures; this is often a problem as most formulas have been developed for (fluvial or marine) sands which are much smaller and more rounded;

- it must be suitable to describe loads below the (assumed) threshold of motion, because this is the load situation (leading to limited/occasional movement of stones) that near-bed structures should be designed for. Many transport formulas will not meet this criterion because they explicitly predict zero movement below a threshold of motion, others do not use this concept explicitly but have only been tested for loads above this threshold (and thus predict a *bulk* transport rate).

Unfortunately, no transport formulas have been found that meet all four criteria; so if we want to use a transport-based design approach we will have to find a suitable transport formula ourselves. It would be logical to base such a new formula on an existing formula that comes closest to meeting all four criteria. The two most promising candidates for this purpose are the Paintal formula (that has been developed for stones and for loads below the threshold of motion, but does not include waves) and the Bijker bed-load formula (that does include waves but has not been validated for stones or loads below the threshold of motion). In their most general forms, these two formulas can be expressed as:

- Paintal: $\Phi = a \cdot \Psi^b$
- Bijker: $\Phi = a \cdot (\Psi_c)^b \cdot \exp(c/\Psi_{wc})$

In the second phase of this research we will fit these two types of formula on existing data sets to see which expression gives the best results.

Both these expressions are based on a (probabilistic) analysis of the complex processes that set a sediment particle into motion, performed by Paintal (1969) and Kalinske (1947), respectively. Of these two analyses, we believe that Paintal's model more closely resembles the 'true physics' of the motion of stones at low mobility values, and we expect that his expression will better match the data sets. It must be stated, however, that both analyses were originally performed for a situation with current only, and it could be expected that some of the underlying assumptions do no longer hold for oscillatory flow. So, instead of simply trying to include waves in the resulting expression, as we intend to do, it would have been better to completely re-do the original analysis first to see if the resulting expression still has the same form for oscillatory flow. However, such a very fundamental analysis is beyond the scope of this research.

As we have seen in Chapter 3, there is an ongoing dispute about the exact values of the fit parameters *a* and *b* in Paintal's formula, and his original formulation has been 'corrected' twice after. We believe that this dispute is – of course – an important and interesting one, but in our view it must be held with some care and sense of relativity, as may be illustrated by the following observations. First of all, it is not clear exactly how

Paintal arrived at his formula. In his thesis he writes that “curves can be fitted into the data which show that bed load transport varies as the 16th power of fluid shear” (quote from Paintal 1969). From his theoretical analysis we may deduce that the exponent of Ψ in the resulting expression is high, but not necessarily 16; depending on the assumptions underlying this model we could expect exponents in the order of 7.5 to 14 (see appendix 4), so there does not appear to be a theoretical basis for this value.

Also, the stochastic nature of the processes involved make it very difficult to measure the ‘correct’ transport rates for lower Ψ-values, unless the experiments are run for a very long time. In this light it is not surprising that similar experiments as conducted by De Boer (1998) or Forschelen (1999) gave different results.

These observations illustrate that it the Paintal formula is based on just one dataset with quite a large scatter and that the exact value of the fit parameters is very sensitive to a slight change in the analysis. It must be remarked that the true power of Paintal’s research does not lie in the exact values of the parameters of his transport formula; it lies in his observation that stones also move at hydraulic loads below the threshold of motion, in his stochastic analysis of this type of transport and in the fact that he has given the engineering community a first tool to analyse this important phenomenon.

We have also studied some transport formulae that are specifically aimed at predicting transport rates under waves only: the formulae by Madsen and Grant (1976) and Hallermeijer (1982), see paragraph 3.5.3. We have seen that the main form of the Madsen and Grant formula is essentially the same as the Paintal formula: $\Phi = a \cdot \Psi^b$, and so there is no need to treat this formula separately in this thesis. The Hallermeijer formula, though, uses a different way of making transport dimensionless and can be seen as an alternative formulation. When appropriate (ie in wave dominated situations) this formula will be included in our analysis.

4.3.2 The damage profile method

The damage profile method has its roots in offshore engineering, where quite a few researchers have measured and studied the development of damage to a specific type of near-bed structure: a pipeline cover under wave attack, sometimes combined with a small current. Their results can be very interesting for our purposes.

Unfortunately these studies have led to as many proposed engineering methods: there appears to be no consensus on the parameters that should be included in a design formula. Some researchers have included the side slope of the structure or propose other structural parameters, others have not; some assume a time-dependency

proportional to the square root of the number of waves (S ~ √N), one study insists this should be S ~ log(N) and yet another study does not include the number of waves at all. Another disagreement among the various studies is the way in which the governing velocities must be defined: as the undisturbed horizontal velocity at the level of the crest of the structure ($\hat{u}_c$, see Figure 3.22) or as the 'near-bed' orbital velocity at the crest of the structure as if the water depth were equal to h_c everywhere (u_{hc}). Lomónaco *et al* (2005) report that the use of u_{hc} matches their (prototype) measurements better, but they measured only one structure and do not show that this agreement should be the case in general; it could be a coincidental agreement for the structure (dimensions, layout) that they measured (ie the Santander sewer outfall). For this reason we will treat the velocity definition as an 'open issue' in this thesis; in our analysis we will use both definitions and see which one gives the best results. For sake of completeness we will also include the undisturbed near-bed velocity $\hat{u}_0$ in our analysis, giving a total of 3 different velocity definitions.

Most researchers have attempted to use transport formulas to explain the measured damages, but they could not find good agreement. Instead, they have opted for a black-box method in which the measured damage profiles are directly related to load parameters. Van Gent and Wallast (2001) have tried various load parameters, more or less in line with our intended analysis, and have found that the best agreement was obtained with a load parameter that was directly based on the wave orbital velocity. They also found, perhaps surprisingly, that the influence of the current could be left out of the design formula without compromising the accuracy. However, it must be stated that they only tested for wave-dominated situations.

In short, these studies seem to point to the conclusions that:

- no transport formula can be found that accurately predicts damage to near-bed structures under combined wave-current attack;
- a velocity parameter based on the wave orbital velocity provides better results than other parameters that are closer related to the actual physical processes;
- given all the uncertainties involved in the stability of near-bed structures, it is better to use a black-box design approach than a transport-based approach that is, again, closer related to actual physical processes.

These conclusions may be a little dispiriting in the light of this present research, but the number of stability parameters and transport formulas that have been tested in these studies is not quite as large as the number of parameters we intend to test (eg: neither researcher tested the Paintal formula, or used a more complex wave-current interaction

model than Bijker).

Another disadvantage of these researches into damage to pipeline covers is that all researchers have opted to express the damage as a dimensionless erosion area S, as defined in paragraph 3.5.6. It is not clear a priori how this measure can be used in practical design. This is one of the questions that we will need to answer in the second stage of this research.

4.4 Specific research questions

This overview completes the first phase of this research. In the second phase we will work things out in a quantitative way, by testing the concepts that we have found in literature against a data set of measured damage to near-bed structures under combined wave-current attack. These datasets will be introduced in more detail in chapter 5, after which chapter 6 will describe the actual analysis and the results.

The datasets contain test data on two different types of structure: horizontal bed protections (Bijman 2000) and pipeline covers (Lomónaco (1994), Van Gent and Wallast (2001) and Saers (2005)). In combination with the two design methods that we discussed in the previous paragraph, and the fact that the present design practice is based on the critical stability approach, the outline of the second stage of this thesis breaks down into four logical parts:

The design of horizontal bed protections with a transport-based method: The critical scour method predicts reductions in layer thickness for these type of structure (see Figure 3.19), and the simple transport method predicts erosion areas. Unfortunately Bijman did not measure either of these, so the design philosophy behind these methods as such cannot be tested. Bijman explicitly measured transport rates for coarse material under various combinations of waves and current attack, so what we *can* do with the Bijman data set is test the second main ingredient of these methods: the transport formula. The research question for the second stage is:

> *Which combination of transport formula (Paintal-type or Bijker-type) and stability parameter (the 18 parameters identified in paragraph 4.2.6) best fits the transport rates measured by Bijman?*

The design of pipeline covers with a transport based method: For this type of structure the critical scour method predicts reductions in crest level (Δz), which are only given in part of our intended dataset (tests by Lomónaco 1994). The other two sources only give damage in terms of S, so we must find a way to translate S-values into crest

height reductions. Various ways of doing so will be investigated; the best one will be applied to the full dataset to find Δz for all tests. Then, with these reductions, the given durations *D* of the tests and an estimate of the scour length we can calculate the transport rates that are associated with the critical scour method using:

$$\Delta z = \frac{q_{\max}}{L_s} D \quad \Rightarrow \quad q_s = \frac{\Delta z \cdot L_s}{D} \tag{4.6}$$

(which follows from equations 3.88 and 3.89 with $\Delta z = SC = SV \cdot D$).

With the simple transport method we can estimate the transport rates as:

$$q_s = \frac{A_e}{D} \tag{4.7}$$

We can then proceed as we did before and fit these transport rates to the various stability parameters, but we have to keep in mind that for pipeline covers the governing velocity can be defined in three different ways. In addition, we discussed in paragraph 4.3 how the damage to these kind of structures could be related to wave-induced transport rather than current-induced transport. For this reason we will also test the applicability of a Hallermeijer-type transport formula. With these additions, the research question becomes:

> *Which combination of transport formula (Paintal-type, Bijker-type or Hallermeijer-type), stability parameter (the 18 parameters identified in paragraph 4.2.6) and velocity definition (see Figure 3.22) best fits the transport rates associated with a transport-based design method (Critical scour method or simple transport method)?*

The result will be compared to the results obtained for horizontal bed protections; ideally the two methods should yield the same transport formula. We will perform this analysis first for the tests with waves only (which is the majority of the tests in our dataset), only when the results are encouraging we will seek to include the effect of the current. This is done because in practice, especially during a design storm, wave-dominated situations can be expected; therefore we prefer to develop a design formula that works well in these situations, the correct inclusion of the presence of a current, although important, has a lower priority.

The design of pipeline covers with the damage profile method: This method predicts the damage to a structure in terms of the dimensionless erosion area S. In our

discussion in paragraph 3.6.2 we have seen that, apart from a lack of consensus on which stability parameter to use and how to define the governing velocity, there is no consensus either on which other parameters should be included in such a design formula. So, in this thesis we will adopt a very general approach and try all stability parameters and velocity definitions that we used before in combination with a whole range of possible other parameters and simply see which one works best (and which do not work at all). The 'other parameters' in this case include the number of waves, the structure slope and the Saers parameter as well as various dimensionless combinations of parameters like h_c/h, B_c/L and so on. The research question is:

> *Which combination of stability parameter (the 18 parameters identified in paragraph 4.2.6), velocity definition (see Figure 3.22) and other dimensionless parameters best fits the measured erosion areas?*

The result of this analysis will be compared (in terms of its goodness-of-fit) to the existing design formulas for S (eg Van Gent and Wallast (2001)) to see if any improvements are possible. Finally, we will use the analysis results to see which design method is more promising: the critical scour method or the damage profile method.

The disadvantage of the parameter S is that it does not relate directly to a clear and tangible measure of damage. A designer must be able to answer such questions as "what does S = 5 mean?" and "When can I expect failure of the structure?" In order for the damage profile method to have any practical applicability we must solve this problem, so we can ask a second research question:

> *Once we know the value of the dimensionless erosion area S, how can we use this value to obtain a practical assessment of the damage to the structure?*

The design of near-bed structures with the critical stability method: Although the main purpose of this thesis is to discuss damage-based design methods (see chapter 1) we can use the datasets to test the correctness of the present design method based on critical stability. We will do so for both types of structure. Also, we can shed some light on a few questions associated with it. The main research question is:

> *How well can we use the critical stability approach for the design of near-bed structures? How must we calculate the combined shear stress and what should the value of Ψ_{cr} be?*

5 Data sets

To answer the questions that we asked in the last paragraph of chapter 4 we need measurement data. In the present research we have not conducted any scale model tests of our own, instead we will refer to measurements by other researchers. The four most important data sources for our analysis are:

- Measurements by Bijman (2000) who conducted flume experiments at the TU Delft for horizontal bed protections (no structures) and measured transport rates for coarse bed material under combined current and (regular) wave attack;
- Measurements by Saers (2005) who measured damage profiles for pipeline covers in the flume at the TU Delft, for (irregular) waves only;
- Measurements by Lomónaco (1994) who measured damage profiles for pipeline covers in the flume at WL|Delft Hydraulics, for a combination of (irregular) waves and a current;
- Measurements by Van Gent and Wallast (2001), quite similar to those of Lomónaco, conducted in the same flume at WL|Delft Hydraulics.

These last three sources will be combined into one large dataset. The next paragraphs will describe these datasets in more detail.

5.1 Bijman (2000)

Bijman conducted classic transport measurements using coloured strips of bed material, using a relatively narrow flume (width B = 80 cm). His dataset is described extensively in his report (Bijman 2000). The most important results (the ones that were used in this present research) are re-printed in appendix 5. The range of parameters that were varied in his research is given in table 5.1. This table shows the model scale parameters such as h, H and T, but also all relevant dimensionless parameters. Most parameters were introduced earlier in this thesis and need no further explanation here, except perhaps for

the wave Reynolds number which is defined as:

$$\mathrm{Re}_w = \frac{\hat{u}_0 a_0}{\nu} \tag{5.1}$$

This parameter can be used in combination with the dimensionless bed roughness a_0/k_s to assess the flow regime in the wave boundary layer (smooth or rough, laminar or turbulent) with the help of a graph devised by Jonsson (1966). The relevant part of this graph (reproduced from Jonsson 1966), with the corresponding data points from the Bijman data set, is given in Figure 5.1. In nature, the flow can be assumed to be rough turbulent, so ideally we want these same conditions in the scale model tests. It turns out that Bijman's experiments were carried out at the very edge of the rough turbulent zone; some of his experiments are actually in the transition zone from laminar to rough turbulent. Apparently this was inevitable given the limitations of the flume used in his research. This means that viscous effects may play a role in his experiments and that we must be careful not to draw too firm conclusions from them.

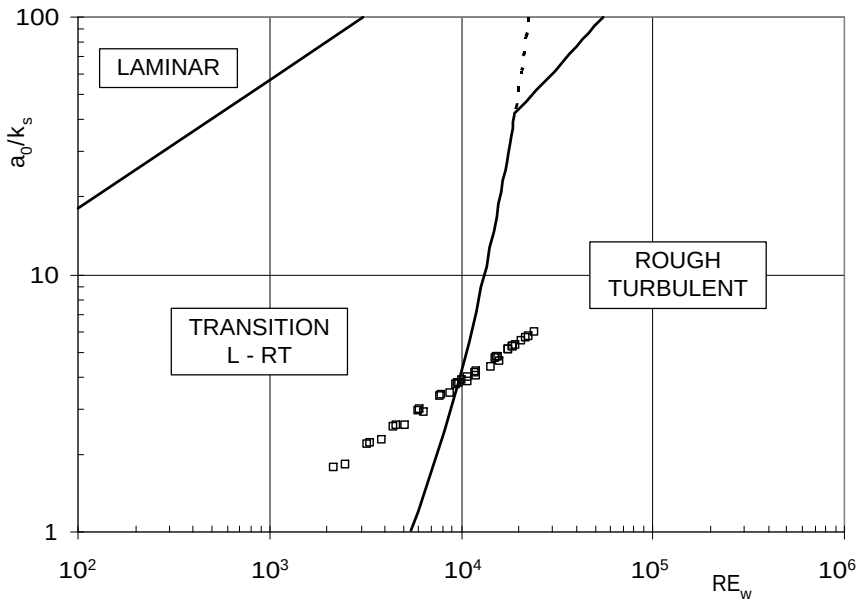

Figure 5.1 – Flow regime for Bijman data set

The parameters shown in table 5.1 and appendix 5 follow from our own analysis of Bijman's measurement data and may deviate from Bijman's original values in a few ways. These are discussed below.

Correction for wall effects: The first deviation arises from the limitations of the test facility (a relatively narrow flume, for the given water depths we have approximately B/h ˜ 2). This results in side effects caused by the wall of the flume that cannot be ignored. The most important wall effect that must be accounted for is the fact that the velocity profile over the depth is no longer logarithmic, which means that the classic way of calculating the current bed shear stress using the Chézy coefficient (equation 2.14) cannot be used. Bijman realised this and, after he finished his experiments, he measured the actual velocity profiles for depth-averaged flow velocities similar to the ones he used in his experiments. These measured profiles indeed proved to be non-logarithmic; the slower the average flow velocity, the larger the deviation from a logarithmic profile. However, the velocity profiles close to the bed *did* prove to be logarithmic, so the actual bed shear stress could be calculated using only these data points, in a way similar to the method described in paragraph 2.1.3 under 'non-developed flow'. The only problem that remained was that this bed shear stress could not be related to the depth-averaged flow velocity which was the only parameter that was measured in the earlier tests, so effectively the bed shear stress in these tests could not be calculated. Bijman solved this problem by re-defining the roughness of the bed in such a way that, for the tests he conducted at the end of his research programme, the measured bed shear stress could be calculated using the Chézy-based method, the measured depth-averaged flow velocity, the measured water depth and this new roughness. This new roughness, expressed as a correction factor to the classic roughness value $k = 2 \cdot d_{n50}$, was then also used in the calculations for the previous tests and it was assumed that this would lead to –more or less- correct bed shear stresses.

We do not agree with this method, because we believe that the bed roughness is a very important parameter in the determination of the bed shear stress. In addition, using a new artificial roughness not only influences the calculation of the current bed shear stress, but also the wave bed shear stress! Instead, we have opted for an alternative way to solve this problem: by not changing the bed roughness, but the depth-averaged flow velocity. In other words, we have re-calculated the depth-averaged flow velocity in such a way that, for the tests conducted at the end of his research programme, the measured bed shear stress could be calculated using the Chézy-based method, the measured water depth, the real bed roughness ($k = 2 \cdot d_{n50}$) and this new flow velocity. This new velocity, again expressed as a correction factor to the measured flow velocities, was then also used in the calculations for the previous tests. This is explained in more detail in appendix 5. This new way of analysing Bijman's data means that our results may deviate somewhat from Bijman's original results.

Dispersion relation: Another way in which our results deviate from Bijman's is caused

by the fact that Bijman takes into account the effect that the current has on the wave period (a following current means a longer wave, an opposing current means a shorter wave. In this experiment Bijman only used following currents). In other words, Bijman uses the adopted dispersion relation (including Doppler effects) to calculate the wave number k for a given period, water depth and current velocity:

$$\omega = \sigma + ku = \sqrt{gk\tanh(kh)} + ku \tag{5.2}$$

in which ω is the wave angular frequency relative to a fixed reference frame, σ is the wave angular frequency relative to a reference frame moving with the current (intrinsic angular frequency), h is the water depth, u is the current velocity and k is the wave number. Bijman then uses this k and σ to calculate the orbital velocity near the bed:

$$\hat{u}_0 = (H/2)\sigma\frac{1}{\sinh(kh)} \tag{5.3}$$

Physically correct as this approach may be, we will not use it in our analysis. Instead, we prefer to use the standard dispersion relation

$$\omega = \sqrt{gk\tanh(kh)} \tag{5.4}$$

to find the wave number for a given frequency ω and water depth, as if there were no current, and continue to calculate the orbital velocity as

$$\hat{u}_0 = (H/2)\omega\frac{1}{\sinh(kh)} \tag{5.5}$$

This is mainly done because this is also the standard way of calculating in design practice. A comparison between the two methods is made in Figure 5.2; the left pane shows the calculated orbital velocity with and without adapted dispersion relation, the right pane shows the same comparison for the dimensionless combined shear stress Ψ (we have used the Bijker averaged method $\tau_{wc} = \tau_c + \frac{1}{2}\tau_w$ here as an example). The figure shows that the error made by using (5.4) instead of (5.2) is not very large in absolute terms (roughly 20% on $\hat{u}_0$ and 15% on Ψ), but more importantly the points tend to collapse onto a straight line indicating that they are highly correlated. In other words: the values obtained by (5.4) differ only by a constant factor from the values obtained by (5.2); this will not bias our intended analysis in Chapter 6 as long as we are clear and consistent in our definitions.

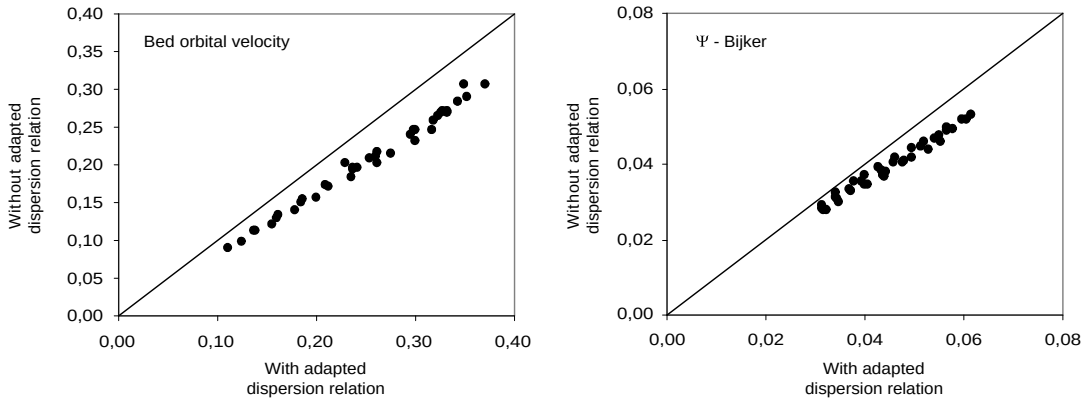

Figure 5.2 – Comparison of parameters with or without adapted dispersion relation for the Bijman data set

Transport and roughness: Finally there are two more ways in which our analysis deviates from Bijman's. The first reason is the fact that Bijman uses a slightly different definition of dimensionless transport than we do (equation 3.74) in the sense that he uses d_{50} and we use d_{n50}. The second reason lies in the definition of the bed roughness: we use $k_s = 2 \cdot d_{n50}$, Bijman uses $k_s = 2.5 \cdot d_{n50}$.

5.2 Lomónaco (1994), Van Gent and Wallast (2001) and Saers (2005)

Lomónaco (1994), Van Gent and Wallast (2001) and Saers (2005) all tested the stability of pipeline covers under wave attack, the first two studies also included combinations of waves and a steady current. Their respective tests are essentially the same and therefore their results will be combined into one large dataset. The parameter ranges that were varied in these tests are given in table 5.2 (for the tests with only waves) and table 5.3 (for the tests with waves and a current). The flow regimes for these two sub-sets using the Jonsson plot are given in Figure 5.3.

The damage that was measured in these tests was expressed as a dimensionless erosion area $S = A_e/(d_{n50})^2$ as defined in paragraph 3.5.6. The definitions of the other (mainly geometric) parameters involved are illustrated in figure 3.20 (repeated here for convenience as Figure 5.4). In addition to the measured erosion area S, Lomónaco also reports the structure height after damage z_d, and gives detailed drawings of all measured damage profiles. Especially these drawings are very insightful, interested readers are referred to Lomónaco (1994). Van Gent and Wallast only report S for their tests, Saers gives some plots of damaged profiles but these are not very clear.

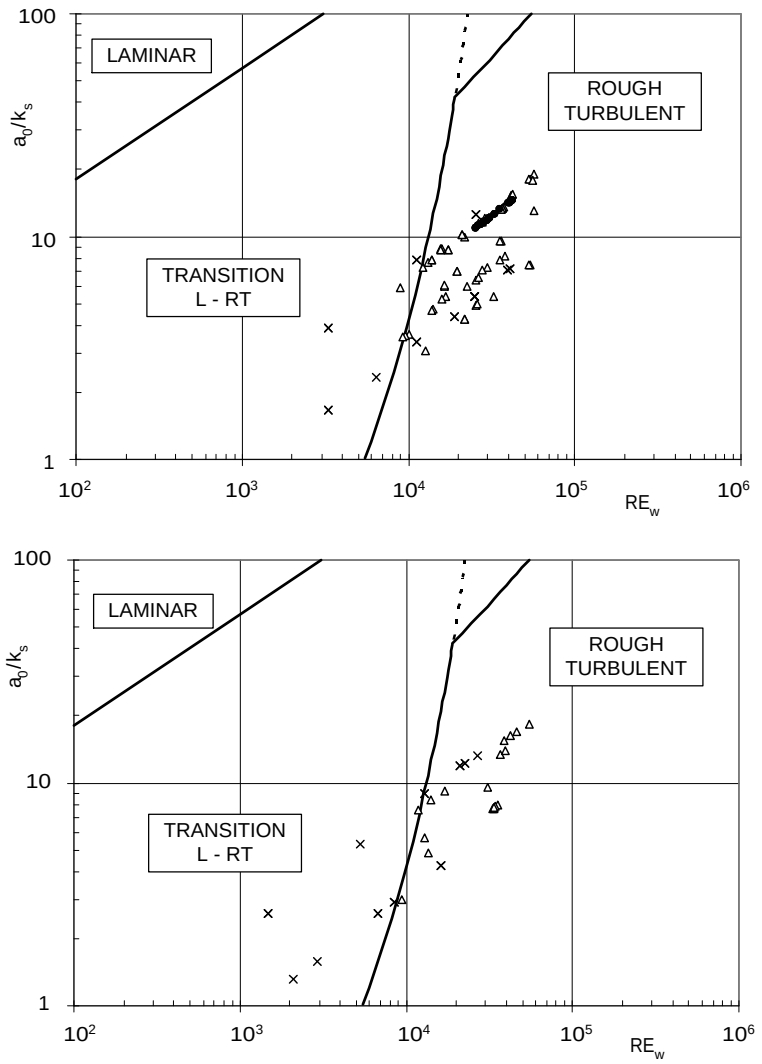

Figure 5.3 – Flow regime for the Lomónaco (triangles) – Van Gent and Wallast (crosses) – Saers (dots) data set. Tests with waves only (top) and a combination of waves and a current (bottom)

When a structure like a pipeline cover is studied the question arises where the characteristic velocities and depths must be evaluated. This has been discussed in paragraph 3.6.2. The parameter ranges given in table 5.2 and 5.3 are based on the approach in which the water depth is assumed equal to h_c everywhere.

In addition to the above, the following remarks must be made:

- Again, the parameter ranges given in these tables are calculated with the standard dispersion relation (equation 5.4), thus neglecting the effect that the current has on the wave length, just as we did for the Bijman data. This approach

is also followed by Van Gent and Wallast in their analysis, so in this respect all analyses are equal.

- All three studies used irregular waves (with a JONSWAP spectrum). The wave heights were reported in terms of $H_{1/3}$ (which we consider to be equal to H_s), H_{max} and H_{rms}, the wave period as $T_{m-1,0}$, T_m, T_p and T_s. Of these, we chose to use H_s and T_m, as these are the two parameters most probably encountered in design practice. In addition, we will calculate $H_{1\%}$ for all tests with equation 2.38 to see if this wave parameter (used by the software package BPP) performs better than H_s. We will then use $H_{1\%}$ in combination with T_p.
- In their reports, neither Lomónaco, Van Gent and Wallast, nor Saers make reference to water-working prior to their tests. This means that their test results may be biased towards over-emphasising small damages (initial movement of unfavourably placed stones).
- The ranges for Re_w and a_0/k_s indicate that not all tests were performed for fully rough turbulent conditions. Apparently using a larger flume than the one Bijman used did not completely solve this problem.
- The original studies (those by Lomónaco and Van Gent and Wallast) included a few tests that were performed with (rather severely) breaking waves (defined as $H_s/h_c > 0.50$, in the original dataset values were as high as $H_s/h_c = 0.76$). Breaking waves cause a fluid motion that is significantly different from the fluid motion under non-breaking waves, and it can be expected that the results from the stability analysis may be biased when these are included. In this thesis we have chosen to focus on non-breaking waves only (see chapter 1) and therefore we will drop the tests with breaking waves from our analysis. This reduces the total data set from 142 test to 118 (81 test with only waves, 37 tests with current and waves). Tables 5.2 and 5.3 are based on this reduced dataset.

An overview of the combined data set of Lomónaco, Van Gent and Wallast and Saers, as far as used in this present research, is given in appendix 6.

Table 5.1 – Parameter ranges for Bijman data set

	parameter	symbol	range
model	stone diameter	d_{n50}	4.86 mm
parameters	stone grading	d_{n85}/d_{n15}	1.3
	stone density	ρ_s	2534 kg/m^3
	relative density	Δ	1.55
	depth-averaged flow velocity	u_{da}	0.35 – 0.66 m/s
	wave height (regular waves)	H	0.05 – 0.15 m
	wave period (regular waves)	T	1.0 – 1.1 s
	water depth	h	0.275 – 0.317 m
dimensionless	combined shear stress	Ψ	0.032 – 0.062
parameters	orbital velocity	Ψ_{u0}	0.148 – 1.658
	wave height	H/h	0.16 – 0.54
	wave length	L/h	6.80 – 8.58
	current dominance	X	0.09 – 0.55
	bed roughness	z_0/h	$1.15\cdot10^{-3}$ - $1.32\cdot10^{-3}$
		a_0/k_s	1.78 – 5.95
		a_0/z_0	53.4 – 178.6
	wave-current angle	φ	0 deg
	number of waves	N	3600
	particle Reynolds number	Re_*	279 – 391
	current Reynolds number	Re	$1.0\cdot10^6$ – $1.9\cdot10^6$
	wave Reynolds number	Re_w	2150 – 24000

Remarks

- The bed roughness is taken as $k_s = 2\cdot d_{n50}$, $z_0 = k_s/30$
- Water-working has been applied: 1800 seconds uniform flow followed by 2400 waves prior to testing
- The combined shear stress in this overview was calculated with the Bijker method: $\tau_{wc} = \tau_c + \frac{1}{2}\cdot\tau_w$
- The particle Reynolds number is based on the combined shear stress velocity
- The current dominance parameter X is defined according to Soulsby (equation 3.4)

Table 5.2 – Parameter ranges for combined Lomónaco – Van Gent and Wallast – Saers data set. tests with waves only

parameter		symbol	range
model parameters	stone diameter	d_{n50}	3.10 – 8.33 mm
	stone shape	-	round – angular – irregular
	stone density	ρ_s	2463 – 2712 kg/m3
	relative density	Δ	1.46 – 1.72
	wave height	H_s	0.085 – 0.29 m
	wave period	T_m	1.1 – 2.1 s
	water depth	h	0.375 – 0.900 m
	structure crest width	B_c	0.040 – 0.25 m
	structure slope	$1:m_0$	1 – 8
	structure height	z_c	0.030 – 0.26 m
dimensionless parameters	shear stress	Ψ	0.023 – 0.090
	orbital velocity	θ	0.16 – 3.61
	wave height	H_s/h	0.24 – 0.50
	wave length	L/h	4.36 – 9.32
	bed roughness	z_0/h	$2.8\cdot10^{-4}$ – $1.9\cdot10^{-3}$
		a_0/k_s	1.67 – 19.0
		a_0/z_0	50 – 570
	number of waves	N	900 – 6500
	particle Reynolds number	Re_*	111 – 745
	wave Reynolds number	Re_w	3200 – 57000
	structure height	h_c/h	0.63 – 0.97
	structure width	B_c/L	0.013 – 0.12
Remarks	• All parameters were determined as if $h = h_c$ and the structure has an infinite width • The shear stress in this overview was determined with the Jonsson/Bijker approach • The bed roughness is taken as $k_s = 2\cdot d_{n50}$ • No reference is made to water-working prior to the tests		

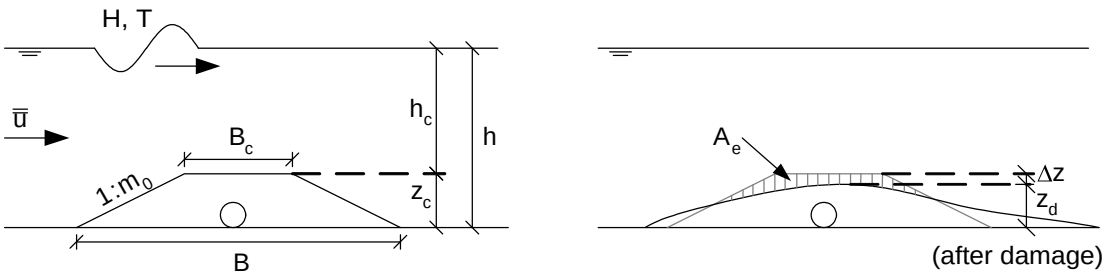

Figure 5.4 - General definition sketch of damage profiles for pipeline covers

Table 5.3 – Parameter ranges for combined Lomónaco – Van Gent and Wallast data set. tests with current and waves

parameter		symbol	range
model parameters	stone diameter	d_{n50}	3.10 – 8.33 mm
	stone shape	-	round – angular
	stone density	ρ_s	2463 – 2712 kg/m3
	relative density	Δ	1.46 – 1.72
	current velocity	u_{da}	0.10 – 0.74 m/s
	wave height	H_s	0.067 – 0.26 m
	wave period	T_m	1.1 – 2.1 s
	water depth	h	0.375 – 0.900 m
	structure crest width	B_c	0.060 – 0.25 m
	structure slope	$1{:}m_0$	1 – 8
	structure height	z_c	0.031 – 0.25 m
dimensionless	shear stress	Ψ_{wc}	0.015 – 0.097
parameters	orbital velocity	θ	0.10 – 3.24
	wave height	H_s/h	0.20 – 0.49
	wave length	L/h	4.57 – 10.7
	current dominance	X	0.01 – 0.57
	bed roughness	z_0/h	$2.8{\cdot}10^{-4}$ – $1.9{\cdot}10^{-3}$
		a_0/k_s	1.32 – 18.4
		a_0/z_0	39 – 552
	wave-current angle	φ	0 deg
	number of waves	N	914 – 3000
	particle Reynolds number	Re_*	72 – 383
	flow Reynolds number	Re	37500 –370000
	wave Reynolds number	Re_w	1500 – 55300
	structure height	h_c/h	0.67 – 0.95
	structure width	B_c/L	0.013 – 0.078

Remarks

- All parameters were determined as if $h = h_c$ and the structure has an infinite width, except for the flow Reynolds number which is based on the full water depth
- The shear stress in this overview was determined with the Jonsson/Bijker approach, $\tau_{wc} = \tau_c + \frac{1}{2}{\cdot}\tau_w$
- The bed roughness is taken as $k_s = 2{\cdot}d_{n50}$
- The current dominance parameter X is defined according to Soulsby (equation 3.4). The value X = 0.57 is an outlier, for the majority of the tests X < 0.2
- No reference is made to water-working prior to the tests

6 Quantitative analysis

In this chapter we will seek to answer the questions that were asked in the last paragraph of chapter 4. We will do so by a quantitative analysis of data sets of scale model tests as described in chapter 5. To do so, we will use some statistical concepts that the reader may not be familiar with. These concepts are described in appendix 7.

We emphasise here that we use the adapted forms of the datasets, as was described in chapter 5. That is, for the Bijman dataset we will re-calculate both the orbital velocities (without the normal dispersion relation, ignoring the influence of the current) and the bed roughness; for the combined Lomónaco – Van Gent and Wallast – Saers dataset we will discard all tests with breaking waves ($H_s/h_c > 0.50$).

The Lomónaco - Van Gent and Wallast – Saers data set uses irregular waves. In the present analysis we have mainly used H_s and T_m as representative parameters, as these are the most practical parameters to use. When applicable we have tested for $H_{1\%}$ and T_p as well. The Bijman data set uses regular waves only.

A worked calculation example, based on the results from this chapter, is included in appendix 9.

6.1 Transport of rock under waves and current

In this paragraph we will focus on the use of a transport-based design method for horizontal bed protections. As we discussed in Chapter 4 we can not test these methods explicitly given the limitations of the dataset in question, and we had to narrow the discussion down to the question of transport of rock. The question we seek to answer in this section is:

> *Which combination of transport formula (Paintal-type or Bijker-type) and stability parameter (Shields-type, for the 16 selected combinations of wave-current*

interaction models and averaging procedures, Morison-type or velocity-based) best fits the transport rates measured by Bijman?

For completeness we repeat here that the '16 selected combinations' include the wave-current interaction models of Bijker (1969), Grant and Madsen (1979) and Fredsøe (1984) and the 'base case' without wave-current interaction; for each method we can either use the maximum shear stress, the average shear stress in the direction of the current, the average shear stress (regardless of current direction) over the whole wave period and the average shear stress (regardless of the current direction) over half the wave period.

The procedure is simple. For all tests performed by Bijman (see appendix 5) we have calculated the combined wave-current shear stresses with the 16 mentioned methods, according to our description in chapter 3; next, we have made all shear stresses dimensionless by dividing them by ($\rho g \Delta d$), which in the case of the Bijman data set is a constant with a value of 82.87 Pa.

In addition, we have calculated the Morison parameters using C_M/C_B = 6.8 as found by Tromp; in that case the Morison parameter becomes (see equation 4.2):

$$\Theta = \frac{\frac{1}{2}\hat{u}_0^2 + 6.8\hat{a}_0 d}{g\Delta d_{n50}} \tag{6.1}$$

In (6.1) the horizontal near-bed orbital velocity $\hat{u}_0$ is taken as the governing velocity, the governing acceleration is simply calculated as the time derivative of the velocity using linear wave theory: $\hat{a}_0 = \omega\hat{u}_0$ (see equation 4.3).

Finally, we have calculated the velocity parameter θ according to equation 4.4, again using $\hat{u}_0$ as the governing velocity.

These 18 stability parameters and the dimensionless transport rates Φ_q measured by Bijman have been fitted to the two selected models (Paintal and Bijker) using the procedures described in appendix 7. The results are discussed next.

6.1.1 Paintal-type formula

The fit of a Paintal-type formula $\Phi_q = a\Psi^b$ can be done by simple linear regression on two variables and has been performed in Excel. The results, in terms of r^2, are given in appendix 8 and summarised in table 6.1. The exact values of the regression coefficients

a and b are not deemed relevant at this moment.

Table 6.1 Goodness-of-fit of various stability parameters in a Paintal-type transport formula. Based on data of Bijman (2000)

Model		r^2
Ψ - No WCI	Maximum	0.22
	Average in current direction	0.65
	Average over full period	0.65
	Average over half period	0.65
Ψ - Bijker	Maximum	0.37
	Average in current direction	0.73
	Average over full period [a)]	0.53
	Average over half period [b)]	0.55
Ψ - Grant and Madsen	Maximum	0.36
	Average in current direction	0.80
	Average over full period	0.50
	Average over half period	0.52
Ψ - Fredsøe	Maximum	0.57
	Average in current direction	0.77
	Average over full period	0.80
	Average over half period	0.79
Θ		0.02
θ		0.03
Notes:	a) CUR/CIRIA method	
	b) BPP method	

This table shows that

- The Morison-type stability parameter and the velocity parameter perform very bad as indicators of transport;
- For all shear stress models, the stability parameters based on the maximum shear stress perform worse than stability parameters based on the average shear stress;
- For the Fredsøe model the average shear stress in the current direction performs (roughly) just as good as the other two averaging procedures, for all other models the average shear stress in the current direction provides the best fit; it therefore appears the be best parameter to use in a Paintal-type transport formula;

- The goodness-of-fit increases considerably when wave-current interaction is taken into account, so this phenomenon cannot be ignored;
- The more advanced wave-current interaction models by Grant and Madsen, and Fredsøe, fit the data better than the simpler model by Bijker. The Fredsøe model performs just as well as the model by Grant and Madsen when the average shear stress in the current direction is used; it performs better for all other averaging procedures.

A visual assessment of what a value of $r^2 = 0.02$ or $r^2 = 0.80$ means can be obtained from figure 6.1 in which we show the scatter plots of the measured Φ_q-values against the calculated Ψ-values for a selection of models.

Table 6.1 shows that there are five models that appear to be useful in a Paintal-type transport equation (in terms of their goodness-of-fit being significantly higher than the other models):

- The average shear stress in the direction of the flow according to Bijker;
- The average shear stress in the direction of the flow according to Grant and Madsen;
- The average shear stress in the direction of the flow according to Fredsøe;
- The average shear stress over the whole wave period according to Fredsøe;
- The average shear stress over half the wave period according to Fredsøe.

The fact that the respective r^2 values vary between 0.73 and 0.80 can not be used to make a final choice between these methods, all methods are deemed ‘just as good’ in this aspect. The final choice will be made on other criteria, being:

- **simplicity / practical use**. A simpler and more practical model will be preferred over a more complicated one;
- **relation to other known concepts**. Ideally, the model of our choice should have a sound physical basis and it should be possible to relate the model to other known concepts, rather than proposing the model “just because it fits our data so nicely”.

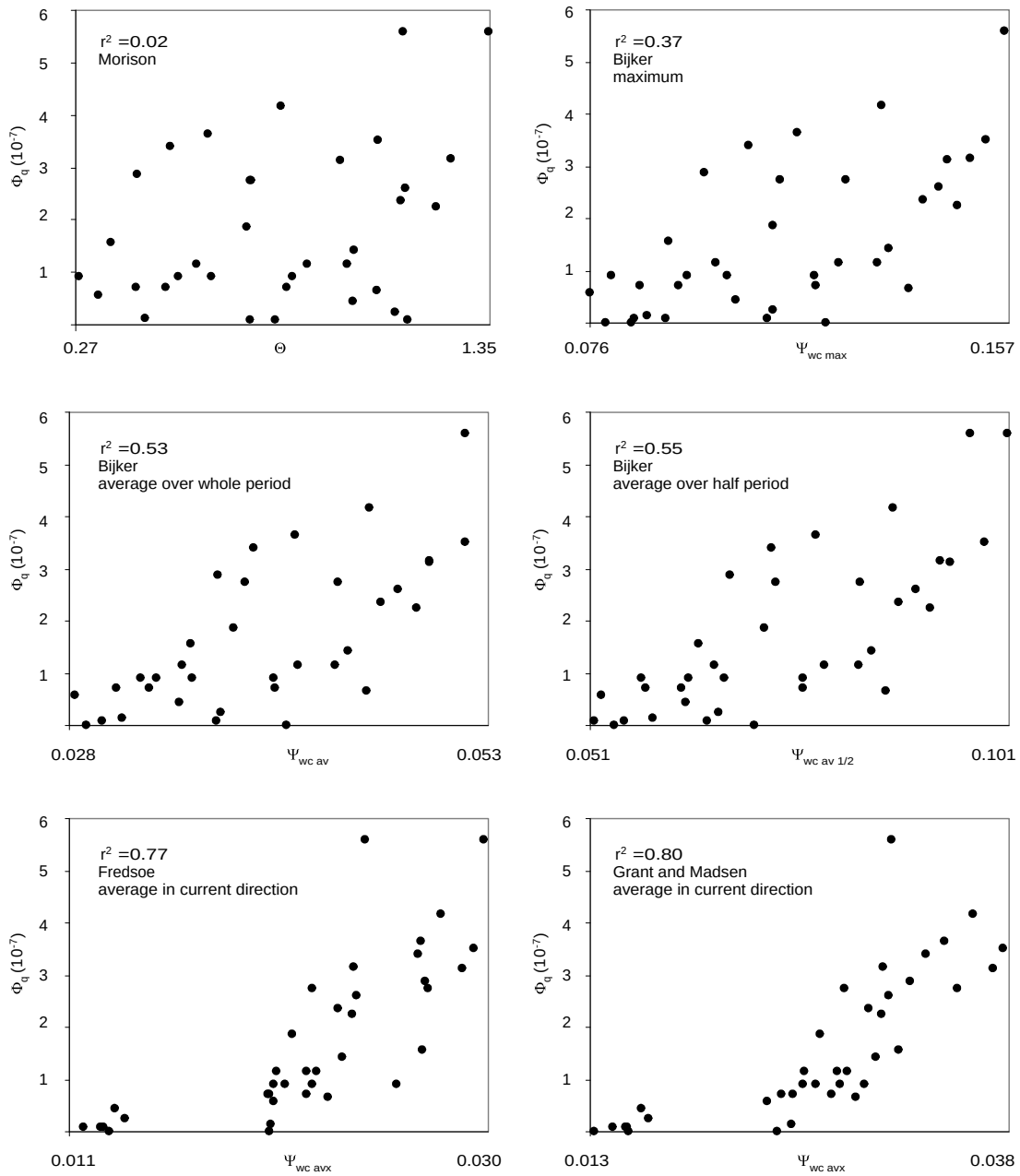

Figure 6.1 – Examples of fit of Φ_q against Ψ for various stability parameters (Bijman data set). Top left: Morison approach (eq 6.1); top right: maximum shear stress according to Bijker; middle left: average shear stress over the whole wave period according to Bjker (CUR/CIRIA method); middle right: average shear stress over half the wave period according to Bijker (BPP method); bottom left: average shear stress in the direction of the current according to Fredsøe; bottom right: average shear stress in the direction of the current according to Grant and Madsen

To start with the last criterion: the Paintal formula was originally derived to describe the transport of rock under a current alone, and ideally our present “current and waves” version should tend towards the “current only” version when the waves grow weaker and weaker. The see which of the five remaining models best meets this criterion, we have plotted the Bijman data against the existing Paintal formula (in the second corrected version by Mosselman and Akkerman):

$$\Phi_q = 3 \cdot 10^7 \cdot \Psi^{8.9} \qquad \text{for } \Psi < 0.05 \qquad \text{(3.77 repeated)}$$

for each of the five remaining wave-current interaction models. The results are given in figure 6.2.

These plots show quite clearly that if Ψ is calculated according to either:

- The average shear stress in the direction of the flow according to Fredsøe;
- The average shear stress over the whole wave period according to Fredsøe;

the measured transport collapses quite nicely onto the Paintal curve. In other words the existing Paintal formula appears to be valid for a combination of currents and waves, too, if we replace the bed shear stress by the combined shear stress according to either of these two methods. This is an important result, because it means that we can cover the whole range of hydraulic conditions from ‘current only’ to ‘current and waves’ with one single formula.

Of these two remaining models, we prefer to use the average shear stress in the direction of the flow according to Fredsøe, for two reasons:

- This is the more practical model to use, because this model has been parameterised by Soulsby et al (1993, see appendix 2) whereas the other model has not;
- The average shear stress in the direction of the current is effectively the bed shear stress caused by the current alone enhanced by the presence of the waves. It seems very logical to use this measure in the Paintal transport formula, because in the original version it also included the bed shear stress caused by the current. This also fits the physical explanation that the current transports the bed material and the waves only enhance the transport capacity.

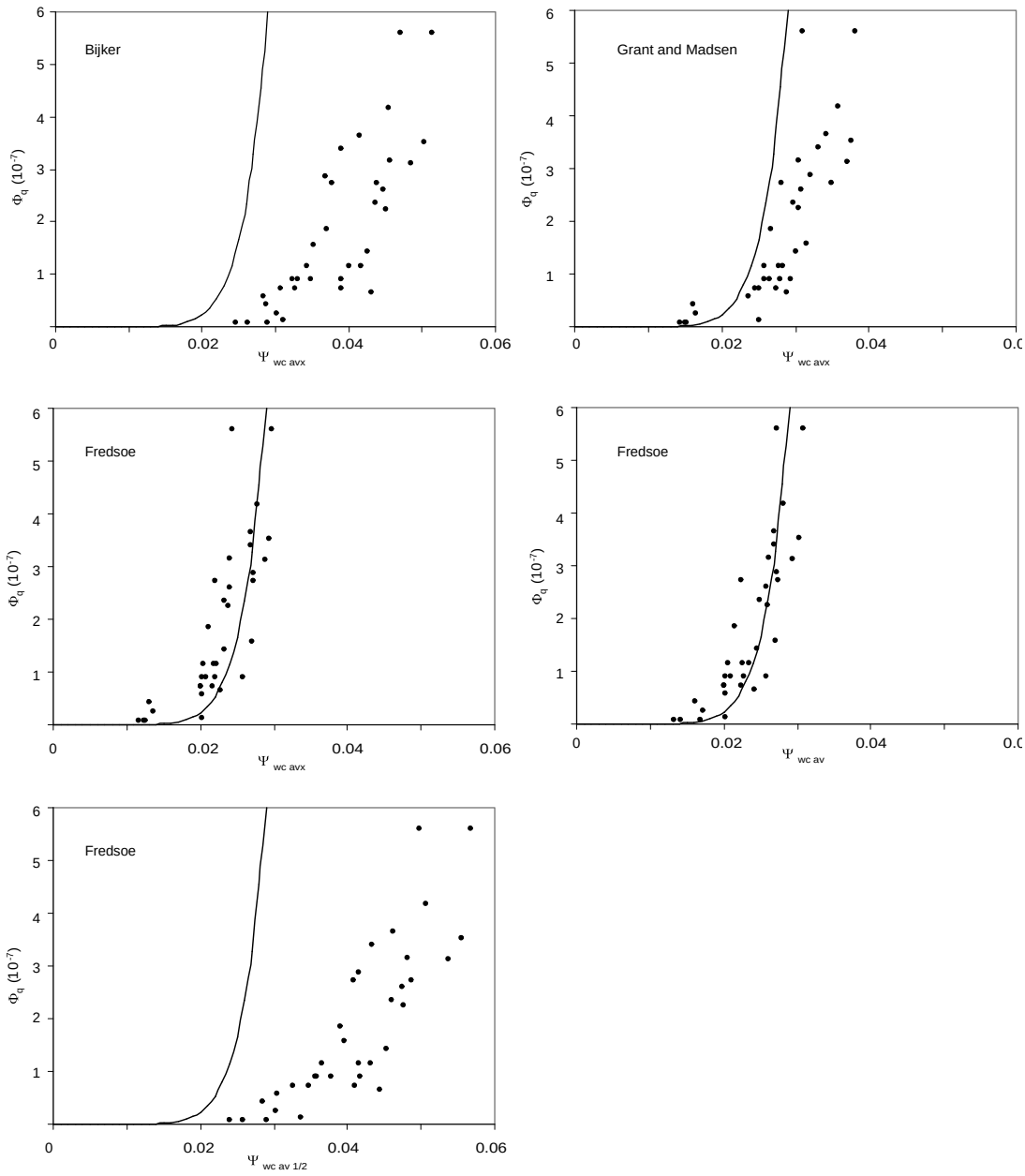

Figure 6.2 – Match Bijman data with existing Paintal formula for various wave-current interaction models

6.1.2 Bijker-type formula

A Bijker-type formula is of the form $\Phi_q = a \cdot (\Psi_c)^b \cdot \exp(c/\Psi_{wc})$, so essentially it consists of a part related to the current shear stress Ψ_c only (responsible for the actual transport of the bed material) and a part related to the combined wave-current shear stress Ψ_{wc}

(responsible for the stirring up of the sediments). This formula is widely used in morphological transport calculations for sand, in which case[4] a = 5, b = 0.5 and c = -0.27; in this paragraph we will investigate whether the formula may also be used for stones, in which case it is expected that the values of the coefficients a, b and c will be different.

In a Bijker-type formula three parameters must be fitted, so we have used the software package SPSS to perform a multivariate linear regression on our data, after the appropriate log-transformation (see Appendix 7). In our analysis we have always used Ψ_c based on the current only and Ψ_{wc} according to the various wave-current interaction models as indicated in the table. In this context the Morison stability parameter and the velocity parameter have no meaning, because they cannot be split in a 'current' part and a 'waves and current' part. They have not been included in the analysis.

Finally, in a multivariate regression analysis the significance (in the true statistical meaning of the word) of the contributions of the various parameters must always be checked, as described in Appendix 7; models in which there is no significant contribution of either Ψ_c or Ψ_{wc} will be rejected. The same is true for models for which colinearity occurs among the dependent variables.

The results are summarised in Table 6.2; the full SPSS output is given in appendix 8.

From this table it is clear that:

- Some models give statistical problems, in terms of a non-significant contribution of one of the two parameters, or colinearity. This last problem occurs mainly when we try to use the averaged combined shear stress in the direction of the current. Apparently this parameter is strongly correlated to the shear stress caused by the current alone (which is not too hard to imagine);
- The models that do pass the statistical tests all show a very high goodness-of-fit, comparable to the best Paintal-type models. There is no apparent preference for a wave-current interaction model, the simpler models (even the model without wave-current interaction whatsoever) perform just as well as the more complex ones.

[4] There is some debate among morphological researchers as to the exact value of *a*. The value given here, a = 5, is used for transport calculations within the surf zone. Outside the surf zone, ie in the absence of breaking waves, *a* is probably lower, perhaps as low as a = 1. However, the exact values are not of importance to us here, we are only interested in order of magnitude

Table 6.2 Goodness-of-fit of various stability parameters in a Bijker-type transport formula. Based on data of Bijman (2000)

Model		adjusted r^2
Ψ - without WCI	Maximum	0.81
	Average in current direction	a) b) c)
	Average over full period	a) b) c)
	Average over half period	a) b) c)
Ψ - Bijker	Maximum	0.81
	Average in current direction	c)
	Average over full period [d]	0.81
	Average over half period [e]	0.81
Ψ - Grant and Madsen	Maximum	0.81
	Average in current direction	a) c)
	Average over full period	0.80
	Average over half period	0.81
Ψ - Fredsøe	Maximum	0.81
	Average in current direction	a) c)
	Average over full period	a) c)
	Average over half period	a) c)
Notes:	a) No significant contribution of Ψ_c b) No significant contribution of Ψ_{wc} c) Colinearity occurs d) CIRIA/CUR method e) BPP method	

We will select two models for further analysis here:

- The maximum shear stress without wave-current interaction, because it is the simplest model to use. The full equation, including the fit parameters a, b and c is:

$$\Phi_q = 0.116 \cdot \Psi_c^{2.97} e^{-0.118/\Psi_{wc}} \tag{6.2}$$

- The average shear stress according to Bijker, because it is the model most often used in the present design practice (a reminder: this is the '$\tau_{wc} = \tau_c + \frac{1}{2}\tau_w$' model). It is also the model used in the Bijker formula for sand transport, on which this new formula is based. The full equation is:

$$\Phi_q = 0.0175 \cdot \Psi_c^{2.27} e^{-0.114/\Psi_{wc}} \tag{6.3}$$

We see that the value of the fit parameters a,b and c deviate strongly from the values that are used in the original Bijker formula for sand. This is probably due to the different nature of the transport of stones (low mobility, occasional transport – see chapter 4).

The two remaining models will be evaluated on a final criterion: their ability to relate to other known concepts. Just as we did for a Paintal-type formula, we would like the new Bijker-type formula to predict stone transport for currents only just as well as for a combination of currents and waves. Evidently, when the waves grow weaker and weaker the combined shear stress τ_{wc} tends towards the current-only shear stress τ_c, so if there is only a current we must replace Ψ_{wc} in (6.3) and (6.4) by Ψ_c.

We can check the applicability of the thus obtained formulas for current-only situations by comparing their predictions to the transport rates measured by Paintal (1969). We have plotted both formulas against Paintal's original dataset in Figure 6.4, in which we also include the Paintal formula (3.77) in the version by Mosselman and Akkerman.

We can see that neither formula predicts the transport rates very well, especially around Ψ = 0.04 – 0.05 the deviations become strong and the new formulas appear to under-predict the measured transport by a factor 100 (note the logarithmic Φ-axis!).

We conclude that, although a Bijker-type formula fits the Bijman data really well and has the advantage that the simplest of wave-current interaction models can be used, it does not work for 'current only' situations. We will therefore reject this type of formula in favour of a Paintal-type formula.

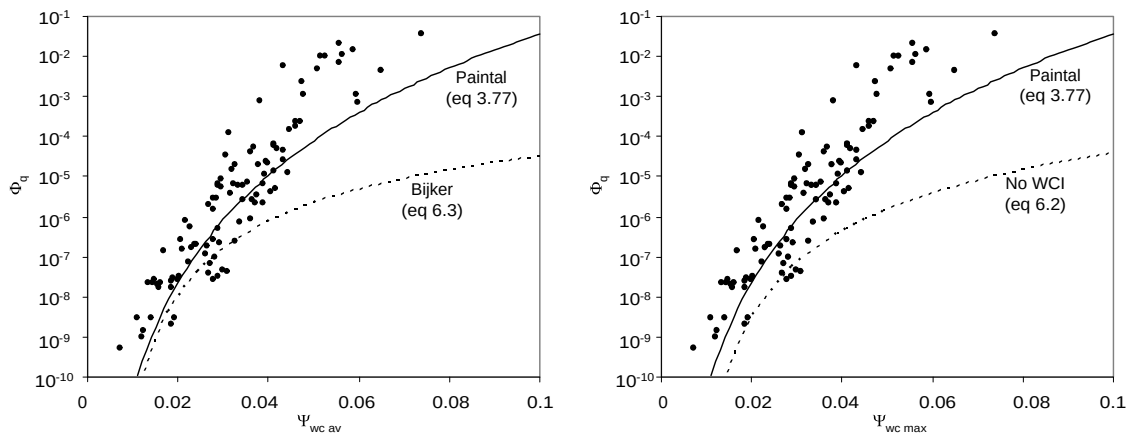

Figure 6.3 – Plots of Bijker-type formulas against Paintal data set (limit for current only)

6.1.3 Conclusions and discussion

In the previous two paragraphs we have seen that both a Paintal-type formula and a Bijker-type formula can be used to predict the transport rates of rock under a combination of waves and currents.

For a Bijker-type formula a simple wave-current interaction model appears to perform just as well as a more complex one, which makes this type of formula easy to use in practice. However, the Bijker-type formulas that were fitted for a combination of currents and waves do not match the measured transport rates for currents only. We believe that a more thorough investigation into transport of rock by a wide range of wave-current flow situations, including a large number of tests for currents only, could potentially result in an all-encompassing transport formula of this kind. But for the time being we will abandon the Bijker-type approach in favour of Paintal-type transport formulas.

When a Paintal-type formula is used, we have found that shear-stress based stability parameters give far better results than other (ie Morison and velocity) stability parameters. Furthermore, the applicability of the formula depends to a large extent on the wave-current interaction model that is used. In general we can say that the more complex models give better results than the simpler ones, and that the maximum combined shear stress is not a good indicator for transport; instead, the average shear stress in the direction of the current appears to be the best parameter to use.

Contrary to Bijker-type formulas, a Paintal-type formula *can* be used for the full range of expected flow situations, from currents only to a combination of currents and waves including strongly wave-dominated situations. In particular we have found that the Paintal formula (as corrected by Mosselman and Akkerman), originally derived for current only, can also be used to predict transport of rock by a combination of currents and waves *provided that the combined bed shear stress is calculated as the average shear stress in the direction of the current according to Fredsøe*. This can be seen as the main conclusion from this part of the present research.

We note that we have assumed that the waves in Bijman's experiment were symmetrical (ie sinusoidal) and that the measured transport was therefore entirely due to the (wave-enhanced) current. This is not really the case: for the water depths and wave heights that Bijman used it is almost impossible to get pure sinusoidal waves in a laboratory flume. Bijman does indeed report that his waves were a little asymmetrical (Bijman 2000). This means that the transport measured by Bijman was at least in part wave-induced; unfortunately we cannot tell to which extent. The conclusion that transport of rock under currents and waves can be described with the Paintal formula in combination

with the shear stress according to Fredsøe can only be justified if we can safely assume that the wave-induced transport in Bijman's experiments was small.

In our calculations we have neglected the influence that the current has on the wave length and period (in other words: we have *not* used the adapted dispersion relation, see chapter 5). Before we can finalize our conclusion we will test the impact of this simplification. We have re-calculated the average shear stress in the direction of the current according to Fredsøe, this time using the adapted dispersion relation, and plotted the results in a similar way as we did in Figure 6.3. In this plot (Figure 6.4) we see that the data point with adapted dispersion relation (dots) are grouped closely to our original points (crosses). Therefore our main conclusions seems equally valid for both calculation methods and the simplification is justified.

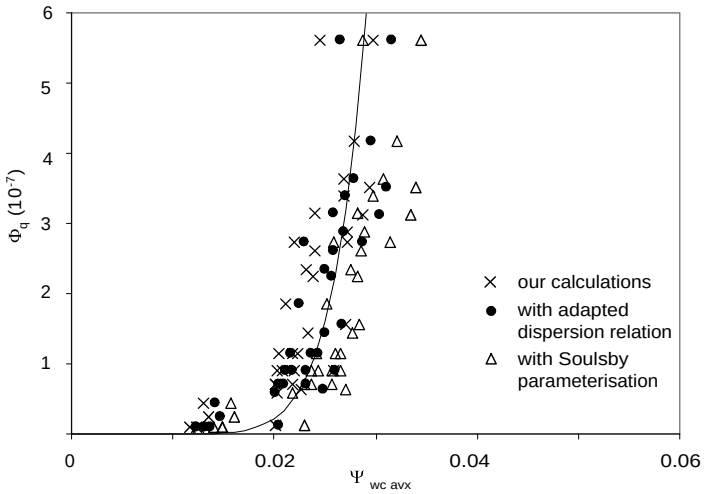

Figure 6.4 – Influence on simplification and parameterization on the main conclusion

In a similar way we can test the recommendation to use the Soulsby parameterisation to calculate $\tau_{wc\ avx}$ instead of the full Fredsøe method. This is also indicated in Figure 6.4. The points obtained with the Soulsby parameterisation (triangles) are slightly to the right of our original points (indicating higher shear stresses), but they are still close enough to support our recommendation.

6.2 Design of pipeline covers with a transport-based method

This paragraph focuses on the use of transport-based design methods for the design of pipeline covers. In Chapter 4 we have discussed various possibilities of doing so, and we have posed this research question:

Which combination of transport formula (Paintal-type, Bijker-type or Hallermeijer-type), stability parameter (the 19 parameters identified in paragraph 4.2.6) and velocity definition (see Figure 3.22) best fits the transport rates associated with a transport-based design method (Critical scour method or simple transport method)?

Before we can proceed to answer this question we will have to find a way to translate the erosion area (in terms of A_e or S) to a reduction in crest height (Δz). This serves two purposes:

- The starting point to calculate the transport rates associated with the critical scour method is a (measured) reduction in crest height, which is not known for all tests in our dataset. For some tests this reduction has been given (Lomónaco 1994, Saers 2005), for other tests it has not (Van Gent and Wallast 2001). This means that for these last tests we will have to find a way to calculate Δz from the measured damage S.
- The simple transport method predicts the erosion area A_e, where in practice designers may be more interested in Δz. If we have a relationship between these two parameters we can use this to make the simple transport method more practical.

Various ways of linking A_e to Δz will be investigated in paragraph 6.3.1. The actual analysis, the fitting of the calculated transport rates to the hydraulic parameters, is performed in paragraph 6.3.2

The damage to a near-bed structure is mainly related to wave action; in design practice the waves commonly form the governing load. Also the data set that we use focuses mainly on wave load, it contains only a relatively small number of tests for waves and currents. For these reasons we will analyse the tests with 'waves only' first; when the results are promising we will seek to include the influence of the current as well. This focus on 'waves only' means we can reduce the research question a little: the number of shear-stress based stability parameters reduces to only three (for each velocity definition), as all wave-current interaction models and averaging procedures loose their significance (the difference between maximum and average is a constant factor in this case). We only keep the (maximum) shear stress according to Bijker, Grant and Madsen, and Fredsøe; these parameters differ because they use different friction factors (see Figure 2.4). In addition we can drop the Bijker-type transport formula if we consider waves only as this formula will always predict zero transport for $\tau_c = 0$.

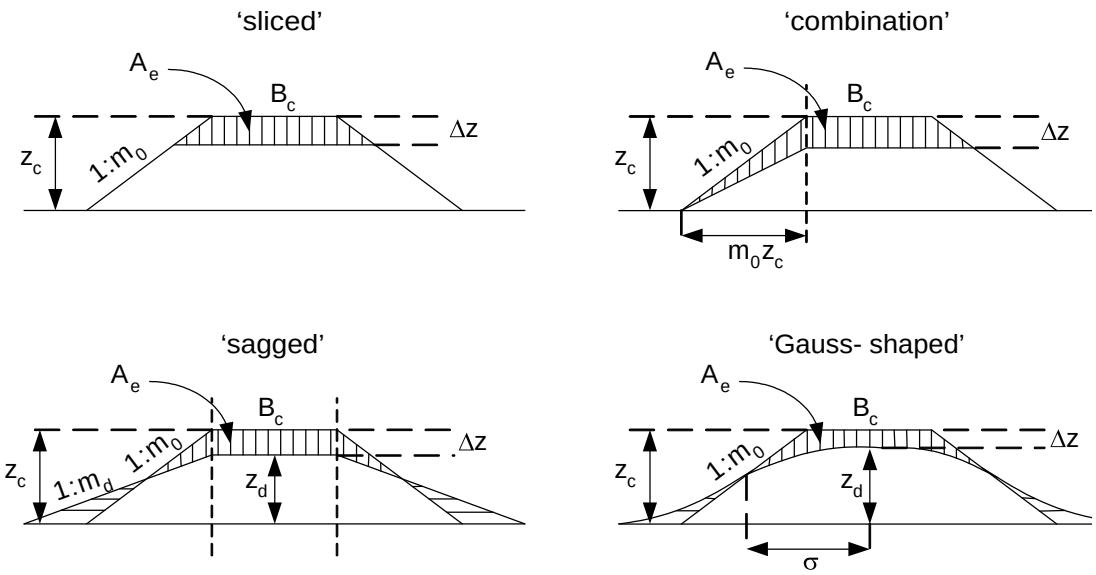

Figure 6.5 –Various damage profiles for pipeline covers

6.2.1 Prediction of structure height after damage

The reduction in crest height Δz can be calculated from the measured erosion areas ($A_e = S*d_{n50}^2$) if we assume a (schematised) profile for the damaged structure. From looking at the damage profiles reported by Lomónaco (1994) we have found four possible ways of doing so. We will test the applicability of each schematisation by comparing the calculated crest reductions to the measured ones (for the part of the dataset for which both Δz and S have been given). We will select the best method and apply that method to calculate Δz for the part of the dataset for which only S has been given.

The four possible schematisations are sketched in figure 6.5 and will be described next.

'Sliced' profile: The first schematisation is the simplest, and assumes that a slice with a constant thickness (the required Δz) is taken from the crest of the structure. We will refer to this schematisation as the 'sliced' profile. The erosion area (the hatched area in figure 6.5) can than simply be calculated as the area of a trapezoid:

$$A_e = \Delta z\left(B_c + m_0 \cdot \Delta z\right) \tag{6.5}$$

For a given boundary condition that the predicted erosion area must match the measured erosion area A_e the required crest reduction follows from the inverse:

$$\Delta z = \frac{-B_c + \sqrt{B_c^2 + 4m_0 A_e}}{2m_0} \tag{6.6}$$

When Δz is calculated for each test and compared to the measured Δz the result can be plotted as in figure 6.6, top left pane. It this plot we have used a dimensionless form, for which we have chosen the relative crest reduction $\Delta z/d_{n50}$, We see that, although the overall prediction is good, the 'sliced' schematisation appears to over-predict the measured damage; it can be seen as a safe upper limit estimation of the real crest reduction.

'Combination' profile: The over-prediction of the crest reduction with the 'sliced' profile is understandable: in this profile it is assumed that all damage occurs at the crest. Looking at the reported profiles learns that the damage also occurs on the slopes of the structure. The damage profile is usually not symmetrical: damage occurs mainly on the 'upstream' slope (in terms of the propagation direction of the waves), the stones are mainly deposited on the downstream slope. This asymmetry is reported by all researchers and probably occurs because the waves in the laboratory flume were not purely sinusoidal (even though they may originally have been intended as such). A schematisation that incorporates this effect is the 'combination' profile, see Figure 6.5, in which it has been assumed that the most upstream point of the structure does not move and that the transition point between the slope and the crest is exactly below the original transition point. The total damage area can be calculated as:

$$A_e = \Delta z B_c + \frac{1}{2}(\Delta z)^2 m_0 + \frac{1}{2} z_c m_0 \cdot \Delta z \tag{6.7}$$

The required crest reduction follows from the inverse:

$$\Delta z = \frac{-(B_c + z_c m_0 / 2) + \sqrt{(B_c + z_c m_0 / 2)^2 + 2m_0 A_e}}{m_0} \tag{6.8}$$

The results from this schematisation are given in Figure 6.6, top right pane. As can be seen, this schematisation tends to under-predict the measured crest height reductions – apparently the extent of the damage on the slopes is over-predicted by this model.

'Sagged' profile: The third schematisation allows for some damage to occur on the slopes of the structure as well, but disregards the reported asymmetry of the damage profile; it assumes that the damage profile is a symmetrical trapezoid with the same crest width B_c as the original profile, but a new height z_d and a new slope m_d. The new profile

can thus be described as a 'sagged' version of the original profile, which is why we will refer to this as the 'sagged' schematisation.

We now use two unknown parameters to describe the damaged profile (z_d and m_d) and consequently we need a second boundary condition to close the set of equations. We will do so by assuming the waves only redistribute the material, so no material is lost and the total cross sectional area of the damaged profile must be equal to the total cross sectional area of the original profile. If we call this area A_0 we have

$$A_0 = z_c\left(B_c + m_0 \cdot z_c\right) \tag{6.9}$$

for the original profile and

$$A_0 = z_d\left(B_c + m_d \cdot z_d\right) \tag{6.10}$$

for the damaged profile.

The calculation now proceeds by iteration: we assume a damaged crest level z_d and calculate the corresponding m_d. Then we can calculate the erosion area (as the area between the resulting two profiles) and see if it matches the measured erosion area. If it does not we must choose a different z_d.

The crest height reductions that were obtained in this way are plotted in figure 6.6, bottom left pane. We see that, despite the more sophisticated calculation, the results from this method are almost similar to those from the 'combination' profile.

'Gauss shaped' profile: In the final schematisation the damage profile is described by a Gauss-shaped profile with a given height z_d and a given width ('standard deviation') σ. This profile is inspired by looking at the actual shapes of the reported damage profiles, that do not show straight lines as assumed in the previous schematisations but appear to have a more 'natural' shape. The Gauss shape is described mathematically as

$$z = z_d e^{-\frac{x^2}{2\sigma^2}} \tag{6.11}$$

with the x-coordinate horizontally along the bed and x = 0 in the symmetry-axis of the structure. The calculation procedure is analogous to the 'sagged' profile with the exception that the cross sectional area of a Gauss-shaped profile is calculated as:

$$A_0 = z_d \sigma \sqrt{2\pi} \tag{6.12}$$

The erosion area follows from the area between the Gauss curve and the original profile and is calculated by a numerical procedure. The results of this schematisation are plotted in figure 6.6, bottom right pane. It is clear that this schematisation again under-predicts the measured damage, and in addition it does not work well for small amounts of damage (which is the main area of interest for a designer and thus for this research).

Conclusion: From this analysis we conclude that the more sophisticated schematisations of the damage profile, the 'sagged' profile and the 'Gauss-shaped' profile, do not work better than the cruder 'sliced' profile and 'combination' profile. As the latter two are easier to calculate (they do not require iteration) they are to be preferred.

The 'sliced' profile over-estimates the measured crest height reduction and can thus be seen as a conservative, upper limit approximation of the real value. Given all the uncertainties involved in the design of pipeline covers it is recommended to use this schematisation in practice whenever a translation from A_e to Δz must be made.

For our purposes (ie testing of the critical scour method) we need a slightly more accurate way of making this translation. We observe that the 'sliced' profile tends to

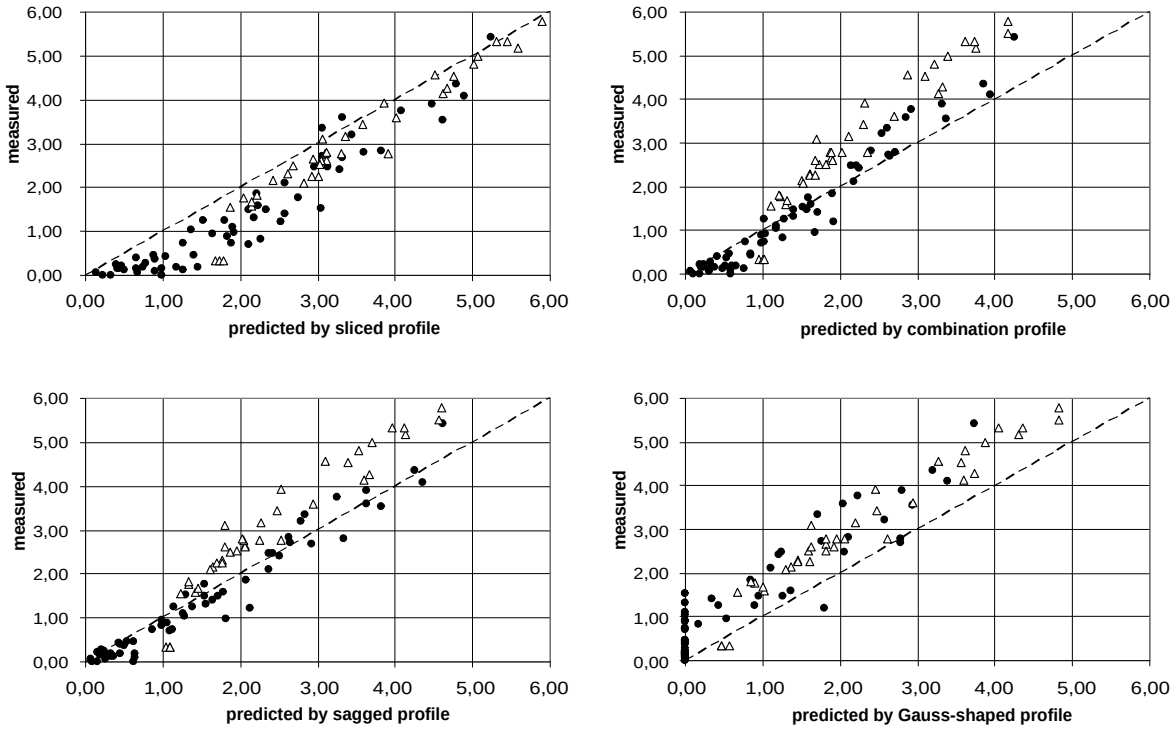

Figure 6.6 – Calculated relative crest reductions ($\Delta z/d_{n50}$) against measured values for four schematizations of the damage profile. Dots: data by Lomónaco (1994); triangles: data by Saers (2005)

over-estimate the measured Δz, whereas the 'combination' profile under-estimates it. An obvious assumption would be that the real Δz is 'somewhere in between'. In Figure 6.8 we have plotted the average value of $\Delta z/d_{n50}$ obtained from both schematisations. We can see that this average predicts the measured values reasonably well: we will use this measure to translate S to Δz for the remaining part of our dataset (the tests by Van Gent and Wallast 2001).

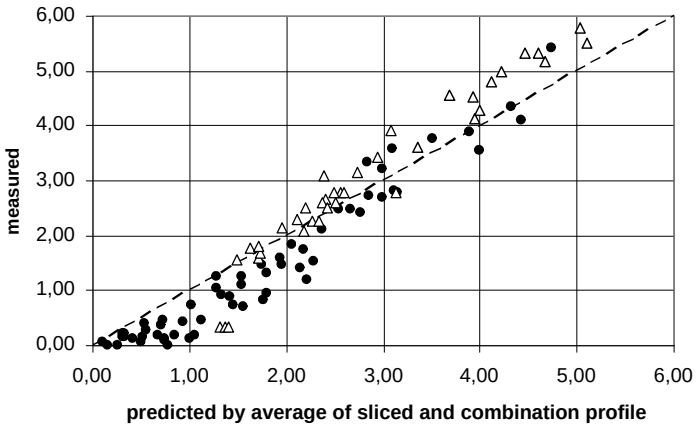

Figure 6.7 – Calculated relative crest reductions ($\Delta z/d_{n50}$) against measured values for average of 'sliced' and 'combination' damage profile.
Dots: data by Lomónaco (1994); triangles: data by Saers (2005)

6.2.2 Transport equations

Now that we have obtained the crest reductions for all tests in the combined Lomónaco – Van Gent and Wallast – Saers dataset we can proceed to analyse which transport equation is best able to predict these reductions in combination with the simple transport method or the critical scour method.

The duration *D* of each test is given, and we will estimate the scouring length as $L_s = m \cdot z_c$ (see Figure 3.20). Now we can calculate the transport rates associated with the critical scour method as

$$q_s = L_s \frac{\Delta z}{D} \tag{6.13}$$

and those associated with the simple transport method as

$$q_s = \frac{A_e}{D} \tag{6.14}$$

We can proceed to make the transport dimensionless in the classic way:

$$\Phi_q = \frac{q_s}{\sqrt{g\Delta d_{n50}^3}} \tag{6.15}$$

or in the way used in the Hallermeijer formula:

$$\Phi_{Hall} = \frac{q_s}{\omega d_{n50}^2} \tag{6.16}$$

Keeping in mind that we only analyse wave-only situations, the shear-stress based stability parameters (Ψ according to Bijker, Grant and Madsen and Fredsøe) are calculated using $\tau_{w,max} = \frac{1}{2}\rho f_w \hat{u}^2$ in combination with the appropriate friction factors (figure 2.4 – the Bijker method uses the Jonsson friction factor). The Morison-type stability parameter Θ is calculated as before (equation 6.1), neglecting the convective acceleration term as discussed in chapter 4. Finally, the velocity parameter follows from equation 4.4. For all stability parameters we will use all three velocity definitions as discussed before (see Figure 3.22). Then, for each combination we can assess the goodness-of-fit of a transport formula $\Phi = a \cdot (\text{stability})^b$. The results are given in table 6.3 (calculations performed with Microsoft Excel, see appendix 8).

The results given in this table lead to the following conclusions:

- The use of the Morison and velocity parameters works roughly just as well as most shear-stress based methods;
- There is hardly any difference between the simple transport method and the critical scour method, or between the various velocity definitions;
- A Hallermeijer-type definition of dimensionless transport works slightly better than a standard definition.

However the overall result in terms of goodness-of-fit is poor: no coefficient of determination higher than $r^2 = 0.39$ was obtained. The general conclusion must be that *no* transport formula can be found that, combined with a transport based design method, correctly predicts the crest level reductions of the near-bed structures as measured by Lomónaco (1994), Van Gent and Wallast (2001) and Saers (2005).

Given this negative conclusion, we will not proceed to analyse the tests with a combination of waves and a current.

We have seen that the critical scour method can not really be used for the design of near-bed structures in the case of wave-dominated loads. This is of course not surprising, since the method was originally developed for current-only situations. This means that we will need to look for other design methods. In the next stage of this thesis we will investigate the applicability of the 'damage profile' methods that were described in paragraph 3.6.2.

Table 6.3 –Goodness-of-fit of various stability parameters in a transport equation (r^2), in combination with a transport-based design method.
Based on data of Lomónaco (1994), Van Gent and Wallast (2001) and Saers (2005)

definition of orbital velocity	Stability parameter	Simple transport method		Critical scour method	
		Φ_q	Φ_{Hall}	Φ_q	Φ_{Hall}
$\hat{u}_0$	Ψ - Bijker	0.16	0.25	0.16	0.23
	Ψ - Grant and Madsen	0.19	0.28	0.18	0.26
	Ψ - Fredsøe	0.21	0.31	0.21	0.30
	Θ	0.21	0.31	0.22	0.31
	θ	0.23	0.33	0.23	0.32
$\hat{u}_c$	Ψ - Bijker	0.17	0.25	0.18	0.25
	Ψ - Grant and Madsen	0.19	0.28	0.19	0.27
	Ψ - Fredsøe	0.22	0.32	0.23	0.32
	Θ	0.22	0.31	0.24	0.33
	θ	0.23	0.34	0.25	0.34
$\hat{u}_{hc}$	Ψ - Bijker	0.16	0.24	0.23	0.30
	Ψ - Grant and Madsen	0.19	0.27	0.24	0.32
	Ψ - Fredsøe	0.22	0.32	0.28	0.37
	Θ	0.22	0.32	0.29	0.38
	θ	0.24	0.34	0.30	0.39

6.3 Design of pipeline covers with the damage profile method

6.3.1 The use of S in practice

A key feature of the damage profile methods is that they predict an expected amount of damage to the structure, expressed as an erosion area A_e. This erosion area can be seen as the amount of material that is eroded from a cross section, and is commonly made dimensionless as:

$$S = \frac{A_e}{d_{n50}^2} \qquad \text{(3.87 repeated)}$$

As such, this parameter S is not a very practical parameter for design purposes. A designer should have some idea, or feeling, as to what a certain value of S means in terms of damage to the structure. For comparison we can look at the design of granular armour layers on revetments (from which the use of this parameter S originates), where a value of, say, S = 2 is directly related to a qualitative assessment of the expected damage, in this case “initial damage” (CIRIA/CUR 1991).

It would be practical to have such a qualitative assessment of damage for near-bed structures as well. This can be obtained by looking at the damage profiles reported by Lomónaco (1994) and categorising them according to a visual assessment of the amount of damage. Roughly speaking, four levels of damage can be discerned:

- category 1: no damage, or rounding off of the edges. Apparently damage starts at the edges of the crest; the most unstable stones are those at the intersection of the crest and the slopes. These stones move first, but this is not considered serious damage.
- category 2: initial damage. A reduction in crest height is clearly visible and the slopes tend to flatten out a little.
- category 3: intermediate damage: Same as level 2, but the structures looks more seriously damaged. The distinction between level 2 and level 3 is not very easy to make and is solely based on arbitrary judgement.
- category 4: severe damage: the structure has completely lost its shape and it is unlikely that it still fulfils its function as a pipeline cover.

Examples from each of these four categories are given in figure 6.8. We have categorised all tests by Lomónaco (1994) in this way, both the tests with waves only and the tests with a combination of currents and waves, details of this categorisation are given in appendix 8.

When we try to relate these damage categories to the dimensionless erosion area S we get the plot given in figure 6.9 (left pane). Clearly there is some relationship between damage category and S but the distinction between the categories is not sharp: for instance the highest category 1 and the lowest category 4 profiles both occur around S = 80. A clearer relationship is obtained in the right pane of figure 6.9. This picture is based on the reasoning that the crest width of the structure should be incorporated in the definition of (dimensionless) damage. For instance, suppose there are two near-bed structures, a narrow one and a wide one, that both have a layer with a thickness of 1 stone diameter removed from their crests. One could argue that both structures are equally damaged, but the wider structure will have a larger erosion area and thus a

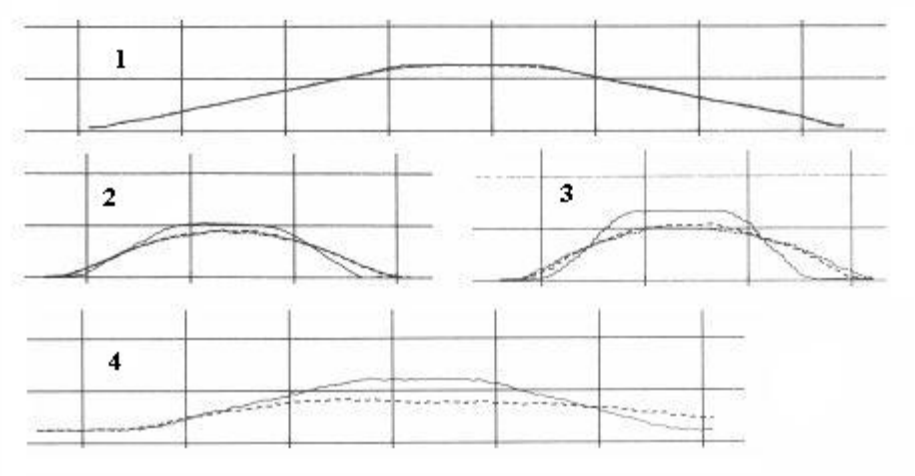

Figure 6.8 - Examples of damage categories (profiles taken from Lomónaco 1994)

larger value of S. In order to correct for this bias, we will introduce an alternative measure of dimensionless damage called S* that is defined as the erosion area per unit crest width and stone diameter.

$$S* = \frac{A_e}{B_c d_{n50}} \tag{6.17}$$

Very roughly speaking this measure S* can be seen as 'the number of stones removed as a layer from the crest of the structure'. A comparison of equation 6.17 and equation 3.87 shows that S* can be calculated as

$$S* = S \frac{d_{n50}}{B_c} \tag{6.18}$$

From the right pane of figure 6.9 we see that this measure S* gives a better indication of the expected damage. The distinction between category 2 and category 3 is still not very clear and may have to be dropped, but we can safely say that 'no damage' corresponds to S* < 1 and 'severe damage' to S* > 4.5. If we want to keep the distinction between 'initial damage' and 'intermediate damage' we can see from figure 6.9 that the boundary between these categories lies at approximately S* = 2.5. This gives a qualitative damage assessment, that may be used for design purposes (see table 6.4).

Apart from this qualitative assessment a designer could also try to relate a given S-value to 'actual damage' by calculating the corresponding reduction in crest level of the structure (and more specifically the remaining cover thickness on the pipe). As we have

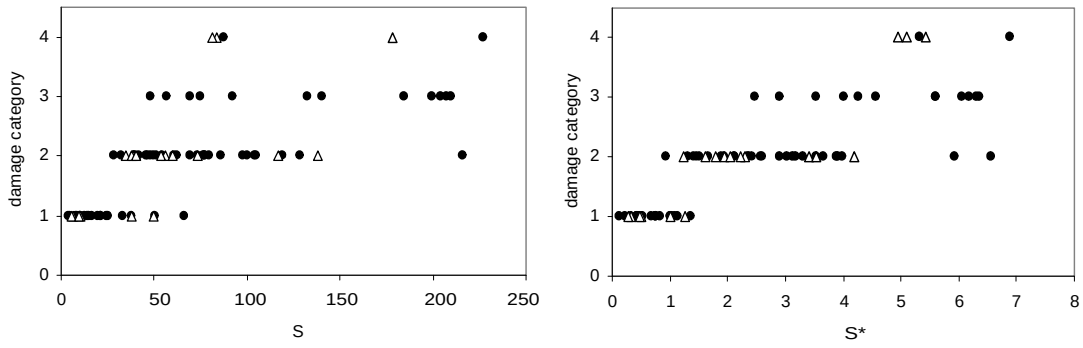

Figure 6.9 – Damage category against dimensionless erosion area

discussed in the previous paragraph we cannot do that without assuming some kind of damaged profile, for which we have seen that the 'sliced' profile (using the explicit relationship (6.6)) provides an easy and safe upper limit estimation.

Table 6.4 - Qualitative damage assessment for pipeline covers

Dimensionless erosion area per unit width	Damage assessment
$S^* < 1$	No damage or rounding off of corners
$1 < S^* < 2.5$	Initial damage
$2.5 < S^* < 4.5$	Intermediate damage
$S^* > 4.5$	Severe damage

It is emphasised here that these categories are based on a subjective assessment of the damage to the structures, obtained from looking at drawings of cross sections of the damaged structures. In reality the qualitative damage will also be related to the structure type, eg a homogeneous rubble mound or a construction with an armour layer with a thickness of $2 \cdot d_{n50}$, and categories like 'filter layer exposed' may have to be used. This leaves room for further research.

6.3.2 Prediction of S

We can now proceed to find answers to the research question we asked in chapter 4:

> *Which combination of stability parameter (the 19 parameters identified in paragraph 4.2.6), velocity definition (see Figure 3.21) and other dimensionless parameters best fits the measured erosion areas?*

This question was asked given the fact that the existing design formulas for S as put forward in literature (Van Gent and Wallast (equation 3.91), Lomónaco and Klomp

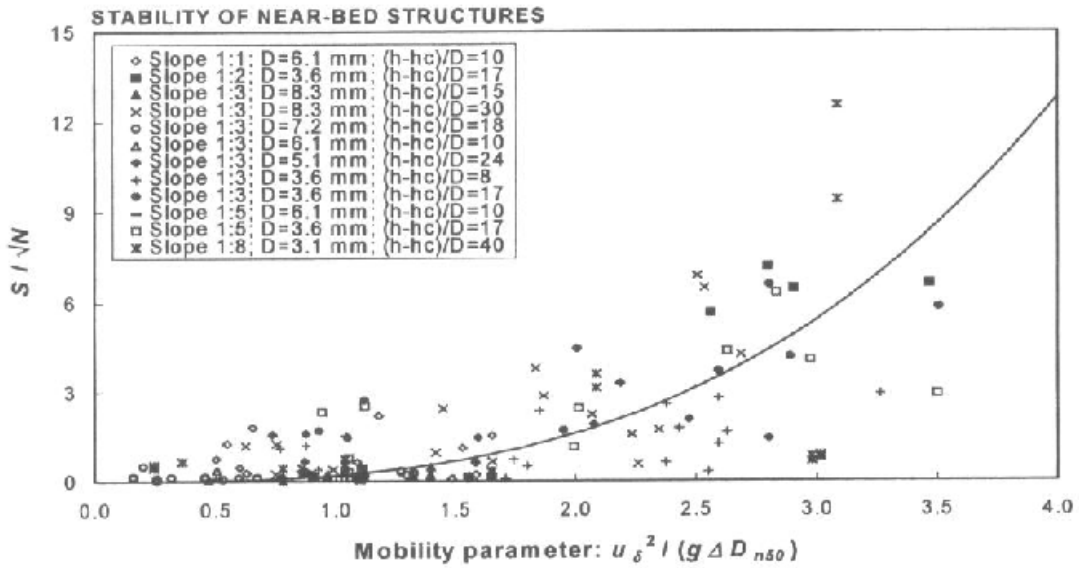

Figure 6.10 – Goodness-of-fit of Van Gent and Wallast formula (taken from Van Gent and Wallast 2001)

(equation 3.90) or Saers (equation 3.92)) contradict each other in terms of the parameters that should be included and the way the governing velocity should be defined. There is another reason why we could be interested in a new design formula, which is illustrated in Figure 6.10: the overall fit of the Van Gent and Wallast formula is poor. Van Gent and Wallast do not quantify this in terms of r^2, but we can estimate this by re-doing their analysis. A regression analysis of $S/\sqrt{N}$ on θ (with u defined as $\hat{u}_{hc}$) on the combined Lomónaco – Van Gent and Wallast data set indicates that the coefficient of determination $r^2 = 0.50$ for this fit. We will use this value as a target value for our new design formula and seek to improve this fit by including more parameters.

Just as we did in paragraph 6.2, we will first analyse the tests with waves only (which reduces the number of stability parameters) and only seek to include the current when the results are encouraging. We will use the same stability parameters as before, ie the shear stress parameters according to Bijker, Grant and Madsen, and Fredsøe, the Morison-type parameter (equation 6.1) and the velocity parameter θ; also, we try all three velocity definitions.

The fit may also be improved by including more dimensionless parameters, other than stability parameters. In this thesis we will investigate the influence of:

- **the number of waves:** N. We will leave this parameter as a 'free' parameter in the analysis, ie we will not force a dependency like $\sqrt{N}$ or log(N);

- **the structure slope**: The most obvious way to describe the effect of the structure slope is through the slope angle m_0. This parameter directly influences the stability of the stones on the slope, but it can also be seen as a measure for the fluid motion around the structure. An alternative slope parameter that is meant to describe the possible influence of the fluid acceleration around the structure is the Saers parameter: $Sa = z_c m_0/a_0$.;
- **the relative structure height**, expressed as the relative water depth h_c/h. This parameter can be seen as an indirect indicator for the type of water motion over the structure; in fact it can be seen as a flow contraction parameter. As such, it describes the degree to which the governing near-bed velocities are disturbed (ie increased);
- **the relative structure width**, in which the structure width is expressed either as the crest width B_c or the full 'footprint' width B (at the base). These parameters can be related to either the wave length L or the excursion of the orbital motion a_0. In short, this gives four possible relative structure width parameters: B_c/L, B/L, B_c/a_0, and B/a_0. These parameters can be seen as a measure of how strongly the wave 'feels' the structure, in other words how strong the interaction between the wave and the structure (and the resulting damage) will be;
- **the relative crest width:** B_c/d_{n50}. We will add this parameter since we have seen in the previous paragraph that it is useful in finding a well-defined measure of the damage (cf the difference between S and S*).

In general terms the purpose of this analysis is to find a design formula of the following form:

$$S = A \cdot (stability)^a \cdot N^b \cdot (slope\ \ factor)^c \cdot \left(rel\ \ height\right)^d \cdot \left(rel\ \ width\right)^e \cdot \left(\frac{B_c}{d_{n50}}\right)^f \tag{6.19a}$$

in which A is a constant. This means that we will have to perform a multivariate linear regression on:

$$\ln(S) = B + a\ln(stability) + b\ln N + c\ln(slope\ \ factor) + d\ln(rel\ \ height) + e\ln\left(rel\ \ width\right) + f\ln\left(\frac{B_c}{d_{n50}}\right) \tag{6.19b}$$

after which the required parameters can be calculated as explained in appendix 7. We

will use SPSS to perform this regression analysis. Since we do not know beforehand which parameters play a role in the design formula and which do not we will use a 'stepwise' regression analysis (see appendix 7).

The results from an analysis of this kind must be interpreted very carefully; it is easy to obtain trivial or non-physical models. In the present analysis we have paid special attention to:

- **completeness**: a 'stepwise' regression analysis uses purely statistical criteria to decide whether a parameter should be in the formula or not. When this leads to the omission of parameters that are absolutely necessary in the formula for physical reasons we will reject the model;
- **physical reality**: when the model predicts a relationship between the parameters that is clearly non-physical (for instance when d in (6.20) is negative indicating that the damage reduces when the load in increased) the model is rejected;
- **colinearity**: as explained in appendix 7, this is the effect that the goodness-of-fit of the model is largely determined by (implicit) correlations between the independent parameters among themselves. This is a large risk in our analysis, since we use quite a lot of dimensionless parameters that are somehow related. For instance, many of them share the fact that they have the wave length or the water depth included in them. We will use the 'tolerance' statistic to check for colinearity and reject all models for which the tolerance is below 0.60 (this in an arbitrary choice; there is no clear criterion other than that this value "should not be too low").

The procedure is as follows: for each combination of stability parameter and velocity definition we will first fit a model that includes only N and m_0 as extra parameters; these two parameters are selected because these are the only ones that can safely be assumed to be statistically independent (from each other as well as from the other parameters), so any statistical complications are ruled out. We will see this model as the base case. Then we will *separately* add h_c/h, B_c/d_{n50} and each of the four relative width parameters to the regression analysis. If none, or only one of these parameters gives an improved goodness-of-fit with respect to the base case, the analysis ends; if two or more parameters give an improved goodness-of-fit we will try all combinations of these parameters as well. Finally, the complete procedure is repeated with Sa instead of m_0 as the slope parameter.

The fit results are given in appendix 8, tables A8.1 – A8.3 and summarised in table 6.5. These tables show the best goodness-of-fit that can be obtained for each combination of

parameters, after rejecting the models that did not meet the criteria stated above. Note that we have used the *adapted* r^2 as a measure of the goodness-of-fit since we are comparing models with a different number of variables.

Table 6.5 –Goodness-of-fit of various models to predict S
Based on data of Lomónaco (1994), Van Gent and Wallast (2001) and Saers (2005)

definition of orbital velocity	stability parameter	adjusted r^2 of best model	parameters in model
$\hat{u}_0$	θ	0.61	N, m_0, B_c/d_{n50}
	Θ	0.58	N, m_0, B_c/d_{n50}
	Ψ - Bijker	0.50	N, B_c/d_{n50}
	Ψ - Grant and Madsen	0.53	N, B_c/d_{n50}
	Ψ - Fredsøe	0.59	N, m_0, B_c/d_{n50}
$\hat{u}_c$	θ	0.62	N, m_0, B_c/d_{n50}
	Θ	0.59	N, m_0, B_c/d_{n50}
	Ψ - Bijker	0.52	N, m_0, B_c/d_{n50}
	Ψ - Grant and Madsen	0.55	N, m_0, B_c/d_{n50}
	Ψ - Fredsøe	0.60	N, m_0, B_c/d_{n50}
$\hat{u}_{hc}$	θ	0.64	N, m_0, B_c/d_{n50}, h_c/h
	Θ	0.61	N, m_0, B_c/d_{n50}, h_c/h
	Ψ - Bijker	0.55	N, B_c/d_{n50}, h_c/h
	Ψ - Grant and Madsen	0.56	N, B_c/d_{n50}, h_c/h
	Ψ - Fredsøe	0.62	N, m_0, B_c/d_{n50}, h_c/h

This table shows that:

- All models include the number of waves, most include the structure slope as well. The relative width parameters are not included in any model; neither is the Saers parameter. The relative height parameter h_c/h is only included in combination with the velocity defined as $\hat{u}_{hc}$;
- The overall goodness-of-fit does improves compared to the Van Gent and Wallast formula (r^2 = 0.50), but significant improvements are only obtained with the velocity parameter, the Morison parameter and the shear-stress based parameter according to Fredsøe;
- The differences between the results from the various wave-current interaction models are small; this can be explained by the fact that we have looked at waves only;

- The best results are obtained with the velocity defined at the crest of the structure $\hat{u}_{hc,}$ but the differences between the results from the various velocity definitions are small;
- Then still, the goodness-of-fit is moderate at best (highest $r^2 = 0.64$).

Now, which model is the best? To answer that question we will follow the same procedure as we did in the previous paragraph; we will select a few models based on their goodness-of-fit and compare them on their ability to predict the damage not only for the scale model tests with waves only but also for the scale model tests with a combination of currents and waves. The selected models are:

- **Case 1: The velocity parameter in combination with $\hat{u}_{hc}$.** This model is selected because it has the highest goodness-of-fit. Its full form (as follows from the full SPSS output – see the enclosed CD-ROM) is:

$$S = 0.34 \cdot \theta_{hc}^{1.24} \cdot N^{0.28} \cdot m_0^{-0.45} \cdot \left(\frac{h_c}{h}\right)^{1.81} \cdot \left(\frac{B_c}{d_{n50}}\right)^{1.02} \tag{6.20}$$

  The velocity parameter θ has no analogy for the combination of waves and a current, so the only way to include the currents in this case is to neglect the current altogether. This is also done by Van Gent and Wallast (2001) in their analysis.

- **Case 2: The velocity parameter in combination with $\hat{u}_{c:}$** This model has a goodness-of-fit that is only slightly lower than case 1, but it contains fewer parameters and could therefore be preferred:

$$S = 0.32 \cdot \theta_c^{1.19} \cdot N^{0.28} \cdot m_0^{-0.45} \cdot \left(\frac{B_c}{d_{n50}}\right)^{1.04} \tag{6.21}$$

  Again, the inclusion of the current in this case comes down to neglecting the current altogether.

- **Case 3: The shear stress according to Fredsøe in combination with $\hat{u}_{hc}$**: This model also has only a slightly lower fit than case 1; in addition it provides and interesting alternative approach as it is shear-stress based:

$$S = 230 \cdot \left(\Psi_{F,\max,hc}\right)^{1.48} \cdot N^{0.28} \cdot m_0^{-0.42} \cdot \left(\frac{h_c}{h}\right)^{2.10} \cdot \left(\frac{B_c}{d_{n50}}\right)^{1.03} \tag{6.22a}$$

This design formula was fitted on the scale model data for waves only, and the wave shear stress used is the maximum wave shear stress (equivalent to the standard way of defining wave shear stresses, see eg equation 2.28). This means that if we seek to include the current we will have to replace the shear stress in (6.22a) by the *maximum* combined shear stress. Alternatively we can try to use the average combined shear stress, but in that case we will need to use the average shear stress in the 'waves only' case as well, and rewrite (6.22a) using $\tau_{av} = ½\tau_{max}$:

$$S = 642 \cdot \left(\Psi_{F,av,hc}\right)^{1.48} \cdot N^{0.28} \cdot m_0^{-0.42} \cdot \left(\frac{h_c}{h}\right)^{2.10} \cdot \left(\frac{B_c}{d_{n50}}\right)^{1.03} \qquad (6.22b)$$

The calculation of the combined shear stress proceeds as described in chapter 3. However, for near-bed structures that still leaves two possible ways to define the current velocity: the structure causes a contraction in the flow and thus the (depth-averaged) velocity over the crest is increased compared to the (depth-averaged) velocity in front of the structure. We can choose to correct for this phenomenon (ie use $u = u_{da} \cdot (h/h_c)$, or not (ie use $u = u_{da}$). In the present analysis we will try both methods.

This gives rise to four different versions of case 3:

Case 3a: maximum combined shear stress and increased current velocity

Case 3b: average combined shear stress and increased current velocity

Case 3c: maximum combined shear stress and undisturbed current velocity

Case 3d: average combined shear stress and undisturbed current velocity

We note that, despite the high r^2 values in table 6.5, we have not selected any models based on the Morison parameter. This is essentially a generalisation of the velocity parameter; given the fact that it does not perform significantly better than the velocity parameter (in fact, slightly worse) and given the uncertainties associated with the Morison method (see chapter 4) we will not treat this parameter separately.

The results of this analysis, in terms of scatter plots of the predicted damage S against the measured damage S is given in figure 6.11. In these plots, the degree in which the accuracy of the design formula for a combination of currents and waves matches the accuracy for waves only can be judged from the degree in which the data points for the model tests with a combination of waves and a current (open circles) lie within the scatter of the data points for the model tests with waves only (dots).

This figure shows that using the shear stress method (case 3) does not work very well in the combined case, regardless of whether the average or the maximum shear stress is used, or the increased or undisturbed current velocity. Neglecting the currents altogether in combination with a velocity parameter, however, does. This is in line with the original conclusion of Van Gent and Wallast (2001). Once again we emphasise here that the data set on which this conclusion is based only includes relatively weak currents; in

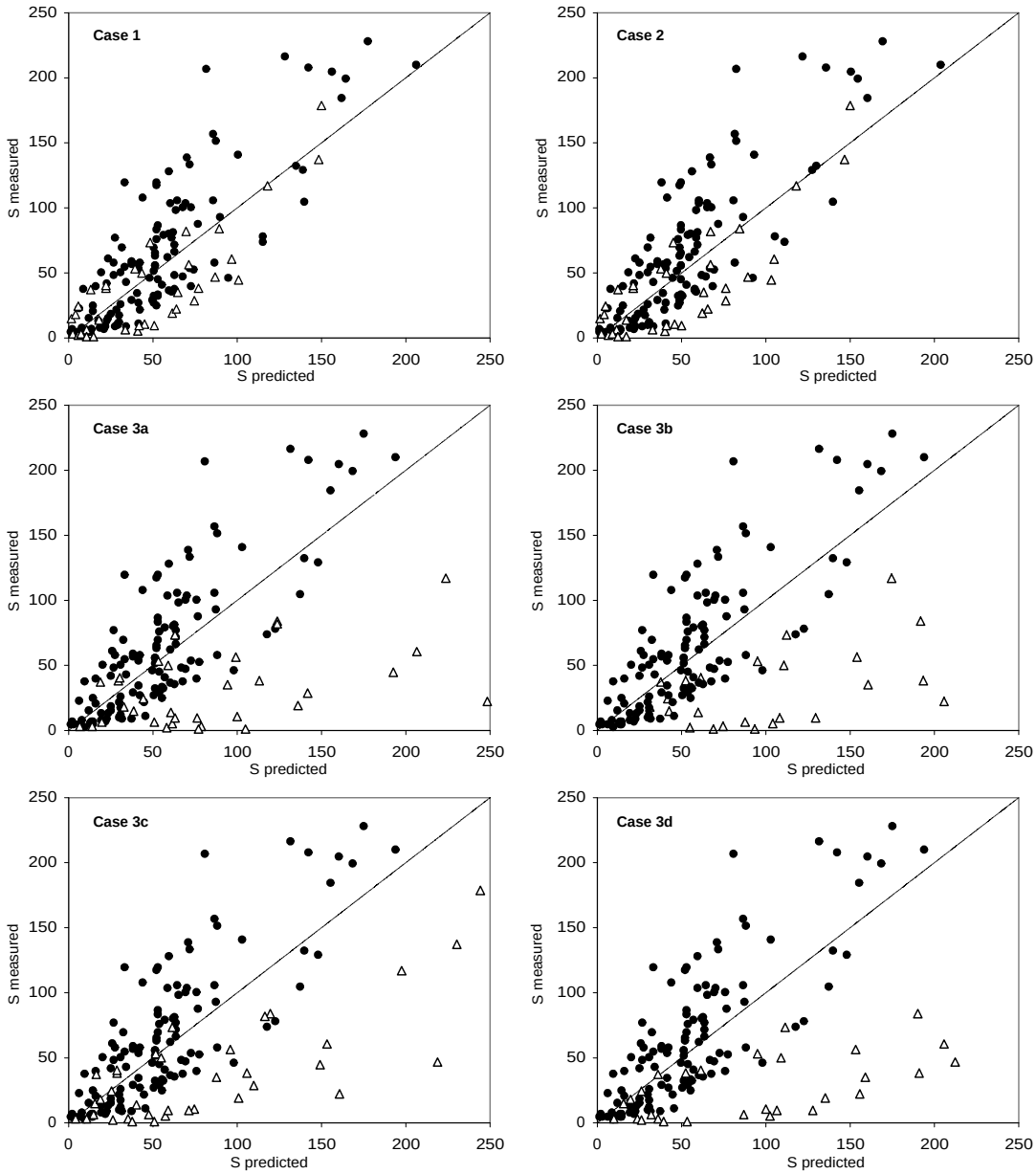

Figure 6.11 – Predicted dimensionless erosion area (equations 6.20 – 6.22) against measurements. Dots: waves only. Triangles: current and waves

terms of the current strength parameter X (defined by Soulsby, see chapter 3) we have approximately $X < 0.2$.

So, at this point we drop the shear-stress based method from our analysis and continue only with the velocity-based methods. Before we make a choice between case 1 and case 2 we will see if we can improve the goodness-of-fit further.

So far we have used H_s and T_m as wave parameters. It could be argued that the damage to a structure is caused by the highest waves in the wave field, in which case $H_{1\%}$ and T_p would be better parameters to characterise the load on the structure. If we re-calculate θ_{hc} and θ_c (for case 1 and 2, respectively) using $H_{1\%}$ (equation 2.38) and T_p instead we get the results given in Table 6.6.

Table 6.6 –Goodness-of-fit of selected models to predict S
Wave parameters based on $H_{1\%}$ and T_p

Case	definition of orbital velocity	stability parameter	adjusted r^2 of best model	parameters in model
1	$\hat{u}_{hc}$	θ	0.68	N, m_0, B_c/d_{n50}
2	$\hat{u}_c$	θ	0.66	N, m_0, B_c/d_{n50}

We see that the goodness-of-fit improves somewhat and that the dependency of S on h_c/h in case 1 disappears (this may be explained by considering that the conversion factor from H_s to $H_{1\%}$ is dependent on water depth, so the water depth is now implicitly present in $\hat{u}$ and thus θ).

A second possible improvement of the goodness-of-fit is inspired by the observation that the exponent of (B_c/d_{n50}) in equations 6.20 and 6.21 is very close to 1. This suggests that S* could be a better way to express the damage than S (divide both sides of the equation by (B_c/d_{n50}) and use the definition of S*, equation 6.17). If we re-do the regression analysis with S* as the dependent parameter (keeping $H_{1\%}$ and T_p as wave parameters) we get the results given in Table 6.7.

Table 6.7 –Goodness-of-fit of selected models to predict S*
Wave parameters based on $H_{1\%}$ and T_p

Case	definition of orbital velocity	stability parameter	adjusted r^2 of best model	parameters in model
1	$\hat{u}_{hc}$	θ	0.73	N, m_0
2	$\hat{u}_c$	θ	0.71	N, m_0

We see that the goodness-of-fit has improved even further. There is still hardly any difference between the two methods in terms of r^2, simplicity, physical reality or any

other criterion that we used before, so will make our final choice simply for the model with the highest goodness-of-fit, which is case 1. In its final form the design formula becomes:

$$\frac{S^*}{N^{0.3}} = 0.048 \cdot \left(\theta_{hc\ 1\%}\right)^{1.6} \cdot m_0^{-0.6} \tag{6.23}$$

A more traditional scatter plot of this formula against the data set is given in figure 6.12 along with a similar plot for the Van Gent and Wallast formula. We see that although the fit is improved, the scatter is still considerable. The data points in this plot are for the full Van Gent and Wallast – Lomónaco – Saers data set (waves and current as well as waves only, but excluding all tests with breaking waves), which explains some of the differences with figure 6.10 which is based on the data of Van Gent and Wallast and Lomónaco only.

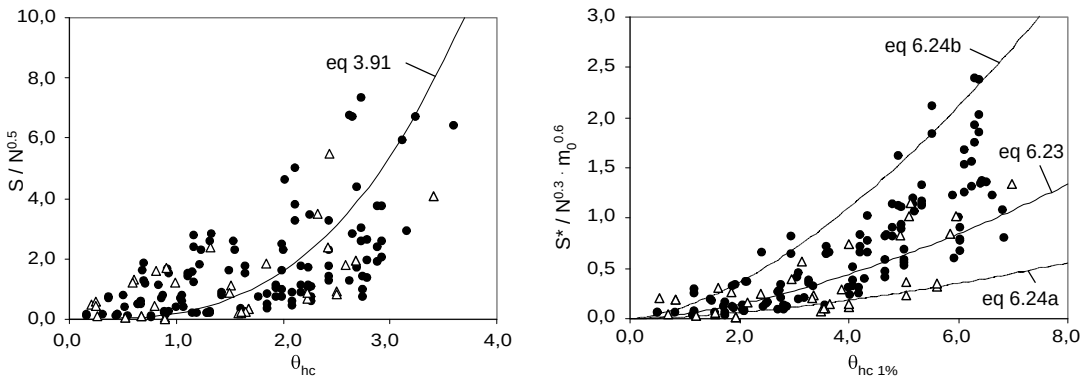

Figure 6.12 – Existing design formula (Van Gent and Wallast 2001) and new design formula for S. Dots: waves only. Triangles: current and waves

Figure 6.12 also shows the confidence bounds of the new design formula. In principle these could be obtained from the standard errors of the regression analysis (given by SPSS), but in this research we have opted a for a simpler approach. For the upper bound we have raised the constant in equation 6.23 until 90% of the measured values were lower than the predicted value, keeping all other fit parameters (exponents) constant. Similarly, lowering the constant until 90% of the measured values were higher gives the lower boundary. This gives:

$$\text{lower bound: } \frac{S^*}{N^{0.3}} = 0.02 \cdot \left(\theta_{hc\ 1\%}\right)^{1.6} \cdot m_0^{-0.6} \tag{6.24a}$$

$$\text{upper bound: } \frac{S^*}{N^{0.3}} = 0.12 \cdot \left(\theta_{hc\ 1\%}\right)^{1.6} \cdot m_0^{-0.6} \qquad (6.24b)$$

This closes our analysis of the prediction of damage to a pipeline cover using the dimensionless erosion area S. A final remark can be made on the time-dependency: our regression analysis shows that S ~ $N^{0.3}$, which is somewhere in between the views expressed by Van Gent and Walllast (S ~ $N^{0.5}$) and Saers (S ~ log N). This is further illustrated in Figure 6.13.

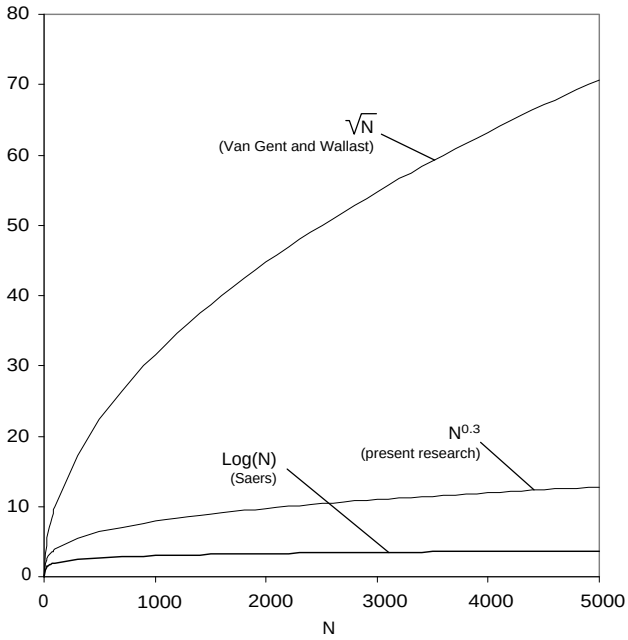

Figure 6.13 – Time dependency of damage according to various studies

6.3.3 Conclusions

This paragraph briefly summarises the main findings considering the design of pipeline covers with the damage profile method:

The damage to a pipeline cover can best be predicted by the following formula:

$$\frac{S^*}{N^{0.3}} = a \cdot \left(\theta_{hc\ 1\%}\right)^{1.6} \cdot m_0^{-0.6} \qquad (6.23)$$

The most likely value for the model constant is a = 0.048, the upper bound is a = 0.12, the lower bound is a = 0.02. In this formula and $\theta_{hc\ 1\%}$ is a stability

parameter based on the near-bed orbital velocity calculated with $H_{1\%}$ and T_p assuming that the water depth is equal to h_c everywhere.

In the case of a combination waves and a weak current ($\tau_c / (\tau_c + \hat{\tau}_w) < 0.2$) the influence of the current can be neglected.

Once S has been calculated a qualitative assessment of the damage to the structure can be found in table 6.4.*

When an quantitative estimate of the reduction of the crest level is required, a conservative estimate can be obtained assuming that a slice with a constant thickness is removed from the crest of the structure:

$$\Delta z = \frac{-B_c + \sqrt{B_c^2 + 4m_0 A_e}}{2m_0} \tag{6.6}$$

The approximate range of validity for formula (6.23) is $0.5 < \theta_{hc\,1\%} < 8$. The ranges of the other (structural) parameters are given in table 5.2 and 5.3. Application of (6.23) outside this range of validity is not recommended.

6.4 Design of near-bed structures with the critical stability approach

The previous paragraphs have been devoted to the damage-based design of near-bed structures, and we have explored various ways of expressing and calculating the damage to a structure. In the present design practice a completely different approach is taken: the stone size needed for a structure is determined with a critical stability calculation. In this paragraph we will use our datasets to briefly investigate the validity of this approach, and to answer some practical questions.

For horizontal bed protections the method explained in Chapter 2 is commonly followed: for current only it is recommended (CIRIA/CUR 1991) to use $\Psi_{cr} = 0.030$; for waves only it is recommended to use either $\Psi_{cr} = 0.030$ in combination with the average shear stress or $\Psi_{cr} = 0.055$ in combination with the maximum shear stress. For a combination of waves and a current the recommendations are less clear; we can use the results of Bijman's tests to shed some light on these matters. This is done in paragraph 6.4.1.

For pipeline covers the the stability of a single stone in the structure is calculated as if the stone were in a horizontal bed protection (it is assumed that $h = h_c$ everywhere), Commonly, the stability parameter is either based on the average shear stress according

to Bijker (CIRIA/CUR method: $\tau_{wc} = \tau_c + \frac{1}{2}\tau_w$) with $\Psi_{cr} = 0.03$, or the software program BPP is used in which case the stability parameter is based on the average shear stress under half a wave period according to Bijker (see chapter 2), also with $\Psi_{cr} = 0.03$. In the case of irregular waves, BPP uses $H_{1\%}$. The validity of this approach is examined in paragraph 6.4.2, along with answers to questions like: "what should the value of Ψ_{cr} be should we use the velocity at the crest or at the bed?".

6.4.1 Design of horizontal bed protections with the critical stability approach

In our analysis of the Bijman data for horizontal bed protections we have used 18 different stability parameters. For each stability parameter we can obtain a critical value by plotting it against the measured transport rates and (linearly) extrapolating the transport to zero; this is equivalent to the way in which Shields originally derived his critical mobility parameter (Shields 1936). An example of this procedure (for the CIRIA/CUR method) is given in figure 6.14.

In mathematical terms we can find the critical value of a stability parameter by fitting a regression line directly onto the Φ_q,Ψ points (so not onto the log-transformed data points as we did earlier). This gives a linear equation $\Phi_q = a\cdot\Psi + b$; the critical value of Ψ can now simply be found as the intersection of this line and the Ψ-axis by letting $\Phi_q = 0$ and solving for Ψ; this gives $\Psi_{cr} = -b/a$. This calculation has been performed in Microsoft Excel; the results are given in appendix 8 and summarized in table 6.8.

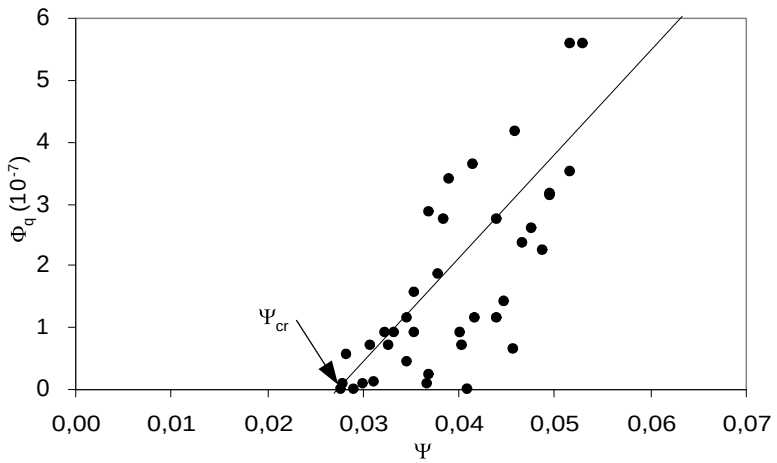

Figure 6.14 – Example of linear extrapolation to obtain Ψ_{cr}

Table 6.8 - Critical values of various stability parameters
Based on data of Bijman (2000)

Model		Ψ_{cr}
Ψ - No WCI	Maximum	0.034
	Average in current direction	0.010
	Average over full period	0.018
	Average over half period	0.018
Ψ - Bijker	Maximum	0.076
	Average in current direction	0.027
	Average over full period [a)]	0.029
	Average over half period [b)]	0.053
Ψ - Grant and Madsen	Maximum	0.039
	Average in current direction	0.018
	Average over full period	0.023
	Average over half period	0.034
Ψ - Fredsøe	Maximum	0.036
	Average in current direction	0.014
	Average over full period	0.017
	Average over half period	0.028
Θ		-0.603
θ		-0.526
Notes:	a) CUR/CIRIA method	
	b) BPP method	

From this table we see that:

- The critical values for the velocity parameter and the Morison parameter (θ and Θ) are negative, which is of course non-physical. This is caused by the large scatter in the plots for these stability parameters (note the very low r^2 values in table 6.2) and is yet another illustration that these parameters are not suitable for design purposes;
- The critical stability parameter for the CIRIA/CUR method is Ψ_{cr} = 0.029 which is close to the 'theoretical' value Ψ_{cr} = 0.030. This is promising and gives some confidence in the calculation procedure;
- An important conclusion to draw from this analysis is that the critical value of the stability parameter is strongly dependent on the wave-current interaction model that is used and on the way in which the resulting shear stress is calculated. Methods that use, for instance, a maximum shear stress will predict higher shear

stresses than methods that use an average shear stress and therefore require a higher critical stability parameter as well.

In practice there is some discussion on what the value of the critical stability parameter should be when the software programme BPP is used. Should it be $\Psi_{cr} = 0.030$ as in the CIRIA/CUR method, or can it be higher? Table 6.10 seems to point to the conclusion that when we use the BPP method we may use a higher critical stability parameter than when we use the CIRIA/CUR method; therefore the present design practice to use $\Psi_{cr} = 0.030$ in BPP seems unjustified. However, we must keep in mind that the present analysis is valid only in the cases that we have a combination of waves and a current. In the limit case, for current only, both the CIRIA/CUR method and the BPP method predict the same shear stress ($\tau = \tau_c$, cf equations 2.34 and 2.37 with $\hat{\tau}_w = 0$) and would therefore need the same critical stability parameter ($\Psi_{cr} = 0.03$). So we see that, for the BPP method, the value of the critical stability parameter appears to be dependent on the situation, and perhaps on the relative current strength; whereas for the CIRIA/CUR method we always have $\Psi_{cr} = 0.030$. This is a very useful property in practice, and since the overall goodness-of-fit fit of the both methods in a transport equation is comparable (see table 6.1) there is no reason in that aspect to prefer one over the other. Therefore we arrive at the following conclusion:

When a critical stability approach is used for the design of horizontal bed protections, it is best to calculate the combined wave-current shear stress with the CIRIA/CUR method ($\tau_{wc} = \tau_c + ½\,\hat{\tau}_w$) in combination with $\Psi_{cr} = 0.03$.

6.4.2 Design of pipeline covers with the critical stability approach

The validity of the critical stability approach for the design of pipeline covers can be assessed with the help of our dataset. We will do so by calculating the stability parameters for each model test as we did before (for H_s and T_m and the three different velocity definitions) and plotting these against the qualitative damage categories as we defined in paragraph 6.3.1. Since we only have defined these damage categories for the test performed by Lomónaco we can only use part of the dataset. The idea is that if there is a critical value of the stability parameter, we should see a clear distinction between category 1 (no damage) and category 2 (initial damage) occurring at that value. We will do this analysis for waves only (to get the general picture), as well as for the combination of waves and a current (but only for the CIRIA/CUR method and the BPP methods as these are the two methods used in the present design practice; we have only used the undisturbed current velocity u_{da} here and not the increased velocity $u_{da}\cdot(h/h_c)$ in order to avoid having to test too many combinations).

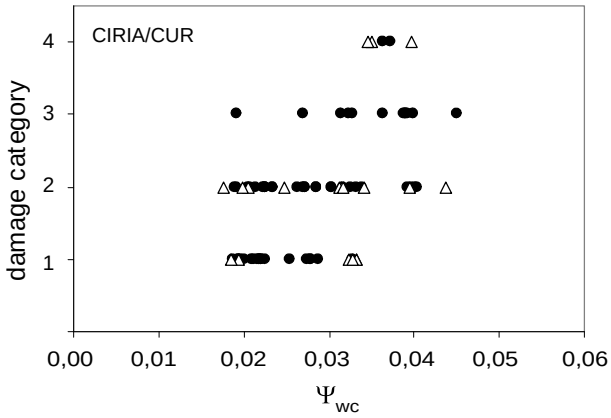

Figure 6.15 - Typical example of relationship between stability parameter and qualitative damage category, for $\hat{u}_{hc}$, H_s and T_m. Dots: tests with waves only. Triangles: tests with current and waves

These plots are given in appendix 8. A typical example (for the CIRIA/CUR method and the velocity defined as $\hat{u}_{hc}$) is given in figure 6.15. As can be seen from these plots there is no relationship whatsoever between the stability parameter and the damage category for any wave-current interaction model or velocity and roughness definition. Apparently there is no relationship between the stability of a single stone and the stability of the structure as a whole. This means that the critical stability approach is not a good design method for near-bed structures.

A second thing that can be seen from the Figure 6.15 (and the figures in appendix 8) is that there are many model tests which resulted in some damage (categories 2, 3 or 4) for Ψ-values less than the commonly used critical value Ψ_{cr} = 0.030. This could be seen as an indication that this value is not safe, but it must be borne in mind that the values in figure 6.15 were obtained using H_s and T_m. When we re-do the calculation with $H_{1\%}$ and

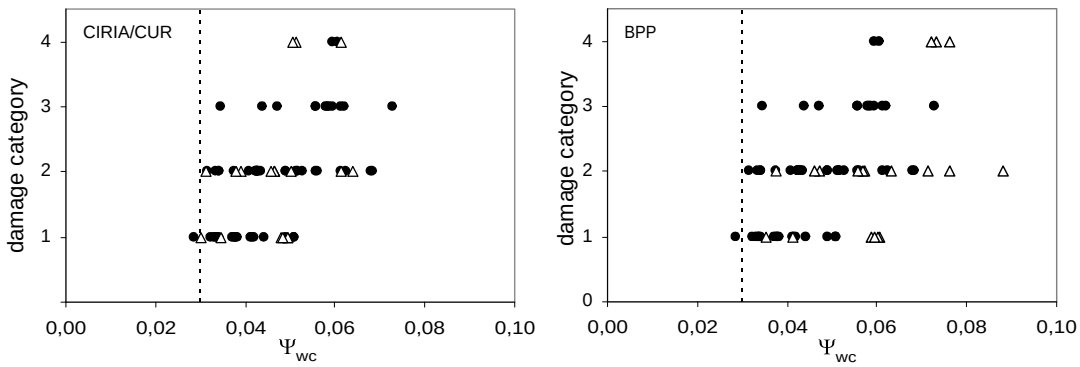

Figure 6.16 - Relationship between stability parameter and qualitative damage category with $\hat{u}_{hc}$, $H_{1\%}$ and T_n. Dots: tests with waves only. Triangles: tests with current and waves

T_p (as BPP does) we get the picture shown in figure 6.16 (for the CIRIA/CUR method and the BPP method, both with the velocity defined as $\hat{u}_{hc}$). Now we see that, although the overall correlation does not improve, the Ψ-values for the damage categories 2, 3 and 4 do lie above $\Psi_{cr} = 0.030$. We note that we only get these results if we define the velocity as $\hat{u}_{hc}$, for the other velocities we still get Ψ-values below $\Psi_{cr} = 0.030$.

Despite our conclusion that no critical stability parameter exists we can observe in figure 6.16 that for the CIRIA/CUR method the lowest Ψ-value for which we find a category 2 damage is indeed roughly $\Psi = 0.030$. So, in very broad terms we could say that the use of Ψ_{cr} could be correct, but very conservative as there are many model tests for which no damage occurred (category 1) that have $\Psi > 0.030$. For the BPP method we see the same Ψ-value of roughly 0.030. This confirms our conclusion from paragraph 6.4.1 that the critical value of the stability parameter for the BPP method is not well defined and may depend on the situation; in contrast, for the CIRIA/CUR method the use of $\Psi_{cr} = 0.030$ seems to be universal.

From this brief analysis we can conclude that:

> *The stability of a single stone cannot be related to the stability of the near-bed structure as a whole, so the critical stability method is strictly speaking not a suitable design method for these type of structures, no matter which wave-current interaction model is used, or in which way the orbital velocity is defined.*
>
> *However, if we do want to use the method (for practical reasons and as a conservative upper limit to the required stone size) we must use the 1%-exceedance wave height $H_{1\%}$ (equation 2.38) and T_p in combination with the orbital velocity at the crest $\hat{u}_{hc}$; the use of the significant wave height H_s and T_m, or other velocity definitions, seriously under-predicts the governing shear stresses. Again, the use of the CIRIA/CUR method ($\tau_{wc} = \tau_c + \frac{1}{2}\hat{\tau}_w$) in combination with $\Psi_{cr} = 0.030$ is recommended*

.

7 Conclusions

This chapter summarises and discusses the main results from the present study; the conclusions will be formulated in terms of answers to the research questions. First we will answer the specific research questions formulated in chapter 4. After that we will discuss the general research goal set in chapter 1.

7.1 Answers to the specific research questions

7.1.1 The design of horizontal bed protections with a transport-based method

question: *Which combination of transport formula (Paintal-type or Bijker-type) and stability parameter (the 18 parameters identified in paragraph 4.2.6) best fits the transport rates measured by Bijman?*

answer: Purely based on a goodness-of-fit analysis for transport rates of rock under a combination of waves and currents, we found that in principle both a Paintal-type formula and a Bijker-type formula can be used. A choice between them was made based on their general applicability: not only for the combination of waves and currents but also for the limit case 'current only'. Then it turns out that the Bijker-type formulas that were fitted for a combination of currents and waves do *not* match the measured transport rates for currents only, whereas the Paintal-type formulas do.

When a Paintal-type formula is used, we have found that stability parameters based on shear stresses give far better results than other (ie Morison and velocity) stability parameters. We believe that this is due to the fact that both the Morison parameters and the velocity parameters only relate to the wave-induced motion; apparently they underestimate the influence of the current. Furthermore, the applicability of the formula depends to a large extent on the wave-current interaction model that is used. In general we can say that the more complex models give better results than the simpler ones. Also, it turns out that the maximum combined shear stress is not a good indicator for

transport; instead, the average shear stress in the direction of the current appears to be the best parameter to use.

In particular we have found that the Paintal formula (corrected by Mosselman and Akkerman (1998)) as originally derived to predict transport of rock by currents only:

$$\Phi_q = 3 \cdot 10^7 \cdot \Psi^{8.9} \qquad \text{for } \Psi < 0.05 \tag{3.77}$$

can also be used to predict transport of rock by a combination of currents and waves, provided that the combined bed shear stress is calculated as the average shear stress in the direction of the current according to Fredsøe (1984).

In design practice, the average shear stress in the direction of the flow according to Fredsøe can best be calculated with the aid of the parameterisation by Soulsby (1993), see appendix 2. (The 'mean' shear stress that follows from this method is the desired average shear stress in the direction of the current).

This Paintal-type formula predicts zero transport for wave-only situations. Physically speaking this means that there is always a current needed, no matter how weak, to actually transport the stones. As discussed previously, transport under waves only is a completely different phenomenon: stones will be moved backwards and forwards under each half wave cycle, but the net transport will indeed be zero (unless the waves are asymmetrical). The magnitude of this half-cycle transport cannot be predicted with a Paintal-type formula; instead the formulas by Hallermeijer (3.81) or Madsen and Grant (3.80) may be used for a first estimation, keeping in mind that the typical dimensions of stones used in near-bed structures is officially (well) beyond the limits of applicability of these formulas.

7.1.2 The design of pipeline covers with a transport based method

Question: *Which combination of transport formula (Paintal-type, Bijker-type or Hallermeijer-type), stability parameter (the 18 parameters identified in paragraph 4.2.6) and velocity definition (see Figure 3.22) best fits the transport rates associated with a transport-based design method (Critical scour method or simple transport method)?*

Answer: The crest level reductions of the near-bed structures as measured by Lomónaco (1994), Van Gent and Wallast (2001) and Saers (2005) could not be related at all to a transport-based design method; we conclude that neither the critical scour method nor the simple transport method is a suitable method for the design of pipeline covers. Instead, these designs must be made with a damage profile method.

7.1.3 The design of pipeline covers with the damage profile method

Question 1: *Which combination of stability parameter (the 18 parameters identified in paragraph 4.2.6), velocity definition (see Figure 3.22) and other dimensionless parameters best fits the measured erosion areas?*

Question 2: *Once we know the value of the dimensionless erosion area S, how can we use this value to obtain a practical assessment of the damage to the structure?*

Answer to question 1: We have tried many dimensionless parameters in our regression analysis to see if inclusion of these parameters in a design formula would improve its fit on the test data. For most parameters, including the dimensionless structure height h_c/h, the dimensionless structure width (B_c/L, B_c/a_0, B/L or B/a_0) and the Saers parameter $z_c m_0/a_0$ we found that this was not the case.

In the end we found that the dimensionless erosion area S was only dependent on the number of waves N, the side slope m_0, the dimensionless crest width B_c/d_{n50} and the velocity parameter θ. The best way to express the velocity turned out to be $\hat{u}_{hc}$: the orbital velocity at the crest of the structure, as if the water depth is equal to h_c everywhere. This is in line with the observation of Lomonaco *et al* (2005) and the suggestion by Van Gent and Wallast (2001). We also found that the fit of the design formula improved if the orbital velocity was calculated using $H_{1\%}$ and T_p as wave parameters instead of H_s and T_m. This can be seen as a suggestion that the highest waves in the wave field are mainly responsible for the damage.

Our analysis has led to the following design formula:

$$\frac{S^*}{N^{0.3}} = a \cdot \left(\theta_{hc\ 1\%}\right)^{1.6} \cdot m_0^{-0.6} \tag{6.23}$$

The most likely value for the model constant is a = 0.048, the upper bound is a = 0.12, the lower bound is a = 0.02.

In this formula S* is the dimensionless erosion area per unit of crest width:

$$S^* = \frac{A_e}{B_c d_{n50}} \tag{6.17}$$

and $\theta_{hc\ 1\%}$ is the velocity parameter:

$$\theta_{hc\ 1\%} = \frac{\left(\hat{u}_{hc\ 1\%}\right)^2}{g\Delta d_{n50}} \tag{4.4}$$

$$\hat{u}_{hc\ 1\%} = \pi \frac{H_{1\%}}{T_p} \frac{1}{\sinh\left(k_c h_c\right)} \tag{2.29}$$

$$\frac{2\pi}{T_p} = \sqrt{g k_c \tanh(k_c h_c)} \qquad \text{(local dispersion relation)} \tag{5.4}$$

$$H_{1\%} = H_s \frac{1.52}{\sqrt[3]{1 + \frac{H_s}{h}}} \tag{2.38}$$

In the case of a combination waves and a weak current ($\tau_c / (\tau_c + \hat{\tau}_w) < 0.2$) the influence of the current can be neglected. Definitions of the parameters used in these formulae can be found in Figure 3.20 and Figure 3.21. It is remarked that more recent formulas for $H_{1\%}$ exist than the one use in the present research; the method by Battjes and Groenendijk (2000) is recommended.

A case study (Santander outfall) based on prototype measurements (see appendix 9) shows that both the Van Gent and Wallast formula and the new design formula can well be used to predict the damage to a structure.

Answer to question 2: Once S* has been calculated a qualitative assessment of the damage to the structure can be found in table 6.4. However, the case study (appendix 9) indicates that the values in this table may well be too high; a value of S* = 0.75 for the start of damage appears more reasonable. More research is required to find a good relationship between qualitative (subjective) damage assessment and S*.

When an quantitative estimate of the reduction of the crest level is required, a conservative estimate can be obtained assuming that a slice with a constant thickness is removed from the crest of the structure:

$$\Delta z = \frac{-B_c + \sqrt{B_c^2 + 4 m_0 A_e}}{2 m_0} \tag{6.6}$$

7.1.4 The design of near-bed structures with the critical stability method

Question: *How well can we use the critical stability approach for the design of near-bed structures? How must we calculate the combined shear stress and what should the value of Ψ_{cr} be?*

Answer: When a critical stability approach is used for the design of horizontal bed protections, it is best to calculate the combined wave-current shear stress with the CIRIA/CUR method ($\tau_{wc} = \tau_c + \frac{1}{2}\hat{\tau}_w$ in combination with $\Psi_{cr} = 0.03$. We note that in the limit of current only ($\tau = \tau_c$) this recommendation equals the classic Shields approach, and in the limit for waves only ($\tau = \frac{1}{2}\hat{\tau}_w$) it equals the present recommendation in CIRIA/CUR (1991) to use $\Psi = 0.030$ in combination with the average shear stress. Therefore it forms a good 'bridge' between these two situations.

It is interesting to note that here, where we study critical stability, it turns out that the combined shear stress under waves and currents can best be expressed as the average shear stress ($\tau_{wc\,av}$); previously we concluded that for transport of stones we could best use the average combined shear stress in the direction of the current ($\tau_{wc\,avx}$). A physical explanation for this difference could be that transport is a phenomenon with a clear direction (the direction of the flow is the direction of transport), whereas critical stability is not (the stones are merely entrained from their position or not, the direction in which this happens is of lesser importance).

For pipeline covers we found that the stability of a single stone could not be related to the stability of the structure as a whole, so the critical stability method is strictly speaking not a suitable design method for this type of structure, no matter which wave-current interaction model is used, or in which way the orbital velocity is defined. However, if we do want to use the method (for practical reasons and as a conservative upper limit to the required stone size) we must use the 1%-exceedance wave height $H_{1\%}$ (equation 2.38 or Battjes and Groenendijk (2000)) and T_p in combination with the velocity at the crest $\hat{u}_{hc}$; the use of the significant wave height H_s and other velocity definitions seriously under-predicts the governing shear stresses. We note that these are the same parameters that are recommended for use in the damage-based design approach.

Again, the use of the CIRIA/CUR method in combination with $\Psi_{cr} = 0.030$ is recommended. This conclusion is supported by the results from the case study (see appendix 9).

7.2 Discussion of the general research question

In Chapter 1 we formulated the research goal as follows:

> *To find a design curve, expressing damage to a near-bed structure as a function of the stability of the individual stones, that can be used for the preliminary design of such structures based on an 'allowable damage' design approach. The stability parameter should be expressed in such a way that it represents the true physics of the destabilising mechanisms and includes a wide range of flow situations, including waves*

There are three main elements in this goal: damage based-design, true physics and a wide range of flow situations. These elements form the basis of the following discussion.

Damage-based design: we have seen how we can adopt two different approaches: a *transport-based method* in which we can calculate a transport rate of the stones under a given flow situation and link this to a certain degree of damage, and a *damage profile method* in which we directly calculate the damage to the structure expressed as an erosion area.

The transport-based approach has not proven very successful in our analysis. The main weakness of the method turns out to be the relationship between transport and damage: for pipeline covers we could not find such a relationship at all, for horizontal bed protections we could not attempt to find such a relation for lack of data. However, we have found an interesting result concerning the transport rates as such: in the case of a combination of waves and a current, the transport rate as such can be calculated with the same formula as used for current-only situations, provided that the shear stress is replaced by the combined shear stress in the direction of the current according to Fredsøe.

The damage profile method provides better results: we have found a design formula for the design of pipeline covers with a reasonable goodness-of-fit on the scale model test data. We have also found a way to translate the obtained damage parameter (the dimensionless erosion area per unit of crest width S*) to the actual damage of the structure, both qualitatively (in terns of a general description of the expected damage) and quantitatively (in terms of the reduction in crest height of the structure). The disadvantage of this method is its lack of physical basis: it is effectively a black-box method linking large-scale fluid parameters directly to the damage without providing any insight into the physical processes that cause this damage. The results from the case study with prototype data from the Santander outfall indicates that S* = 0.7 can be used

as a design criterion for a damage-based design of pipeline covers – this value corresponds with 'no damage' and results in stone sizes equivalent to those obtained with a critical stability method.

True physics: in the introduction we described how one of the main problems with the Shields method was its use of the shear stress as the governing parameter, leading to a lack of understanding of the actual physical processes that entrain a stone and, consequently, its lack of applicability in non-uniform flow situations. In this study we have described two alternative approaches that seek to overcome this problem: the Morison approach and a turbulence-based approach.

From the Morison approach we have learnt that fluid accelerations *do* play a role in the entrainment of stones from a near-bed structure, especially in the case of asymmetric (shoaling) waves. However, in terms of practical applicability the Morison approach seems to invoke more questions than answers. Firstly, the old problem of where 'the' velocity and 'the' acceleration should be defined (which is why Shields proposed his shear-stress based approach in the first place) has not been solved yet. Secondly, the values of the empirical parameters C_B and C_M are very difficult to measure and are subject to a lot of discussion. Finally, although the potential power of the method lies in the description of wave asymmetry, the exact way in which this asymmetry should be included has not been established yet (and especially not in terms of practical parameters).

Some of these disadvantages may be circumvented by applying a 'hybrid' approach in which the drag-and-lift part of the Morison equation is replaced by a shear stress-based expression; this effectively leads to a 'Shields-type stability parameter with accelerations'. Such a parameter is briefly explored in this thesis, but not included in our main analysis.

The turbulence-based approach probably offers the best description of the actual physical processes: Hofland (2005) found strong evidence that the entrainment of stones is related to turbulence structures in the flow. The main disadvantage of the method is that it requires numerical modelling of the flow situation, which makes it less suitable for preliminary design. However, we note that this is perhaps inevitable if we seek an all-encompassing, versatile design method; all simplifications to avoid numerical modelling and make a method suitable for preliminary, 'back of an envelope'-type of calculations come at the expense of physical reality and, in the extreme case, bring us right back to where we started: a shear-stress based design approach.

We believe that in the future the turbulence-based calculations will be the main approach

to the design of near-bed structures. At this moment however, the method is not developed far enough to be applicable in practice. There is no consensus yet on the actual way in which the turbulence characteristics must be included in the stability parameter, and the method does not include waves. Especially, the most recent method (Hofland 2005) still uses the assumption of a Bakhmetev mixing length distribution (which is associated with uniform flow); ideally we would have a design method that is completely based on numerical model output so it can really be used in any flow situation. This suggests that more advanced turbulence closure models (eg Large Eddy Simulation) may have to be used instead of the presently used k-ε model.

In this 'true physics' discussion it is interesting to note that the two main results of this present research (concerning the transport of stones under waves and currents and the design of pipeline covers) do not use these more advanced approaches. The transport of stones is related to the shear stress, the design of pipeline covers is related to the local velocity.

Wide range of flow situations: this final element of the research goal has only partly been reached. For the transport of stones we have managed to find a formulation that can be used in the case of current only, and the combination of currents and waves. Transport under pure wave load remains unclear. Our result concerning the design of pipeline covers is mainly valid for waves only; for situations with waves and a small current we found that the results can also be applied provided that the current is neglected altogether. It is of course expected that we can only do this up to a certain point, but where this point lies is unknown. Also the limit case of current only was not investigated.

8 Recommendations

This chapter contains recommendations for the design of near-bed structures as well as recommendations for further research.

In general terms, the recommendations for the design of near-bed structures follow from the present design practice and from the questions that were answered in this research. The recommendations for further research follow from the questions that were asked in this research, but not answered.

These recommendations can be given per structure type (horizontal bed protections and pipeline covers), per load type (current only, waves only and a combination of both) and per design approach (static stability and dynamic stability). They are given in table 8.1 and 8.2 on the next pages.

A few of these recommendations have a general validity and are worth mentioning explicitly here:

- For horizontal bed protections we have only studied the transport rates of rock. As such, these transport rates are not a good indication of the expected damage to a structure; for design purposes they must be translated into quantitative measures such as the reduction in layer thickness. How this translation must be made is not clear at the moment. The suggestion by De Groot *et al* (1988) to use the critical scour method is followed here, but it is stressed that we have not been able to test this method in this research. It is recommended to study the relationship between transport rates and damage to a structure in more detail.
- The waves used in the scale model tests by Bijman (2000) were asymmetrical. This means that the measured transport rates were in fact a combination of (wave-enhanced) current-induced transport and net wave-induced transport. It is not clear to what extent this phenomenon biases our conclusions; this may be investigated further.

- Because our dataset did not contain measurements of erosion areas and/or layer thickness for the horizontal bed protections we could not test the application of a damage profile method for this type of structure (ie develop a design formula in terms of S). This could be an interesting subject for further research.
- We have combined the Morison approach with linear wave theory, although in literature it has been strongly associated with asymmetric waves. We believe that, when wave asymmetry is correctly included in the analysis, our conclusion that the applicability of the Morison approach is limited may be falsified. For this purpose it is helpful to investigate the relationship between asymmetry and accelerations in more detail, and find a method to correctly account for this asymmetry in the Morison formula (perhaps following some suggestions made by Terrile (2005, Terrile *et al* 2006) – in any case this method should be related to large-scale wave parameters like H, T and h, probably in combination with a higher order wave theory). With this knowledge part of our analysis (likely, but not necessarily based on the same datasets) can be re-done.
- In terms of new design methods that do include correct descriptions of the actual physical processes we recommend to focus more on the turbulence-based methods instead of on the Morison approach. Main research topics could be the inclusion of waves, and the development of a stability parameter that is fully based on model output and no longer relies on simplifications like the Bakhmetev distribution – this means that perhaps other, more advanced turbulence closure models must be considered (eg LES) instead of k-ε models.
- The relation between S* and an assessment of the qualitative damage to a structure, as given in table 6.4 of this thesis, is probably not correct – the values in that table are obtained from looking at drawings, not real structures, and may well be too high. It is recommended to conduct a specific research into this topic using a set of pre-defined, reasonably well described damage criteria (such as 'no damage', 'small holes', 'large holes', 'underlayer visible' and so on) and possibly different types of structure (simple homogeneous rubble mounds, structures with an armour layer of $2 \cdot d_{n50}$ thickness and so on). This research may also seek to quantify the relationship between an average reduction in crest level (as for instance obtained with equation 6.6) and the deepest damage holes in the structure so that a design criterion for $\Delta z/d_{n50}$ may be set.
- In paragraph 4.2.3 we suggested the introduction of the hybrid 'Shields-plus' stability parameter that combines shear stresses with acceleration effects. The – theoretical and practical – possibilities of such a stability parameter may be investigated further.

Table 8.1 Recommendations for the design of horizontal bed protections

CURRENT ONLY	Static stability	Design philosophy	There is an assumed threshold of motion that can be expressed as a critical shear stress.
		Proposed design method	Use the classic Shields approach.
		Questions asked in this thesis	none
		Remaining questions	none
	Dynamic stability	Design philosophy	The current transports stones away from the structure causing ongoing damage.
		Proposed design method	Use Paintal formula to estimate transport rate.
		Questions asked in this thesis	*How can we relate a transport rate to the actual damage to a structure?* **Answer**: It is suggested to use the critical scour method.
		Remaining questions	*Given a transport rate, can we indeed use the critical scour method to assess the damage to a structure?*
WAVES ONLY	Static stability	Design philosophy	There is an assumed threshold of motion that can be expressed as a critical shear stress.
		Proposed design method	Use the Shields approach and replace the bed shear stress by the maximum or average wave shear stress. Follow the recommendations in CIRIA/CUR.
		Questions asked in this thesis	none
		Remaining questions	none
	Dynamic stability	Design philosophy	No ongoing damage, no reshaping. Only transport (back and fro) during half a wave cycle. Possible net transport by asymmetric waves.
		Proposed design method	Use Madsen and Grant or Hallermeier formula to assess magnitude of movement under half a wave cycle, or net transport under asymmetric waves.
		Questions asked in this thesis	none
		Remaining questions	*Which transport formula is best suitable to predict the transport of stones under waves? Do the coefficients in the formula need to be adapted?*

Table 8.1 Recommendations for the design of horizontal bed protections (CONTINUED)

CURRENT + WAVES	Static stability	Design philosophy	There is an assumed threshold of motion that can be expressed as a critical shear stress.
		Proposed design method	Use the Shields approach and replace the bed shear stress with the combined wave-current shear stress. Use a wave-current interaction model and corresponding critical Shields parameter.
		Questions asked in this thesis	*Which WCI model gives the best results and what is the corresponding critical Shields parameter?* **Answer**: the critical stability parameter depends strongly on the WCI model used. It is recommended to use the Bijker average model (CIRIA/CUR) with $\Psi_{cr} = 0.030$.
		Remaining questions	This answer is based on Bijman data set which has a limited applicability. More research in larger flume (no wall effects, hydraulically rough bottom), with wider range of d_{n50}, Δ, wave-current dominance etc is required to support these conclusions.
	Dynamic stability	Design philosophy	Waves cause transport during half a wave cycle, but also increase current-induced transport.
		Proposed design method	As for current only, but using a transport formula that adapted for current + waves. Use method for waves only to assess transport during half a wave cycle.
		Questions asked in this thesis	*Which transport formula can best be used? Should it be adapted to include the effect of waves?* **Answer**: the Paintal formula (correction by Mosselman and Akkerman 1996) can best be used. It does not need to be adapted; it can also be used for currents and waves provided that the combined shear stress is calculated as the average shear stress in the direction of the current according to Fredsøe.
		Remaining questions	This answer is based on Bijman data set which has a limited applicability. More research in larger flume (no wall effects, hydraulically rough bottom), with wider range of d_{n50}, Δ, wave-current dominance etc is required to support these conclusions. It is recommended to include Bijker-type transport formulas in this research.

Table 8.2 Recommendations for the design of pipeline covers

WAVES ONLY	Static stability	Design philosophy	There is an assumed threshold of motion that can be expressed as a critical shear stress.
		Proposed design method	Use the Shields approach and replace the bed shear stress by the average wave shear stress.
		Questions asked in this thesis	*Where to define velocities (undisturbed or over crest)? What is the critical Shields parameter?* **Answer**: There is no clear threshold of motion for near-bed structures; a critical stability approach as for bed protections gives a conservative estimate of the required stone size, provided that the velocity is defined at the crest and $H_{1\%}$ and T_p are taken as the governing wave parameters.
		Remaining questions	The stability of a single stone cannot be assessed well with the data sets used in this research. Separate scale model tests aimed specifically at this purpose are required to answer this question.
	Dynamic stability	Design philosophy	Ongoing damage in terms of reshaping of the structure.
		Proposed design method	Use a design formula to assess damage in terms of the erosion area S.
		Questions asked in this thesis	*How can we relate S to practical measures of damage? Can we find a formula that shows less scatter than the present design formulas?* **Answer:** The dimensionless erosion area per unit crest width S* can best be used to obtain a qualitative assessment of the damage to the structure. When an quantitative assessment is required, a simple but conservative estimate of the crest height reduction of the structure can be obtained from equation 6.6. The present design formulas can be improved by using equation 6.23 instead.
		Remaining questions	Validation of these formulae by more scale model tests and -preferably- prototype tests.

Table 8.2 Recommendations for the design of pipeline covers (CONTINUED)

CURRENT ONLY	Static stability	Design philosophy	There is an assumed threshold of motion that can be expressed as a critical shear stress.
		Proposed design method	Use the classic Shields approach.
		Questions asked in this thesis	none
		Remaining questions	none
	Dynamic stability	Design philosophy	The current transports stones away from the structure causing ongoing damage.
		Proposed design method	Use Paintal formula to estimate transport rate.
		Questions asked in this thesis	*How can we relate a transport rate to the actual damage to a structure?* **Answer**: It is suggested to use the critical scour method.
		Remaining questions	*Given a transport rate, can we indeed use the critical scour method to assess the damage to a structure?*
CURRENT + WAVES	Static stability	Design philosophy	There is an assumed threshold of motion that can be expressed as a critical shear stress.
		Proposed design method	Use the Shields approach and replace the bed shear stress with the combined wave-current shear stress. Use a wave-current interaction model and corresponding critical Shields parameter.
		Questions asked in this thesis	*Which WCI model gives the best results and what is the corresponding critical Shields parameter? Where to define velocities (undisturbed or over crest)?* **Answer**: see 'waves only'.
		Remaining questions	see 'waves only'
	Dynamic stability	Design philosophy	Current causes ongoing damage. Waves cause reshaping of the structure, but also increase current-induced transport.
		Proposed design method	Current dominates: use critical scour method + transport formula adapted for currents + waves. Waves dominate: use method for waves only and incorporate current.
		Questions asked in this thesis	*How must the current be incorporated in the waves-only approach?* **Answer**: in the design formula (6.23) the current can be neglected, provided that the hydraulic conditions are strongly wave-dominated ($X < 0.2$).
		Remaining questions	See 'waves only'. Also: more tests with stronger currents to test up to where the current can be neglected.

References

(TU Delft MSc theses can be downloaded from http://www.waterbouw.tudelft.nl. Choose ‘education’ and then ‘MSc theses’.)

BATTJES, J A and GROENENDIJK, H W (2000) ‘Wave height distributions on shallow foreshores’, *Coastal Engineering,* Vol 40 (2000), pp 161-182, Elsevier

BIJKER, E W (1967) *Some considerations about scales for Coastal Models with Movable Bed*, TH Delft, Delft, The Netherlands, PhD thesis

BIJMAN, W (2000) *Transport van stortsteen door golven en stroming*, TU Delft, Delft, The Netherlands, MSc thesis (in Dutch)

BRYMAN, A and CRAMER, D (2005) *Quantitative Data Analysis with SPSS 12 and 13*, Routlegde, New York, USA

CIRIA / CUR (1991) *Manual on the use of rock in coastal and shoreline engineering*, CIRIA special publication 083 / CUR report 154

DAVIES, A G, SOULSBY, R L and KING, H L (1988) 'A Numerical Model of the Combined Wave and Current Bottom Boundary Layer', *Journal of Geophysical Research, Vol 93 no C1*, pp 491-508

DEAN, R G and DALRYMPLE, R A (1991) *Water wave mechanics for scientists and engineers*, advanced series on ocean engineering, volume 2, World Scientific, Singapore

DE BOER, G M (1998) *Transport van stenen van een granulaire bodemverdediging*, TU Delft, Delft, The Netherlands, MSc thesis (in Dutch)

DE GROOT, M B, BLIEK, A J and VAN ROSSUM, H (1988) 'Critical scour: new bed

protection design method', *Journal of Hydraulic Engineering, Vol 114 (10*), pp 1227-1240, ASCE, New York, USA

DESSENS, M (2004) *The influence of flow acceleration on stone stability*, TU Delft, Delft, The Netherlands, MSc thesis

FORSCHELEN, P (1999) *Transport van granulair bodemmateriaal. Een onderzoek naar transport bij lage hydraulische belasting*, TU Delft, Delft, The Netherlands, MSc thesis (in Dutch)

FREDSOE, J (1984) 'Turbulent Boundary Layer in Wave-Current Motion', *Journal of Hydraulic Engineering*, *Vol 110 (8),* pp 1103-1120

FREDSOE, J, and DEIGAARD, R (1992) *Mechanics of coastal sediment transport,* advanced series on ocean engineering, volume 3, World Scientific Singapore

GRANT, W D, and MADSEN, O S (1979) 'Combined Wave and Current interaction with a Rough Bottom', *Journal of Geophysical Research, Vol 84 no C4*, pp 1797-1808

GRANT, W D, and MADSEN, O S (1986) 'The Continental Shelf Bottom Boundary Layer', *Annual Review of Fluid Mechanics, Vol 18*, pp 265-305

HOFLAND, B (2004) *Modelling damage to Granular Bed Protections under Non-Uniform Flows*, TU Delft, Delft, The Netherlands, Faculty of Civil Engineering and Geosciences, Report 01-04

HOFLAND, B (2005) *Rock and roll; Turbulence-induced damage to granular bed protections*, TU Delft, Delft, The Netherlands, PhD thesis

HUYNH-THANH, S, and TEMPERVILLE, A (1991) 'A numerical model of the rough turbulent boundary layer in combined wave and current interaction', *R L Soulsby and R Bettes (ed) Sand transport in Rivers, Estuaries and the Sea*, pp 93 - 100, Balkema, Rotterdam, The Netherlands

JONSSON, I G (1966) 'Wave boundary layers and friction factor', *Proc 10th ICCE Tokyo, Vol 1* pp 127-148, ASCE, New York, USA

LAMMERS, J C (1997) *Shields in de praktijk*, TU Delft, Delft, The Netherlands, MSc thesis (in Dutch)

LEVIT, M (1996) *Stability of pipeline cover material*, TU Delft, Delft, The Netherlands,

MSc thesis; WL|Delft Hydraulics report H3043

LEVIT, M, VAN GENT, M R A and MASSIE, W W (1997) 'Stability of pipeline covers under waves and currents', *Proc 8th Int Conf on the behaviour of offshore structures, Vol 1*, pp 195-210, Delft, The Netherlands

LOMÓNACO , P (1994) *Design of Rock Cover for Underwater Pipelines*, International Institute for Infrastructural Hydraulic and Environmental Engineering (IHE), Delft, The Netherlands, MSc thesis

LOMÓNACO , P, and KLOMP, W G H (1997) 'Pipeline cover damage assessment'*, Proc 8th Int Conf on the behaviour of offshore structures, Vol 1*, pp 179-193, Delft, The Netherlands

LOMÓNACO , P, VIDAL, C, LOSADA, I J, GARCIA, N and LARA, J L (2005) 'Flow measurements and numerical simulation on low-crested structures for coastal protection', in: Zimmermann, C (ed) *Environmentally Friendly Coastal Protection*, Springer, The Netherlands, pp 191-210

MORISON, J R, O'BRIEN, M P, JOHNSON, J W and SCHAAF, S A (1950) 'The forces exerted by surface waves on piles'*, Petroleum Transactions AIME, Vol 189*, pp 149-154

MOSSELMAN, E, and AKKERMAN, G J (1998) *Low-mobility transport of coarse-grained material*, WL|Delft Hydraulics, Delft, The Netherlands, Tech. Rept. Q2395.40

NIELSEN, P (1992) *Coastal bottom boundary layers and sediment transport*, advanced series on ocean engineering, volume 4, World Scientific, Singapore

NIEUWSTADT, F T M (1998) Turbulentie: inleiding in de theorie en toepassingen van turbulente stromingen, Epsilon, Utrecht, The Netherlands (in Dutch)

PAINTAL, A P (1969) *The probabilistic characteristics of bed load transport in alluvial channels*, University of Minnesota, Minneapolis / Saint Paul, USA. Ph.D. thesis

PAINTAL, A P (1971) 'Concept of critical shear stress in loose boundary open channels', *Journal of Hydraulic Research, Vol 9 (1)*, pp 91-113

RANCE, P J, and WARREN, N F (1968) 'The treshold of movement of Coarse Material in oscillatory flow', *Proc 11th ICCE London, Vol 1*, pp 487-491, ACSE, New York, USA

SAERS, W (2005) *Erosion of rubble mound near-bed structures under irregular waves*,

TU Delft, Delft, The Netherlands, MSc thesis

SCHIERECK, G J (2001) *Introduction to bed, bank and shore protection*, Delft University Press, Delft, The Netherlands

SHIELDS, A (1936) *Anwendung der Aenhnlichkeitsmechanik und der Turbulenzforschung auf die Geschiebebewegung*, Mitteilungen der Preuszichen Versuchsanhalt fuer Wasserbau und Schiffbau (no 26), Berlin, Germany, PhD thesis

SLEATH, J F A (1978) 'Measurements of bed-load in oscillatory flows', *ASCE Journal of the Waterway Port Coastal and Ocean division, Vol 104* (WW4) pp 291-307, ASCE, USA

SOULSBY, R L (1997) *Dynamics of Marine Sands*, Thomas Telford Publications, London, UK

SOULSBY, R L, HAMM, L, KLOPMAN, G, MYRHAUG, D, SIMONS, R R and THOMAS, G P (1993) 'Wave-current interaction within and outside the Bottom Boundary Layer', *Coastal engineering,* Vol 21, pp 41-69, Elsevier

TENNEKES, H, and LUMLEY, J L (1972) *A first course in turbulence*, MIT Press, Cambridge, Mass, USA

TERRILE, E (2004) *The threshold of motion of coarse sediment particles by regular non-breaking waves*, TU Delft, Delft, The Netherlands, MSc thesis

TERRILE, E, RENIERS, A J H M, STIVE, M J F, TROMP, M and VERHAGEN, H J (2006) 'Incipient motion of coarse particles under regular shoaling waves', *Coastal engineering*, Vol 53 (2006), pp 81-92, Elsevier

TROMP, M (2004) *Influences of fluid accelerations on the threshold of motion*, TU Delft, Delft, The Netherlands, MSc thesis

UIJTTEWAAL, W (2005) *Turbulence in hydraulics*, TU Delft, Delft, The Netherlands, Lecture notes

UITTENBOGAARD, R E, HOFMANS, G J C M and AKKERMAN, G J (1999) *Turbulence schermatization for stone stability assessment*, WL|Delft Hydraulics report Q 2395.30, Delft, The Netherlands

US ARMY CORPS OF ENGINEERS (1995) *Coastal Engineering Manual*, Washington, DC, USA

VAN GENT, M R A, and WALLAST, I (2001) *Stability of near-bed structures and bed protections; analysis of physical model tests with waves and currents*, WL|Delft Hydraulics, Delft, The Netherlands, Delft Cluster Report HC030204H3804

VAN RIJN, L C (1993) *Principles of Sediment Transport in Rivers, Estuaries and Coastal Seas*, Aqua Publications, Amsterdam, The Netherlands

VIDAL, C, LOMÓNACO, P and MARTIN, F L (2002) 'Prototype analysis of stability of rubble mound protections for submarine outfalls', *Proc 28th ICCE Cardiff, Vol 2*, pp 1936-1948, ACSE, New York, USA

VIDAL, C, LOSADA, I J and MARTIN, F L (1998) 'Stability of near-bed rubble mound structures', *Proc ICCE 1998 Copenhagen, Vol 2* pp 1730 - 1743, ASCE, New York, USA

WALLAST, I, and VAN GENT, M R A (2002) 'Stability of near-bed structures under waves and currents', *Proc 28th ICCE Cardiff, Vol 2*, pp 1744-1756, ACSE, New York, USA

WL|DELFT HYDRAULICS (1985?) *BPP user Manual*, Delft, The Netherlands

Appendix 1 Turbulence

Many concepts discussed in this thesis are somehow related to turbulence. This appendix introduces some of the most important ideas in turbulence research, and provides some background information. The contents of this appendix are largely based on the lecture notes 'Turbulence in hydraulics' of Delft University (Uijttewaal 2005) and two introductory books on the subject: (Tennekes and Lumley 1972) and (Nieuwstadt 1992).

A1.1 The problem of turbulence closure

Fluid motion is described by the Navier-Stokes equations. These equations form a set of three nonlinear partial differential equations, for four variables (three velocity components u, v and w, and the pressure p). Together with a fourth equation describing the conservation of mass (the continuity equation) we get a closed set of equations that could in principle be solved for any flow problem with a given set of boundary conditions. Unfortunately no analytical solution to the Navier-Stokes equations exists. Solutions may be sought by numerical computations, but for turbulent flow this is practically impossible as will be discussed later.

Throughout the history of hydraulic engineering, various researchers have proposed methods to solve this dilemma, but a satisfactory solution still has not been found. This appendix will introduce some of the best-known methods.

In a broad sense, turbulence can be seen as an instability phenomenon: small disturbances in the flow have large consequences. So when a turbulent flow experiment is repeated a number of times the outcome for each experiment (in terms of local, instantaneous values of velocity and pressure) will be different, unless we manage to reproduce the exact boundary conditions and initial conditions with infinite accuracy,

which is impossible. However, each separate outcome can be seen as a mean value (ensemble averaged over all experiments) plus a deviation from this mean (different for each experiment), written as:

$$u = \overline{u} + u' \quad v = \overline{v} + v' \quad w = \overline{w} + w' \quad p = \overline{p} + p' \tag{A1.1}$$

Since we are only interested in the mean values we can try to write the Navier Stokes equations in terms of these mean values and solve them.

In a simplified case, when we consider only 2D flow (x horizontally in the direction of the flow, z vertically), the Navier-Stokes equation for flow in the x-direction becomes:

$$\rho\left(\frac{\partial u}{\partial t} + u\frac{\partial u}{\partial x} + v\frac{\partial u}{\partial z}\right) = -\frac{\partial p}{\partial x} + \rho\nu\frac{\partial^2 u}{\partial z^2} \tag{A1.2}$$

in which ν is the (molecular) kinematic viscosity of the fluid. The equation expresses that the fluid inertia (left hand side) is balanced by a gradient in the normal stress ?p/?x and the viscous shear stress $\rho\nu(?^2u/?z^2)$. Applying (A1.1) and averaging gives, after some algebra:

$$\rho\left(\frac{\partial \overline{u}}{\partial t} + \overline{u}\frac{\partial \overline{u}}{\partial x} + \overline{v}\frac{\partial \overline{u}}{\partial z}\right) = -\left(\frac{\partial \overline{p}}{\partial x} + \rho\frac{\partial \overline{u'^2}}{\partial x}\right) + \rho\nu\frac{\partial^2 \overline{u}}{\partial z^2} + \rho\frac{\partial \overline{u'v'}}{\partial z} \tag{A1.3}$$

We can now see that averaging the Navier Stokes equation did not simply yield the same equation in terms of average quantities. Instead, we now have two new terms that appear as (the gradients of) an extra normal stress $\rho\left(\partial\overline{u'^2}/\partial x\right)$ and an extra shear stress $\rho\left(\partial\overline{u'v'}/\partial z\right)$. These stresses are the so-called *Reynolds* stresses.

Note that, even though the average value of the fluctuating component $\overline{u'}$ equals zero by definition, the same is not true for the average value of the *product* of two fluctuating components $\overline{u'v'}$. Statistically, this parameter is analogous to the covariance of the velocity components *u* and *v*. In other words, the larger this value is, the larger the probability that a strong fluctuation in horizontal velocity occurs simultaneously with a strong fluctuation in vertical velocity. This means that the Reynolds stresses can be related to some kind of pattern, or structure, in the flow. So, although we refer to statistical methods to analyse turbulent flow, the flow is in a strict sense *not random*.

The Reynolds normal stress is typically much smaller than the mean pressure gradient, but the Reynolds shear stress is much larger than the viscous shear stress, so (A1.3)

can be simplified to:

$$\rho\left(\frac{\partial \overline{u}}{\partial t}+\overline{u}\frac{\partial \overline{u}}{\partial x}+\overline{v}\frac{\partial \overline{u}}{\partial z}\right)=-\frac{\partial \overline{p}}{\partial x}+\rho\frac{\partial \overline{u'v'}}{\partial z} \tag{A1.4}$$

The Reynolds shear stress is expressed in terms of the fluctuating components u' and v', so we now have two extra unknown variables but still only four equations. This means we no longer have a closed set of equations, and (A1.4) (known as the Reynolds equation) can only be solved if we can find expressions for the Reynolds stresses in terms of the average quantities $\overline{u}$, $\overline{v}$ and $\overline{p}$. This problem, which is one of the largest unsolved problems in fluid mechanics, is known as the *turbulence closure problem*.

A1.2 The eddy viscosity concept

The classic hypothesis to close the Reynolds equation is the introduction of a so-called turbulence viscosity (or *eddy viscosity*). From an analogy between the viscous shear stress gradient term in the Navier-Stokes equation:

$$\rho\nu\frac{\partial^2 \overline{u}}{\partial z^2}=\frac{\partial}{\partial z}\left(\rho\nu\frac{\partial \overline{u}}{\partial z}\right)=\frac{\partial \tau_{visc}}{\partial z} \tag{A1.5}$$

and the Reynolds shear stress gradient term:

$$\rho\frac{\partial \overline{u'v'}}{\partial z}=\frac{\partial}{\partial z}\left(\rho\overline{u'v'}\right)=\frac{\partial \tau_{turb}}{\partial z} \tag{A1.6}$$

we can see that we can write the turbulent shear stress as:

$$\tau_{turb}=\rho\overline{u'v'}=\rho\nu_T\frac{\partial \overline{u}}{\partial z} \tag{A1.7}$$

in which ν_T is the eddy viscosity, which is a yet unknown property. Note that unlike the molecular viscosity ν, this eddy viscosity is not a property of the fluid, but a property of the flow, so ν_T is different for each flow problem. This equation relates the Reynolds shear stress to the mean flow velocity $\overline{u}$ and thus closes the Reynolds equation. The problem has, of course, only shifted to determining ν_T. For this, again, various solutions have been proposed. The most important methods are listed below.

A1.2.1 Constant eddy viscosity

The simplest method is to assume that the eddy viscosity is a constant (for a given flow problem). Measurements have shown that this assumption is an over-simplification: the eddy viscosity really varies with z-coordinate, and, for unsteady flow, also with time. Nevertheless, the assumption of a constant eddy viscosity is still used in some older computer flow models (especially 2D transport models) as a 'tuning' parameter.

A1.2.2 Mixing length models

From dimensional analysis we can see that we can write ν_T as the product of a length scale L and a velocity scale U; but since we know that it is more the velocity *gradient* that determines the shear stresses, we can better write the eddy viscosity as the product of this velocity gradient and a length scale squared:

$$\nu_T = LU = L^2 \frac{\partial U}{\partial z} \tag{A1.8}$$

For the velocity scale we can take the mean flow velocity $\overline{u}$, and for the length scale Prandtl has introduced the concept of the *mixing length* l_m, that can be thought of as the characteristic dimension of the turbulent eddies. So:

$$\nu_T = l_m{}^2 \frac{\partial \overline{u}}{\partial z} \tag{A1.9}$$

The remaining problem is now to determine the mixing length. The simplest way would be to assume that l_m is constant. This is physically dubious (there is no reason why the turbulent eddies should have the same size everywhere in the fluid). Alternatively, Von Kármán has suggested that the mixing length is proportional to the distance from the bed, so the further away from the bed, the larger the turbulent eddies can grow:

$$l_m = \kappa z \tag{A1.10}$$

in which the constant of proportionality κ (called Von Kármán's constant) has been measured in numerous experiments and appears to have the universal value $\kappa = 0.4$.

Combining (A1.9) and (A1.10) gives the Prandtl-Von Kármán eddy viscosity:

$$\nu_T = (\kappa z)^2 \frac{\partial \overline{u}}{\partial z} \tag{A1.11}$$

Other suggestions for the distribution of the mixing length have been proposed, of which the Bakhmetev distribution:

$$l_m = \kappa z \sqrt{1 - \frac{z}{h}} \tag{A1.12}$$

is the most prominent. This distribution expresses that the turbulent eddies grow larger with increasing distance from the bed, but their growth is not unlimited: near the free surface ($z \rightarrow h$) the eddy size reduces again to $l_m = 0$ at the free surface.

A1.2.3 One equation model

The turbulent fluctuations in a fluid can be associated with a *turbulent kinetic energy* defined as:

$$k = \frac{1}{2}\rho\left(\overline{u'^2} + \overline{v'^2} + \overline{w'^2}\right) \tag{A1.13}$$

An important result from turbulence research is that the energy that is contained in the turbulent motion originates from the kinetic energy of the mean motion; in fact, the turbulent motion forms the most effective mechanism for dissipation of this mean kinetic energy. This means that *k* can be related to the mean motion, or more specifically, that we can derive a balance equation for *k* in terms of the mean motion properties $\overline{u}$, $\overline{v}$ and $\overline{w}$ so that *k* can in principle be calculated at any point in the flow.

From a dimensional analysis we can write the eddy viscosity as:

$$\nu_T = C_\nu \sqrt{k} L \tag{A1.14}$$

in which C_ν is a tuning parameter, and L is the length scale of the process.

In numerical models, the Reynolds equation (A1.4) can be solved along with the balance equation for *k,* after which (A1.14) and (A1.7) can be used to close the equations. The parameter C_ν can be used to tune the results. Uijttewaal (2005) gives $C_\nu \sim 0.53$. The balance equation for *k* also contains two tuning parameters.

The disadvantage of this method is that the length scale L still needs to be estimated.

A1.2.4 Two equation model (k-ε closure)

The disadvantage of the one-equation model can be overcome by adding another

balance equation, this time for ε, which is the *dissipation rate* of the turbulent kinetic energy. Note that this makes hardly any sense in physical terms, because energy dissipation (unlike energy itself) is not a conserved quantity, so there is no reason why a balance equation for dissipation should hold. Such a balance equation would contain physically doubtful terms as the 'production of dissipation', 'transport of dissipation' and 'dissipation of dissipation'. Nevertheless this approach appears to give reasonable results, and it is quite popular in modern engineering applications.

After ε is calculated from its balance equation, the eddy viscosity is calculated as:

$$\nu_T = C_1 \frac{k^2}{\varepsilon} \tag{A1.16}$$

which, again, follows purely from dimensional arguments.

The advantage is this method is that is does not require an additional estimation of L. The disadvantage, apart from its dubious physical basis, is that it introduces more tuning parameters (C_1 in the above equation, and another two in the balance equation for ε), so it takes some practice and skill to run such a model correctly.

A1.3 Other turbulence closure methods

The eddy viscosity concept, described above in all its varieties, is one way of closing the Reynolds equations, but there are more. These are not very relevant for the research described in this thesis, so they will only be treated briefly below, for the sake of completeness.

A1.3.1 Direct numerical simulation (DNS)

This method circumvents the Reynolds equation altogether, and seeks to solve the Navier-Stokes equation directly (numerically), on a spatial grid that is fine enough to resolve all the relevant motion.

For turbulent flow this is practically impossible. It can be shown that the ratio between the largest and the smallest spatial scales at which turbulence plays a role is equal to $Re^{3/4}$, so for a 'normal' turbulent flow with Re =10^6 ~ 10^7 this ratio is in the order 10^5. In numerical applications this number is roughly equal to the number of gridpoints at which the Navier-Stokes equations must be evaluated. When it is also considered that the problem needs to be solved in three spatial dimensions and for a reasonably long period in time, it is seen that the total number of computations needed to solve a given fluid

problem is in the order 10^{20} or more, which is well beyond the capacity of modern computers.

DNS has been applied in theoretical research, but only for very simple flow geometries at low Reynolds numbers.

A1.3.2 Reynolds stress modelling

This method seeks to find direct balance equations for the Reynolds stresses, as in:

$$\frac{\partial\left(\rho\overline{u'v'}\right)}{\partial t}+\overline{u}\frac{\partial\left(\rho\overline{u'v'}\right)}{\partial x}=f\left(...\right) \tag{A1.17}$$

The function *f* can be shown to contain higher order closure terms, like the triple product $\overline{u'u'v'}$ and so on; so effectively the problem is only shifted to finding closure schemes for these higher order terms. It is hoped that these terms are easier to close; or at least that the assumptions involved in their closure do not have very far-reaching complications. So far, this approach has yielded few results.

A1.3.3 Large eddy simulation (LES)

This method can be seen as a simplified way of Direct Numerical Simulation. The difference with DNS is that the computational grid is much coarser, so only the largest turbulent motions can be resolved (hence the name of the method). This greatly reduces the computational capacity involved, and makes the method more suitable for practical applications. The smaller motions that are not resolved on the numerical grid are represented in the model by a so-called *sub-grid stress*. Modeling these sub-grid stresses, of course, requires some assumptions regarding turbulence closure again, but the powerful idea behind LES is that this is easier and less critical than finding a turbulence closure for the larger-scale motions.

A1.4 Velocity profiles

Once the Reynolds equations have been closed by one method or another, the resulting expression can be used to find the velocity profile $\overline{u}(z)$ of the flow. This is used extensively throughout this thesis, so a short introduction to the ideas behind it is given below.

For open channel flow it can be shown (from a momentum balance) that the shear stress varies linearly from a value $\tau = \tau_0$ at the bed to $\tau = 0$ at the free surface. Close to the bed,

it can be assumed that the shear stress is constant with a value equal to the bed shear stress τ_0. When it is further assumed that the turbulent shear stress is far larger than the molecular shear stress, we can write that close to the bed:

$$\tau = \tau_0 = \rho u_*^2 = \tau_{turb} = \rho \overline{u'v'} = \rho \nu_T \frac{\partial \overline{u}}{\partial z} \tag{A1.18}$$

or, in short:

$$u_*^2 = \nu_T \frac{\partial \overline{u}}{\partial z} \tag{A1.19}$$

When a constant mixing length is assumed, (A1.19) becomes:

$$u_*^2 = l_m{}^2 \left| \frac{\partial \overline{u}}{\partial z} \right| \frac{\partial \overline{u}}{\partial z} \tag{A1.20a}$$

or

$$\frac{\partial \overline{u}}{\partial z} = \frac{u_*}{l_m} \tag{A1.20b}$$

which integrates to a linear velocity profile:

$$\overline{u}(z) = \frac{u_*}{l_m} z \tag{A1.21}$$

with boundary condition u = 0 at z = 0. Constant mixing lengths and the resulting linear velocity profiles are not commonly applied, but they are introduced here because a linear velocity profile is an important part of the wave-current interaction model by Bijker (1967).

From (A1.21) and the definition of the mixing length (A1.9) it follows that assuming a constant mixing length is equivalent to assuming a constant eddy viscosity with $\nu_T = u_* l_m$.

Using the Prandtl-Von Kármán mixing length hypothesis leads to:

$$u_*^2 = (\kappa z)^2 \left| \frac{\partial \overline{u}}{\partial z} \right| \frac{\partial \overline{u}}{\partial z} \tag{A1.22a}$$

or

$$\frac{\partial \overline{u}}{\partial z} = \frac{u_*}{\kappa}\frac{1}{z} \tag{A1.22b}$$

which integrates to

$$\overline{u}(z) = \frac{u_*}{\kappa}\ln\left(\frac{z}{z_0}\right) \tag{A1.23}$$

with boundary condition u = 0 at z = z_0. This is the well-known logarithmic velocity profile. So, strictly speaking, this profile was derived for the assumption that $\tau = \tau_0$, so it is only valid close to the wall. However, measurements have shown that the logarithmic velocity profile appears to be a more 'universal law' which is valid throughout the whole water column.

Mathematically it can be shown that, if we want the logarithmic profile to hold for the whole water column, and so the assumption of a constant shear stress must be dropped in favour of the linear varying shear stress distribution, we need to use the mixing length distribution according to Bakhmetev (equation A1.12).

A1.5 Turbulent flows in design practice

Practically all flows in civil engineering are turbulent, both in nature as in scale models (in laboratories). This means that design methods, being based on either empirical evidence on prototype scale or on physical model research, have turbulence implicitly included in them. Therefore, it is not necessary to account for turbulence explicitly in the design of structures, unless of course the expected turbulence levels in the design situation deviate strongly from the 'normal' turbulence levels. Situations when this can be expected include the reattachment point after a sill, the outer bends of rivers or sudden transitions in bottom roughness.

The most common way to express turbulence levels is by the *turbulence intensity r*, defined as:

$$r_u = \frac{\sqrt{\overline{u'^2}}}{\overline{u}} \tag{A1.24a}$$

with similar expressions for the intensities in the other two dimensions r_v and r_w. Usually

only flow in the *x* direction is considered and *r* is used without a subscript. Statistically speaking, the root of the average of the fluctuating component squared $\sqrt{\overline{u'^2}}$ is equivalent to the standard deviation of *u*, so *r* can be interpreted as the coefficient of variance of *u*:

$$r_u = \frac{\sigma(u)}{\mu(u)} \qquad \text{(A1.24b)}$$

In a turbulent flow it is commonly assumed that movement of stones is caused by an extreme velocity, say 3 standard deviations higher than the mean value. In other words, the governing velocity is $u = \mu(u) + 3\sigma(u) = (1+3r)u$. When we expect higher turbulence levels, we can use this assumption to scale the design velocity as follows (Schiereck 2001):

$$u_{design} = \frac{(1+3r_{design})}{(1+3r_{natural})}\bar{u} \qquad \text{(A1.25)}$$

in which r_{design} is the expected increased turbulence intensity (estimated or taken from a 3D flow model), and $r_{natural}$ is the natural turbulence intensity that is implicitly used in the design method. This natural intensity is linked to the bed roughness (a higher roughness causes more turbulence) and can be calculated with the expression given by Nezu (1977, cf Uittenbogaard 1999):

$$r_{natural} = \sqrt{\frac{1.45g}{C^2}} \qquad \text{(A1.26)}$$

in which C is the Chézy coefficient related to the bed roughness. Measurements have shown that in nature, turbulence intensities are usually of the order $r_{natural} = 0.1$ (which corresponds to C ~ 40 $m^{1/2}/s$ in equation A1.26), so equation A1.25 can also be written as:

$$u_{design} = \frac{(1+3r_{design})}{1.3}\bar{u} \qquad \text{(A1.26)}$$

Appendix 2 Soulsby parameterisation

Soulsby (Soulsby *et al* 1993, Solusby 1997) gives a very useful parameterisation of some often-used wave-current interaction models, including the models used in this thesis. Their results can be used to obtain an approximation of the maximum and mean shear combined stresses predicted by the various models, without having to go into the details of the models themselves. Soulsby does not specify which measure of the 'mean' shear stress is used, but a comparison with our own simulation results (see Chapter 3) indicates that they have used the average shear stress in the direction of the flow, averaged over the whole period.

The parameterisation requires three input parameters, the relative bed roughness z_0/h, the relative wave excursion a_0/z_0 and the angle between the current and the wave propagation φ. The dimensionless parameters X, Y and Z are defined in paragraph 3.1.

For the Bijker model, Soulsby *et al* (1993) give the following exact solution for the maximum shear stress:

$$Z = 1 + 2X^{1/2}(1-X)^{1/2}\cos\phi$$

They do not give an approximation for the mean shear stress.

For the other models Soulsby suggests approximations of the form:

$$Y = X\left(1 + bX^{p}(1-X)^{q}\right)$$

$$Z = 1 + aX^{m}(1-X)^{n}$$

which they stress has no physical meaning but is merely suggested by the shape of the curves in Figure 3.3.

The appropriate values of the fitting parameters can be calculated from:

$$a = \left(a_1 + a_2\left|\cos\phi\right|^I\right) + \left(a_3 + a_4\left|\cos\phi\right|^I\right)\log\left(\frac{f_w}{C_D}\right)$$

with analogous expressions for *m*, *n*, *b*, *p* and *q*.

The values of a_1, a_2 etc vary between the models and can be read from table A2.1. The values of f_w and C_D can be calculated directly from the various models themselves (eg equation 2.18 and 2.25 for Bijker etc), or read from table A2.2 for various values of a_0/z_0 and z_0/h (by linear interpolation).

Table A2.1 –Fitting coefficients for various wave-current interaction models (Soulsby 1997)

Model*	a_1	a_2	a_3	a_4	m_1	m_2	m_3	m_4	n_1	n_2	n_3	n_4	I
GM79	0·11	1·95	−0·49	−0·28	0·65	−0·22	0·15	0·06	0·71	−0·19	0·17	−0·15	0·67
F84	−0·06	1·70	−0·29	0·29	0·67	−0·29	0·09	0·42	0·75	−0·27	0·11	−0·02	0·80
HT91	−0·07	1·87	−0·34	−0·12	0·72	−0·33	0·08	0·34	0·78	−0·23	0·12	−0·12	0·82
DSK88	0·05	1·62	−0·38	0·25	1·05	−0·72	−0·08	0·59	0·66	−0·25	0·19	−0·03	0·82
	b_1	b_2	b_3	b_4	p_1	p_2	p_3	p_4	q_1	q_2	q_3	q_4	J
GM79	0·73	0·40	−0·23	−0·24	−0·68	0·13	0·24	−0·07	1·04	−0·56	0·34	−0·27	0·50
F84	0·29	0·55	−0·10	−0·14	−0·77	0·10	0·27	0·14	0·91	0·25	0·50	0·45	3·0
HT91	0·27	0·51	−0·10	−0·24	−0·75	0·13	0·12	0·02	0·89	0·40	0·50	−0·28	2·7
DSK88	0·22	0·73	−0·05	−0·35	−0·86	0·26	0·34	−0·07	−0·89	2·33	2·60	−2·50	2·7
DATA13	0·47	0·69	−0·09	−0·08	−0·53	0·47	0·07	−0·02	2·34	−2·41	0·45	0·61	8·8
DATA2	1·2	0·0	0·0	0·0	0·0	0·0	0·0	0·0	3·2	0·0	0·0	0·0	0·0

* GM79 = Grant and Madsen (1979); F84 = Fredsøe (1984); HT91 = Huynh-Thanh and Temperville (1991); DSK88 = Davies *et al.* (1988); DATA13, DATA2 = fit to 131 data points using 13,2 coefficients.

Table A2.2 – Friction parameters for various wave-current interaction models (Soulsby 1997)

Model*	Values of f_w			
A/z_0	10^2	10^3	10^4	10^5
GM79	0·1057	0·0316	0·0135	0·00690
F84	0·0592	0·0221	0·0102	0·0056
HT91	0·0750	0·0272	0·0121	0·0062
DSK88	0·0701	0·0209	0·0120	0·00661
DATA13, DATA2	0·1268	0·0383	0·0116	0·0035
	Values of C_D			
z_0/h	10^{-2}	10^{-3}	10^{-4}	10^{-5}
GM79, F84, DATA13, DATA2	0·01231	0·00458	0·00237	0·00145
HT91	–	0·00482	0·00237	0·00141
DSK88	–	0·00429	0·00222	0·00130

* GM79 = Grant and Madsen (1979); F84 = Fredsøe (1984); HT91 = Huynh-Thanh and Temperville (1991); DSK88 = Davies *et al.* (1988); DATA13, DATA2 from Equation (62a).
[b] Models GM79, F84, DATA2 and DATA13 use the logarithmic profile expression for C_D, Equation (37).

Appendix 3 Fredsøe's wave-current interaction model

The explanation of the Fredsoe model as given in paragraph 3.2.6 is in fact a simplification, introduced in order to explain the main features of the model without having to go into the (complex) details of it. In our analysis of the flat bed protection data and the pipeline cover data we have not used this simplification, but the full model as given in Fredsøe and Deigaard (1992). The main differences between the simplified version of chapter 3 and the full version are given below. An accompanying definition sketch is given in Figure A3.1.

Notation: Fredsøe uses a different notation than we do. This appendix follows Fredsoe's notation. A translation table for the most important parameters is given below.

Table A3.1- Differences in notation between Fredsoe and Deigaard (1992) and this thesis

parameter	Fredsoe and Deigaard (1992)	This thesis
maximum wave orbital velocity	u_{1m}	$\hat{u}_0$
current only shear stress velocity	u_{f0}	
enhanced current shear stress velocity	u_{fc}	u_{*c}
combined shear stress velocity	u_f	u_{*wc}

Fredsøe also uses the notation $u_0(\omega t)$ for the instantaneous wave orbital velocity: $u_0(\omega t) = \hat{u}_0 \sin(\omega t)$.

Current profile: In the full model the current velocity profile is split in two (logarithmic) parts. Inside the boundary layer the profile is influenced by the physical bed roughness z_0 and the shear stress velocity u_{f0}. Outside the boundary layer the boundary layer itself acts as a roughness element and so the current velocity profile in influenced by the apparent roughness z_A and the corresponding shear stress velocity u_{fc}. (see figure A3.1).

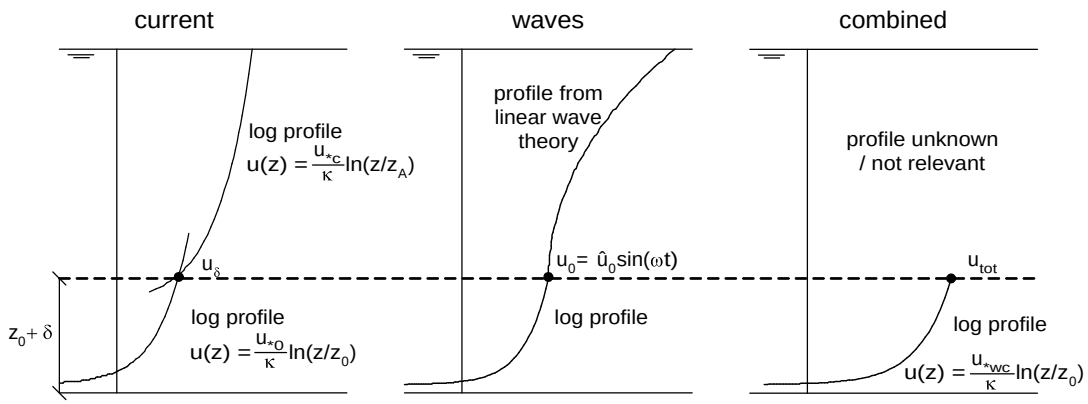

Figure A3.1 –Definition sketch for the Fredsøe model

Iteration: In chapter 3 we described how we had to iteratively find a correct value for the current velocity at the edge of the boundary layer u_δ. Fredsøe does not iterate on u_δ but on the current-only shear stress velocity in the boundary layer u_{f0}. The value of u_δ then follows as part of the solution:

$$u_\delta(\omega t) = \frac{u_{f0}}{\kappa} Z(\omega t) \tag{A3.1}$$

This equation follows from the boundary condition at the edge of the boundary layer and the definition of Z (see chapter 3), and shows the same dependency between u_δ and u_{f0} as between the corresponding parameters u_{tot} and u_f (cf eq 3.49). We now see that u_δ is in fact a time-dependent parameter,. and not a constant as assumed in chapter 3. The rest of the procedure (ie calculate u_{tot} and so on) now proceeds as in chapter 3. The value of u_{f0} must be chosen arbitrarily at the first iteration loop, and updated until the correct value of u_{da} is obtained.

Angle between instantaneous combined shear stress and current velocity: in chapter 3 we already introduced that:

$$\cos\Phi(\omega t) = \frac{u_\delta + u_0 \cos\phi}{u_{tot}} \tag{A3.2}$$

This expression follows quite straightforwardly from the geometry of the situation, as sketched in Figure A3.2. Fredsøe and Deigaard give a far more complex expression, introducing yet another parameter u_f^*, but we do not follow their suggestion. Instead, we use equation A2.2 in our analysis.

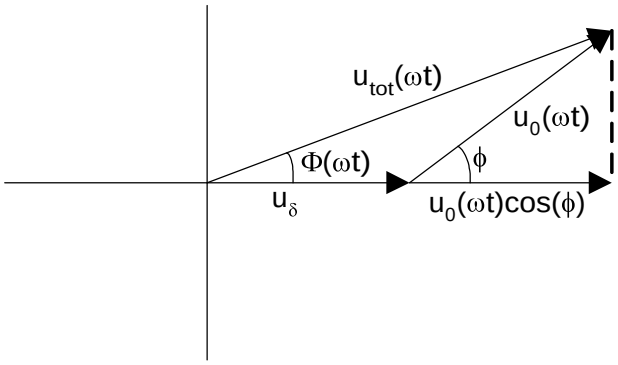

Figure A3.2 –Determination of $\Phi(\omega t)$

Differential equation: The full expression for the differential equation dZ/d(ωt) is given in Fredsøe and Deigaard (1992) and in Fredsøe (1984) in two different forms, and in either source the exact formulation is a little unclear**.** We believe this may be due to typesetting errors. After re-doing the calculus involved in solving the momentum integral (eq 3.44) we believe that the correct version should be:

$$\frac{dZ}{d(\omega t)} = \frac{Z(1+Z-e^Z)}{e^Z(Z-1)+1}\frac{1}{u_0}\frac{du_0}{d(\omega t)} + \beta\frac{\kappa}{u_{f0}}\frac{u_{tot}}{e^Z(Z-1)+1} \tag{A3.3a}$$

with

$$\beta = 30\kappa\frac{a_0/k_s}{u_{1m}/u_{f0}} \tag{A3.3b}$$

and

$$u_{tot} = \sqrt{u_\delta^2 + u_0^2 + 2u_\delta u_0\cos\phi} \tag{A3.3c}$$

In this version we have already substituted u_{tot} (cf equation 3.48) which simplifies the notation somewhat. In addition, in the version of the differential equation used in our software application (in Microsoft Excel) we have replaced the factor

$$\frac{1}{u_0}\frac{du_0}{d(\omega t)} = \frac{1}{\tan(\omega t)} \tag{A3.4}$$

as follows readily from $u_0 = \hat{u}_0\cdot\sin(\omega t)$.

The initial condition for the differential equation (A3.2) is $\omega t = 0 \Rightarrow Z = 0$. Unfortunately the differential equation is singular for $\omega t = 0$, so it cannot directly be solved. However, Fredsøe notes that for small ωt equation (A3.2) can be approximated by another differential equation which has the analytical solution:

$$Z(\omega t) = \sqrt{\frac{4}{3}\beta}\sqrt{\omega t} \tag{A3.5}$$

Equation A3.5 can be used to obtain the initial values for $Z(\omega t)$, after which the full expression (A3.2) can be used to further solve $Z(\omega t)$ for higher ωt values (Note: Fredsoe gives a factor 2/3 in his version of A3.5, but he also has a factor 60 in the definition of β (eq A3.3b) instead of 30 as we do)

Apparent roughness: The introduction of u_{f0} as a parameter means that the apparent roughness can now be found by equating the two logarithmic velocity profiles at $z = \delta_m$ (the mean boundary layer thickness):

$$\frac{u_{f0}}{\kappa}\ln\left(\frac{\delta_m}{z_0}\right) = \frac{u_{fc}}{\kappa}\ln\left(\frac{\delta_m}{z_A}\right) \quad \Rightarrow \quad z_A = z_0\left(\frac{\delta_m}{z_0}\right)^{1-\frac{u_{f0}}{u_{fc}}} \tag{A3.6a}$$

or, as expressed by Fredsøe in terms of Nikuradze roughness heights ($k = 30 \cdot z_0$):

$$\frac{k_A}{k_s} = \left(\frac{30\delta_m}{k_s}\right)^{1-\frac{u_{f0}}{u_{fc}}} \tag{A3.6a}$$

This replaces equation 3.53. We note that in his whole analysis Fredsøe has always assumed the edge of the boundary layer to be at a height $z = z_0 + \delta_m$ (see chapter 3). It is not clear why he chooses to equate the logarithmic profiles at $z = \delta_m$ instead of $z = z_0 + \delta_m$ this time.

Appendix 4 Paintal's bed load model

Paintal reasoned that there are four different stochastic parameters that play a role in the bed load transport of stones at low Ψ-values.

First, there is the fluctuating load (Paintal only considered drag and lift forces) caused by the fluctuations in the flow velocity due to turbulence. This load is assumed to have a normal distribution with a standard deviation 0.5 times the mean value (which Paintal based on earlier measurements by other researchers).

The second stochastic parameter is the embedment: stones that happen to protrude more from the bed are exposed more to the flow and will have a higher probability of movement. Paintal's embedment model is sketched in Figure A4.1. The stones undergo a drag force D_r and a lift force L, which is balanced by the stone weight W (note: these are Paintal's original notations, deviating from the notation used in this thesis). A stone can leave its position in the bed through the *escape angle* β. Both the magnitude of the hydraulic forces and the escape angle depend on the exposure of a stone (e_2 in Figure A4.1) relative to the exposure of its neighbours (e_1 and e_3). Paintal assumed a uniform distribution for a stone's relative exposure.

A stone will move when $D_r > (W-L)\cdot\tan\beta$. Using this inequality, expressing all parameters in terms of e_1, e_2, and e_3 and combining this with the assumed distribution of the loads, Paintal derives a theoretical expression for the probability p_0 that a given stone is at the point of incipient motion. The function was found to be a function of Ψ only. The full expression for p_0 is rather complicated, but for low Ψ values Paintal states that it can be roughly approximated with a 4th power relation: $p_0 \sim \Psi^4$. Paintal also plots this function in his thesis (Paintal 1969); measurements in this plot reveal that the 4th power is a crude approximation and that the real relationship is $p_0 = 1.92\cdot\Psi^{4.5}$ (for $\Psi < 0.06$)

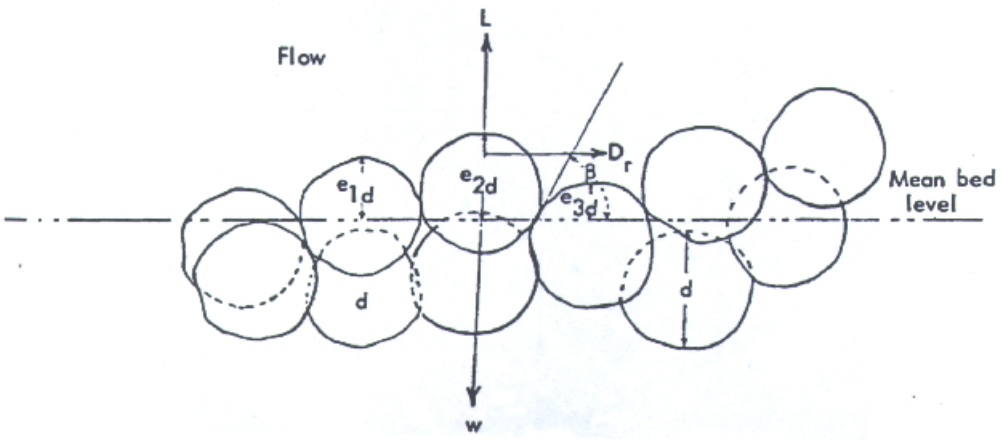

Figure A4.1- Embedment model of Paintal (taken from Paintal, 1969)

The third stochastic parameter is the step length, being the distance a stone would travel once set into motion. Paintal used a negative exponential distribution here with an unknown mean value λ, made dimensionless as $\lambda_0 = \lambda/d$.

The fourth and last parameter is the time in between steps. Paintal simply stated this parameter should be dependent on the flow and the sediment characteristics, and assumed from purely dimensional arguments that it should be proportional to d/u_*, In addition, Paintal assumed it to be related to the probability p_0, reasoning that a more exposed stone having a higher p_0 would need a shorter time before it starts moving. This is perhaps the most disputable of Paintal's assumptions, as we could argue that this exposure has already been accounted for elsewhere in the model.

Following a simple argument, originating from H A Einstein (1942), Paintal is now able to show that: (for a full derivation see Paintal, 1969)

$$\Phi_q = A\frac{p_0^3}{(1-p_0)}\sqrt{\Psi} \qquad \text{(A4.1)}$$

in which A denotes a collection of dimensionless proportionality constants. We have re-written equation A4.1 in the notation used in this thesis, Paintal's original notation is different.

When we substitute the previously found relationship $p_0 = 1.92\cdot\Psi^{4.5}$, equation A4.1 seems to induce that $\Phi_q \sim \Psi^{14}$. It is interesting to note that Paintal does not draw this conclusion anywhere in his thesis, nor does he link this to his measured correlation between Φ and Ψ^{16}.

To show the sensitivity of the value of the exponent to a change in the analysis, we will see what happens if we drop the questionable assumption that the time between two consecutive steps depends on p_0, but otherwise follow the same reasoning as Paintal in his thesis. This eventually leads to a general relationship

$$\Phi_q = A\frac{p_0^2}{(1-p_0)}\sqrt{\Psi} \tag{A4.2}$$

which would induce $\Phi \sim \Psi^{7.5}$. So, we see that Paintal's theoretical analysis does seem to justify a rather high exponent of Ψ, though probably not quite as high as 16, and that the exact value of the exponent is very sensitive to a slight change in the assumptions.

Appendix 5 Data set for horizontal bed protections

Bijman performed five test series with four different current velocities: To check his assumption that the velocity profiles during his tests were logarithmic, he performed EMS measurements at the end of his test programme, for (roughly) the same current velocities. These measurements showed that the velocity profiles were in fact *not* logarithmic; especially for the smaller velocities the deviations were large. However, in all cases the velocity profile close to the bed (ie the first five measurement points or so) *were* approximately logarithmic. This enabled Bijman to calculate the bed shear stress for his four EMS measurements, by fitting a logarithmic profile:

$$u(z) = \frac{u_*}{\kappa} \ln\left(\frac{z}{z_0}\right) \tag{A5.1}$$

to these data points by a least squares method; the values of u_* (and thus $\tau = \rho u_*^2$) and z_0 then follow as a fit parameter. The flow velocities and bed shear stresses measured by Bijman are given in table A5.1.

As explained in chapter 5 Bijman proceeds to obtain an artificial bed roughness from these measurements (defined as that roughness that must be used to calculate the measured shear stress, using the measured current velocity and a calculation method based on the assumption of a logarithmic profile) – this artificial bed roughness is then also used in the analysis of the results from the main tests (with the corresponding current velocity). This comes down to calculating an artificial Chézy value (cf eq 2.13):

$$C = \frac{\sqrt{g}}{u_*} \overline{\overline{u}} \tag{A5.2}$$

from the measured current velocity and shear stress, and finally the artificial roughness: (cf eq 2.16, using the water depth *h* from the EMS measurements)

$$k_s = \frac{12h}{10^{C/18}} \tag{A5.3}$$

For the reasons explained in chapter 5 we adopt a slightly different approach, in which we do not change the bed roughness but the current velocity. In other words we ask the question "what should the current velocity have been in order to calculate the measured bed shear stress using the calculation procedure for a logarithmic profile and keeping $k_s = 2 \cdot d_{n50}$". The ratio between this new current velocity and the measured current velocity is then determined, and the current velocities in the main tests are corrected with the same factor. This comes down to calculating C according to equation 2.16 (with the water depth from the EMS measurements and $k_s = 2 \cdot d_{n50}$) and letting the artificial ('corrected') current velocity follow from (cf eq 2.13)

$$\overline{\overline{u}}_{corr} = \frac{C}{\sqrt{g}} u_* \tag{A5.4}$$

The required correction factor then simply follows from $f = u_{da\ corr}/u_{da\ meas}$.

The results from these calculations is given in Table A5.1. The full dataset for the main tests, including the corrected current velocities, is given in Table A5.2 on the next page.

Table A5.1 – Correction factors for current velocity in Bijman data set

main test		**EMS measurements (Bijman 2000)**			**Correction (present research)**		
Test series	**u_{da}**	**u_{da}**	**h**	**u_***	**C**	**u_{corr}**	**f**
	m/s	m/s	m	cm/s	m1/2/s	m/s	-
1	0.35	0.35	0.281	2.65	44.8	0.38	1.08
2	0.45	0.43	0.310	2.84	45.6	0.41	0.96
3	0.60	0.54	0.296	3.73	45.2	0.54	1.00
4	0.65	0.66	0.282	4.52	44.9	0.65	0.98

Table A5.2 – Data set for horizontal bed protections (Bijman data set)
Hydraulic conditions and transport parameters

Test nr	Original nr	Hydraulic conditions								Transport parameters	
		T	H	u_{da}	correction	u_{da} corr	h	N	Duration	q_s	Φ_q
		s	m	m/s	factor	m/s	m	-	s	10^{-10} m^2/s	10^{-8}
BM 1	TS 1	1,1	0,1007	0,35	1,08	0,38	0,2858	3600	3960	0	0
BM 2		1,1	0,1536	0,35	1,08	0,38	0,2858	3600	3960	0	0
BM 3	Test series 2	1,1	0,1421	0,44	0,96	0,42	0,3061	3600	3960	0,39	2,46
BM 4		1,1	0,1511	0,42	0,96	0,40	0,3172	3600	3960	0,13	0,86
BM 5		1,1	0,1324	0,44	0,96	0,42	0,3079	3600	3960	0,68	4,36
BM 6		1,1	0,1116	0,44	0,96	0,42	0,3073	3600	3960	0,13	0,86
BM 7		1,1	0,1052	0,43	0,96	0,41	0,3096	3600	3960	0,13	0,86
BM 8	Test series 3	1,1	0,0549	0,57	1,00	0,57	0,2775	3600	3960	0	0
BM 9		1,1	0,0654	0,57	1,00	0,57	0,2783	3600	3960	0,21	1,32
BM 10		1,1	0,0757	0,57	1,00	0,57	0,2802	3600	3960	1,43	9,11
BM 11		1,1	0,0846	0,57	1,00	0,57	0,2782	3600	3960	1,43	9,11
BM 12		1,1	0,0947	0,58	1,00	0,58	0,2769	3600	3960	4,29	27,34
BM 13		1,1	0,1060	0,57	1,00	0,57	0,2796	3600	3960	1,43	9,11
BM 14		1,1	0,1190	0,58	1,00	0,58	0,2752	3600	3960	2,25	14,33
BM 15		1,1	0,1308	0,58	1,00	0,58	0,2759	3600	3960	4,09	26,08
BM 16		1,1	0,1323	0,57	1,00	0,57	0,2815	3600	3960	3,69	23,50
BM 17		1,1	0,1374	0,57	1,00	0,57	0,2759	3600	3960	3,53	22,47
BM 18		1,1	0,1421	0,57	1,00	0,57	0,2794	3600	3960	4,95	31,53
BM 19		1,1	0,1495	0,57	1,00	0,57	0,2786	3600	3960	8,79	56,00
BM 20	Test series 4	1,1	0,0451	0,65	0.98	0,64	0,2873	3600	3960	1,43	9,11
BM 21		1,1	0,0556	0,66	0.98	0,65	0,2833	3600	3960	2,46	15,65
BM 22		1,1	0,0646	0,66	0.98	0,65	0,2859	3600	3960	4,50	28,66
BM 23		1,1	0,0745	0,66	0.98	0,65	0,2849	3600	3960	5,32	33,88
BM 24		1,1	0,0849	0,66	0.98	0,65	0,2823	3600	3960	5,72	36,46
BM 25		1,1	0,0976	0,66	0.98	0,65	0,2861	3600	3960	4,29	27,34
BM 26		1,1	0,1039	0,66	0.98	0,65	0,2817	3600	3960	6,54	41,67
BM 27		1,1	0,1187	0,66	0.98	0,65	0,2821	3600	3960	4,90	31,24
BM 28		1,1	0,1283	0,66	0.98	0,65	0,2840	3600	3960	5,52	35,20
BM 29		1,1	0,1338	0,66	0.98	0,65	0,2839	3600	3960	8,79	56,00
BM 30	Test series 5	1	0,0524	0,57	1,00	0,57	0,2783	3600	3600	0,90	5,73
BM 31		1	0,0651	0,57	1,00	0,57	0,2785	3600	3600	1,12	7,16
BM 32		1	0,0749	0,57	1,00	0,57	0,2784	3600	3600	1,12	7,16
BM 33		1	0,0839	0,57	1,00	0,57	0,2778	3600	3600	1,80	11,47
BM 34		1	0,0989	0,57	1,00	0,57	0,2790	3600	3600	2,91	18,52
BM 35		1	0,1099	0,57	1,00	0,57	0,2792	3600	3600	1,12	7,16
BM 36		1	0,1153	0,57	1,00	0,57	0,2786	3600	3600	1,80	11,47
BM 37		1	0,1268	0,57	1,00	0,57	0,2817	3600	3600	1,80	11,47
BM 38		1	0,1330	0,57	1,00	0,57	0,2793	3600	3600	1,01	6,45

Notes: d_{n50} = 5,45 mm (constant for all tests)
Δ = 1,55 (constant for all tests)

Appendix 6 Data set for pipeline covers

The next pages contain the raw data from the tests performed by Lomónaco (1994), Van Gent and Wallast (2001) and Saers (2005), denoted LOM, VGW and SAE, respectively. No further analysis has been applied to these data, with the exception of the parameters printed in *italics*:

- The 'maximum' wave height $H_{1./100}$ has been calculated for all tests using equation 2.38
- Only T_m was given for the tests by Van Gent and Wallast, T_p has been calculated as $T_p = T_m/0.8$
- Conversely, only T_p was given for the other tests, T_m has been calculated as $T_m = T_p/0.8$
- The original numbers refer to the numbering in the original reports by Lomónaco, Van Gent and Wallast and Saers
- Only Lomónaco states the duration of his tests explicitly; the others mention only a number of waves. In that case the test duration is estimated as $D = N \cdot T_m$

There are a few gaps in our numbering. The missing tests are the tests with breaking waves (as explained in chapter 5, these tests will not be used in the present research). All analyses in chapter 6 are based on the data sets *without* these tests.

Table A6.1 – Data set for pipeline covers. Tests with waves only
Hydraulic conditions and stone parameters

Test nr	Original nr	Data set	Hydraulic conditions							Stone parameters			
			H_s	$H_{1\%}$	T_m	T_p	N	h	h_c	ρ_s	d_{n50}	shape	Δ
			m	m	s	s	-	m	m	kg/m^3	mm	-	-
W 1	A310	VGW	0,090	*0,129*	1,11	*1,39*	1000	0,500	0,375	2650	7,20		1,65
W 2	A310	VGW	0,090	*0,129*	1,11	*1,39*	3000	0,500	0,375	2650	7,20		1,65
W 3	A311	VGW	0,127	*0,179*	1,32	*1,65*	1000	0,500	0,375	2650	7,20		1,65
W 4	A311	VGW	0,127	*0,179*	1,32	*1,65*	3000	0,500	0,375	2650	7,20		1,65
W 5	A312	VGW	0,163	*0,225*	1,51	*1,89*	1000	0,500	0,375	2650	7,20		1,65
W 6	A312	VGW	0,163	*0,225*	1,51	*1,89*	3000	0,500	0,375	2650	7,20		1,65
W 7	H312	VGW	0,162	*0,224*	1,51	*1,89*	1000	0,500	0,375	2650	7,20		1,65
W 8	H312	VGW	0,162	*0,224*	1,51	*1,89*	3000	0,500	0,375	2650	7,20		1,65
W 9	A313	VGW	0,188	*0,256*	1,66	*2,08*	1000	0,500	0,375	2650	7,20		1,65
W 10	A313	VGW	0,188	*0,256*	1,66	*2,08*	3000	0,500	0,375	2650	7,20		1,65
W 11	H313	VGW	0,186	*0,254*	1,66	*2,08*	1000	0,500	0,375	2650	7,20		1,65
W 12	H313	VGW	0,186	*0,254*	1,66	*2,08*	3000	0,500	0,375	2650	7,20		1,65
W 13	A320	VGW	0,085	*0,120*	1,10	*1,38*	1000	0,375	0,250	2650	7,20		1,65
W 14	A321	VGW	0,119	*0,165*	1,32	*1,65*	1000	0,375	0,250	2650	7,20		1,65
W 15	A321	VGW	0,119	*0,165*	1,32	*1,65*	3000	0,375	0,250	2650	7,20		1,65
W 18	A410	VGW	0,090	*0,129*	1,11	*1,39*	1000	0,500	0,375	2650	3,10		1,65
W 19	A410	VGW	0,090	*0,129*	1,11	*1,39*	3000	0,500	0,375	2650	3,10		1,65
W 20	A411	VGW	0,127	*0,179*	1,32	*1,65*	1000	0,500	0,375	2650	3,10		1,65
W 21	A411	VGW	0,127	*0,179*	1,32	*1,65*	3000	0,500	0,375	2650	3,10		1,65
W 22	A412	VGW	0,164	*0,226*	1,51	*1,89*	1000	0,500	0,375	2650	3,10		1,65
W 23	A412	VGW	0,164	*0,226*	1,51	*1,89*	3000	0,500	0,375	2650	3,10		1,65
W 26	T1 D2	LOM	0,149	*0,207*	*1,28*	1,61	2897	0,500	0,470	2463	3,65	Round	1,46
W 27	T1 D3	LOM	0,153	*0,212*	*1,26*	1,58	2870	0,500	0,444	2512	6,12	Round	1,51
W 28	T1 D4	LOM	0,149	*0,207*	*1,26*	1,58	2845	0,500	0,444	2512	6,12	Round	1,51
W 29	T1 D5	LOM	0,148	*0,206*	*1,26*	1,58	2840	0,500	0,446	2512	6,12	Round	1,51
W 30	T1 D6	LOM	0,140	*0,196*	*1,28*	1,61	2806	0,500	0,375	2712	8,33	Sharp	1,71
W 32	T2 D2	LOM	0,186	*0,254*	*1,49*	1,86	1864	0,500	0,468	2463	3,65	Round	1,46
W 33	T2 D3	LOM	0,191	*0,260*	*1,49*	1,86	1850	0,500	0,441	2512	6,12	Round	1,51
W 34	T2 D4	LOM	0,183	*0,250*	*1,56*	1,95	1853	0,500	0,442	2512	6,12	Round	1,51
W 35	T2 D5	LOM	0,181	*0,247*	*1,49*	1,86	1846	0,500	0,448	2512	6,12	Round	1,51
W 36	T2 D6	LOM	0,178	*0,244*	*1,56*	1,95	1799	0,500	0,374	2712	8,33	Sharp	1,71
W 38	T3 D2	LOM	0,213	*0,287*	*1,64*	2,05	928	0,500	0,470	2463	3,65	Round	1,46
W 40	T3 D4	LOM	0,209	*0,282*	*1,64*	2,05	898	0,500	0,442	2512	6,12	Round	1,51
W 41	T3 D5	LOM	0,202	*0,273*	*1,64*	2,05	919	0,500	0,442	2512	6,12	Round	1,51
W 44	T5A D2	LOM	0,208	*0,289*	*1,46*	1,82	953	0,700	0,670	2463	3,65	Round	1,46
W 45	T5A D3	LOM	0,233	*0,322*	*1,46*	1,82	970	0,700	0,636	2463	3,65	Round	1,46
W 46	T5A D4	LOM	0,201	*0,280*	*1,49*	1,86	950	0,700	0,638	2463	3,65	Round	1,46
W 47	T5A D5	LOM	0,203	*0,283*	*1,49*	1,86	938	0,700	0,640	2512	6,12	Round	1,51
W 48	T5A D6	LOM	0,202	*0,281*	*1,46*	1,82	920	0,700	0,572	2613	5,13	Sharp	1,61
W 49	T5A D7	LOM	0,180	*0,253*	*1,46*	1,82	956	0,700	0,440	2712	8,33	Sharp	1,71
W 50	T5B D2	LOM	0,208	*0,289*	*1,49*	1,86	1897	0,700	0,670	2463	3,65	Round	1,46
W 51	T5B D3	LOM	0,233	*0,322*	*1,46*	1,82	1935	0,700	0,636	2463	3,65	Round	1,46
W 52	T5B D4	LOM	0,201	*0,281*	*1,49*	1,86	1898	0,700	0,638	2463	3,65	Round	1,46
W 53	T5B D5	LOM	0,202	*0,281*	*1,49*	1,86	1876	0,700	0,640	2512	6,12	Round	1,51
W 54	T5B D6	LOM	0,204	*0,284*	*1,46*	1,82	1842	0,700	0,572	2613	5,13	Sharp	1,61
W 55	T5B D7	LOM	0,181	*0,254*	*1,46*	1,82	1908	0,700	0,440	2712	8,33	Sharp	1,71
W 56	T6A D2	LOM	0,251	*0,344*	*1,64*	2,05	932	0,700	0,662	2463	3,65	Round	1,46
W 57	T6A D3	LOM	0,283	*0,384*	*1,64*	2,05	921	0,700	0,636	2463	3,65	Round	1,46
W 58	T6A D4	LOM	0,244	*0,335*	*1,64*	2,05	929	0,700	0,637	2463	3,65	Round	1,46
W 59	T6A D5	LOM	0,243	*0,333*	*1,68*	2,10	920	0,700	0,630	2512	6,12	Round	1,51
W 60	T6A D6	LOM	0,244	*0,335*	*1,68*	2,10	907	0,700	0,572	2613	5,13	Sharp	1,61
W 61	T6A D7	LOM	0,223	*0,308*	*1,82*	2,28	911	0,700	0,442	2712	8,33	Sharp	1,71
W 62	T6B D2	LOM	0,252	*0,345*	*1,64*	2,05	1871	0,700	0,662	2463	3,65	Round	1,46
W 63	T6B D3	LOM	0,283	*0,383*	*1,64*	2,05	1845	0,700	0,636	2463	3,65	Round	1,46
W 64	T6B D4	LOM	0,244	*0,335*	*1,68*	2,10	1852	0,700	0,637	2463	3,65	Round	1,46
W 65	T6B D5	LOM	0,242	*0,332*	*1,68*	2,10	1842	0,700	0,630	2512	6,12	Round	1,51
W 66	T6B D6	LOM	0,243	*0,334*	*1,68*	2,10	1811	0,700	0,572	2613	5,13	Sharp	1,61
W 67	T6B D7	LOM	0,223	*0,309*	*1,82*	2,28	1822	0,700	0,442	2712	8,33	Sharp	1,71
W 68	T7A D2	LOM	0,255	*0,356*	*1,64*	2,05	975	0,900	0,861	2463	3,65	Round	1,46
W 69	T7A D3	LOM	0,285	*0,395*	*1,64*	2,05	960	0,900	0,837	2463	3,65	Round	1,46
W 70	T7A D4	LOM	0,248	*0,347*	*1,64*	2,05	974	0,900	0,837	2463	3,65	Round	1,46
W 71	T7A D5	LOM	0,252	*0,352*	*1,64*	2,05	957	0,900	0,833	2512	6,12	Round	1,51
W 72	T7A D6	LOM	0,250	*0,350*	*1,64*	2,05	960	0,900	0,773	2613	5,13	Sharp	1,61
W 73	T7A D7	LOM	0,238	*0,334*	*1,64*	2,05	936	0,900	0,646	2712	8,33	Sharp	1,71
W 74	T7B D2	LOM	0,257	*0,358*	*1,64*	2,05	1941	0,900	0,861	2463	3,65	Round	1,46
W 75	T7B D3	LOM	0,286	*0,396*	*1,64*	2,05	1921	0,900	0,837	2463	3,65	Round	1,46

Table A6.1 – Data set for pipeline covers. Tests with waves only
Hydraulic conditions and stone parameters (continued)

Test nr	Original nr	Data set	Hydraulic conditions							Stone parameters			
			H_s	$H_{1\%}$	T_m	T_p	N	h	h_c	ρ_s	d_{n50}	shape	Δ
			m	m	s	s	-	m	m	kg/m^3	mm	-	-
W 76	T7B D4	LOM	0,248	*0,347*	*1,64*	2,05	1949	0,900	0,837	2463	3,65	Round	1,46
W 77	T7B D5	LOM	0,250	*0,349*	*1,64*	2,05	1914	0,900	0,833	2512	6,12	Round	1,51
W 78	T7B D6	LOM	0,252	*0,352*	*1,64*	2,05	1910	0,900	0,773	2613	5,13	Sharp	1,61
W 79	T7B D7	LOM	0,241	*0,338*	*1,64*	2,05	1871	0,900	0,646	2712	8,33	Sharp	1,71
W 80	T9 D2	LOM	0,207	*0,280*	*2,05*	2,56	1011	0,500	0,461	2463	3,65	Round	1,46
W 82	T9 D4	LOM	0,199	*0,270*	*2,05*	2,56	976	0,500	0,438	2463	3,65	Round	1,46
W 83	T9 D5	LOM	0,201	*0,273*	*2,11*	2,64	973	0,500	0,441	2463	3,65	Round	1,46
W 86	T11 D2	LOM	0,263	*0,358*	*1,87*	2,34	968	0,700	0,669	2463	3,65	Round	1,46
W 87	T11 D3	LOM	0,293	*0,396*	*1,87*	2,34	973	0,700	0,636	2463	3,65	Round	1,46
W 88	T11 D4	LOM	0,253	*0,346*	*1,87*	2,34	955	0,700	0,640	2463	3,65	Round	1,46
W 89	T11 D5	LOM	0,257	*0,351*	*1,87*	2,34	955	0,700	0,641	2463	3,65	Round	1,46
W 90	T11 D6	LOM	0,259	*0,353*	*1,96*	2,45	919	0,700	0,571	2613	5,13	Sharp	1,61
W 92	T12 D2	LOM	0,215	*0,289*	*1,64*	2,05	931	0,500	0,469	2463	3,65	Round	1,46
W 94	T12 D4	LOM	0,206	*0,278*	*1,64*	2,05	905	0,500	0,443	2463	3,65	Round	1,46
W 95	T12 D5	LOM	0,203	*0,274*	*1,64*	2,05	908	0,500	0,442	2463	3,65	Round	1,46
W 96	0a6	SAE	0,208	*0,284*	*1,71*	2,14	1096	0,550	0,490	2470	3,70	Irregular	1,47
W 97	0a6	SAE	0,208	*0,284*	*1,71*	2,14	3177	0,550	0,490	2470	3,70	Irregular	1,47
W 100	1a4	SAE	0,209	*0,282*	*1,71*	2,14	1052	0,500	0,455	2470	3,70	Irregular	1,47
W 101	1a4	SAE	0,209	*0,282*	*1,71*	2,14	3114	0,500	0,455	2470	3,70	Irregular	1,47
W 102	1a4	SAE	0,209	*0,282*	*1,71*	2,14	6196	0,500	0,455	2470	3,70	Irregular	1,47
W 103	1a5	SAE	0,209	*0,282*	*1,71*	2,14	1028	0,500	0,451	2470	3,70	Irregular	1,47
W 104	1a5	SAE	0,209	*0,282*	*1,71*	2,14	2820	0,500	0,451	2470	3,70	Irregular	1,47
W 105	1a5	SAE	0,209	*0,282*	*1,71*	2,14	5855	0,500	0,451	2470	3,70	Irregular	1,47
W 106	1a6	SAE	0,209	*0,282*	*1,71*	2,14	982	0,500	0,436	2470	3,70	Irregular	1,47
W 107	1a6	SAE	0,209	*0,282*	*1,71*	2,14	2941	0,500	0,436	2470	3,70	Irregular	1,47
W 108	1a6	SAE	0,209	*0,282*	*1,71*	2,14	5961	0,500	0,436	2470	3,70	Irregular	1,47
W 109	1a6 her	SAE	0,209	*0,282*	*1,71*	2,14	1015	0,500	0,440	2470	3,70	Irregular	1,47
W 110	1a6 her	SAE	0,209	*0,282*	*1,71*	2,14	3079	0,500	0,440	2470	3,70	Irregular	1,47
W 111	1a6 her	SAE	0,209	*0,282*	*1,71*	2,14	6296	0,500	0,440	2470	3,70	Irregular	1,47
W 112	1b4	SAE	0,180	*0,244*	*1,62*	2,02	1023	0,450	0,408	2470	3,70	Irregular	1,47
W 113	1b4	SAE	0,180	*0,244*	*1,62*	2,02	3063	0,450	0,408	2470	3,70	Irregular	1,47
W 114	1b4	SAE	0,180	*0,244*	*1,62*	2,02	6083	0,450	0,408	2470	3,70	Irregular	1,47
W 115	1b6	SAE	0,180	*0,244*	*1,62*	2,02	1052	0,450	0,390	2470	3,70	Irregular	1,47
W 116	1b6	SAE	0,180	*0,244*	*1,62*	2,02	3114	0,450	0,390	2470	3,70	Irregular	1,47
W 117	1b6	SAE	0,180	*0,244*	*1,62*	2,02	6196	0,450	0,390	2470	3,70	Irregular	1,47
W 121	2b4	SAE	0,173	*0,236*	*1,62*	2,02	1046	0,450	0,409	2470	3,70	Irregular	1,47
W 122	2b4	SAE	0,173	*0,236*	*1,62*	2,02	3073	0,450	0,409	2470	3,70	Irregular	1,47
W 123	2b4	SAE	0,173	*0,236*	*1,62*	2,02	6128	0,450	0,409	2470	3,70	Irregular	1,47
W 124	2b5	SAE	0,173	*0,236*	*1,62*	2,02	1104	0,450	0,399	2470	3,70	Irregular	1,47
W 125	2b5	SAE	0,173	*0,236*	*1,62*	2,02	3330	0,450	0,399	2470	3,70	Irregular	1,47
W 126	2b5	SAE	0,173	*0,236*	*1,62*	2,02	6546	0,450	0,399	2470	3,70	Irregular	1,47
W 127	2b6	SAE	0,173	*0,236*	*1,62*	2,02	1079	0,450	0,390	2470	3,70	Irregular	1,47
W 128	2b6	SAE	0,173	*0,236*	*1,62*	2,02	3221	0,450	0,390	2470	3,70	Irregular	1,47
W 129	2b6	SAE	0,173	*0,236*	*1,62*	2,02	6369	0,450	0,390	2470	3,70	Irregular	1,47
W 130	3c4	SAE	0,148	*0,202*	*1,61*	2,01	990	0,400	0,358	2470	3,70	Irregular	1,47
W 131	3c4	SAE	0,148	*0,202*	*1,61*	2,01	2956	0,400	0,358	2470	3,70	Irregular	1,47
W 132	3c4	SAE	0,148	*0,202*	*1,61*	2,01	5621	0,400	0,358	2470	3,70	Irregular	1,47
W 133	3c5	SAE	0,148	*0,202*	*1,61*	2,01	10414	0,400	0,348	2470	3,70	Irregular	1,47
W 134	3c5	SAE	0,148	*0,202*	*1,61*	2,01	3112	0,400	0,348	2470	3,70	Irregular	1,47
W 135	3c5	SAE	0,148	*0,202*	*1,61*	2,01	6028	0,400	0,348	2470	3,70	Irregular	1,47
W 136	3c6	SAE	0,148	*0,202*	*1,61*	2,01	980	0,400	0,340	2470	3,70	Irregular	1,47
W 137	3c6	SAE	0,148	*0,202*	*1,61*	2,01	2910	0,400	0,340	2470	3,70	Irregular	1,47
W 138	3c6	SAE	0,148	*0,202*	*1,61*	2,01	5967	0,400	0,340	2470	3,70	Irregular	1,47

Table A6.2 – Data set for pipeline covers. Tests with waves only
Structure parameters and damage parameters

Test nr	Original nr	Data set	Structure parameters				Damage parameters			
			m_0	z_c	B_c	B	S	z_d	Duration	A_e
			-	m	m	m	-		s	cm^2
W 1	A310	VGW	3	0,1250	0,125	0,875	4,4		*1110*	2,28
W 2	A310	VGW	3	0,1250	0,125	0,875	6,1		*3330*	3,16
W 3	A311	VGW	3	0,1250	0,125	0,875	4,6		*1320*	2,38
W 4	A311	VGW	3	0,1250	0,125	0,875	7,3		*3960*	3,78
W 5	A312	VGW	3	0,1250	0,125	0,875	6,3		*1510*	3,27
W 6	A312	VGW	3	0,1250	0,125	0,875	7,4		*4530*	3,84
W 7	H312	VGW	3	0,1250	0,125	0,875	6,3		*1510*	3,27
W 8	H312	VGW	3	0,1250	0,125	0,875	13,0		*4530*	6,74
W 9	A313	VGW	3	0,1250	0,125	0,875	8,3		*1660*	4,30
W 10	A313	VGW	3	0,1250	0,125	0,875	11,8		*4980*	6,12
W 11	H313	VGW	3	0,1250	0,125	0,875	5,9		*1660*	3,06
W 12	H313	VGW	3	0,1250	0,125	0,875	10,0		*4980*	5,18
W 13	A320	VGW	3	0,1250	0,125	0,875	4,3		*1100*	2,23
W 14	A321	VGW	3	0,1250	0,125	0,875	2,1		*1320*	1,09
W 15	A321	VGW	3	0,1250	0,125	0,875	5,8		*3960*	3,01
W 18	A410	VGW	8	0,1250	0,125	2,125	22,3		*1110*	2,14
W 19	A410	VGW	8	0,1250	0,125	2,125	37,3		*3330*	3,58
W 20	A411	VGW	8	0,1250	0,125	2,125	18,5		*1320*	1,78
W 21	A411	VGW	8	0,1250	0,125	2,125	43,0		*3960*	4,13
W 22	A412	VGW	8	0,1250	0,125	2,125	103,6		*1510*	9,96
W 23	A412	VGW	8	0,1250	0,125	2,125	206,4		*4530*	19,84
W 26	T1 D2	LOM	3	0,0298	0,060	0,239	60,4	0,0254	3960	8,03
W 27	T1 D3	LOM	5	0,0562	0,120	0,682	4,5	0,0562	3960	1,70
W 28	T1 D4	LOM	3	0,0559	0,120	0,455	20,0	0,0554	3960	7,50
W 29	T1 D5	LOM	1	0,0540	0,120	0,228	41,5	0,0481	3960	15,55
W 30	T1 D6	LOM	3	0,1253	0,250	1,002	4,0	0,1248	3960	2,81
W 32	T2 D2	LOM	3	0,0320	0,060	0,252	32,0	0,0274	3000	4,25
W 33	T2 D3	LOM	5	0,0589	0,120	0,709	8,9	0,0579	3000	3,35
W 34	T2 D4	LOM	3	0,0576	0,120	0,466	8,3	0,0562	3000	3,10
W 35	T2 D5	LOM	1	0,0523	0,120	0,225	28,8	0,0459	3000	10,79
W 36	T2 D6	LOM	3	0,1265	0,250	1,009	10,2	0,1265	3000	7,06
W 38	T3 D2	LOM	3	0,0298	0,060	0,239	39,1	0,0252	1680	5,20
W 40	T3 D4	LOM	3	0,0579	0,120	0,467	10,6	0,0571	1680	3,99
W 41	T3 D5	LOM	1	0,0579	0,120	0,236	48,3	0,0466	1680	18,11
W 44	T5A D2	LOM	3	0,0300	0,060	0,240	12,3	0,0286	1680	1,63
W 45	T5A D3	LOM	5	0,0637	0,120	0,757	24,5	0,0635	1680	3,26
W 46	T5A D4	LOM	3	0,0625	0,120	0,495	46,2	0,0598	1680	6,13
W 47	T5A D5	LOM	1	0,0598	0,120	0,240	15,0	0,0586	1680	5,62
W 48	T5A D6	LOM	3	0,1280	0,250	1,018	21,3	0,1272	1680	5,62
W 49	T5A D7	LOM	3	0,2601	0,250	1,811	14,5	0,2584	1680	10,07
W 50	T5B D2	LOM	3	0,0300	0,060	0,240	16,8	0,0283	3360	2,23
W 51	T5B D3	LOM	5	0,0637	0,120	0,757	37,6	0,0632	3360	5,00
W 52	T5B D4	LOM	3	0,0625	0,120	0,495	62,1	0,0591	3360	8,25
W 53	T5B D5	LOM	1	0,0598	0,120	0,240	21,2	0,0571	3360	7,96
W 54	T5B D6	LOM	3	0,1280	0,250	1,018	33,5	0,1272	3360	8,80
W 55	T5B D7	LOM	3	0,2601	0,250	1,811	24,9	0,2579	3360	17,28
W 56	T6A D2	LOM	3	0,0376	0,060	0,286	75,0	0,0286	1680	9,97
W 57	T6A D3	LOM	5	0,0640	0,120	0,760	77,6	0,0608	1680	10,30
W 58	T6A D4	LOM	3	0,0630	0,120	0,498	140,4	0,0542	1680	18,65
W 59	T6A D5	LOM	1	0,0696	0,120	0,259	69,3	0,0491	1680	26,00
W 60	T6A D6	LOM	3	0,1277	0,250	1,016	46,0	0,1258	1680	12,11
W 61	T6A D7	LOM	3	0,2576	0,250	1,796	77,0	0,2518	1680	53,40
W 62	T6B D2	LOM	3	0,0376	0,060	0,286	97,7	0,0274	3360	12,98
W 63	T6B D3	LOM	5	0,0640	0,120	0,760	128,7	0,0576	3360	17,09
W 64	T6B D4	LOM	3	0,0630	0,120	0,498	215,9	0,0501	3360	28,69
W 65	T6B D5	LOM	1	0,0696	0,120	0,259	76,1	0,0476	3360	28,55
W 66	T6B D6	LOM	3	0,1277	0,250	1,016	73,7	0,1253	3360	19,40
W 67	T6B D7	LOM	3	0,2576	0,250	1,796	119,3	0,2449	3360	82,80
W 68	T7A D2	LOM	3	0,0386	0,060	0,292	48,0	0,0332	1680	6,37
W 69	T7A D3	LOM	5	0,0628	0,120	0,748	80,0	0,0601	1680	10,63
W 70	T7A D4	LOM	3	0,0632	0,120	0,499	85,9	0,0584	1680	11,41
W 71	T7A D5	LOM	1	0,0674	0,120	0,255	57,0	0,0545	1680	21,36
W 72	T7A D6	LOM	3	0,1270	0,250	1,012	50,6	0,1270	1680	13,32
W 73	T7A D7	LOM	3	0,2542	0,250	1,775	39,1	0,2527	1680	27,16
W 74	T7B D2	LOM	3	0,0386	0,060	0,292	54,5	0,0332	3360	7,24
W 75	T7B D3	LOM	5	0,0628	0,120	0,748	100,1	0,0598	3360	13,30

Table A6.2 – Data set for pipeline covers. Tests with waves only
Structure parameters and damage parameters (continued)

Test nr	Original nr	Data set	Structure parameters				Damage parameters			
			m_0	z_c	B_c	B	S	z_d	Duration	A_e
			-	m	m	m	-		s	cm^2
W 76	T7B D4	LOM	3	0,0632	0,120	0,499	105,0	0,0581	3360	13,94
W 77	T7B D5	LOM	1	0,0674	0,120	0,255	69,4	0,0508	3360	26,03
W 78	T7B D6	LOM	3	0,1270	0,250	1,012	66,2	0,1263	3360	17,41
W 79	T7B D7	LOM	3	0,2542	0,250	1,775	49,9	0,2527	3360	34,63
W 80	T9 D2	LOM	3	0,0391	0,060	0,295	92,1	0,0274	2100	12,24
W 82	T9 D4	LOM	3	0,0625	0,120	0,495	184,4	0,0488	2100	24,49
W 83	T9 D5	LOM	2	0,0589	0,120	0,356	209,4	0,0440	2100	27,83
W 86	T11 D2	LOM	3	0,0308	0,060	0,245	87,8	0,0210	1920	11,66
W 87	T11 D3	LOM	5	0,0640	0,120	0,760	199,3	0,0537	1920	26,48
W 88	T11 D4	LOM	3	0,0601	0,120	0,481	207,6	0,0459	1920	27,58
W 89	T11 D5	LOM	2	0,0591	0,120	0,356	227,2	0,0393	1920	30,18
W 90	T11 D6	LOM	3	0,1289	0,250	1,023	103,8	0,1233	1920	27,30
W 92	T12 D2	LOM	3	0,0310	0,060	0,246	51,6	0,0252	1680	6,86
W 94	T12 D4	LOM	3	0,0571	0,120	0,463	132,2	0,0481	1680	17,56
W 95	T12 D5	LOM	2	0,0584	0,120	0,354	203,9	0,0425	1680	27,10
W 96	0a6	SAE	2,5	0,0598	0,040	0,339	107,8	0,0514	*1876*	14,76
W 97	0a6	SAE	2,5	0,0598	0,040	0,339	128,2	0,0508	*5439*	17,54
W 100	1a4	SAE	2,5	0,0448	0,040	0,264	45,1	0,0351	*1801*	6,18
W 101	1a4	SAE	2,5	0,0448	0,040	0,264	53,3	0,0340	*5331*	7,30
W 102	1a4	SAE	2,5	0,0448	0,040	0,264	57,6	0,0335	*10608*	7,89
W 103	1a5	SAE	2,5	0,0494	0,040	0,287	83,5	0,0346	*1760*	11,43
W 104	1a5	SAE	2,5	0,0494	0,040	0,287	103,1	0,0325	*4828*	14,12
W 105	1a5	SAE	2,5	0,0494	0,040	0,287	104,9	0,0322	*10024*	14,36
W 106	1a6	SAE	2,5	0,0637	0,040	0,359	117,2	0,0451	*1681*	16,04
W 107	1a6	SAE	2,5	0,0637	0,040	0,359	138,6	0,0431	*5035*	18,97
W 108	1a6	SAE	2,5	0,0637	0,040	0,359	156,5	0,0419	*10205*	21,42
W 109	1a6 her	SAE	2,5	0,0596	0,040	0,338	119,0	0,0407	*1738*	16,29
W 110	1a6 her	SAE	2,5	0,0596	0,040	0,338	133,2	0,0395	*5271*	18,24
W 111	1a6 her	SAE	2,5	0,0596	0,040	0,338	150,6	0,0375	*10779*	20,62
W 112	1b4	SAE	2,5	0,0420	0,040	0,250	34,5	0,0342	*1653*	4,72
W 113	1b4	SAE	2,5	0,0420	0,040	0,250	40,6	0,0330	*4950*	5,56
W 114	1b4	SAE	2,5	0,0420	0,040	0,250	46,9	0,0321	*9830*	6,42
W 115	1b6	SAE	2,5	0,0604	0,040	0,342	56,7	0,0489	*1700*	7,76
W 116	1b6	SAE	2,5	0,0604	0,040	0,342	78,9	0,0459	*5032*	10,80
W 117	1b6	SAE	2,5	0,0604	0,040	0,342	99,6	0,0435	*10013*	13,64
W 121	2b4	SAE	2,5	0,0412	0,040	0,246	29,0	0,0343	*1690*	3,97
W 122	2b4	SAE	2,5	0,0412	0,040	0,246	32,4	0,0336	*4966*	4,43
W 123	2b4	SAE	2,5	0,0412	0,040	0,246	34,8	0,0332	*9903*	4,77
W 124	2b5	SAE	2,5	0,0509	0,040	0,295	58,0	0,0394	*1784*	7,94
W 125	2b5	SAE	2,5	0,0509	0,040	0,295	64,5	0,0385	*5381*	8,83
W 126	2b5	SAE	2,5	0,0509	0,040	0,295	70,9	0,0377	*10578*	9,71
W 127	2b6	SAE	2,5	0,0603	0,040	0,342	56,0	0,0491	*1744*	7,67
W 128	2b6	SAE	2,5	0,0603	0,040	0,342	62,9	0,0481	*5205*	8,61
W 129	2b6	SAE	2,5	0,0603	0,040	0,342	80,5	0,0459	*10292*	11,01
W 130	3c4	SAE	2,5	0,0425	0,040	0,253	25,3	0,0364	*1592*	3,46
W 131	3c4	SAE	2,5	0,0425	0,040	0,253	26,3	0,0364	*4753*	3,59
W 132	3c4	SAE	2,5	0,0425	0,040	0,253	27,0	0,0362	*9039*	3,70
W 133	3c5	SAE	2,5	0,0518	0,040	0,299	36,1	0,0439	*16746*	4,94
W 134	3c5	SAE	2,5	0,0518	0,040	0,299	57,7	0,0403	*5004*	7,90
W 135	3c5	SAE	2,5	0,0518	0,040	0,299	55,6	0,0406	*9693*	7,61
W 136	3c6	SAE	2,5	0,0596	0,040	0,338	50,2	0,0492	*1576*	6,88
W 137	3c6	SAE	2,5	0,0596	0,040	0,338	53,1	0,0488	*4679*	7,27
W 138	3c6	SAE	2,5	0,0596	0,040	0,338	55,2	0,0486	*9595*	7,56

Table A6.3 – Data set for pipeline covers. Tests with current and waves
Hydraulic conditions and stone parameters

Test nr	Original nr	Data set	Hydraulic conditions								Stone parameters			
			H_s	$H_{1\%}$	T_m	T_p	N	u_{da}	h	h_c	ρ_s	d_{n50}	Shape	Δ
			m	m	s	s	-	m/s	m	m	kg/m³	mm	-	-
WC 1	B320	VGW	0,078	*0,111*	1,08	*1,35*	1000	0,11	0,375	0,250	2650	7,20		1,65
WC 2	B321	VGW	0,112	*0,156*	1,29	*1,61*	1000	0,10	0,375	0,250	2650	7,20		1,65
WC 3	B321	VGW	0,112	*0,156*	1,29	*1,61*	3000	0,10	0,375	0,250	2650	7,20		1,65
WC 6	D320	VGW	0,067	*0,096*	1,12	*1,40*	1000	0,35	0,375	0,250	2650	7,20		1,65
WC 7	D321	VGW	0,098	*0,138*	1,30	*1,63*	1000	0,35	0,375	0,250	2650	7,20		1,65
WC 8	D321	VGW	0,098	*0,138*	1,30	*1,63*	3000	0,35	0,375	0,250	2650	7,20		1,65
WC 9	D322	VGW	0,122	*0,169*	1,46	*1,83*	1000	0,35	0,375	0,250	2650	7,20		1,65
WC 10	D322	VGW	0,122	*0,169*	1,46	*1,83*	3000	0,35	0,375	0,250	2650	7,20		1,65
WC 11	C410	VGW	0,076	*0,110*	1,09	*1,36*	1000	0,20	0,500	0,375	2650	3,10		1,65
WC 12	C410	VGW	0,076	*0,110*	1,09	*1,36*	3000	0,20	0,500	0,375	2650	3,10		1,65
WC 13	C411	VGW	0,113	*0,160*	1,28	*1,60*	1000	0,19	0,500	0,375	2650	3,10		1,65
WC 14	C412	VGW	0,147	*0,205*	1,49	*1,86*	1000	0,18	0,500	0,375	2650	3,10		1,65
WC 15	C412	VGW	0,147	*0,205*	1,49	*1,86*	3000	0,18	0,500	0,375	2650	3,10		1,65
WC 16	C413	VGW	0,172	*0,237*	1,62	*2,03*	1000	0,18	0,500	0,375	2650	3,10		1,65
WC 17	C413	VGW	0,172	*0,237*	1,62	*2,03*	3000	0,18	0,500	0,375	2650	3,10		1,65
WC 18	D413	VGW	0,163	*0,225*	1,60	*2,00*	1000	0,32	0,500	0,375	2650	3,10		1,65
WC 19	D413	VGW	0,163	*0,225*	1,60	*2,00*	3000	0,32	0,500	0,375	2650	3,10		1,65
WC 20	F423	VGW	0,141	*0,197*	1,57	*1,96*	1000	0,74	0,500	0,375	2650	3,10		1,65
WC 22	T4A D2	LOM	0,210	*0,284*	*1,64*	2,05	953	0,13	0,500	0,468	2463	3,65	round	1,46
WC 23	T4A D3	LOM	0,208	*0,281*	*1,64*	2,05	943	0,13	0,500	0,439	2512	6,12	round	1,51
WC 24	T4A D4	LOM	0,203	*0,275*	*1,68*	2,10	934	0,13	0,500	0,438	2512	6,12	round	1,51
WC 25	T4A D5	LOM	0,200	*0,271*	*1,68*	2,10	950	0,13	0,500	0,443	2512	6,12	round	1,51
WC 28	T4B D2	LOM	0,211	*0,284*	*1,68*	2,10	1899	0,13	0,500	0,468	2463	3,65	round	1,46
WC 29	T4B D3	LOM	0,208	*0,281*	*1,68*	2,10	1886	0,13	0,500	0,439	2512	6,12	round	1,51
WC 30	T4B D4	LOM	0,205	*0,277*	*1,68*	2,10	1883	0,13	0,500	0,438	2512	6,12	round	1,51
WC 31	T4B D5	LOM	0,199	*0,270*	*1,68*	2,10	1890	0,13	0,500	0,443	2512	6,12	round	1,51
WC 34	T8 D2	LOM	0,236	*0,331*	*1,64*	2,05	976	0,10	0,900	0,859	2463	3,65	round	1,46
WC 35	T8 D3	LOM	0,262	*0,365*	*1,64*	2,05	961	0,10	0,900	0,834	2463	3,65	round	1,46
WC 36	T8 D4	LOM	0,228	*0,320*	*1,60*	2,00	976	0,10	0,900	0,839	2463	3,65	round	1,46
WC 37	T8 D5	LOM	0,233	*0,328*	*1,64*	2,05	953	0,10	0,900	0,832	2512	6,12	round	1,51
WC 38	T8 D6	LOM	0,234	*0,329*	*1,64*	2,05	976	0,10	0,900	0,771	2613	5,13	sharp	1,61
WC 39	T8 D7	LOM	0,219	*0,309*	*1,64*	2,05	967	0,10	0,900	0,648	2712	8,33	sharp	1,71
WC 40	T10 D2	LOM	0,183	*0,251*	*2,05*	2,56	1177	0,21	0,500	0,469	2463	3,65	round	1,46
WC 41	T10 D3	LOM	0,207	*0,280*	*2,05*	2,56	1128	0,21	0,500	0,436	2463	3,65	round	1,46
WC 42	T10 D4	LOM	0,172	*0,237*	*2,05*	2,56	1107	0,21	0,500	0,440	2463	3,65	round	1,46
WC 43	T10 D5	LOM	0,175	*0,241*	*2,11*	2,64	1063	0,21	0,500	0,445	2463	3,65	round	1,46
WC 44	T10 D6	LOM	0,175	*0,240*	*1,93*	2,41	1041	0,21	0,500	0,374	2613	5,13	sharp	1,61

Table A6.4 – Data set for pipeline covers. Tests with current and waves
Structure parameters and damage parameters

Test nr	Original nr	Data set	Structure parameters				Damage parameters		
			m_0	z_c	B_c	B	S	z_d	A_e
			-	m	m	m	-	m	cm^2
WC 1	B320	VGW	3	0,1250	0,125	0,875	2,9		1,50
WC 2	B321	VGW	3	0,1250	0,125	0,875	3,0		1,56
WC 3	B321	VGW	3	0,1250	0,125	0,875	6,3		3,27
WC 6	D320	VGW	3	0,1250	0,125	0,875	14,6		7,57
WC 7	D321	VGW	3	0,1250	0,125	0,875	2,0		1,04
WC 8	D321	VGW	3	0,1250	0,125	0,875	3,1		1,61
WC 9	D322	VGW	3	0,1250	0,125	0,875	1,0		0,52
WC 10	D322	VGW	3	0,1250	0,125	0,875	1,3		0,67
WC 11	C410	VGW	8	0,1250	0,125	2,125	18,0		1,73
WC 12	C410	VGW	8	0,1250	0,125	2,125	25,0		2,40
WC 13	C411	VGW	8	0,1250	0,125	2,125	14,1		1,36
WC 14	C412	VGW	8	0,1250	0,125	2,125	10,4		1,00
WC 15	C412	VGW	8	0,1250	0,125	2,125	18,9		1,82
WC 16	C413	VGW	8	0,1250	0,125	2,125	28,9		2,78
WC 17	C413	VGW	8	0,1250	0,125	2,125	44,2		4,25
WC 18	D413	VGW	8	0,1250	0,125	2,125	22,0		2,11
WC 19	D413	VGW	8	0,1250	0,125	2,125	47,3		4,55
WC 20	F423	VGW	8	0,1250	0,125	2,125	769,0		73,90
WC 22	T4A D2	LOM	3	0,0325	0,060	0,255	56,0	0,0261	7,44
WC 23	T4A D3	LOM	5	0,0613	0,120	0,733	6,3	0,0613	2,36
WC 24	T4A D4	LOM	3	0,0618	0,120	0,491	5,4	0,0615	2,04
WC 25	T4A D5	LOM	1	0,0571	0,120	0,234	35,0	0,0491	13,12
WC 28	T4B D2	LOM	3	0,0325	0,060	0,255	83,8	0,0256	11,14
WC 29	T4B D3	LOM	5	0,0613	0,120	0,733	10,1	0,0613	3,79
WC 30	T4B D4	LOM	3	0,0618	0,120	0,491	9,6	0,0615	3,61
WC 31	T4B D5	LOM	1	0,0571	0,120	0,234	38,3	0,0491	14,37
WC 34	T8 D2	LOM	3	0,0415	0,060	0,309	38,0	0,0369	5,04
WC 35	T8 D3	LOM	5	0,0657	0,120	0,777	73,5	0,0628	9,76
WC 36	T8 D4	LOM	3	0,0615	0,120	0,489	53,5	0,0589	7,11
WC 37	T8 D5	LOM	1	0,0679	0,120	0,256	40,3	0,0584	15,11
WC 38	T8 D6	LOM	3	0,1292	0,250	1,025	49,7	0,1287	13,08
WC 39	T8 D7	LOM	3	0,2520	0,250	1,762	37,5	0,2520	26,04
WC 40	T10 D2	LOM	3	0,0308	0,060	0,245	81,6	0,0291	10,84
WC 41	T10 D3	LOM	5	0,0640	0,120	0,760	137,7	0,0611	18,29
WC 42	T10 D4	LOM	3	0,0596	0,120	0,478	116,6	0,0574	15,49
WC 43	T10 D5	LOM	2	0,0554	0,120	0,342	178,4	0,0466	23,70
WC 44	T10 D6	LOM	3	0,1260	0,250	1,006	60,2	0,1248	15,82

Appendix 7 Statistical tools

A7.1 The coefficient of determination r^2

The single most often used statistical notion in this thesis is the coefficient of determination r^2. This is a measure of how well a given model, e.g a Paintal-type transport formulation $\Phi_q = a\Psi^b$ fits a given dataset, on a normalised scale from 0 to 1. In general terms, r^2 can be seen as the amount of variation in the dependent variable (in our example the transport rate Φ_q) that can be explained by the model under investigation (in our example the formula $a\Psi^b$). In other words: if a model, say $\Phi_q = 5 \cdot \Psi^2$, has a coefficient of determination $r^2 = 0.80$, that means that calculating Φ_q as $5 \cdot \Psi^2$ explains 80% of the observed (measured) values of Φ.

There is no common guideline as to what value of r^2 can be accepted as a good fit, but Bryman and Cramer (2005) give the following rules of thumb:

Table A7.1 - Goodness-of-fit assessment using r^2

r	r^2	goodness-of-fit
< 0.19	< 0.039	very low
0.20 – 0.39	0.04 – 0.159	low
0.40 – 0.69	0.16 – 0.489	modest
0.70 – 0.89	0.49 – 0.809	high
> 0.90	> 0.81	very high

Other measures for the goodness-of-fit of a model exist, but r^2 is by far the most common one in research. This is also the measure that a program like Microsoft Excel automatically calculates when a trend line is fitted through a scatter cloud of data points.

A7.1.1 Transformation of variables and linear regression

In this thesis we will try to fit non-linear models (like $\Phi_q = a\Psi^b$) to a dataset. The tool that

we use for this purpose is a simple linear regression, which means that we will have to transform our models to a linear form.

A Paintal-type model $\Phi_q = a\Psi^b$ is linearized by taking the (natural) logarithm of both sides of the equation:

$$\ln(\Phi_q) = \ln(a) + b \cdot \ln(\Psi) \tag{6.1}$$

The coefficients can now simply be found by fitting a linear equation $Y = p_0 + p_1.X_1$ with $Y = \ln(\Phi_q)$ and $X_1 = \ln(\Psi)$, for instance by a standard least-squares regression analysis. From (6.1) it follows that $a = e^{p0}$ and $b = p_1$

For a Bijker-type model $\Phi_q = a\cdot(\Psi_c)^b\cdot\exp(c/\Psi_{wc})$ linearization results in

$$\ln(\Phi_q) = \ln(a) + b \cdot \ln(\Psi_c) + c \cdot (1/\Psi_{wc}) \tag{6.2}$$

The coefficients in the model can be found by fitting a linear equation $Y = p_0 + p_1 \bullet X_1 + p_2 \bullet X_2$ with $Y = \ln(\Phi_q)$, $X_1 = \ln(\Psi_c)$ and $X_2 = 1/\Psi_{wc}$, using a multivariate regression analysis. From (6.2) it follows that $a = e^{p0}$, $b = p_1$ and $c = p_2$

In general, any model that is built of a product of variables can be fitted by a linear regression on the logarithms of the variables. Essentially, the variable r^2 is the correlation coefficient (squared) between the measured Y-values and the Y-values predicted with the linear regression model. The correlation between the non-transformed variables (such as Φ_q and Ψ) will be different!

A7.2 Software package SPSS

For a simple analysis on two variables (eg $\Phi_q = a\Psi^b$) we can use Microsoft Excel to calculate a, b and r^2. This is essentially what happens when we plot Φ_q against Ψ and ask Excel to calculate a (power) trend line. When we want to fit more than two parameters (as is for instance the case when we want to fit a Bijker-type transport formula, or want to explore the influence of various variables on the stability of near-bed structures) we can no longer use Excel. Instead we will have to refer to more powerful statistical software. In this thesis we have used the standard software for this purpose: SPSS for Windows, version 12.

A package like SPSS produces more output than simply the regression coefficients (a, b and c in our examples) and r^2. This output must be understood well. An example of a typical SPSS output (in the format that we will use in this research) is given in Figure A7.1. The most important parameters on this output will be discussed next. This discussion is largely based on Bryman and Cramer (2005)

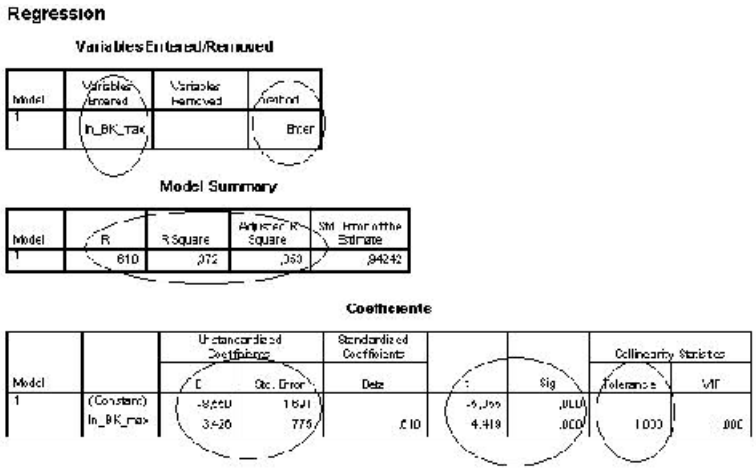

Figure A7.1 – Example of SPSS output

- **Variables entered/removed**: This table shows which variables are currently in the model as dependent (X) variables (the independent variable Y is not shown). Note that SPSS always shows the results of the linear analysis on the transformed variables. The 'method' that is referred to is the procedure that SPSS uses to enter the variables into the equation. In this thesis we will use two different methods: 'enter' and 'stepwise'. In the 'enter' method all variables are 'forced' into the equation. We will use this method when we seek to fit a existing formula, like the Bijker transport equation, and we are certain that all variables should be in the equation. The 'stepwise' allows the software program to decide whether a variable must be entered into the equation or not. In general terms, a variable is only entered into the equation when it really adds any information to the resulting model. If the model performs just as good (or almost just as good) without it, a variable is indeed left out. We will use this method when we investigate the stability of near-bed structures and we do not know a priori whether a variable should be in the equation. It must be said that the 'stepwise' method is a simple but rather crude way of achieving this goal, and more sophisticated ways do exist.

- **Model summary:** this gives the value of r, r^2 and an adjusted r^2. The first two measures have been discussed above; the adjusted r^2 must be used when we compare the goodness-of-fit of two models with a different number of variables (for instance a Paintal-type formula and a Bijker-type formula). In our results given in this chapter we will always use this adjusted r^2 in order to avoid any complications.
- **Coefficients**: This table gives the calculated regression coefficients (B) of the various variables in the model. Again, it is stressed that these are the coefficients for the linear model (p_0, p_1 and p_2 in our example in the previous paragraph); the coefficients for the 'real' non-linear model must be calculated by backwards transformation as described above. The standard errors in the next column are an indication of the accuracy of the results and can be used to calculate the confidence bounds; eg the 95% confidence bounds can be calculated as B $\pm$ 1.96·(standard error). Next, the columns 't' and 'sig' provide information on the relative contribution of the variable in question to the overall goodness-of-fit of the model. The SPSS documentation states that as a rule of thumb, a variable must have a t-value of well above 2 (or below -2) to have a serious influence; or equivalently the significance level of the variable ('sig') must be low enough (say < 0.005). This information is particularly of interest when the 'enter' method has been used to calculated the regression; when the 'stepwise' method has been used these values should automatically be fine (but of course it will do no harm to double-check that). Finally, the 'tolerance' statistic is an important indicator of the 'correctness' of a model. It is a measure of the correlation between a dependent variable and the other dependent variables in the model. Ideally, an independent variable (Y) must be predicted by a model of dependent variables X that have no correlation among themselves. If this is not the case the (implicit) correlation between the X variables may eclipse the (desired) correlation between the X and Y variables, and as a result the model can be severely biased. Because of the way it is formally defined, the tolerance statistic should be high; a low value indicates that the X variables are closely correlated and that the resulting model is very likely to yield false results.

Appendix 8 Calculation results

The next pages contain:

- The Excel output for the fit of a Paintal-type transport formula on the data of Bijman, see § 6.1.1
- The Excel output for the calculation of the various damage profiles based on the data of Lomónaco, Van Gent and Wallast and Saers, see § 6.2.1
- The Excel output for the fit of a transport equation on the data of Lomónaco, Van Gent and Wallast and Saers using a transport-based design method, see § 6.2.2
- The categorisation of the damaged structures in the dataset of Lomónaco, see § 6.3.1
- A summary of the SPSS output for the fit of the dimensionless erosion area S on the data by Lomónaco, Van Gent and Wallast and Saers, tables A8.1 – A8.3, see § 6.3.2
- The Excel output for the calculation of the critical values of the stability parameters based on the data of Bijman, see § 6.4.1

See appendix 7 for some remarks on the way in which the full SPSS output must be interpreted. The full SPSS output on which the tables A7.1 – A7.3 are based, as well as the SPSS output for the fit of a Bijker-type formula on the data for flat bed protections (§ 6.1.2) is included on a CD-rom (.SPO files).

Fit of transport formula on data of Bijman (2000)
Sheet 1 Calculation of stability parameters

Test nr	C	tau c	u_0	fw	tau w	Psi - Bijker				Psi - Grant and Madsen				Psi - Fredsoe				Psi - No WCI				Theta	Morison
	m1/2 /s	Pa	m/s	-	Pa	max	av x	av	av 1/2	max	av x	av	av 1/2	max	av x	av	av 1/2	max	av x	av	av 1/2	-	-
BM 1	45,0	0,693	0,201	0,161	3,263	0,084	0,024	0,028	0,051	0,046	0,013	0,022	0,034	0,034	0,011	0,013	0,023	0,048	0,008	0,016	0,016	0,49	0,76
BM 2	45,0	0,693	0,307	0,116	5,477	0,121	0,030	0,041	0,071	0,072	0,015	0,037	0,051	0,049	0,013	0,019	0,031	0,074	0,008	0,016	0,016	1,14	1,35
BM 3	45,5	0,846	0,266	0,130	4,574	0,113	0,031	0,037	0,067	0,064	0,017	0,032	0,047	0,047	0,014	0,018	0,031	0,065	0,010	0,019	0,019	0,85	1,10
BM 4	45,8	0,761	0,271	0,128	4,696	0,111	0,030	0,037	0,066	0,064	0,016	0,032	0,046	0,045	0,013	0,017	0,030	0,066	0,009	0,017	0,017	0,89	1,14
BM 5	45,5	0,844	0,246	0,138	4,162	0,106	0,029	0,035	0,063	0,060	0,017	0,029	0,044		0,014	0,017	0,029	0,060	0,010	0,019	0,019	0,73	0,99
BM 6	45,5	0,844	0,208	0,157	3,391	0,092	0,027	0,030	0,056	0,050	0,016	0,024	0,037		0,013	0,015	0,026	0,051	0,010	0,019	0,019	0,52	0,79
BM 7	45,6	0,804	0,194	0,166	3,132	0,086	0,025	0,028	0,052	0,046	0,015	0,022	0,035	0,035	0,012	0,013	0,025	0,048	0,010	0,018	0,018	0,46	0,72
BM 8	44,7	1,593	0,113	0,264	1,679	0,079	0,029	0,029	0,054	0,042	0,024	0,024	0,035	0,039	0,020	0,020	0,031	0,039	0,019	0,029	0,029	0,15	0,36
BM 9	44,8	1,591	0,134	0,227	2,035	0,087	0,031	0,031	0,059	0,047	0,025	0,025	0,039	0,042	0,020	0,020	0,034	0,044	0,019	0,029	0,029	0,22	0,45
BM 10	44,8	1,588	0,154	0,201	2,386	0,095	0,033	0,033	0,063	0,052	0,026	0,026	0,042	0,046	0,020	0,020	0,036	0,048	0,019	0,029	0,029	0,29	0,54
BM 11	44,8	1,592	0,173	0,182	2,736	0,103	0,035	0,035	0,067	0,056	0,026	0,027	0,045	0,049	0,021	0,021	0,038	0,052	0,019	0,029	0,029	0,36	0,62
BM 12	44,7	1,651	0,195	0,165	3,142	0,113	0,038	0,038	0,073	0,063	0,028	0,030	0,050	0,054	0,022	0,022	0,041	0,058	0,020	0,030	0,030	0,46	0,73
BM 13	44,8	1,589	0,216	0,152	3,557	0,119	0,039	0,040	0,076	0,067	0,028	0,031	0,053		0,022	0,023	0,042	0,062	0,019	0,029	0,029	0,56	0,83
BM 14	44,7	1,654	0,246	0,137	4,169	0,134	0,043	0,045	0,085	0,077	0,030	0,036	0,059		0,023	0,025	0,045	0,070	0,020	0,030	0,030	0,73	1,00
BM 15	44,7	1,653	0,270	0,128	4,671	0,143	0,045	0,048	0,090	0,083	0,031	0,039	0,064	0,066	0,024	0,026	0,047	0,076	0,020	0,030	0,030	0,88	1,13
BM 16	44,8	1,585	0,268	0,129	4,628	0,140	0,044	0,047	0,088	0,081	0,030	0,038	0,062	0,064	0,023	0,025	0,046	0,075	0,019	0,029	0,029	0,87	1,12
BM 17	44,7	1,596	0,284	0,123	4,965	0,147	0,045	0,049	0,092	0,086	0,030	0,040	0,065	0,067	0,024	0,026	0,048	0,079	0,019	0,029	0,029	0,97	1,21
BM 18	44,8	1,589	0,290	0,121	5,103	0,149	0,046	0,049	0,093	0,087	0,030	0,041	0,066	0,068	0,024	0,026	0,048	0,081	0,019	0,029	0,029	1,02	1,25
BM 19	44,8	1,591	0,306	0,117	5,456	0,156	0,047	0,052	0,096	0,092	0,031	0,043	0,069	0,071	0,024	0,027	0,050	0,085	0,019	0,029	0,029	1,13	1,35
BM 20	45,0	1,966	0,090	0,300	1,206	0,078	0,031	0,031	0,056	0,043	0,028	0,028	0,037	0,040	0,025	0,025	0,035	0,038	0,024	0,034	0,034	0,10	0,28
BM 21	44,9	2,036	0,112	0,266	1,667	0,089	0,034	0,034	0,062	0,049	0,030	0,030	0,042	0,045	0,026	0,026	0,038	0,045	0,025	0,035	0,035	0,15	0,36
BM 22	45,0	2,030	0,129	0,234	1,950	0,096	0,036	0,036	0,066	0,053	0,031	0,031	0,045	0,049	0,026	0,026	0,040	0,048	0,024	0,035	0,035	0,20	0,43
BM 23	44,9	2,032	0,149	0,206	2,301	0,104	0,038	0,038	0,071	0,058	0,032	0,032	0,048	0,053	0,026	0,026	0,042	0,052	0,025	0,035	0,035	0,27	0,52
BM 24	44,9	2,039	0,172	0,184	2,704	0,114	0,040	0,041	0,076	0,064	0,033	0,033	0,052	0,057	0,026	0,026	0,045	0,057	0,025	0,035	0,035	0,36	0,62
BM 25	45,0	2,029	0,195	0,165	3,140	0,123	0,043	0,043	0,081	0,070	0,034	0,034	0,056	0,061	0,026	0,026	0,047	0,062	0,024	0,035	0,035	0,46	0,73
BM 26	44,8	2,040	0,210	0,156	3,444	0,130	0,044	0,045	0,085	0,074	0,035	0,035	0,059		0,027	0,027	0,049	0,066	0,025	0,035	0,035	0,53	0,80
BM 27	44,9	2,039	0,240	0,140	4,040	0,143	0,047	0,049	0,092	0,082	0,036	0,039	0,065		0,028	0,029	0,052	0,073	0,025	0,035	0,035	0,70	0,96
BM 28	44,9	2,035	0,258	0,133	4,410	0,150	0,049	0,051	0,096	0,087	0,036	0,041	0,068	0,073	0,028	0,029	0,054	0,078	0,025	0,035	0,035	0,80	1,06
BM 29	44,9	2,035	0,269	0,128	4,647	0,155	0,050	0,052	0,099	0,090	0,037	0,042	0,070	0,074	0,028	0,030	0,055	0,081	0,025	0,035	0,035	0,87	1,12
BM 30	44,8	1,591	0,097	0,300	1,417	0,076	0,028	0,028	0,052	0,040	0,024	0,024	0,033	0,036	0,020	0,020	0,030	0,036	0,019	0,029	0,029	0,11	0,33
BM 31	44,8	1,591	0,121	0,271	1,971	0,086	0,031	0,031	0,058	0,045	0,024	0,024	0,037	0,041	0,020	0,020	0,033	0,043	0,019	0,029	0,029	0,18	0,43
BM 32	44,8	1,591	0,139	0,239	2,302	0,093	0,033	0,033	0,062	0,049	0,025	0,025	0,040	0,044	0,020	0,020	0,035	0,047	0,019	0,029	0,029	0,23	0,51
BM 33	44,7	1,592	0,156	0,216	2,624	0,100	0,034	0,035	0,066	0,053	0,026	0,026	0,043	0,047	0,020	0,021	0,037	0,051	0,019	0,029	0,029	0,29	0,58
BM 34	44,8	1,590	0,183	0,189	3,154	0,111	0,037	0,038	0,072	0,060	0,027	0,028	0,048	0,051	0,021	0,022	0,039	0,057	0,019	0,029	0,029	0,40	0,72
BM 35	44,8	1,590	0,203	0,173	3,566	0,120	0,039	0,040	0,077	0,066	0,027	0,031	0,051		0,022	0,022	0,041	0,062	0,019	0,029	0,029	0,50	0,82
BM 36	44,8	1,591	0,214	0,166	3,785	0,124	0,040	0,042	0,079	0,068	0,028	0,032	0,053		0,022	0,023	0,042	0,065	0,019	0,029	0,029	0,55	0,88
BM 37	44,8	1,585	0,232	0,155	4,180	0,132	0,042	0,044	0,083	0,073	0,028	0,034	0,057		0,022	0,023	0,043	0,070	0,019	0,029	0,029	0,65	0,98
BM 38	44,8	1,589	0,246	0,148	4,477	0,138	0,043	0,046	0,086	0,077	0,029	0,036	0,059	0,062	0,023	0,024	0,044	0,073	0,019	0,029	0,029	0,73	1,05

Fit of transport formula on data of Bijman (2000)
Sheet 2 Fit of Paintal-type transport formula

Test nr	ln (Phi_q)	ln(Psi Bijker)				ln(Psi Grant and Madsen)				ln (Psi Fredsoe)				ln(Psi No WCI)				ln (Theta)	ln (Morison)
		max	avx	av	av12	max	avx	av	av12	max	avx	av	av12	max	avx	av	av12		
BM 1																			
BM 2																			
BM 3	-17,52	-2,19	-3,50	-3,30	-2,71	-2,75	-4,10	-3,45	-3,07	-3,08	-4,30	-4,06	-3,50	-2,73	-4,63	-4,01	-4,01	-0,16	0,10
BM 4	-18,57	-2,21	-3,54	-3,30	-2,73	-2,76	-4,19	-3,45	-3,09	-3,11	-4,38	-4,08	-3,54	-2,73	-4,73	-4,07	-4,07	-0,12	0,13
BM 5	-16,95	-2,26	-3,55	-3,37	-2,77	-2,83	-4,13	-3,55	-3,15		-4,34	-4,13	-3,56	-2,81	-4,63	-4,01	-4,01	-0,31	-0,01
BM 6	-18,57	-2,40	-3,64	-3,51	-2,90	-3,00	-4,18	-3,74	-3,30		-4,39	-4,26	-3,66	-2,98	-4,63	-4,01	-4,01	-0,65	-0,23
BM 7	-18,57	-2,47	-3,70	-3,58	-2,96	-3,08	-4,25	-3,82	-3,38	-3,37	-4,45	-4,33	-3,73	-3,06	-4,68	-4,04	-4,04	-0,79	-0,32
BM 8																			
BM 9	-18,14	-2,44	-3,47	-3,47	-2,84	-3,06	-3,69	-3,69	-3,25	-3,16	-3,90	-3,90	-3,39	-3,13	-3,95	-3,55	-3,55	-1,53	-0,80
BM 10	-16,21	-2,35	-3,41	-3,40	-2,77	-2,96	-3,66	-3,66	-3,17	-3,09	-3,90	-3,90	-3,33	-3,04	-3,96	-3,55	-3,55	-1,25	-0,62
BM 11	-16,21	-2,28	-3,35	-3,34	-2,70	-2,87	-3,63	-3,61	-3,10	-3,02	-3,87	-3,86	-3,28	-2,95	-3,95	-3,55	-3,55	-1,01	-0,47
BM 12	-15,11	-2,18	-3,28	-3,26	-2,62	-2,77	-3,57	-3,52	-3,00	-2,92	-3,81	-3,80	-3,20	-2,85	-3,92	-3,52	-3,52	-0,78	-0,32
BM 13	-16,21	-2,12	-3,25	-3,21	-2,57	-2,70	-3,58	-3,46	-2,95		-3,82	-3,78	-3,18	-2,78	-3,95	-3,55	-3,55	-0,57	-0,18
BM 14	-15,76	-2,01	-3,15	-3,11	-2,47	-2,57	-3,50	-3,33	-2,83		-3,76	-3,71	-3,10	-2,66	-3,91	-3,52	-3,52	-0,31	0,00
BM 15	-15,16	-1,94	-3,11	-3,04	-2,41	-2,49	-3,48	-3,25	-2,76	-2,72	-3,73	-3,66	-3,05	-2,57	-3,91	-3,52	-3,52	-0,13	0,12
BM 16	-15,26	-1,96	-3,13	-3,07	-2,43	-2,51	-3,52	-3,27	-2,78	-2,74	-3,76	-3,69	-3,08	-2,59	-3,96	-3,55	-3,55	-0,14	0,11
BM 17	-15,31	-1,92	-3,10	-3,02	-2,39	-2,46	-3,49	-3,21	-2,73	-2,70	-3,74	-3,65	-3,04	-2,54	-3,95	-3,54	-3,54	-0,03	0,19
BM 18	-14,97	-1,90	-3,09	-3,01	-2,38	-2,44	-3,49	-3,19	-2,72	-2,68	-3,73	-3,64	-3,03	-2,52	-3,95	-3,55	-3,55	0,01	0,22
BM 19	-14,40	-1,86	-3,06	-2,96	-2,34	-2,39	-3,47	-3,14	-2,67	-2,64	-3,71	-3,60	-3,00	-2,46	-3,95	-3,55	-3,55	0,12	0,30
BM 20	-16,21	-2,53	-3,43	-3,43	-2,86	-3,12	-3,53	-3,53	-3,26	-3,19	-3,66	-3,66	-3,33	-3,24	-3,70	-3,36	-3,36	-2,33	-1,28
BM 21	-15,67	-2,40	-3,34	-3,34	-2,75	-2,99	-3,46	-3,46	-3,14	-3,07	-3,61	-3,61	-3,23	-3,09	-3,67	-3,33	-3,33	-1,89	-1,02
BM 22	-15,07	-2,32	-3,30	-3,30	-2,69	-2,91	-3,44	-3,44	-3,08	-3,00	-3,61	-3,61	-3,18	-3,02	-3,67	-3,34	-3,34	-1,61	-0,84
BM 23	-14,90	-2,24	-3,24	-3,24	-2,62	-2,82	-3,41	-3,41	-3,01	-2,92	-3,62	-3,62	-3,14	-2,93	-3,67	-3,33	-3,33	-1,31	-0,66
BM 24	-14,82	-2,15	-3,18	-3,18	-2,55	-2,73	-3,38	-3,38	-2,93	-2,84	-3,61	-3,61	-3,07	-2,84	-3,66	-3,33	-3,33	-1,03	-0,48
BM 25	-15,11	-2,08	-3,13	-3,12	-2,49	-2,64	-3,35	-3,35	-2,86	-2,77	-3,60	-3,60	-3,02	-2,76	-3,67	-3,34	-3,34	-0,78	-0,32
BM 26	-14,69	-2,02	-3,09	-3,08	-2,44	-2,58	-3,33	-3,31	-2,80		-3,58	-3,57	-2,98	-2,70	-3,66	-3,33	-3,33	-0,63	-0,22
BM 27	-14,98	-1,93	-3,02	-3,01	-2,36	-2,48	-3,30	-3,24	-2,72		-3,55	-3,53	-2,92	-2,60	-3,66	-3,33	-3,33	-0,36	-0,04
BM 28	-14,86	-1,88	-2,99	-2,96	-2,32	-2,42	-3,28	-3,18	-2,67	-2,59	-3,53	-3,50	-2,89	-2,54	-3,67	-3,33	-3,33	-0,22	0,06
BM 29	-14,40	-1,85	-2,97	-2,94	-2,29	-2,39	-3,27	-3,15	-2,63	-2,58	-3,51	-3,48	-2,87	-2,51	-3,67	-3,33	-3,33	-0,14	0,12
BM 30	-16,67	-2,58	-3,56	-3,56	-2,95	-3,23	-3,75	-3,75	-3,40	-3,32	-3,90	-3,90	-3,49	-3,32	-3,95	-3,55	-3,55	-2,17	-1,11
BM 31	-16,45	-2,46	-3,48	-3,48	-2,85	-3,11	-3,71	-3,71	-3,29	-3,20	-3,91	-3,91	-3,42	-3,15	-3,95	-3,55	-3,55	-1,74	-0,85
BM 32	-16,45	-2,37	-3,42	-3,42	-2,78	-3,02	-3,68	-3,68	-3,22	-3,12	-3,91	-3,91	-3,36	-3,06	-3,95	-3,55	-3,55	-1,46	-0,68
BM 33	-15,98	-2,30	-3,37	-3,36	-2,72	-2,93	-3,66	-3,65	-3,15	-3,07	-3,89	-3,89	-3,31	-2,98	-3,95	-3,55	-3,55	-1,23	-0,54
BM 34	-15,50	-2,20	-3,30	-3,27	-2,63	-2,81	-3,62	-3,56	-3,04	-2,98	-3,86	-3,84	-3,24	-2,86	-3,95	-3,55	-3,55	-0,91	-0,33
BM 35	-16,45	-2,12	-3,24	-3,21	-2,57	-2,73	-3,60	-3,49	-2,97		-3,83	-3,80	-3,20	-2,78	-3,95	-3,55	-3,55	-0,70	-0,20
BM 36	-15,98	-2,09	-3,22	-3,18	-2,54	-2,69	-3,58	-3,45	-2,94		-3,83	-3,79	-3,18	-2,74	-3,95	-3,55	-3,55	-0,60	-0,13
BM 37	-15,98	-2,03	-3,18	-3,13	-2,49	-2,61	-3,56	-3,38	-2,87		-3,81	-3,75	-3,14	-2,67	-3,96	-3,55	-3,55	-0,43	-0,02
BM 38	-16,56	-1,98	-3,15	-3,08	-2,45	-2,57	-3,55	-3,32	-2,83	-2,78	-3,79	-3,72	-3,11	-2,61	-3,95	-3,55	-3,55	-0,32	0,05
	a	1,94E-04	2,57	0,39	0,015	3,97E-04	0,19	0,47	0,012	0,017	0,66	23,52	0,62	9,95E-05	0,020	0,63	0,630	1,42E-07	1,29E-07
	b	3,43	5,16	4,65	4,51	2,96	3,97	4,41	3,86	4,01	4,06	5,06	4,82	2,40	3,04	4,37	4,37	0,29	0,44
	rsq	**0,37**	**0,73**	**0,53**	**0,55**	**0,36**	**0,80**	**0,50**	**0,52**	**0,57**	**0,77**	**0,80**	**0,79**	**0,22**	**0,65**	**0,65**	**0,65**	**0,03**	**0,02**

Assessment of damage profiles; data of Lomonaco (1994), Van Gent and Wallast (2001) and Saers (2005)
Sheet 1

	Structure							Measured damage			Gauss-shaped profile			Sliced profile			Sagged profile			Combination profile			Av
Test nr	dn50	m0	Bc	B	zc	A0	S	Ae	zd	delta_z /dn50	zd	sigma	delta_z /dn50	delta_z	zd	delta_z /dn50	zd	md	delta_z /dn50	delta_z	zd	delta_z /dn50	delta_z /dn50
-	m	-	m	m	m	m2	-	m2	m	-	m	m	-	m	m	-	m	-	-	m	m	-	-
W 1	0,0072	3	0,125	0,875	0,125	0,063	4,40	2,28E-04			0,125	0,1820	0,00	0,0018	0,123	0,24	0,124	3,04	0,09	0,0007	0,124	0,10	0,17
W 2	0,0072	3	0,125	0,875	0,125	0,063	6,10	3,16E-04			0,125	0,1820	0,00	0,0024	0,123	0,33	0,124	3,04	0,09	0,0010	0,124	0,14	0,24
W 3	0,0072	3	0,125	0,875	0,125	0,063	4,60	2,38E-04			0,125	0,1820	0,00	0,0018	0,123	0,25	0,124	3,04	0,09	0,0008	0,124	0,11	0,18
W 4	0,0072	3	0,125	0,875	0,125	0,063	7,30	3,78E-04			0,125	0,1820	0,00	0,0028	0,122	0,39	0,124	3,07	0,17	0,0012	0,124	0,17	0,28
W 5	0,0072	3	0,125	0,875	0,125	0,063	6,30	3,27E-04			0,125	0,1820	0,00	0,0025	0,123	0,34	0,124	3,04	0,09	0,0010	0,124	0,14	0,24
W 6	0,0072	3	0,125	0,875	0,125	0,063	7,40	3,84E-04			0,125	0,1820	0,00	0,0029	0,122	0,40	0,124	3,07	0,17	0,0012	0,124	0,17	0,28
W 7	0,0072	3	0,125	0,875	0,125	0,063	6,30	3,27E-04			0,125	0,1820	0,00	0,0025	0,123	0,34	0,124	3,04	0,09	0,0010	0,124	0,14	0,24
W 8	0,0072	3	0,125	0,875	0,125	0,063	13,00	6,74E-04			0,125	0,1820	0,00	0,0048	0,120	0,67	0,123	3,11	0,26	0,0021	0,123	0,30	0,48
W 9	0,0072	3	0,125	0,875	0,125	0,063	8,30	4,30E-04			0,125	0,1820	0,00	0,0032	0,122	0,44	0,124	3,07	0,17	0,0014	0,124	0,19	0,32
W 10	0,0072	3	0,125	0,875	0,125	0,063	11,80	6,12E-04			0,125	0,1820	0,00	0,0044	0,121	0,61	0,123	3,11	0,26	0,0019	0,123	0,27	0,44
W 11	0,0072	3	0,125	0,875	0,125	0,063	5,90	3,06E-04			0,125	0,1820	0,00	0,0023	0,123	0,32	0,124	3,04	0,09	0,0010	0,124	0,14	0,23
W 12	0,0072	3	0,125	0,875	0,125	0,063	10,00	5,18E-04			0,125	0,1820	0,00	0,0038	0,121	0,53	0,124	3,07	0,17	0,0016	0,123	0,23	0,38
W 13	0,0072	3	0,125	0,875	0,125	0,063	4,30	2,23E-04			0,125	0,1820	0,00	0,0017	0,123	0,24	0,124	3,04	0,09	0,0007	0,124	0,10	0,17
W 14	0,0072	3	0,125	0,875	0,125	0,063	2,10	1,09E-04			0,125	0,1820	0,00	0,0009	0,124	0,12	0,125	3,00	0,00	0,0003	0,125	0,05	0,08
W 15	0,0072	3	0,125	0,875	0,125	0,063	5,80	3,01E-04			0,125	0,1820	0,00	0,0023	0,123	0,32	0,124	3,04	0,09	0,0010	0,124	0,13	0,22
W 18	0,0031	8	0,125	2,125	0,125	0,141	22,30	2,14E-04			0,12	0,4675	1,61	0,0016	0,123	0,50	0,125	8,00	0,00	0,0003	0,125	0,11	0,31
W 19	0,0031	8	0,125	2,125	0,125	0,141	37,30	3,58E-04			0,12	0,4675	1,61	0,0025	0,123	0,80	0,125	8,00	0,00	0,0006	0,124	0,18	0,49
W 20	0,0031	8	0,125	2,125	0,125	0,141	18,50	1,78E-04			0,12	0,4675	1,61	0,0013	0,124	0,42	0,125	8,00	0,00	0,0003	0,125	0,09	0,26
W 21	0,0031	8	0,125	2,125	0,125	0,141	43,00	4,13E-04			0,12	0,4675	1,61	0,0028	0,122	0,90	0,124	8,09	0,20	0,0007	0,124	0,21	0,56
W 22	0,0031	8	0,125	2,125	0,125	0,141	103,60	9,96E-04			0,12	0,4675	1,61	0,0058	0,119	1,87	0,124	8,17	0,40	0,0016	0,123	0,51	1,19
W 23	0,0031	8	0,125	2,125	0,125	0,141	206,40	1,98E-03			0,12	0,4675	1,61	0,0098	0,115	3,15	0,122	8,44	1,01	0,0031	0,122	1,00	2,08
W 26	0,0036	3	0,060	0,239	0,030	0,004	60,44	8,03E-04	0,0254	1,21	0,023	0,0764	1,80	0,0092	0,021	2,52	0,022	6,43	2,13	0,0070	0,023	1,91	2,22
W 27	0,0061	5	0,120	0,682	0,056	0,023	4,53	1,70E-04	0,0562	0,00	0,056	0,1365	0,00	0,0013	0,055	0,22	0,056	5,12	0,09	0,0006	0,056	0,11	0,16
W 28	0,0061	3	0,120	0,455	0,056	0,016	20,01	7,50E-04	0,0554	0,08	0,056	0,1004	0,00	0,0055	0,050	0,90	0,052	3,64	0,64	0,0036	0,052	0,59	0,74
W 29	0,0061	1	0,120	0,228	0,054	0,009	41,45	1,55E-03	0,0481	0,96	0,051	0,0738	0,53	0,0118	0,042	1,93	0,043	2,30	1,81	0,0102	0,044	1,67	1,80
W 30	0,0083	3	0,250	1,002	0,125	0,078	4,05	2,81E-04	0,1248	0,06	0,125	0,1829	0,00	0,0011	0,124	0,13	0,125	3,04	0,08	0,0006	0,125	0,08	0,10
W 32	0,0036	3	0,060	0,252	0,032	0,005	31,99	4,25E-04	0,0274	1,26	0,030	0,0655	0,44	0,0055	0,026	1,52	0,028	4,29	1,14	0,0037	0,028	1,03	1,27
W 33	0,0061	5	0,120	0,709	0,059	0,024	8,93	3,35E-04	0,0579	0,16	0,059	0,1429	0,00	0,0025	0,056	0,41	0,058	5,25	0,19	0,0012	0,058	0,20	0,31
W 34	0,0061	3	0,120	0,466	0,058	0,017	8,26	3,10E-04	0,0562	0,23	0,058	0,0838	0,00	0,0024	0,055	0,40	0,056	3,21	0,24	0,0015	0,056	0,24	0,32
W 35	0,0061	1	0,120	0,225	0,052	0,009	28,77	1,08E-03	0,0459	1,05	0,052	0,0635	0,00	0,0084	0,044	1,37	0,044	1,86	1,28	0,0072	0,045	1,18	1,27
W 36	0,0083	3	0,250	1,009	0,127	0,080	10,18	7,06E-04	0,1265	0,00	0,127	0,1843	0,00	0,0027	0,124	0,33	0,125	3,08	0,15	0,0016	0,125	0,19	0,26
W 38	0,0036	3	0,060	0,239	0,030	0,004	39,13	5,20E-04	0,0252	1,26	0,027	0,0670	0,90	0,0065	0,023	1,79	0,025	4,85	1,39	0,0047	0,025	1,28	1,53
W 40	0,0061	3	0,120	0,467	0,058	0,017	10,63	3,99E-04	0,0571	0,13	0,058	0,0841	0,00	0,0031	0,055	0,50	0,056	3,30	0,33	0,0019	0,056	0,31	0,41
W 41	0,0061	1	0,120	0,236	0,058	0,010	48,28	1,81E-03	0,0466	1,85	0,053	0,0780	0,85	0,0136	0,044	2,21	0,045	2,39	2,08	0,0117	0,046	1,91	2,06
W 44	0,0036	3	0,060	0,240	0,030	0,005	12,28	1,63E-04	0,0286	0,38	0,030	0,0495	0,00	0,0024	0,028	0,67	0,028	3,48	0,45	0,0015	0,028	0,42	0,54
W 45	0,0036	5	0,120	0,757	0,064	0,028	24,52	3,26E-04	0,0635	0,05	0,064	0,1548	0,00	0,0025	0,061	0,68	0,063	5,18	0,26	0,0012	0,063	0,32	0,50
W 46	0,0036	3	0,120	0,495	0,063	0,019	46,17	6,13E-04	0,0598	0,74	0,063	0,0997	0,00	0,0046	0,058	1,26	0,059	3,43	0,86	0,0028	0,060	0,77	1,02
W 47	0,0061	1	0,120	0,240	0,060	0,011	15,00	5,62E-04	0,0586	0,20	0,060	0,0454	0,00	0,0045	0,055	0,74	0,056	1,29	0,63	0,0037	0,056	0,61	0,67
W 48	0,0051	3	0,250	1,018	0,128	0,081	21,35	5,62E-04	0,1272	0,16	0,128	0,1861	0,00	0,0022	0,126	0,43	0,127	3,08	0,25	0,0013	0,127	0,25	0,34
W 49	0,0083	3	0,250	1,811	0,260	0,268	14,52	1,01E-03	0,2584	0,20	0,260	0,3791	0,00	0,0039	0,256	0,46	0,259	3,04	0,16	0,0016	0,259	0,19	0,33
W 50	0,0036	3	0,060	0,240	0,030	0,005	16,79	2,23E-04	0,0283	0,47	0,030	0,0543	0,00	0,0032	0,027	0,88	0,028	3,17	0,54	0,0021	0,028	0,57	0,72
W 51	0,0036	5	0,120	0,757	0,064	0,028	37,64	5,00E-04	0,0632	0,14	0,064	0,1548	0,00	0,0036	0,060	0,99	0,063	5,12	0,23	0,0018	0,062	0,48	0,74
W 52	0,0036	3	0,120	0,495	0,063	0,019	62,08	8,25E-04	0,0591	0,93	0,063	0,1078	0,00	0,0060	0,057	1,64	0,059	3,12	0,99	0,0038	0,059	1,03	1,34
W 53	0,0061	1	0,120	0,240	0,060	0,011	21,23	7,96E-04	0,0571	0,44	0,060	0,0531	0,00	0,0063	0,053	1,03	0,057	1,11	0,44	0,0052	0,055	0,85	0,94
W 54	0,0051	3	0,250	1,018	0,128	0,081	33,45	8,80E-04	0,1272	0,16	0,128	0,1861	0,00	0,0034	0,125	0,66	0,127	3,04	0,28	0,0020	0,126	0,39	0,52
W 55	0,0083	3	0,250	1,811	0,260	0,268	24,90	1,73E-03	0,2579	0,26	0,260	0,3791	0,00	0,0064	0,254	0,77	0,258	3,00	0,20	0,0027	0,257	0,32	0,55

Assessment of damage profiles; data of Lomonaco (1994), Van Gent and Wallast (2001) and Saers (2005)
Sheet 2

	Structure						Measured damage				Gauss-shaped profile			Sliced profile			Sagged profile			Combination profile			Av
Test nr	dn50	m0	Bc	B	zc	A0	S	Ae	zd	delta_z /dn50	zd	sigma	delta_z /dn50	delta_z	zd	delta_z /dn50	zd	md	delta_z /dn50	delta_z	zd	delta_z /dn50	delta_z /dn50
-	m	-	m	m	m	m2	-	m2	m	-	m	m	-	m	m	-	m	-	-	m	m	-	-
W 56	0,0036	3	0,060	0,286	0,038	0,006	75,04	9,97E-04	0,0286	2,47	0,030	0,0862	2,06	0,0108	0,027	2,96	0,029	5,68	2,37	0,0078	0,030	2,14	2,55
W 57	0,0036	5	0,120	0,760	0,064	0,028	77,56	1,03E-03	0,0608	0,88	0,064	0,1684	0,00	0,0067	0,057	1,84	0,060	5,79	1,05	0,0036	0,060	0,98	1,41
W 58	0,0036	3	0,120	0,498	0,063	0,019	140,38	1,87E-03	0,0542	2,41	0,059	0,1326	1,21	0,0120	0,051	3,28	0,054	4,48	2,51	0,0082	0,055	2,26	2,77
W 59	0,0061	1	0,120	0,259	0,070	0,013	69,32	2,60E-03	0,0491	3,35	0,059	0,0890	1,70	0,0187	0,051	3,06	0,052	2,54	2,84	0,0160	0,054	2,61	2,83
W 60	0,0051	3	0,250	1,016	0,128	0,081	46,02	1,21E-03	0,1258	0,37	0,128	0,1857	0,00	0,0046	0,123	0,89	0,125	3,16	0,50	0,0027	0,125	0,53	0,71
W 61	0,0083	3	0,250	1,796	0,258	0,263	76,95	5,34E-03	0,2518	0,70	0,258	0,3751	0,00	0,0176	0,240	2,12	0,249	3,26	1,08	0,0082	0,249	0,99	1,55
W 62	0,0036	3	0,060	0,286	0,038	0,006	97,71	1,30E-03	0,0274	2,80	0,027	0,0944	2,79	0,0131	0,025	3,59	0,025	4,08	3,33	0,0099	0,028	2,71	3,15
W 63	0,0036	5	0,120	0,760	0,064	0,028	128,66	1,71E-03	0,0576	1,76	0,061	0,1848	0,88	0,0100	0,054	2,76	0,058	5,51	1,55	0,0058	0,058	1,59	2,17
W 64	0,0036	3	0,120	0,498	0,063	0,019	215,94	2,87E-03	0,0501	3,54	0,052	0,1485	2,94	0,0168	0,046	4,62	0,049	3,92	3,83	0,0123	0,051	3,38	4,00
W 65	0,0061	1	0,120	0,259	0,070	0,013	76,14	2,86E-03	0,0476	3,59	0,057	0,0922	2,05	0,0203	0,049	3,32	0,047	1,17	3,63	0,0175	0,052	2,85	3,09
W 66	0,0051	3	0,250	1,016	0,128	0,081	73,74	1,94E-03	0,1253	0,47	0,128	0,1857	0,00	0,0071	0,121	1,39	0,125	3,08	0,62	0,0043	0,123	0,84	1,12
W 67	0,0083	3	0,250	1,796	0,258	0,263	119,33	8,28E-03	0,2449	1,52	0,258	0,3751	0,00	0,0254	0,232	3,05	0,247	3,14	1,30	0,0126	0,245	1,52	2,28
W 68	0,0036	3	0,060	0,292	0,039	0,007	47,96	6,37E-04	0,0332	1,48	0,035	0,0771	0,95	0,0077	0,031	2,11	0,033	4,41	1,54	0,0051	0,034	1,39	1,75
W 69	0,0036	5	0,120	0,748	0,063	0,027	80,00	1,06E-03	0,0601	0,74	0,063	0,1679	0,00	0,0069	0,056	1,89	0,059	5,86	1,12	0,0037	0,059	1,02	1,45
W 70	0,0036	3	0,120	0,499	0,063	0,020	85,88	1,14E-03	0,0584	1,32	0,063	0,1197	0,00	0,0079	0,055	2,18	0,058	3,83	1,56	0,0051	0,058	1,41	1,79
W 71	0,0061	1	0,120	0,255	0,067	0,013	56,96	2,14E-03	0,0545	2,11	0,061	0,0831	1,10	0,0157	0,052	2,57	0,053	2,24	2,37	0,0133	0,054	2,18	2,37
W 72	0,0051	3	0,250	1,012	0,127	0,080	50,64	1,33E-03	0,1270	0,00	0,127	0,1849	0,00	0,0050	0,122	0,98	0,124	3,21	0,62	0,0030	0,124	0,58	0,78
W 73	0,0083	3	0,250	1,775	0,254	0,257	39,15	2,72E-03	0,2527	0,18	0,254	0,3711	0,00	0,0097	0,244	1,17	0,250	3,11	0,46	0,0043	0,250	0,51	0,84
W 74	0,0036	3	0,060	0,292	0,039	0,007	54,52	7,24E-04	0,0332	1,48	0,034	0,0797	1,27	0,0085	0,030	2,33	0,032	3,20	1,71	0,0057	0,033	1,57	1,95
W 75	0,0036	5	0,120	0,748	0,063	0,027	100,10	1,33E-03	0,0598	0,82	0,062	0,1749	0,17	0,0082	0,055	2,26	0,059	5,18	0,99	0,0046	0,058	1,26	1,76
W 76	0,0036	3	0,120	0,499	0,063	0,020	104,96	1,39E-03	0,0581	1,40	0,062	0,1260	0,35	0,0094	0,054	2,58	0,057	3,17	1,64	0,0062	0,057	1,71	2,14
W 77	0,0061	1	0,120	0,255	0,067	0,013	69,39	2,60E-03	0,0508	2,71	0,057	0,0890	1,76	0,0188	0,049	3,06	0,051	1,28	2,64	0,0161	0,051	2,63	2,85
W 78	0,0051	3	0,250	1,012	0,127	0,080	66,16	1,74E-03	0,1263	0,14	0,127	0,1849	0,00	0,0065	0,121	1,26	0,125	3,04	0,36	0,0039	0,123	0,76	1,01
W 79	0,0083	3	0,250	1,775	0,254	0,257	49,91	3,46E-03	0,2527	0,18	0,254	0,3711	0,00	0,0121	0,242	1,45	0,251	3,04	0,33	0,0054	0,249	0,65	1,05
W 80	0,0036	3	0,060	0,295	0,039	0,007	92,11	1,22E-03	0,0274	3,21	0,030	0,0931	2,57	0,0125	0,027	3,44	0,029	6,21	2,79	0,0092	0,030	2,53	2,99
W 82	0,0036	3	0,120	0,495	0,063	0,019	184,36	2,45E-03	0,0488	3,76	0,054	0,1410	2,23	0,0149	0,048	4,08	0,051	5,13	3,26	0,0107	0,052	2,92	3,50
W 83	0,0036	2	0,120	0,356	0,059	0,014	209,44	2,78E-03	0,0440	4,09	0,047	0,1201	3,39	0,0179	0,041	4,90	0,043	4,79	4,36	0,0144	0,045	3,95	4,43
W 86	0,0036	3	0,060	0,245	0,031	0,005	87,76	1,17E-03	0,0210	2,69	0,021	0,0907	2,79	0,0121	0,019	3,32	0,020	8,56	2,92	0,0097	0,021	2,65	2,99
W 87	0,0036	5	0,120	0,760	0,064	0,028	199,30	2,65E-03	0,0537	2,83	0,056	0,1995	2,11	0,0140	0,050	3,83	0,054	7,31	2,63	0,0088	0,055	2,41	3,12
W 88	0,0036	3	0,120	0,481	0,060	0,018	207,61	2,76E-03	0,0459	3,90	0,050	0,1443	2,80	0,0163	0,044	4,48	0,047	5,65	3,63	0,0121	0,048	3,32	3,90
W 89	0,0036	2	0,120	0,356	0,059	0,014	227,15	3,02E-03	0,0393	5,43	0,046	0,1234	3,73	0,0191	0,040	5,23	0,042	5,04	4,62	0,0155	0,044	4,25	4,74
W 90	0,0051	3	0,250	1,023	0,129	0,082	103,77	2,73E-03	0,1233	1,09	0,129	0,2071	0,00	0,0098	0,119	1,91	0,122	3,43	1,26	0,0060	0,123	1,18	1,54
W 92	0,0036	3	0,060	0,246	0,031	0,005	51,64	6,86E-04	0,0252	1,59	0,026	0,0727	1,36	0,0081	0,023	2,23	0,024	5,46	1,79	0,0059	0,025	1,63	1,93
W 94	0,0036	3	0,120	0,463	0,057	0,017	132,15	1,76E-03	0,0481	2,47	0,053	0,1263	1,25	0,0114	0,046	3,12	0,048	4,66	2,43	0,0081	0,049	2,21	2,67
W 95	0,0036	2	0,120	0,354	0,058	0,014	203,95	2,71E-03	0,0425	4,36	0,047	0,1181	3,20	0,0175	0,041	4,80	0,043	4,71	4,25	0,0141	0,044	3,86	4,33
W 96	0,0037	2,5	0,04	0,339	0,0598	0,011	107,83	1,48E-03	0,0431	4,53	0,047	0,0969	3,56	0,0176	0,042	4,75	0,047	4,23	3,39	0,0114	0,048	3,09	3,92
W 97	0,0037	2,5	0,04	0,339	0,0598	0,011	128,15	1,75E-03	0,0401	5,33	0,045	0,1008	4,04	0,0197	0,040	5,32	0,045	4,67	3,96	0,0133	0,046	3,61	4,46
W 100	0,0037	2,5	0,04	0,264	0,0448	0,007	45,13	6,18E-04	0,0363	2,30	0,039	0,0689	1,45	0,0096	0,035	2,61	0,038	3,60	1,76	0,0060	0,039	1,61	2,11
W 101	0,0037	2,5	0,04	0,264	0,0448	0,007	53,30	7,30E-04	0,0349	2,66	0,038	0,0713	1,82	0,0109	0,034	2,94	0,037	3,85	2,06	0,0070	0,038	1,88	2,41
W 102	0,0037	2,5	0,04	0,264	0,0448	0,007	57,60	7,89E-04	0,0345	2,78	0,037	0,0731	2,06	0,0115	0,033	3,10	0,037	4,01	2,24	0,0075	0,037	2,02	2,56
W 103	0,0037	2,5	0,04	0,287	0,0494	0,008	83,50	1,14E-03	0,0361	3,60	0,039	0,0836	2,94	0,0148	0,035	4,01	0,039	4,40	2,94	0,0100	0,039	2,70	3,36
W 104	0,0037	2,5	0,04	0,287	0,0494	0,008	103,14	1,41E-03	0,0341	4,14	0,036	0,0894	3,60	0,0171	0,032	4,62	0,036	5,10	3,60	0,0121	0,037	3,27	3,94
W 105	0,0037	2,5	0,04	0,287	0,0494	0,008	104,88	1,44E-03	0,0336	4,27	0,036	0,0906	3,74	0,0173	0,032	4,67	0,036	5,18	3,67	0,0123	0,037	3,31	3,99
W 106	0,0037	2,5	0,04	0,3585	0,0637	0,013	117,16	1,60E-03	0,0459	4,82	0,050	0,1006	3,62	0,0186	0,045	5,02	0,051	4,16	3,53	0,0119	0,052	3,22	4,12
W 107	0,0037	2,5	0,04	0,3585	0,0637	0,013	138,56	1,90E-03	0,0446	5,16	0,048	0,1060	4,30	0,0207	0,043	5,59	0,048	4,59	4,13	0,0139	0,050	3,74	4,67
W 108	0,0037	2,5	0,04	0,3585	0,0637	0,013	156,50	2,14E-03	0,0433	5,51	0,046	0,1104	4,82	0,0223	0,041	6,04	0,047	4,94	4,56	0,0154	0,048	4,17	5,10

Assessment of damage profiles; data of Lomonaco (1994), Van Gent and Wallast (2001) and Saers (2005)
Sheet 3

	Structure						Measured damage				Gauss-shaped profile			Sliced profile			Sagged profile			Combination profile			Av
Test nr	dn50	m0	Bc	B	zc	A0	S	Ae	zd	delta_z /dn50	zd	sigma	delta_z /dn50	delta_z	zd	delta_z /dn50	zd	md	delta_z /dn50	delta_z	zd	delta_z /dn50	delta_z /dn50
-	m	-	m	m	m	m2	-	m2	m	-	m	m	-	m	m	-	m	-	-	m	m	-	-
W 109	0,0037	2,5	0,04	0,338	0,0596	0,011	118,97	1,63E-03	0,0411	4,99	0,045	0,0992	3,87	0,0187	0,041	5,07	0,046	4,48	3,70	0,0125	0,047	3,38	4,22
W 110	0,0037	2,5	0,04	0,338	0,0596	0,011	133,20	1,82E-03	0,0399	5,32	0,044	0,1033	4,35	0,0202	0,039	5,45	0,044	4,81	4,11	0,0138	0,046	3,74	4,60
W 111	0,0037	2,5	0,04	0,338	0,0596	0,011	150,60	2,06E-03	0,0381	5,80	0,042	0,1077	4,83	0,0218	0,038	5,89	0,043	5,26	4,59	0,0154	0,044	4,17	5,03
W 112	0,0037	2,5	0,04	0,25	0,042	0,006	34,50	4,72E-04	0,0361	1,59	0,038	0,0636	1,02	0,0079	0,034	2,14	0,037	3,42	1,42	0,0048	0,037	1,30	1,72
W 113	0,0037	2,5	0,04	0,25	0,042	0,006	40,63	5,56E-04	0,0340	2,16	0,037	0,0657	1,36	0,0089	0,033	2,41	0,036	3,61	1,65	0,0056	0,036	1,51	1,96
W 114	0,0037	2,5	0,04	0,25	0,042	0,006	46,87	6,42E-04	0,0328	2,50	0,036	0,0673	1,59	0,0099	0,032	2,68	0,035	3,81	1,87	0,0064	0,036	1,73	2,20
W 115	0,0037	2,5	0,04	0,342	0,0604	0,012	56,70	7,76E-04	0,0489	3,10	0,054	0,0847	1,63	0,0114	0,049	3,07	0,054	3,25	1,80	0,0063	0,054	1,70	2,38
W 116	0,0037	2,5	0,04	0,342	0,0604	0,012	78,90	1,08E-03	0,0459	3,92	0,051	0,0896	2,45	0,0143	0,046	3,86	0,051	3,65	2,53	0,0086	0,052	2,31	3,09
W 117	0,0037	2,5	0,04	0,342	0,0604	0,012	99,60	1,36E-03	0,0435	4,57	0,048	0,0952	3,26	0,0167	0,044	4,51	0,049	4,00	3,10	0,0106	0,050	2,86	3,69
W 121	0,0037	2,5	0,04	0,246	0,0412	0,006	29,00	3,97E-04	0,0354	1,56	0,039	0,0607	0,67	0,0069	0,034	1,87	0,037	3,29	1,22	0,0041	0,037	1,11	1,49
W 122	0,0037	2,5	0,04	0,246	0,0412	0,006	32,37	4,43E-04	0,0346	1,78	0,038	0,0620	0,89	0,0075	0,034	2,04	0,036	3,38	1,34	0,0046	0,037	1,23	1,63
W 123	0,0037	2,5	0,04	0,246	0,0412	0,006	34,83	4,77E-04	0,0350	1,67	0,037	0,0627	1,00	0,0080	0,033	2,15	0,036	3,47	1,45	0,0049	0,036	1,32	1,74
W 124	0,0037	2,5	0,04	0,2945	0,0509	0,009	58,02	7,94E-04	0,0412	2,61	0,044	0,0776	1,93	0,0115	0,039	3,12	0,043	3,62	2,06	0,0071	0,044	1,91	2,51
W 125	0,0037	2,5	0,04	0,2945	0,0509	0,009	64,52	8,83E-04	0,0392	3,16	0,043	0,0794	2,20	0,0124	0,038	3,36	0,043	3,77	2,27	0,0078	0,043	2,11	2,73
W 126	0,0037	2,5	0,04	0,2945	0,0509	0,009	70,94	9,71E-04	0,0382	3,44	0,042	0,0814	2,48	0,0133	0,038	3,59	0,042	3,93	2,48	0,0085	0,042	2,30	2,94
W 127	0,0037	2,5	0,04	0,3415	0,0603	0,012	56,04	7,67E-04	0,0507	2,61	0,054	0,0846	1,63	0,0113	0,049	3,04	0,054	3,25	1,79	0,0062	0,054	1,68	2,36
W 128	0,0037	2,5	0,04	0,3415	0,0603	0,012	62,88	8,61E-04	0,0500	2,77	0,053	0,0865	1,96	0,0122	0,048	3,30	0,053	3,37	2,04	0,0069	0,053	1,88	2,59
W 129	0,0037	2,5	0,04	0,3415	0,0603	0,012	80,46	1,10E-03	0,0500	2,77	0,051	0,0906	2,61	0,0145	0,046	3,91	0,051	3,65	2,53	0,0087	0,052	2,36	3,13
W 130	0,0037	2,5	0,04	0,2525	0,0425	0,006	25,26	3,46E-04	0,0412	0,34	0,041	0,0608	0,46	0,0062	0,036	1,68	0,039	3,12	1,03	0,0035	0,039	0,96	1,32
W 131	0,0037	2,5	0,04	0,2525	0,0425	0,006	26,26	3,59E-04	0,0412	0,34	0,041	0,0608	0,46	0,0064	0,036	1,73	0,038	3,16	1,09	0,0037	0,039	0,99	1,36
W 132	0,0037	2,5	0,04	0,2525	0,0425	0,006	27,02	3,70E-04	0,0412	0,34	0,040	0,0614	0,57	0,0066	0,036	1,77	0,038	3,16	1,09	0,0038	0,039	1,02	1,40
W 133	0,0037	2,5	0,04	0,299	0,0518	0,009	36,10	4,94E-04	0,0451	1,82	0,049	0,0719	0,84	0,0082	0,044	2,21	0,047	3,14	1,33	0,0045	0,047	1,21	1,71
W 134	0,0037	2,5	0,04	0,299	0,0518	0,009	57,68	7,90E-04	0,0414	2,80	0,045	0,0777	1,82	0,0115	0,040	3,11	0,044	3,57	2,03	0,0070	0,045	1,88	2,49
W 135	0,0037	2,5	0,04	0,299	0,0518	0,009	55,60	7,61E-04	0,0425	2,52	0,045	0,0777	1,82	0,0112	0,041	3,03	0,045	3,53	1,96	0,0067	0,045	1,82	2,42
W 136	0,0037	2,5	0,04	0,338	0,0596	0,011	50,22	6,88E-04	0,0519	2,09	0,055	0,0820	1,29	0,0104	0,049	2,81	0,054	3,17	1,61	0,0057	0,054	1,53	2,17
W 137	0,0037	2,5	0,04	0,338	0,0596	0,011	53,14	7,27E-04	0,0513	2,26	0,054	0,0829	1,45	0,0108	0,049	2,93	0,053	3,21	1,69	0,0060	0,054	1,61	2,27
W 138	0,0037	2,5	0,04	0,338	0,0596	0,011	55,23	7,56E-04	0,0513	2,26	0,054	0,0838	1,61	0,0111	0,048	3,01	0,053	3,25	1,77	0,0062	0,053	1,67	2,34

Fit of a transport equation to model tests with pipeline covers

Sheet 1 Stability parameters

Test nr	u = u0					u = uc					u = u_hc				
	Psi_BK	Psi_GM	Psi_F	Theta	Morr	Psi_BK	Psi_GM	Psi_F	Theta	Morr	Psi_BK	Psi_GM	Psi_F	Theta	Morr
W 1	0,011	0,009	0,001	0,08	0,30	0,013	0,010	0,002	0,09	0,33	0,023	0,014	0,003	0,16	0,48
W 2	0,011	0,009	0,001	0,08	0,30	0,013	0,010	0,002	0,09	0,33	0,023	0,014	0,003	0,16	0,48
W 3	0,025	0,017	0,004	0,26	0,60	0,027	0,019	0,004	0,28	0,65	0,036	0,026	0,007	0,46	0,92
W 4	0,025	0,017	0,004	0,26	0,60	0,027	0,019	0,004	0,28	0,65	0,036	0,026	0,007	0,46	0,92
W 5	0,036	0,027	0,008	0,55	1,00	0,038	0,029	0,008	0,60	1,06	0,049	0,038	0,012	0,90	1,47
W 6	0,036	0,027	0,008	0,55	1,00	0,038	0,029	0,008	0,60	1,06	0,049	0,038	0,012	0,90	1,47
W 7	0,036	0,027	0,008	0,55	0,99	0,038	0,028	0,008	0,59	1,05	0,049	0,038	0,012	0,89	1,45
W 8	0,036	0,027	0,008	0,55	0,99	0,038	0,028	0,008	0,59	1,05	0,049	0,038	0,012	0,89	1,45
W 9	0,044	0,035	0,011	0,85	1,35	0,046	0,036	0,012	0,90	1,41	0,059	0,048	0,016	1,32	1,94
W 10	0,044	0,035	0,011	0,85	1,35	0,046	0,036	0,012	0,90	1,41	0,059	0,048	0,016	1,32	1,94
W 11	0,043	0,034	0,011	0,83	1,32	0,045	0,036	0,011	0,88	1,39	0,058	0,047	0,016	1,29	1,91
W 12	0,043	0,034	0,011	0,83	1,32	0,045	0,036	0,011	0,88	1,39	0,058	0,047	0,016	1,29	1,91
W 13	0,021	0,013	0,002	0,14	0,44	0,024	0,015	0,003	0,17	0,51	0,033	0,022	0,005	0,32	0,78
W 14	0,033	0,024	0,006	0,40	0,83	0,036	0,026	0,007	0,45	0,92	0,049	0,037	0,011	0,77	1,37
W 15	0,033	0,024	0,006	0,40	0,83	0,036	0,026	0,007	0,45	0,92	0,049	0,037	0,011	0,77	1,37
W 18	0,016	0,011	0,003	0,17	0,40	0,018	0,013	0,003	0,21	0,45	0,026	0,019	0,005	0,37	0,69
W 19	0,016	0,011	0,003	0,17	0,40	0,018	0,013	0,003	0,21	0,45	0,026	0,019	0,005	0,37	0,69
W 20	0,030	0,024	0,008	0,59	0,94	0,033	0,026	0,008	0,66	1,03	0,044	0,037	0,013	1,06	1,52
W 21	0,030	0,024	0,008	0,59	0,94	0,033	0,026	0,008	0,66	1,03	0,044	0,037	0,013	1,06	1,52
W 22	0,047	0,039	0,015	1,30	1,75	0,049	0,040	0,016	1,40	1,87	0,065	0,054	0,022	2,12	2,69
W 23	0,047	0,039	0,015	1,30	1,75	0,049	0,040	0,016	1,40	1,87	0,065	0,054	0,022	2,12	2,69
W 26	0,039	0,031	0,010	0,73	1,18	0,039	0,031	0,010	0,73	1,19	0,043	0,034	0,011	0,84	1,32
W 27	0,034	0,025	0,006	0,42	0,87	0,035	0,025	0,006	0,43	0,88	0,040	0,030	0,008	0,55	1,06
W 28	0,033	0,024	0,006	0,40	0,84	0,034	0,024	0,006	0,41	0,85	0,039	0,029	0,008	0,52	1,02
W 29	0,033	0,023	0,006	0,39	0,83	0,033	0,024	0,006	0,40	0,84	0,038	0,028	0,007	0,51	1,00
W 30	0,026	0,018	0,004	0,24	0,61	0,028	0,019	0,004	0,27	0,66	0,037	0,027	0,007	0,44	0,93
W 32	0,059	0,049	0,018	1,57	2,14	0,059	0,049	0,018	1,58	2,15	0,063	0,054	0,020	1,77	2,38
W 33	0,050	0,039	0,012	0,95	1,52	0,050	0,040	0,013	0,97	1,54	0,058	0,046	0,015	1,19	1,83
W 34	0,048	0,038	0,012	0,94	1,48	0,048	0,038	0,012	0,96	1,50	0,055	0,044	0,014	1,16	1,76
W 35	0,047	0,036	0,011	0,85	1,39	0,047	0,037	0,011	0,87	1,41	0,053	0,042	0,013	1,04	1,64
W 36	0,038	0,028	0,008	0,58	1,04	0,039	0,030	0,009	0,62	1,10	0,051	0,040	0,012	0,93	1,52
W 38	0,073	0,061	0,025	2,38	3,02	0,073	0,061	0,025	2,39	3,03	0,078	0,066	0,028	2,63	3,30
W 40	0,058	0,047	0,016	1,32	1,93	0,058	0,047	0,016	1,33	1,95	0,066	0,054	0,019	1,61	2,28
W 41	0,055	0,045	0,015	1,23	1,82	0,055	0,045	0,015	1,25	1,84	0,063	0,052	0,018	1,50	2,15
W 44	0,041	0,033	0,011	0,90	1,35	0,041	0,033	0,011	0,91	1,35	0,044	0,036	0,012	1,00	1,47
W 45	0,048	0,039	0,014	1,14	1,64	0,049	0,040	0,014	1,16	1,66	0,056	0,046	0,017	1,43	1,99
W 46	0,041	0,033	0,011	0,90	1,34	0,041	0,033	0,011	0,92	1,35	0,047	0,038	0,013	1,12	1,60
W 47	0,034	0,026	0,007	0,53	0,95	0,035	0,026	0,007	0,54	0,96	0,039	0,030	0,009	0,65	1,12
W 48	0,033	0,025	0,007	0,55	0,94	0,034	0,026	0,008	0,59	1,00	0,044	0,035	0,011	0,87	1,36
W 49	0,024	0,017	0,004	0,25	0,58	0,029	0,020	0,005	0,34	0,72	0,043	0,033	0,009	0,67	1,20
W 50	0,042	0,035	0,012	0,96	1,41	0,042	0,035	0,012	0,97	1,42	0,045	0,037	0,013	1,07	1,54
W 51	0,048	0,039	0,014	1,14	1,64	0,049	0,040	0,014	1,16	1,66	0,056	0,046	0,017	1,43	1,99
W 52	0,041	0,033	0,011	0,90	1,34	0,041	0,033	0,011	0,92	1,36	0,047	0,038	0,013	1,12	1,60
W 53	0,034	0,026	0,007	0,52	0,95	0,035	0,026	0,007	0,53	0,96	0,039	0,030	0,009	0,64	1,11
W 54	0,033	0,025	0,008	0,56	0,95	0,035	0,027	0,008	0,60	1,01	0,044	0,035	0,011	0,88	1,38
W 55	0,024	0,017	0,004	0,26	0,59	0,029	0,021	0,005	0,34	0,72	0,044	0,033	0,009	0,68	1,21
W 56	0,060	0,049	0,019	1,77	2,32	0,060	0,049	0,020	1,78	2,33	0,065	0,053	0,022	1,99	2,58
W 57	0,070	0,058	0,024	2,25	2,87	0,071	0,059	0,024	2,28	2,91	0,081	0,068	0,029	2,74	3,43
W 58	0,057	0,047	0,019	1,67	2,21	0,058	0,047	0,019	1,69	2,23	0,065	0,054	0,022	2,03	2,62
W 59	0,047	0,038	0,013	1,01	1,53	0,048	0,039	0,013	1,02	1,55	0,054	0,044	0,015	1,23	1,80
W 60	0,047	0,039	0,014	1,14	1,63	0,049	0,040	0,014	1,20	1,70	0,061	0,051	0,019	1,66	2,24
W 61	0,036	0,028	0,008	0,64	1,05	0,039	0,031	0,010	0,74	1,19	0,057	0,047	0,016	1,32	1,92
W 62	0,060	0,049	0,020	1,78	2,33	0,060	0,049	0,020	1,79	2,34	0,065	0,053	0,022	2,00	2,59
W 63	0,070	0,058	0,024	2,24	2,87	0,071	0,059	0,024	2,27	2,90	0,080	0,068	0,029	2,73	3,42
W 64	0,059	0,048	0,019	1,77	2,31	0,059	0,049	0,020	1,79	2,34	0,067	0,055	0,023	2,12	2,71
W 65	0,047	0,038	0,012	1,00	1,52	0,048	0,038	0,013	1,01	1,54	0,054	0,044	0,015	1,22	1,79
W 66	0,047	0,039	0,014	1,14	1,62	0,049	0,040	0,014	1,19	1,69	0,061	0,051	0,019	1,65	2,24
W 67	0,036	0,028	0,008	0,64	1,06	0,039	0,031	0,010	0,74	1,19	0,057	0,047	0,016	1,33	1,93
W 68	0,042	0,034	0,012	1,03	1,46	0,042	0,035	0,012	1,04	1,46	0,045	0,037	0,013	1,15	1,60
W 69	0,048	0,041	0,015	1,30	1,77	0,049	0,041	0,015	1,31	1,79	0,054	0,044	0,017	1,54	2,06
W 70	0,040	0,033	0,012	0,98	1,39	0,040	0,033	0,012	0,99	1,40	0,045	0,038	0,014	1,16	1,61
W 71	0,034	0,026	0,008	0,58	0,99	0,034	0,026	0,008	0,59	0,99	0,038	0,030	0,009	0,70	1,15
W 72	0,033	0,026	0,008	0,64	1,02	0,034	0,027	0,009	0,67	1,06	0,042	0,034	0,011	0,92	1,37
W 73	0,026	0,019	0,005	0,34	0,67	0,029	0,021	0,006	0,40	0,77	0,041	0,032	0,009	0,70	1,19
W 74	0,042	0,035	0,012	1,05	1,47	0,042	0,035	0,012	1,05	1,48	0,045	0,038	0,014	1,17	1,62
W 75	0,049	0,041	0,015	1,30	1,78	0,049	0,041	0,015	1,32	1,80	0,055	0,045	0,017	1,55	2,07
W 76	0,040	0,033	0,012	0,98	1,39	0,040	0,033	0,012	0,99	1,40	0,045	0,038	0,014	1,17	1,62
W 77	0,034	0,026	0,008	0,57	0,97	0,034	0,026	0,008	0,58	0,98	0,038	0,030	0,009	0,69	1,13
W 78	0,033	0,027	0,008	0,65	1,03	0,034	0,027	0,009	0,68	1,07	0,042	0,034	0,011	0,93	1,39
W 79	0,026	0,019	0,005	0,34	0,69	0,029	0,022	0,006	0,41	0,78	0,042	0,032	0,010	0,72	1,21
W 80	0,072	0,062	0,028	2,83	3,39	0,072	0,063	0,028	2,84	3,40	0,078	0,068	0,031	3,17	3,76
W 82	0,068	0,059	0,026	2,61	3,15	0,069	0,059	0,026	2,63	3,17	0,077	0,067	0,030	3,12	3,71
W 83	0,069	0,060	0,027	2,74	3,28	0,070	0,061	0,027	2,76	3,30	0,078	0,068	0,031	3,24	3,82
W 86	0,069	0,058	0,025	2,46	3,03	0,069	0,059	0,025	2,47	3,04	0,073	0,062	0,027	2,66	3,25
W 87	0,081	0,069	0,030	3,07	3,70	0,081	0,070	0,031	3,10	3,73	0,090	0,078	0,035	3,61	4,30
W 88	0,066	0,055	0,024	2,29	2,84	0,066	0,056	0,024	2,30	2,86	0,073	0,062	0,027	2,66	3,25
W 89	0,067	0,057	0,024	2,36	2,91	0,067	0,057	0,024	2,37	2,94	0,074	0,063	0,028	2,73	3,34

Fit of a transport equation to model tests with pipeline covers
Sheet 1 Stability parameters (continued)

Test nr	u = u0					u = uc					u = u_hc				
	Psi_BK	Psi_GM	Psi_F	Theta	Morr	Psi_BK	Psi_GM	Psi_F	Theta	Morr	Psi_BK	Psi_GM	Psi_F	Theta	Morr
W 90	0,055	0,044	0,018	1,64	2,14	0,056	0,046	0,018	1,69	2,20	0,068	0,057	0,024	2,25	2,84
W 92	0,074	0,061	0,026	2,42	3,07	0,074	0,062	0,026	2,43	3,08	0,080	0,067	0,028	2,69	3,37
W 94	0,070	0,057	0,024	2,22	2,83	0,070	0,058	0,024	2,24	2,87	0,080	0,067	0,028	2,70	3,38
W 95	0,068	0,057	0,023	2,15	2,76	0,069	0,057	0,023	2,18	2,80	0,078	0,065	0,028	2,63	3,31
W 96	0,064	0,053	0,022	2,01	2,58	0,064	0,053	0,022	2,04	2,61	0,072	0,061	0,025	2,43	3,05
W 97	0,064	0,053	0,022	2,01	2,58	0,064	0,053	0,022	2,04	2,61	0,072	0,061	0,025	2,43	3,05
W 100	0,071	0,060	0,025	2,37	2,99	0,072	0,060	0,025	2,39	3,01	0,079	0,067	0,028	2,75	3,41
W 101	0,071	0,060	0,025	2,37	2,99	0,072	0,060	0,025	2,39	3,01	0,079	0,067	0,028	2,75	3,41
W 102	0,071	0,060	0,025	2,37	2,99	0,072	0,060	0,025	2,39	3,01	0,079	0,067	0,028	2,75	3,41
W 103	0,071	0,060	0,025	2,37	2,99	0,072	0,060	0,025	2,39	3,01	0,080	0,068	0,029	2,79	3,46
W 104	0,071	0,060	0,025	2,37	2,99	0,072	0,060	0,025	2,39	3,01	0,080	0,068	0,029	2,79	3,46
W 105	0,071	0,060	0,025	2,37	2,99	0,072	0,060	0,025	2,39	3,01	0,080	0,068	0,029	2,79	3,46
W 106	0,071	0,060	0,025	2,37	2,99	0,072	0,061	0,025	2,41	3,03	0,083	0,070	0,030	2,93	3,62
W 107	0,071	0,060	0,025	2,37	2,99	0,072	0,061	0,025	2,41	3,03	0,083	0,070	0,030	2,93	3,62
W 108	0,071	0,060	0,025	2,37	2,99	0,072	0,061	0,025	2,41	3,03	0,083	0,070	0,030	2,93	3,62
W 109	0,071	0,060	0,025	2,37	2,99	0,072	0,060	0,025	2,40	3,02	0,082	0,069	0,030	2,89	3,57
W 110	0,071	0,060	0,025	2,37	2,99	0,072	0,060	0,025	2,40	3,02	0,082	0,069	0,030	2,89	3,57
W 111	0,071	0,060	0,025	2,37	2,99	0,072	0,060	0,025	2,40	3,02	0,082	0,069	0,030	2,89	3,57
W 112	0,064	0,053	0,021	1,95	2,54	0,065	0,053	0,021	1,96	2,55	0,072	0,059	0,024	2,27	2,91
W 113	0,064	0,053	0,021	1,95	2,54	0,065	0,053	0,021	1,96	2,55	0,072	0,059	0,024	2,27	2,91
W 114	0,064	0,053	0,021	1,95	2,54	0,065	0,053	0,021	1,96	2,55	0,072	0,059	0,024	2,27	2,91
W 115	0,064	0,053	0,021	1,95	2,54	0,065	0,053	0,022	1,98	2,57	0,075	0,063	0,026	2,43	3,09
W 116	0,064	0,053	0,021	1,95	2,54	0,065	0,053	0,022	1,98	2,57	0,075	0,063	0,026	2,43	3,09
W 117	0,064	0,053	0,021	1,95	2,54	0,065	0,053	0,022	1,98	2,57	0,075	0,063	0,026	2,43	3,09
W 121	0,061	0,050	0,020	1,80	2,36	0,061	0,050	0,020	1,81	2,38	0,068	0,055	0,023	2,09	2,70
W 122	0,061	0,050	0,020	1,80	2,36	0,061	0,050	0,020	1,81	2,38	0,068	0,055	0,023	2,09	2,70
W 123	0,061	0,050	0,020	1,80	2,36	0,061	0,050	0,020	1,81	2,38	0,068	0,055	0,023	2,09	2,70
W 124	0,061	0,050	0,020	1,80	2,36	0,062	0,050	0,020	1,82	2,39	0,069	0,057	0,023	2,17	2,79
W 125	0,061	0,050	0,020	1,80	2,36	0,062	0,050	0,020	1,82	2,39	0,069	0,057	0,023	2,17	2,79
W 126	0,061	0,050	0,020	1,80	2,36	0,062	0,050	0,020	1,82	2,39	0,069	0,057	0,023	2,17	2,79
W 127	0,061	0,050	0,020	1,80	2,36	0,062	0,050	0,020	1,83	2,40	0,071	0,059	0,024	2,25	2,88
W 128	0,061	0,050	0,020	1,80	2,36	0,062	0,050	0,020	1,83	2,40	0,071	0,059	0,024	2,25	2,88
W 129	0,061	0,050	0,020	1,80	2,36	0,062	0,050	0,020	1,83	2,40	0,071	0,059	0,024	2,25	2,88
W 130	0,056	0,045	0,018	1,57	2,11	0,056	0,046	0,018	1,59	2,12	0,063	0,051	0,020	1,86	2,44
W 131	0,056	0,045	0,018	1,57	2,11	0,056	0,046	0,018	1,59	2,12	0,063	0,051	0,020	1,86	2,44
W 132	0,056	0,045	0,018	1,57	2,11	0,056	0,046	0,018	1,59	2,12	0,063	0,051	0,020	1,86	2,44
W 133	0,056	0,045	0,018	1,57	2,11	0,056	0,046	0,018	1,59	2,13	0,064	0,052	0,021	1,93	2,52
W 134	0,056	0,045	0,018	1,57	2,11	0,056	0,046	0,018	1,59	2,13	0,064	0,052	0,021	1,93	2,52
W 135	0,056	0,045	0,018	1,57	2,11	0,056	0,046	0,018	1,59	2,13	0,064	0,052	0,021	1,93	2,52
W 136	0,056	0,045	0,018	1,57	2,11	0,057	0,046	0,018	1,60	2,14	0,066	0,054	0,022	2,00	2,60
W 137	0,056	0,045	0,018	1,57	2,11	0,057	0,046	0,018	1,60	2,14	0,066	0,054	0,022	2,00	2,60
W 138	0,056	0,045	0,018	1,57	2,11	0,057	0,046	0,018	1,60	2,14	0,066	0,054	0,022	2,00	2,60

Fit of a transport equation to model tests with pipeline covers

Sheet 2 Transport parameters

Test					Simple transport			Critical scour method		
nr	Ls	omega	Ae	Duration	qs	Phi_q	Phi_Hall	qs	Phi_q	Phi_Hall
-	m	rad/s	m2	s	m3/m/s	-	-	m3/m/s	-	-
W 1	0,375	5,661	2,28E-04	1110	2,05E-07	8,36E-05	7,00E-04	4,19E-07	1,70E-04	1,43E-03
W 2	0,375	5,661	3,16E-04	3330	9,50E-08	3,86E-05	3,24E-04	1,91E-07	7,79E-05	6,52E-04
W 3	0,375	4,760	2,38E-04	1320	1,81E-07	7,35E-05	7,32E-04	3,68E-07	1,50E-04	1,49E-03
W 4	0,375	4,760	3,78E-04	3960	9,56E-08	3,89E-05	3,87E-04	1,91E-07	7,78E-05	7,75E-04
W 5	0,375	4,161	3,27E-04	1510	2,16E-07	8,80E-05	1,00E-03	4,35E-07	1,77E-04	2,02E-03
W 6	0,375	4,161	3,84E-04	4530	8,47E-08	3,45E-05	3,93E-04	1,69E-07	6,89E-05	7,85E-04
W 7	0,375	4,161	3,27E-04	1510	2,16E-07	8,80E-05	1,00E-03	4,35E-07	1,77E-04	2,02E-03
W 8	0,375	4,161	6,74E-04	4530	1,49E-07	6,05E-05	6,90E-04	2,88E-07	1,17E-04	1,34E-03
W 9	0,375	3,785	4,30E-04	1660	2,59E-07	1,05E-04	1,32E-03	5,16E-07	2,10E-04	2,63E-03
W 10	0,375	3,785	6,12E-04	4980	1,23E-07	5,00E-05	6,26E-04	2,40E-07	9,75E-05	1,22E-03
W 11	0,375	3,785	3,06E-04	1660	1,84E-07	7,50E-05	9,39E-04	3,72E-07	1,51E-04	1,90E-03
W 12	0,375	3,785	5,18E-04	4980	1,04E-07	4,24E-05	5,31E-04	2,05E-07	8,34E-05	1,05E-03
W 13	0,375	5,712	2,23E-04	1100	2,03E-07	8,24E-05	6,84E-04	4,13E-07	1,68E-04	1,40E-03
W 14	0,375	4,760	1,09E-04	1320	8,25E-08	3,36E-05	3,34E-04	1,71E-07	6,94E-05	6,91E-04
W 15	0,375	4,760	3,01E-04	3960	7,59E-08	3,09E-05	3,08E-04	1,53E-07	6,24E-05	6,21E-04
W 18	1,000	5,661	2,14E-04	1110	1,93E-07	2,78E-04	3,55E-03	8,56E-07	1,23E-03	1,57E-02
W 19	1,000	5,661	3,58E-04	3330	1,08E-07	1,55E-04	1,98E-03	4,57E-07	6,59E-04	8,41E-03
W 20	1,000	4,760	1,78E-04	1320	1,35E-07	1,94E-04	2,94E-03	6,05E-07	8,71E-04	1,32E-02
W 21	1,000	4,760	4,13E-04	3960	1,04E-07	1,50E-04	2,28E-03	4,37E-07	6,29E-04	9,55E-03
W 22	1,000	4,161	9,96E-04	1510	6,59E-07	9,49E-04	1,65E-02	2,44E-06	3,52E-03	6,11E-02
W 23	1,000	4,161	1,98E-03	4530	4,38E-07	6,31E-04	1,09E-02	1,42E-06	2,05E-03	3,55E-02
W 26	0,089	4,890	8,03E-04	3960	2,03E-07	2,43E-04	3,12E-03	9,93E-08	1,19E-04	1,53E-03
W 27	0,281	4,987	1,70E-04	3960	4,29E-08	2,33E-05	2,29E-04	0,00E+00	0,00E+00	0,00E+00
W 28	0,168	4,987	7,50E-04	3960	1,89E-07	1,03E-04	1,01E-03	2,12E-08	1,15E-05	1,13E-04
W 29	0,054	4,987	1,55E-03	3960	3,93E-07	2,13E-04	2,10E-03	8,05E-08	4,36E-05	4,30E-04
W 30	0,376	4,890	2,81E-04	3960	7,09E-08	2,28E-05	2,09E-04	4,75E-08	1,52E-05	1,40E-04
W 32	0,096	4,218	4,25E-04	3000	1,42E-07	1,70E-04	2,53E-03	1,47E-07	1,77E-04	2,63E-03
W 33	0,295	4,218	3,35E-04	3000	1,12E-07	6,05E-05	7,06E-04	9,82E-08	5,32E-05	6,21E-04
W 34	0,173	4,028	3,10E-04	3000	1,03E-07	5,59E-05	6,83E-04	8,06E-08	4,37E-05	5,34E-04
W 35	0,052	4,218	1,08E-03	3000	3,60E-07	1,95E-04	2,27E-03	1,12E-07	6,05E-05	7,05E-04
W 36	0,380	4,028	7,06E-04	3000	2,35E-07	7,56E-05	8,42E-04	0,00E+00	0,00E+00	0,00E+00
W 38	0,089	3,835	5,20E-04	1680	3,09E-07	3,71E-04	6,07E-03	2,45E-07	2,94E-04	4,80E-03
W 40	0,174	3,835	3,99E-04	1680	2,37E-07	1,29E-04	1,65E-03	8,27E-08	4,48E-05	5,75E-04
W 41	0,058	3,835	1,81E-03	1680	1,08E-06	5,84E-04	7,49E-03	3,89E-07	2,11E-04	2,71E-03
W 44	0,090	4,315	1,63E-04	1680	9,71E-08	1,17E-04	1,69E-03	7,50E-08	9,00E-05	1,31E-03
W 45	0,319	4,315	3,26E-04	1680	1,94E-07	2,33E-04	3,38E-03	3,79E-08	4,55E-05	6,61E-04
W 46	0,188	4,218	6,13E-04	1680	3,65E-07	4,38E-04	6,52E-03	3,01E-07	3,61E-04	5,38E-03
W 47	0,060	4,218	5,62E-04	1680	3,35E-07	1,81E-04	2,12E-03	4,27E-08	2,31E-05	2,70E-04
W 48	0,384	4,315	5,62E-04	1680	3,34E-07	2,29E-04	2,94E-03	1,83E-07	1,25E-04	1,61E-03
W 49	0,780	4,315	1,01E-03	1680	6,00E-07	1,92E-04	2,00E-03	7,90E-07	2,53E-04	2,64E-03
W 50	0,090	4,218	2,23E-04	3360	6,64E-08	7,96E-05	1,18E-03	4,55E-08	5,46E-05	8,13E-04
W 51	0,319	4,315	5,00E-04	3360	1,49E-07	1,79E-04	2,60E-03	4,74E-08	5,69E-05	8,27E-04
W 52	0,188	4,218	8,25E-04	3360	2,45E-07	2,94E-04	4,38E-03	1,90E-07	2,28E-04	3,39E-03
W 53	0,060	4,218	7,96E-04	3360	2,37E-07	1,28E-04	1,50E-03	4,81E-08	2,60E-05	3,04E-04
W 54	0,384	4,315	8,80E-04	3360	2,62E-07	1,79E-04	2,31E-03	9,14E-08	6,26E-05	8,05E-04
W 55	0,780	4,315	1,73E-03	3360	5,14E-07	1,65E-04	1,72E-03	5,11E-07	1,64E-04	1,71E-03
W 56	0,113	3,835	9,97E-04	1680	5,93E-07	7,12E-04	1,16E-02	6,04E-07	7,25E-04	1,19E-02
W 57	0,320	3,835	1,03E-03	1680	6,13E-07	7,36E-04	1,20E-02	6,10E-07	7,31E-04	1,20E-02
W 58	0,189	3,835	1,87E-03	1680	1,11E-06	1,33E-03	2,18E-02	9,90E-07	1,19E-03	1,94E-02
W 59	0,070	3,738	2,60E-03	1680	1,55E-06	8,38E-04	1,10E-02	8,49E-07	4,60E-04	6,06E-03
W 60	0,383	3,738	1,21E-03	1680	7,21E-07	4,93E-04	7,33E-03	4,33E-07	2,97E-04	4,41E-03
W 61	0,773	3,451	5,34E-03	1680	3,18E-06	1,02E-03	1,33E-02	2,67E-06	8,56E-04	1,11E-02
W 62	0,113	3,835	1,30E-03	3360	3,86E-07	4,63E-04	7,58E-03	3,42E-07	4,11E-04	6,72E-03
W 63	0,320	3,835	1,71E-03	3360	5,09E-07	6,10E-04	9,98E-03	6,10E-07	7,31E-04	1,20E-02
W 64	0,189	3,738	2,87E-03	3360	8,54E-07	1,02E-03	1,72E-02	7,26E-07	8,70E-04	1,46E-02
W 65	0,070	3,738	2,86E-03	3360	8,50E-07	4,60E-04	6,06E-03	4,56E-07	2,47E-04	3,25E-03
W 66	0,383	3,738	1,94E-03	3360	5,77E-07	3,95E-04	5,87E-03	2,74E-07	1,87E-04	2,78E-03
W 67	0,773	3,451	8,28E-03	3360	2,46E-06	7,91E-04	1,03E-02	2,92E-06	9,38E-04	1,22E-02
W 68	0,116	3,835	6,37E-04	1680	3,79E-07	4,55E-04	7,44E-03	3,72E-07	4,46E-04	7,31E-03
W 69	0,314	3,835	1,06E-03	1680	6,33E-07	7,59E-04	1,24E-02	5,05E-07	6,05E-04	9,90E-03
W 70	0,190	3,835	1,14E-03	1680	6,79E-07	8,15E-04	1,33E-02	5,42E-07	6,50E-04	1,06E-02
W 71	0,067	3,835	2,14E-03	1680	1,27E-06	6,89E-04	8,84E-03	5,18E-07	2,80E-04	3,60E-03
W 72	0,381	3,835	1,33E-03	1680	7,93E-07	5,43E-04	7,86E-03	0,00E+00	0,00E+00	0,00E+00
W 73	0,763	3,835	2,72E-03	1680	1,62E-06	5,19E-04	6,08E-03	6,81E-07	2,19E-04	2,56E-03
W 74	0,116	3,835	7,24E-04	3360	2,16E-07	2,59E-04	4,23E-03	1,86E-07	2,23E-04	3,65E-03
W 75	0,314	3,835	1,33E-03	3360	3,96E-07	4,75E-04	7,77E-03	2,80E-07	3,36E-04	5,50E-03
W 76	0,190	3,835	1,39E-03	3360	4,15E-07	4,98E-04	8,15E-03	2,88E-07	3,45E-04	5,65E-03
W 77	0,067	3,835	2,60E-03	3360	7,75E-07	4,20E-04	5,39E-03	3,33E-07	1,80E-04	2,32E-03
W 78	0,381	3,835	1,74E-03	3360	5,18E-07	3,55E-04	5,13E-03	7,94E-08	5,43E-05	7,87E-04
W 79	0,763	3,835	3,46E-03	3360	1,03E-06	3,31E-04	3,87E-03	3,40E-07	1,09E-04	1,28E-03
W 80	0,117	3,068	1,22E-03	2100	5,83E-07	6,99E-04	1,43E-02	6,54E-07	7,84E-04	1,60E-02
W 82	0,188	3,068	2,45E-03	2100	1,17E-06	1,40E-03	2,86E-02	1,22E-06	1,47E-03	3,00E-02
W 83	0,118	2,972	2,78E-03	2100	1,33E-06	1,59E-03	3,36E-02	8,36E-07	1,00E-03	2,12E-02
W 86	0,092	3,355	1,17E-03	1920	6,07E-07	7,28E-04	1,36E-02	4,72E-07	5,66E-04	1,06E-02
W 87	0,320	3,355	2,65E-03	1920	1,38E-06	1,65E-03	3,09E-02	1,72E-06	2,06E-03	3,85E-02
W 88	0,180	3,355	2,76E-03	1920	1,44E-06	1,72E-03	3,22E-02	1,33E-06	1,60E-03	2,99E-02

Fit of a transport equation to model tests with pipeline covers

Sheet 2 Transport parameters (continued)

Test					Simple transport			Critical scour method		
nr	Ls	omega	Ae	Duration	qs	Phi_q	Phi_Hall	qs	Phi_q	Phi_Hall
-	m	rad/s	m2	s	m3/m/s	-	-	m3/m/s	-	-
W 89	0,118	3,355	3,02E-03	1920	1,57E-06	1,89E-03	3,53E-02	1,22E-06	1,46E-03	2,73E-02
W 90	0,387	3,207	2,73E-03	1920	1,42E-06	9,73E-04	1,69E-02	1,13E-06	7,72E-04	1,34E-02
W 92	0,093	3,835	6,86E-04	1680	4,08E-07	4,90E-04	8,02E-03	3,21E-07	3,85E-04	6,30E-03
W 94	0,171	3,835	1,76E-03	1680	1,05E-06	1,25E-03	2,05E-02	9,18E-07	1,10E-03	1,80E-02
W 95	0,117	3,835	2,71E-03	1680	1,61E-06	1,93E-03	3,17E-02	1,11E-06	1,33E-03	2,17E-02
W 96	0,150	3,670	1,48E-03	1876	7,87E-07	9,21E-04	1,57E-02	6,67E-07	7,80E-04	1,33E-02
W 97	0,150	3,670	1,75E-03	5439	3,23E-07	3,77E-04	6,42E-03	2,47E-07	2,88E-04	4,91E-03
W 100	0,112	3,670	6,18E-04	1801	3,43E-07	4,01E-04	6,83E-03	6,04E-07	7,06E-04	1,20E-02
W 101	0,112	3,670	7,30E-04	5331	1,37E-07	1,60E-04	2,72E-03	2,26E-07	2,64E-04	4,50E-03
W 102	0,112	3,670	7,89E-04	10608	7,43E-08	8,70E-05	1,48E-03	1,20E-07	1,40E-04	2,39E-03
W 103	0,124	3,670	1,14E-03	1760	6,50E-07	7,60E-04	1,29E-02	1,04E-06	1,22E-03	2,07E-02
W 104	0,124	3,670	1,41E-03	4828	2,92E-07	3,42E-04	5,82E-03	4,32E-07	5,06E-04	8,60E-03
W 105	0,124	3,670	1,44E-03	10024	1,43E-07	1,68E-04	2,85E-03	2,12E-07	2,48E-04	4,22E-03
W 106	0,159	3,670	1,60E-03	1681	9,54E-07	1,12E-03	1,90E-02	1,76E-06	2,06E-03	3,51E-02
W 107	0,159	3,670	1,90E-03	5035	3,77E-07	4,41E-04	7,50E-03	6,53E-07	7,64E-04	1,30E-02
W 108	0,159	3,670	2,14E-03	10205	2,10E-07	2,46E-04	4,18E-03	3,40E-07	3,98E-04	6,77E-03
W 109	0,149	3,670	1,63E-03	1738	9,37E-07	1,10E-03	1,87E-02	1,62E-06	1,89E-03	3,22E-02
W 110	0,149	3,670	1,82E-03	5271	3,46E-07	4,05E-04	6,89E-03	5,67E-07	6,64E-04	1,13E-02
W 111	0,149	3,670	2,06E-03	10779	1,91E-07	2,24E-04	3,81E-03	3,05E-07	3,57E-04	6,07E-03
W 112	0,105	3,888	4,72E-04	1653	2,86E-07	3,34E-04	5,37E-03	4,98E-07	5,83E-04	9,36E-03
W 113	0,105	3,888	5,56E-04	4950	1,12E-07	1,31E-04	2,11E-03	1,90E-07	2,22E-04	3,57E-03
W 114	0,105	3,888	6,42E-04	9830	6,53E-08	7,64E-05	1,23E-03	1,06E-07	1,24E-04	1,99E-03
W 115	0,151	3,888	7,76E-04	1700	4,57E-07	5,34E-04	8,58E-03	1,02E-06	1,19E-03	1,91E-02
W 116	0,151	3,888	1,08E-03	5032	2,15E-07	2,51E-04	4,03E-03	4,35E-07	5,09E-04	8,17E-03
W 117	0,151	3,888	1,36E-03	10013	1,36E-07	1,59E-04	2,56E-03	2,55E-07	2,98E-04	4,79E-03
W 121	0,103	3,888	3,97E-04	1690	2,35E-07	2,75E-04	4,41E-03	4,18E-07	4,90E-04	7,86E-03
W 122	0,103	3,888	4,43E-04	4966	8,92E-08	1,04E-04	1,68E-03	1,57E-07	1,83E-04	2,94E-03
W 123	0,103	3,888	4,77E-04	9903	4,82E-08	5,63E-05	9,05E-04	8,28E-08	9,69E-05	1,56E-03
W 124	0,127	3,888	7,94E-04	1784	4,45E-07	5,21E-04	8,36E-03	8,20E-07	9,60E-04	1,54E-02
W 125	0,127	3,888	8,83E-04	5381	1,64E-07	1,92E-04	3,08E-03	2,94E-07	3,44E-04	5,52E-03
W 126	0,127	3,888	9,71E-04	10578	9,18E-08	1,07E-04	1,72E-03	1,59E-07	1,86E-04	2,99E-03
W 127	0,151	3,888	7,67E-04	1744	4,40E-07	5,15E-04	8,27E-03	9,70E-07	1,13E-03	1,82E-02
W 128	0,151	3,888	8,61E-04	5205	1,65E-07	1,94E-04	3,11E-03	3,53E-07	4,13E-04	6,63E-03
W 129	0,151	3,888	1,10E-03	10292	1,07E-07	1,25E-04	2,01E-03	2,10E-07	2,46E-04	3,95E-03
W 130	0,106	3,907	3,46E-04	1592	2,17E-07	2,54E-04	4,06E-03	4,08E-07	4,78E-04	7,64E-03
W 131	0,106	3,907	3,59E-04	4753	7,56E-08	8,85E-05	1,41E-03	1,37E-07	1,60E-04	2,56E-03
W 132	0,106	3,907	3,70E-04	9039	4,09E-08	4,79E-05	7,65E-04	7,39E-08	8,65E-05	1,38E-03
W 133	0,130	3,907	4,94E-04	16746	2,95E-08	3,45E-05	5,52E-04	6,09E-08	7,12E-05	1,14E-03
W 134	0,130	3,907	7,90E-04	5004	1,58E-07	1,85E-04	2,95E-03	2,98E-07	3,48E-04	5,56E-03
W 135	0,130	3,907	7,61E-04	9693	7,85E-08	9,19E-05	1,47E-03	1,49E-07	1,75E-04	2,79E-03
W 136	0,149	3,907	6,88E-04	1576	4,36E-07	5,10E-04	8,16E-03	9,81E-07	1,15E-03	1,83E-02
W 137	0,149	3,907	7,27E-04	4679	1,55E-07	1,82E-04	2,91E-03	3,45E-07	4,04E-04	6,46E-03
W 138	0,149	3,907	7,56E-04	9595	7,88E-08	9,22E-05	1,47E-03	1,71E-07	2,00E-04	3,20E-03

Fit of a transport equation to model tests with pipeline covers
Sheet 3 Fit Simple transport method - Phi_q

		u = u0					u = uc					u = u_hc				
Test nr	ln(Phi)	ln(Psi_BK)	ln(Psi_GM)	ln(Psi_F)	ln(Theta)	ln(Mor)	ln(Psi_BK)	ln(Psi_GM)	ln(Psi_F)	ln(Theta)	ln(Mor)	ln(Psi_BK)	ln(Psi_GM)	ln(Psi_F)	ln(Theta)	ln(Mor)
W 1	-9,39	-4,49	-4,76	-6,54	-2,59	-1,21	-4,31	-4,64	-6,38	-2,41	-1,10	-3,79	-4,26	-5,88	-1,84	-0,73
W 2	-10,16	-4,49	-4,76	-6,54	-2,59	-1,21	-4,31	-4,64	-6,38	-2,41	-1,10	-3,79	-4,26	-5,88	-1,84	-0,73
W 3	-9,52	-3,68	-4,06	-5,51	-1,36	-0,51	-3,61	-3,98	-5,41	-1,26	-0,43	-3,34	-3,66	-5,00	-0,79	-0,09
W 4	-10,16	-3,68	-4,06	-5,51	-1,36	-0,51	-3,61	-3,98	-5,41	-1,26	-0,43	-3,34	-3,66	-5,00	-0,79	-0,09
W 5	-9,34	-3,32	-3,60	-4,86	-0,59	0,00	-3,28	-3,55	-4,80	-0,52	0,06	-3,02	-3,26	-4,44	-0,10	0,38
W 6	-10,28	-3,32	-3,60	-4,86	-0,59	0,00	-3,28	-3,55	-4,80	-0,52	0,06	-3,02	-3,26	-4,44	-0,10	0,38
W 7	-9,34	-3,33	-3,61	-4,87	-0,60	-0,01	-3,28	-3,56	-4,81	-0,53	0,05	-3,03	-3,27	-4,45	-0,12	0,37
W 8	-9,71	-3,33	-3,61	-4,87	-0,60	-0,01	-3,28	-3,56	-4,81	-0,53	0,05	-3,03	-3,27	-4,45	-0,12	0,37
W 9	-9,16	-3,13	-3,36	-4,52	-0,17	0,30	-3,09	-3,32	-4,47	-0,11	0,34	-2,84	-3,04	-4,13	0,28	0,66
W 10	-9,90	-3,13	-3,36	-4,52	-0,17	0,30	-3,09	-3,32	-4,47	-0,11	0,34	-2,84	-3,04	-4,13	0,28	0,66
W 11	-9,50	-3,14	-3,38	-4,54	-0,19	0,28	-3,10	-3,33	-4,48	-0,13	0,33	-2,85	-3,06	-4,15	0,26	0,65
W 12	-10,07	-3,14	-3,38	-4,54	-0,19	0,28	-3,10	-3,33	-4,48	-0,13	0,33	-2,85	-3,06	-4,15	0,26	0,65
W 13	-9,40	-3,87	-4,35	-6,00	-1,98	-0,81	-3,74	-4,21	-5,81	-1,77	-0,67	-3,40	-3,79	-5,28	-1,15	-0,25
W 14	-10,30	-3,41	-3,75	-5,12	-0,92	-0,18	-3,34	-3,66	-5,00	-0,79	-0,09	-3,01	-3,29	-4,54	-0,26	0,32
W 15	-10,39	-3,41	-3,75	-5,12	-0,92	-0,18	-3,34	-3,66	-5,00	-0,79	-0,09	-3,01	-3,29	-4,54	-0,26	0,32
W 18	-8,19	-4,11	-4,47	-5,90	-1,75	-0,92	-4,00	-4,35	-5,75	-1,57	-0,79	-3,66	-3,96	-5,25	-1,00	-0,37
W 19	-8,77	-4,11	-4,47	-5,90	-1,75	-0,92	-4,00	-4,35	-5,75	-1,57	-0,79	-3,66	-3,96	-5,25	-1,00	-0,37
W 20	-8,55	-3,49	-3,72	-4,88	-0,52	-0,06	-3,42	-3,65	-4,78	-0,41	0,03	-3,11	-3,31	-4,37	0,06	0,42
W 21	-8,80	-3,49	-3,72	-4,88	-0,52	-0,06	-3,42	-3,65	-4,78	-0,41	0,03	-3,11	-3,31	-4,37	0,06	0,42
W 22	-6,96	-3,06	-3,23	-4,22	0,27	0,56	-3,01	-3,23	-4,16	0,34	0,63	-2,73	-2,91	-3,80	0,75	0,99
W 23	-7,37	-3,06	-3,23	-4,22	0,27	0,56	-3,01	-3,23	-4,16	0,34	0,63	-2,73	-2,91	-3,80	0,75	0,99
W 26	-8,32	-3,24	-3,48	-4,65	-0,32	0,17	-3,23	-3,48	-4,65	-0,31	0,17	-3,15	-3,38	-4,53	-0,18	0,28
W 27	-10,67	-3,38	-3,71	-5,07	-0,87	-0,14	-3,36	-3,69	-5,05	-0,84	-0,12	-3,21	-3,52	-4,83	-0,60	0,06
W 28	-9,18	-3,41	-3,74	-5,11	-0,91	-0,18	-3,39	-3,72	-5,09	-0,89	-0,16	-3,24	-3,56	-4,88	-0,65	0,02
W 29	-8,46	-3,42	-3,75	-5,13	-0,93	-0,19	-3,40	-3,74	-5,11	-0,91	-0,17	-3,26	-3,57	-4,90	-0,67	0,00
W 30	-10,69	-3,64	-4,04	-5,54	-1,42	-0,50	-3,57	-3,96	-5,43	-1,30	-0,42	-3,29	-3,63	-5,01	-0,82	-0,07
W 32	-8,68	-2,84	-3,01	-4,02	0,45	0,76	-2,84	-3,01	-4,02	0,46	0,77	-2,76	-2,93	-3,91	0,57	0,87
W 33	-9,71	-3,00	-3,24	-4,40	-0,05	0,42	-2,99	-3,22	-4,38	-0,03	0,43	-2,86	-3,08	-4,20	0,17	0,60
W 34	-9,79	-3,04	-3,27	-4,42	-0,06	0,39	-3,03	-3,26	-4,40	-0,04	0,41	-2,90	-3,12	-4,23	0,15	0,57
W 35	-8,54	-3,07	-3,31	-4,49	-0,16	0,33	-3,06	-3,30	-4,48	-0,14	0,34	-2,94	-3,17	-4,32	0,04	0,49
W 36	-9,49	-3,28	-3,56	-4,82	-0,55	0,04	-3,24	-3,51	-4,76	-0,48	0,10	-2,98	-3,23	-4,41	-0,07	0,42
W 38	-7,90	-2,62	-2,79	-3,68	0,87	1,10	-2,61	-2,79	-3,68	0,87	1,11	-2,55	-2,72	-3,59	0,97	1,20
W 40	-8,96	-2,86	-3,06	-4,14	0,28	0,65	-2,85	-3,05	-4,12	0,29	0,67	-2,72	-2,91	-3,96	0,47	0,82
W 41	-7,45	-2,90	-3,11	-4,20	0,21	0,60	-2,89	-3,10	-4,18	0,22	0,61	-2,77	-2,96	-4,02	0,41	0,77
W 44	-9,06	-3,19	-3,40	-4,50	-0,10	0,30	-3,19	-3,40	-4,49	-0,10	0,30	-3,12	-3,32	-4,40	0,00	0,39
W 45	-8,37	-3,04	-3,23	-4,29	0,13	0,49	-3,02	-3,22	-4,28	0,15	0,51	-2,89	-3,07	-4,10	0,36	0,69
W 46	-7,73	-3,21	-3,41	-4,50	-0,10	0,29	-3,20	-3,40	-4,49	-0,09	0,30	-3,07	-3,26	-4,32	0,11	0,47
W 47	-8,61	-3,37	-3,65	-4,91	-0,64	-0,05	-3,36	-3,64	-4,90	-0,62	-0,04	-3,24	-3,51	-4,73	-0,43	0,11
W 48	-8,38	-3,42	-3,68	-4,90	-0,60	-0,06	-3,37	-3,63	-4,84	-0,53	0,00	-3,13	-3,36	-4,50	-0,14	0,31
W 49	-8,56	-3,72	-4,09	-5,52	-1,37	-0,54	-3,55	-3,89	-5,27	-1,09	-0,33	-3,14	-3,42	-4,68	-0,40	0,19
W 50	-9,44	-3,16	-3,37	-4,45	-0,04	0,35	-3,16	-3,36	-4,44	-0,03	0,35	-3,10	-3,29	-4,36	0,07	0,43
W 51	-8,63	-3,04	-3,23	-4,29	0,13	0,49	-3,02	-3,22	-4,28	0,15	0,51	-2,89	-3,07	-4,10	0,36	0,69
W 52	-8,13	-3,20	-3,41	-4,50	-0,10	0,29	-3,19	-3,40	-4,49	-0,09	0,30	-3,06	-3,26	-4,32	0,11	0,47
W 53	-8,96	-3,37	-3,66	-4,92	-0,65	-0,06	-3,37	-3,65	-4,91	-0,63	-0,04	-3,25	-3,51	-4,74	-0,44	0,10
W 54	-8,63	-3,41	-3,67	-4,89	-0,58	-0,05	-3,36	-3,62	-4,82	-0,51	0,01	-3,12	-3,35	-4,49	-0,12	0,32
W 55	-8,71	-3,71	-4,08	-5,52	-1,36	-0,53	-3,54	-3,89	-5,27	-1,08	-0,32	-3,13	-3,41	-4,67	-0,39	0,19
W 56	-7,25	-2,82	-3,02	-3,94	0,57	0,84	-2,82	-3,02	-3,93	0,58	0,85	-2,74	-2,94	-3,83	0,69	0,95
W 57	-7,21	-2,65	-2,84	-3,73	0,81	1,06	-2,65	-2,83	-3,72	0,82	1,07	-2,52	-2,69	-3,56	1,01	1,23
W 58	-6,62	-2,86	-3,06	-3,99	0,51	0,79	-2,85	-3,06	-3,98	0,52	0,80	-2,73	-2,92	-3,82	0,71	0,96
W 59	-7,08	-3,05	-3,26	-4,38	0,01	0,42	-3,04	-3,25	-4,36	0,02	0,44	-2,92	-3,12	-4,20	0,21	0,59
W 60	-7,61	-3,05	-3,24	-4,30	0,13	0,49	-3,02	-3,21	-4,26	0,18	0,53	-2,80	-2,97	-3,97	0,50	0,81
W 61	-6,89	-3,34	-3,59	-4,78	-0,45	0,05	-3,24	-3,48	-4,64	-0,30	0,17	-2,86	-3,06	-4,14	0,28	0,65
W 62	-7,68	-2,82	-3,02	-3,93	0,58	0,85	-2,81	-3,01	-3,93	0,58	0,85	-2,73	-2,93	-3,83	0,69	0,95
W 63	-7,40	-2,66	-2,84	-3,73	0,81	1,05	-2,65	-2,83	-3,72	0,82	1,06	-2,52	-2,69	-3,56	1,01	1,23
W 64	-6,88	-2,83	-3,04	-3,94	0,57	0,84	-2,83	-3,03	-3,93	0,58	0,85	-2,71	-2,90	-3,79	0,75	1,00
W 65	-7,68	-3,05	-3,27	-4,38	0,00	0,42	-3,04	-3,26	-4,37	0,01	0,43	-2,92	-3,13	-4,21	0,20	0,58
W 66	-7,84	-3,05	-3,25	-4,30	0,13	0,49	-3,02	-3,21	-4,26	0,18	0,53	-2,80	-2,98	-3,98	0,50	0,80
W 67	-7,14	-3,33	-3,58	-4,77	-0,45	0,05	-3,24	-3,48	-4,64	-0,30	0,18	-2,86	-3,06	-4,13	0,28	0,66
W 68	-7,70	-3,18	-3,37	-4,41	0,03	0,38	-3,18	-3,37	-4,40	0,04	0,38	-3,11	-3,29	-4,31	0,14	0,47
W 69	-7,18	-3,03	-3,20	-4,21	0,26	0,57	-3,02	-3,20	-4,20	0,27	0,58	-2,91	-3,12	-4,06	0,43	0,72
W 70	-7,11	-3,22	-3,41	-4,46	-0,02	0,33	-3,21	-3,40	-4,45	-0,01	0,34	-3,10	-3,28	-4,30	0,15	0,48
W 71	-7,28	-3,38	-3,64	-4,85	-0,54	-0,01	-3,37	-3,63	-4,84	-0,53	-0,01	-3,26	-3,51	-4,69	-0,35	0,14
W 72	-7,52	-3,41	-3,64	-4,79	-0,44	0,02	-3,38	-3,61	-4,75	-0,40	0,06	-3,18	-3,39	-4,48	-0,08	0,31
W 73	-7,56	-3,65	-3,97	-5,31	-1,09	-0,40	-3,54	-3,85	-5,16	-0,92	-0,27	-3,20	-3,45	-4,66	-0,35	0,17
W 74	-8,26	-3,17	-3,36	-4,40	0,05	0,39	-3,17	-3,36	-4,39	0,05	0,39	-3,10	-3,28	-4,30	0,15	0,48
W 75	-7,65	-3,03	-3,20	-4,20	0,27	0,58	-3,02	-3,19	-4,20	0,28	0,59	-2,91	-3,11	-4,05	0,44	0,73
W 76	-7,61	-3,22	-3,41	-4,46	-0,02	0,33	-3,21	-3,40	-4,45	-0,01	0,34	-3,10	-3,28	-4,30	0,15	0,48
W 77	-7,78	-3,39	-3,65	-4,87	-0,56	-0,03	-3,38	-3,64	-4,86	-0,55	-0,02	-3,27	-3,52	-4,70	-0,37	0,12
W 78	-7,94	-3,40	-3,63	-4,78	-0,43	0,03	-3,37	-3,60	-4,74	-0,38	0,07	-3,17	-3,37	-4,47	-0,07	0,33
W 79	-8,01	-3,63	-3,95	-5,29	-1,06	-0,38	-3,53	-3,83	-5,14	-0,89	-0,25	-3,18	-3,44	-4,64	-0,33	0,19
W 80	-7,27	-2,63	-2,77	-3,58	1,04	1,22	-2,62	-2,77	-3,58	1,05	1,23	-2,55	-2,69	-3,48	1,15	1,32
W 82	-6,57	-2,69	-2,84	-3,65	0,96	1,15	-2,68	-2,82	-3,65	0,97	1,15	-2,56	-2,70	-3,50	1,14	1,31
W 83	-6,44	-2,67	-2,81	-3,62	1,01	1,19	-2,66	-2,80	-3,61	1,02	1,19	-2,55	-2,69	-3,47	1,18	1,34
W 86	-7,22	-2,67	-2,84	-3,68	0,90	1,11	-2,67	-2,84	-3,68	0,90	1,11	-2,62	-2,78	-3,62	0,98	1,18

Fit of a transport equation to model tests with pipeline covers
Sheet 3 Fit Simple transport method - Phi_q (continued)

		u = u0					u = uc					u = u_hc				
Test nr	ln(Phi)	ln(Psi_BK)	ln(Psi_GM)	ln(Psi_F)	ln(Theta)	ln(Mor)	ln(Psi_BK)	ln(Psi_GM)	ln(Psi_F)	ln(Theta)	ln(Mor)	ln(Psi_BK)	ln(Psi_GM)	ln(Psi_F)	ln(Theta)	ln(Mor)
W 87	-6,40	-2,52	-2,67	-3,49	1,12	1,31	-2,51	-2,66	-3,48	1,13	1,32	-2,40	-2,55	-3,35	1,28	1,46
W 88	-6,36	-2,73	-2,89	-3,75	0,83	1,04	-2,72	-2,89	-3,74	0,83	1,05	-2,62	-2,78	-3,62	0,98	1,18
W 89	-6,27	-2,70	-2,87	-3,72	0,86	1,07	-2,70	-2,86	-3,71	0,86	1,08	-2,60	-2,76	-3,59	1,01	1,20
W 90	-6,94	-2,91	-3,11	-4,02	0,49	0,76	-2,89	-3,09	-3,99	0,52	0,79	-2,69	-2,87	-3,74	0,81	1,04
W 92	-7,62	-2,60	-2,79	-3,66	0,88	1,12	-2,60	-2,79	-3,66	0,89	1,12	-2,53	-2,71	-3,57	0,99	1,21
W 94	-6,68	-2,66	-2,86	-3,74	0,80	1,04	-2,66	-2,84	-3,73	0,81	1,05	-2,53	-2,71	-3,57	0,99	1,22
W 95	-6,25	-2,68	-2,87	-3,77	0,77	1,02	-2,68	-2,87	-3,75	0,78	1,03	-2,55	-2,73	-3,59	0,97	1,20
W 96	-6,99	-2,76	-2,94	-3,84	0,70	0,95	-2,75	-2,94	-3,82	0,71	0,96	-2,63	-2,80	-3,67	0,89	1,11
W 97	-7,88	-2,76	-2,94	-3,84	0,70	0,95	-2,75	-2,94	-3,82	0,71	0,96	-2,63	-2,80	-3,67	0,89	1,11
W 100	-7,82	-2,64	-2,81	-3,69	0,86	1,10	-2,64	-2,81	-3,68	0,87	1,10	-2,54	-2,71	-3,56	1,01	1,23
W 101	-8,74	-2,64	-2,81	-3,69	0,86	1,10	-2,64	-2,81	-3,68	0,87	1,10	-2,54	-2,71	-3,56	1,01	1,23
W 102	-9,35	-2,64	-2,81	-3,69	0,86	1,10	-2,64	-2,81	-3,68	0,87	1,10	-2,54	-2,71	-3,56	1,01	1,23
W 103	-7,18	-2,64	-2,81	-3,69	0,86	1,10	-2,64	-2,81	-3,68	0,87	1,10	-2,53	-2,70	-3,55	1,03	1,24
W 104	-7,98	-2,64	-2,81	-3,69	0,86	1,10	-2,64	-2,81	-3,68	0,87	1,10	-2,53	-2,70	-3,55	1,03	1,24
W 105	-8,69	-2,64	-2,81	-3,69	0,86	1,10	-2,64	-2,81	-3,68	0,87	1,10	-2,53	-2,70	-3,55	1,03	1,24
W 106	-6,80	-2,64	-2,81	-3,69	0,86	1,10	-2,63	-2,80	-3,68	0,88	1,11	-2,49	-2,67	-3,51	1,08	1,29
W 107	-7,73	-2,64	-2,81	-3,69	0,86	1,10	-2,63	-2,80	-3,68	0,88	1,11	-2,49	-2,67	-3,51	1,08	1,29
W 108	-8,31	-2,64	-2,81	-3,69	0,86	1,10	-2,63	-2,80	-3,68	0,88	1,11	-2,49	-2,67	-3,51	1,08	1,29
W 109	-6,82	-2,64	-2,81	-3,69	0,86	1,10	-2,63	-2,81	-3,68	0,88	1,11	-2,50	-2,68	-3,52	1,06	1,27
W 110	-7,81	-2,64	-2,81	-3,69	0,86	1,10	-2,63	-2,81	-3,68	0,88	1,11	-2,50	-2,68	-3,52	1,06	1,27
W 111	-8,40	-2,64	-2,81	-3,69	0,86	1,10	-2,63	-2,81	-3,68	0,88	1,11	-2,50	-2,68	-3,52	1,06	1,27
W 112	-8,00	-2,74	-2,94	-3,85	0,67	0,93	-2,74	-2,94	-3,84	0,67	0,94	-2,64	-2,83	-3,72	0,82	1,07
W 113	-8,94	-2,74	-2,94	-3,85	0,67	0,93	-2,74	-2,94	-3,84	0,67	0,94	-2,64	-2,83	-3,72	0,82	1,07
W 114	-9,48	-2,74	-2,94	-3,85	0,67	0,93	-2,74	-2,94	-3,84	0,67	0,94	-2,64	-2,83	-3,72	0,82	1,07
W 115	-7,53	-2,74	-2,94	-3,85	0,67	0,93	-2,73	-2,93	-3,84	0,68	0,94	-2,59	-2,77	-3,65	0,89	1,13
W 116	-8,29	-2,74	-2,94	-3,85	0,67	0,93	-2,73	-2,93	-3,84	0,68	0,94	-2,59	-2,77	-3,65	0,89	1,13
W 117	-8,74	-2,74	-2,94	-3,85	0,67	0,93	-2,73	-2,93	-3,84	0,68	0,94	-2,59	-2,77	-3,65	0,89	1,13
W 121	-8,20	-2,80	-3,00	-3,92	0,59	0,86	-2,79	-3,00	-3,91	0,59	0,87	-2,69	-2,89	-3,79	0,74	0,99
W 122	-9,17	-2,80	-3,00	-3,92	0,59	0,86	-2,79	-3,00	-3,91	0,59	0,87	-2,69	-2,89	-3,79	0,74	0,99
W 123	-9,78	-2,80	-3,00	-3,92	0,59	0,86	-2,79	-3,00	-3,91	0,59	0,87	-2,69	-2,89	-3,79	0,74	0,99
W 124	-7,56	-2,80	-3,00	-3,92	0,59	0,86	-2,79	-2,99	-3,91	0,60	0,87	-2,67	-2,86	-3,76	0,77	1,03
W 125	-8,56	-2,80	-3,00	-3,92	0,59	0,86	-2,79	-2,99	-3,91	0,60	0,87	-2,67	-2,86	-3,76	0,77	1,03
W 126	-9,14	-2,80	-3,00	-3,92	0,59	0,86	-2,79	-2,99	-3,91	0,60	0,87	-2,67	-2,86	-3,76	0,77	1,03
W 127	-7,57	-2,80	-3,00	-3,92	0,59	0,86	-2,79	-2,99	-3,91	0,60	0,87	-2,64	-2,83	-3,72	0,81	1,06
W 128	-8,55	-2,80	-3,00	-3,92	0,59	0,86	-2,79	-2,99	-3,91	0,60	0,87	-2,64	-2,83	-3,72	0,81	1,06
W 129	-8,99	-2,80	-3,00	-3,92	0,59	0,86	-2,79	-2,99	-3,91	0,60	0,87	-2,64	-2,83	-3,72	0,81	1,06
W 130	-8,28	-2,88	-3,10	-4,04	0,45	0,74	-2,88	-3,09	-4,03	0,46	0,75	-2,77	-2,97	-3,89	0,62	0,89
W 131	-9,33	-2,88	-3,10	-4,04	0,45	0,74	-2,88	-3,09	-4,03	0,46	0,75	-2,77	-2,97	-3,89	0,62	0,89
W 132	-9,95	-2,88	-3,10	-4,04	0,45	0,74	-2,88	-3,09	-4,03	0,46	0,75	-2,77	-2,97	-3,89	0,62	0,89
W 133	-10,27	-2,88	-3,10	-4,04	0,45	0,74	-2,87	-3,08	-4,02	0,47	0,76	-2,74	-2,95	-3,86	0,66	0,93
W 134	-8,60	-2,88	-3,10	-4,04	0,45	0,74	-2,87	-3,08	-4,02	0,47	0,76	-2,74	-2,95	-3,86	0,66	0,93
W 135	-9,30	-2,88	-3,10	-4,04	0,45	0,74	-2,87	-3,08	-4,02	0,47	0,76	-2,74	-2,95	-3,86	0,66	0,93
W 136	-7,58	-2,88	-3,10	-4,04	0,45	0,74	-2,87	-3,08	-4,02	0,47	0,76	-2,72	-2,92	-3,83	0,69	0,95
W 137	-8,61	-2,88	-3,10	-4,04	0,45	0,74	-2,87	-3,08	-4,02	0,47	0,76	-2,72	-2,92	-3,83	0,69	0,95
W 138	-9,29	-2,88	-3,10	-4,04	0,45	0,74	-2,87	-3,08	-4,02	0,47	0,76	-2,72	-2,92	-3,83	0,69	0,95
	a	0,01	0,01	0,01	0,00	0,00	0,01	0,01	0,01	0,00	0,00	0,02	0,02	0,01	0,00	0,00
	b	1,12	1,05	0,77	0,65	0,87	1,23	1,14	0,83	0,70	0,93	1,48	1,36	1,00	0,83	1,09
	rsq	**0,16**	**0,19**	**0,21**	**0,23**	**0,21**	**0,17**	**0,19**	**0,22**	**0,23**	**0,22**	**0,16**	**0,19**	**0,22**	**0,24**	**0,22**

Fit of a transport equation to model tests with pipeline covers
Sheet 4 Fit Simple transport method - Hallermeijer

		u = u0					u = uc					u = u_hc				
Test nr	ln(Phi)	ln(Psi_BK)	ln(Psi_GM)	ln(Psi_F)	ln(Theta)	ln(Mor)	ln(Psi_BK)	ln(Psi_GM)	ln(Psi_F)	ln(Theta)	ln(Mor)	ln(Psi_BK)	ln(Psi_GM)	ln(Psi_F)	ln(Theta)	ln(Mor)
W 1	-7,26	-4,49	-4,76	-6,54	-2,59	-1,21	-4,31	-4,64	-6,38	-2,41	-1,10	-3,79	-4,26	-5,88	-1,84	-0,73
W 2	-8,04	-4,49	-4,76	-6,54	-2,59	-1,21	-4,31	-4,64	-6,38	-2,41	-1,10	-3,79	-4,26	-5,88	-1,84	-0,73
W 3	-7,22	-3,68	-4,06	-5,51	-1,36	-0,51	-3,61	-3,98	-5,41	-1,26	-0,43	-3,34	-3,66	-5,00	-0,79	-0,09
W 4	-7,86	-3,68	-4,06	-5,51	-1,36	-0,51	-3,61	-3,98	-5,41	-1,26	-0,43	-3,34	-3,66	-5,00	-0,79	-0,09
W 5	-6,91	-3,32	-3,60	-4,86	-0,59	0,00	-3,28	-3,55	-4,80	-0,52	0,06	-3,02	-3,26	-4,44	-0,10	0,38
W 6	-7,84	-3,32	-3,60	-4,86	-0,59	0,00	-3,28	-3,55	-4,80	-0,52	0,06	-3,02	-3,26	-4,44	-0,10	0,38
W 7	-6,91	-3,33	-3,61	-4,87	-0,60	-0,01	-3,28	-3,56	-4,81	-0,53	0,05	-3,03	-3,27	-4,45	-0,12	0,37
W 8	-7,28	-3,33	-3,61	-4,87	-0,60	-0,01	-3,28	-3,56	-4,81	-0,53	0,05	-3,03	-3,27	-4,45	-0,12	0,37
W 9	-6,63	-3,13	-3,36	-4,52	-0,17	0,30	-3,09	-3,32	-4,47	-0,11	0,34	-2,84	-3,04	-4,13	0,28	0,66
W 10	-7,38	-3,13	-3,36	-4,52	-0,17	0,30	-3,09	-3,32	-4,47	-0,11	0,34	-2,84	-3,04	-4,13	0,28	0,66
W 11	-6,97	-3,14	-3,38	-4,54	-0,19	0,28	-3,10	-3,33	-4,48	-0,13	0,33	-2,85	-3,06	-4,15	0,26	0,65
W 12	-7,54	-3,14	-3,38	-4,54	-0,19	0,28	-3,10	-3,33	-4,48	-0,13	0,33	-2,85	-3,06	-4,15	0,26	0,65
W 13	-7,29	-3,87	-4,35	-6,00	-1,98	-0,81	-3,74	-4,21	-5,81	-1,77	-0,67	-3,40	-3,79	-5,28	-1,15	-0,25
W 14	-8,00	-3,41	-3,75	-5,12	-0,92	-0,18	-3,34	-3,66	-5,00	-0,79	-0,09	-3,01	-3,29	-4,54	-0,26	0,32
W 15	-8,09	-3,41	-3,75	-5,12	-0,92	-0,18	-3,34	-3,66	-5,00	-0,79	-0,09	-3,01	-3,29	-4,54	-0,26	0,32
W 18	-5,64	-4,11	-4,47	-5,90	-1,75	-0,92	-4,00	-4,35	-5,75	-1,57	-0,79	-3,66	-3,96	-5,25	-1,00	-0,37
W 19	-6,23	-4,11	-4,47	-5,90	-1,75	-0,92	-4,00	-4,35	-5,75	-1,57	-0,79	-3,66	-3,96	-5,25	-1,00	-0,37
W 20	-5,83	-3,49	-3,72	-4,88	-0,52	-0,06	-3,42	-3,65	-4,78	-0,41	0,03	-3,11	-3,31	-4,37	0,06	0,42
W 21	-6,08	-3,49	-3,72	-4,88	-0,52	-0,06	-3,42	-3,65	-4,78	-0,41	0,03	-3,11	-3,31	-4,37	0,06	0,42
W 22	-4,11	-3,06	-3,23	-4,22	0,27	0,56	-3,01	-3,23	-4,16	0,34	0,63	-2,73	-2,91	-3,80	0,75	0,99
W 23	-4,51	-3,06	-3,23	-4,22	0,27	0,56	-3,01	-3,23	-4,16	0,34	0,63	-2,73	-2,91	-3,80	0,75	0,99
W 26	-5,77	-3,24	-3,48	-4,65	-0,32	0,17	-3,23	-3,48	-4,65	-0,31	0,17	-3,15	-3,38	-4,53	-0,18	0,28
W 27	-8,38	-3,38	-3,71	-5,07	-0,87	-0,14	-3,36	-3,69	-5,05	-0,84	-0,12	-3,21	-3,52	-4,83	-0,60	0,06
W 28	-6,89	-3,41	-3,74	-5,11	-0,91	-0,18	-3,39	-3,72	-5,09	-0,89	-0,16	-3,24	-3,56	-4,88	-0,65	0,02
W 29	-6,17	-3,42	-3,75	-5,13	-0,93	-0,19	-3,40	-3,74	-5,11	-0,91	-0,17	-3,26	-3,57	-4,90	-0,67	0,00
W 30	-8,47	-3,64	-4,04	-5,54	-1,42	-0,50	-3,57	-3,96	-5,43	-1,30	-0,42	-3,29	-3,63	-5,01	-0,82	-0,07
W 32	-5,98	-2,84	-3,01	-4,02	0,45	0,76	-2,84	-3,01	-4,02	0,46	0,77	-2,76	-2,93	-3,91	0,57	0,87
W 33	-7,26	-3,00	-3,24	-4,40	-0,05	0,42	-2,99	-3,22	-4,38	-0,03	0,43	-2,86	-3,08	-4,20	0,17	0,60
W 34	-7,29	-3,04	-3,27	-4,42	-0,06	0,39	-3,03	-3,26	-4,40	-0,04	0,41	-2,90	-3,12	-4,23	0,15	0,57
W 35	-6,09	-3,07	-3,31	-4,49	-0,16	0,33	-3,06	-3,30	-4,48	-0,14	0,34	-2,94	-3,17	-4,32	0,04	0,49
W 36	-7,08	-3,28	-3,56	-4,82	-0,55	0,04	-3,24	-3,51	-4,76	-0,48	0,10	-2,98	-3,23	-4,41	-0,07	0,42
W 38	-5,10	-2,62	-2,79	-3,68	0,87	1,10	-2,61	-2,79	-3,68	0,87	1,11	-2,55	-2,72	-3,59	0,97	1,20
W 40	-6,41	-2,86	-3,06	-4,14	0,28	0,65	-2,85	-3,05	-4,12	0,29	0,67	-2,72	-2,91	-3,96	0,47	0,82
W 41	-4,89	-2,90	-3,11	-4,20	0,21	0,60	-2,89	-3,10	-4,18	0,22	0,61	-2,77	-2,96	-4,02	0,41	0,77
W 44	-6,38	-3,19	-3,40	-4,50	-0,10	0,30	-3,19	-3,40	-4,49	-0,10	0,30	-3,12	-3,32	-4,40	0,00	0,39
W 45	-5,69	-3,04	-3,23	-4,29	0,13	0,49	-3,02	-3,22	-4,28	0,15	0,51	-2,89	-3,07	-4,10	0,36	0,69
W 46	-5,03	-3,21	-3,41	-4,50	-0,10	0,29	-3,20	-3,40	-4,49	-0,09	0,30	-3,07	-3,26	-4,32	0,11	0,47
W 47	-6,16	-3,37	-3,65	-4,91	-0,64	-0,05	-3,36	-3,64	-4,90	-0,62	-0,04	-3,24	-3,51	-4,73	-0,43	0,11
W 48	-5,83	-3,42	-3,68	-4,90	-0,60	-0,06	-3,37	-3,63	-4,84	-0,53	0,00	-3,13	-3,36	-4,50	-0,14	0,31
W 49	-6,21	-3,72	-4,09	-5,52	-1,37	-0,54	-3,55	-3,89	-5,27	-1,09	-0,33	-3,14	-3,42	-4,68	-0,40	0,19
W 50	-6,74	-3,16	-3,37	-4,45	-0,04	0,35	-3,16	-3,36	-4,44	-0,03	0,35	-3,10	-3,29	-4,36	0,07	0,43
W 51	-5,95	-3,04	-3,23	-4,29	0,13	0,49	-3,02	-3,22	-4,28	0,15	0,51	-2,89	-3,07	-4,10	0,36	0,69
W 52	-5,43	-3,20	-3,41	-4,50	-0,10	0,29	-3,19	-3,40	-4,49	-0,09	0,30	-3,06	-3,26	-4,32	0,11	0,47
W 53	-6,50	-3,37	-3,66	-4,92	-0,65	-0,06	-3,37	-3,65	-4,91	-0,63	-0,04	-3,25	-3,51	-4,74	-0,44	0,10
W 54	-6,07	-3,41	-3,67	-4,89	-0,58	-0,05	-3,36	-3,62	-4,82	-0,51	0,01	-3,12	-3,35	-4,49	-0,12	0,32
W 55	-6,37	-3,71	-4,08	-5,52	-1,36	-0,53	-3,54	-3,89	-5,27	-1,08	-0,32	-3,13	-3,41	-4,67	-0,39	0,19
W 56	-4,45	-2,82	-3,02	-3,94	0,57	0,84	-2,82	-3,02	-3,93	0,58	0,85	-2,74	-2,94	-3,83	0,69	0,95
W 57	-4,42	-2,65	-2,84	-3,73	0,81	1,06	-2,65	-2,83	-3,72	0,82	1,07	-2,52	-2,69	-3,56	1,01	1,23
W 58	-3,83	-2,86	-3,06	-3,99	0,51	0,79	-2,85	-3,06	-3,98	0,52	0,80	-2,73	-2,92	-3,82	0,71	0,96
W 59	-4,51	-3,05	-3,26	-4,38	0,01	0,42	-3,04	-3,25	-4,36	0,02	0,44	-2,92	-3,12	-4,20	0,21	0,59
W 60	-4,92	-3,05	-3,24	-4,30	0,13	0,49	-3,02	-3,21	-4,26	0,18	0,53	-2,80	-2,97	-3,97	0,50	0,81
W 61	-4,32	-3,34	-3,59	-4,78	-0,45	0,05	-3,24	-3,48	-4,64	-0,30	0,17	-2,86	-3,06	-4,14	0,28	0,65
W 62	-4,88	-2,82	-3,02	-3,93	0,58	0,85	-2,81	-3,01	-3,93	0,58	0,85	-2,73	-2,93	-3,83	0,69	0,95
W 63	-4,61	-2,66	-2,84	-3,73	0,81	1,05	-2,65	-2,83	-3,72	0,82	1,06	-2,52	-2,69	-3,56	1,01	1,23
W 64	-4,06	-2,83	-3,04	-3,94	0,57	0,84	-2,83	-3,03	-3,93	0,58	0,85	-2,71	-2,90	-3,79	0,75	1,00
W 65	-5,11	-3,05	-3,27	-4,38	0,00	0,42	-3,04	-3,26	-4,37	0,01	0,43	-2,92	-3,13	-4,21	0,20	0,58
W 66	-5,14	-3,05	-3,25	-4,30	0,13	0,49	-3,02	-3,21	-4,26	0,18	0,53	-2,80	-2,98	-3,98	0,50	0,80
W 67	-4,58	-3,33	-3,58	-4,77	-0,45	0,05	-3,24	-3,48	-4,64	-0,30	0,18	-2,86	-3,06	-4,13	0,28	0,66
W 68	-4,90	-3,18	-3,37	-4,41	0,03	0,38	-3,18	-3,37	-4,40	0,04	0,38	-3,11	-3,29	-4,31	0,14	0,47
W 69	-4,39	-3,03	-3,20	-4,21	0,26	0,57	-3,02	-3,20	-4,20	0,27	0,58	-2,91	-3,12	-4,06	0,43	0,72
W 70	-4,32	-3,22	-3,41	-4,46	-0,02	0,33	-3,21	-3,40	-4,45	-0,01	0,34	-3,10	-3,28	-4,30	0,15	0,48
W 71	-4,73	-3,38	-3,64	-4,85	-0,54	-0,01	-3,37	-3,63	-4,84	-0,53	-0,01	-3,26	-3,51	-4,69	-0,35	0,14
W 72	-4,85	-3,41	-3,64	-4,79	-0,44	0,02	-3,38	-3,61	-4,75	-0,40	0,06	-3,18	-3,39	-4,48	-0,08	0,31
W 73	-5,10	-3,65	-3,97	-5,31	-1,09	-0,40	-3,54	-3,85	-5,16	-0,92	-0,27	-3,20	-3,45	-4,66	-0,35	0,17
W 74	-5,47	-3,17	-3,36	-4,40	0,05	0,39	-3,17	-3,36	-4,39	0,05	0,39	-3,10	-3,28	-4,30	0,15	0,48
W 75	-4,86	-3,03	-3,20	-4,20	0,27	0,58	-3,02	-3,19	-4,20	0,28	0,59	-2,91	-3,11	-4,05	0,44	0,73
W 76	-4,81	-3,22	-3,41	-4,46	-0,02	0,33	-3,21	-3,40	-4,45	-0,01	0,34	-3,10	-3,28	-4,30	0,15	0,48
W 77	-5,22	-3,39	-3,65	-4,87	-0,56	-0,03	-3,38	-3,64	-4,86	-0,55	-0,02	-3,27	-3,52	-4,70	-0,37	0,12
W 78	-5,27	-3,40	-3,63	-4,78	-0,43	0,03	-3,37	-3,60	-4,74	-0,38	0,07	-3,17	-3,37	-4,47	-0,07	0,33
W 79	-5,55	-3,63	-3,95	-5,29	-1,06	-0,38	-3,53	-3,83	-5,14	-0,89	-0,25	-3,18	-3,44	-4,64	-0,33	0,19
W 80	-4,25	-2,63	-2,77	-3,58	1,04	1,22	-2,62	-2,77	-3,58	1,05	1,23	-2,55	-2,69	-3,48	1,15	1,32
W 82	-3,55	-2,69	-2,84	-3,65	0,96	1,15	-2,68	-2,82	-3,65	0,97	1,15	-2,56	-2,70	-3,50	1,14	1,31
W 83	-3,39	-2,67	-2,81	-3,62	1,01	1,19	-2,66	-2,80	-3,61	1,02	1,19	-2,55	-2,69	-3,47	1,18	1,34
W 86	-4,30	-2,67	-2,84	-3,68	0,90	1,11	-2,67	-2,84	-3,68	0,90	1,11	-2,62	-2,78	-3,62	0,98	1,18

Fit of a transport equation to model tests with pipeline covers
Sheet 4 Fit Simple transport method - Hallermeijer (continued)

		u = u0					u = uc					u = u_hc				
Test nr	ln(Phi)	ln(Psi_BK)	ln(Psi_GM)	ln(Psi_F)	ln(Theta)	ln(Mor)	ln(Psi_BK)	ln(Psi_GM)	ln(Psi_F)	ln(Theta)	ln(Mor)	ln(Psi_BK)	ln(Psi_GM)	ln(Psi_F)	ln(Theta)	ln(Mor)
W 87	-3,48	-2,52	-2,67	-3,49	1,12	1,31	-2,51	-2,66	-3,48	1,13	1,32	-2,40	-2,55	-3,35	1,28	1,46
W 88	-3,43	-2,73	-2,89	-3,75	0,83	1,04	-2,72	-2,89	-3,74	0,83	1,05	-2,62	-2,78	-3,62	0,98	1,18
W 89	-3,34	-2,70	-2,87	-3,72	0,86	1,07	-2,70	-2,86	-3,71	0,86	1,08	-2,60	-2,76	-3,59	1,01	1,20
W 90	-4,08	-2,91	-3,11	-4,02	0,49	0,76	-2,89	-3,09	-3,99	0,52	0,79	-2,69	-2,87	-3,74	0,81	1,04
W 92	-4,83	-2,60	-2,79	-3,66	0,88	1,12	-2,60	-2,79	-3,66	0,89	1,12	-2,53	-2,71	-3,57	0,99	1,21
W 94	-3,89	-2,66	-2,86	-3,74	0,80	1,04	-2,66	-2,84	-3,73	0,81	1,05	-2,53	-2,71	-3,57	0,99	1,22
W 95	-3,45	-2,68	-2,87	-3,77	0,77	1,02	-2,68	-2,87	-3,75	0,78	1,03	-2,55	-2,73	-3,59	0,97	1,20
W 96	-4,16	-2,76	-2,94	-3,84	0,70	0,95	-2,75	-2,94	-3,82	0,71	0,96	-2,63	-2,80	-3,67	0,89	1,11
W 97	-5,05	-2,76	-2,94	-3,84	0,70	0,95	-2,75	-2,94	-3,82	0,71	0,96	-2,63	-2,80	-3,67	0,89	1,11
W 100	-4,99	-2,64	-2,81	-3,69	0,86	1,10	-2,64	-2,81	-3,68	0,87	1,10	-2,54	-2,71	-3,56	1,01	1,23
W 101	-5,91	-2,64	-2,81	-3,69	0,86	1,10	-2,64	-2,81	-3,68	0,87	1,10	-2,54	-2,71	-3,56	1,01	1,23
W 102	-6,52	-2,64	-2,81	-3,69	0,86	1,10	-2,64	-2,81	-3,68	0,87	1,10	-2,54	-2,71	-3,56	1,01	1,23
W 103	-4,35	-2,64	-2,81	-3,69	0,86	1,10	-2,64	-2,81	-3,68	0,87	1,10	-2,53	-2,70	-3,55	1,03	1,24
W 104	-5,15	-2,64	-2,81	-3,69	0,86	1,10	-2,64	-2,81	-3,68	0,87	1,10	-2,53	-2,70	-3,55	1,03	1,24
W 105	-5,86	-2,64	-2,81	-3,69	0,86	1,10	-2,64	-2,81	-3,68	0,87	1,10	-2,53	-2,70	-3,55	1,03	1,24
W 106	-3,96	-2,64	-2,81	-3,69	0,86	1,10	-2,63	-2,80	-3,68	0,88	1,11	-2,49	-2,67	-3,51	1,08	1,29
W 107	-4,89	-2,64	-2,81	-3,69	0,86	1,10	-2,63	-2,80	-3,68	0,88	1,11	-2,49	-2,67	-3,51	1,08	1,29
W 108	-5,48	-2,64	-2,81	-3,69	0,86	1,10	-2,63	-2,80	-3,68	0,88	1,11	-2,49	-2,67	-3,51	1,08	1,29
W 109	-3,98	-2,64	-2,81	-3,69	0,86	1,10	-2,63	-2,81	-3,68	0,88	1,11	-2,50	-2,68	-3,52	1,06	1,27
W 110	-4,98	-2,64	-2,81	-3,69	0,86	1,10	-2,63	-2,81	-3,68	0,88	1,11	-2,50	-2,68	-3,52	1,06	1,27
W 111	-5,57	-2,64	-2,81	-3,69	0,86	1,10	-2,63	-2,81	-3,68	0,88	1,11	-2,50	-2,68	-3,52	1,06	1,27
W 112	-5,23	-2,74	-2,94	-3,85	0,67	0,93	-2,74	-2,94	-3,84	0,67	0,94	-2,64	-2,83	-3,72	0,82	1,07
W 113	-6,16	-2,74	-2,94	-3,85	0,67	0,93	-2,74	-2,94	-3,84	0,67	0,94	-2,64	-2,83	-3,72	0,82	1,07
W 114	-6,70	-2,74	-2,94	-3,85	0,67	0,93	-2,74	-2,94	-3,84	0,67	0,94	-2,64	-2,83	-3,72	0,82	1,07
W 115	-4,76	-2,74	-2,94	-3,85	0,67	0,93	-2,73	-2,93	-3,84	0,68	0,94	-2,59	-2,77	-3,65	0,89	1,13
W 116	-5,51	-2,74	-2,94	-3,85	0,67	0,93	-2,73	-2,93	-3,84	0,68	0,94	-2,59	-2,77	-3,65	0,89	1,13
W 117	-5,97	-2,74	-2,94	-3,85	0,67	0,93	-2,73	-2,93	-3,84	0,68	0,94	-2,59	-2,77	-3,65	0,89	1,13
W 121	-5,42	-2,80	-3,00	-3,92	0,59	0,86	-2,79	-3,00	-3,91	0,59	0,87	-2,69	-2,89	-3,79	0,74	0,99
W 122	-6,39	-2,80	-3,00	-3,92	0,59	0,86	-2,79	-3,00	-3,91	0,59	0,87	-2,69	-2,89	-3,79	0,74	0,99
W 123	-7,01	-2,80	-3,00	-3,92	0,59	0,86	-2,79	-3,00	-3,91	0,59	0,87	-2,69	-2,89	-3,79	0,74	0,99
W 124	-4,78	-2,80	-3,00	-3,92	0,59	0,86	-2,79	-2,99	-3,91	0,60	0,87	-2,67	-2,86	-3,76	0,77	1,03
W 125	-5,78	-2,80	-3,00	-3,92	0,59	0,86	-2,79	-2,99	-3,91	0,60	0,87	-2,67	-2,86	-3,76	0,77	1,03
W 126	-6,36	-2,80	-3,00	-3,92	0,59	0,86	-2,79	-2,99	-3,91	0,60	0,87	-2,67	-2,86	-3,76	0,77	1,03
W 127	-4,80	-2,80	-3,00	-3,92	0,59	0,86	-2,79	-2,99	-3,91	0,60	0,87	-2,64	-2,83	-3,72	0,81	1,06
W 128	-5,77	-2,80	-3,00	-3,92	0,59	0,86	-2,79	-2,99	-3,91	0,60	0,87	-2,64	-2,83	-3,72	0,81	1,06
W 129	-6,21	-2,80	-3,00	-3,92	0,59	0,86	-2,79	-2,99	-3,91	0,60	0,87	-2,64	-2,83	-3,72	0,81	1,06
W 130	-5,51	-2,88	-3,10	-4,04	0,45	0,74	-2,88	-3,09	-4,03	0,46	0,75	-2,77	-2,97	-3,89	0,62	0,89
W 131	-6,56	-2,88	-3,10	-4,04	0,45	0,74	-2,88	-3,09	-4,03	0,46	0,75	-2,77	-2,97	-3,89	0,62	0,89
W 132	-7,18	-2,88	-3,10	-4,04	0,45	0,74	-2,88	-3,09	-4,03	0,46	0,75	-2,77	-2,97	-3,89	0,62	0,89
W 133	-7,50	-2,88	-3,10	-4,04	0,45	0,74	-2,87	-3,08	-4,02	0,47	0,76	-2,74	-2,95	-3,86	0,66	0,93
W 134	-5,83	-2,88	-3,10	-4,04	0,45	0,74	-2,87	-3,08	-4,02	0,47	0,76	-2,74	-2,95	-3,86	0,66	0,93
W 135	-6,52	-2,88	-3,10	-4,04	0,45	0,74	-2,87	-3,08	-4,02	0,47	0,76	-2,74	-2,95	-3,86	0,66	0,93
W 136	-4,81	-2,88	-3,10	-4,04	0,45	0,74	-2,87	-3,08	-4,02	0,47	0,76	-2,72	-2,92	-3,83	0,69	0,95
W 137	-5,84	-2,88	-3,10	-4,04	0,45	0,74	-2,87	-3,08	-4,02	0,47	0,76	-2,72	-2,92	-3,83	0,69	0,95
W 138	-6,52	-2,88	-3,10	-4,04	0,45	0,74	-2,87	-3,08	-4,02	0,47	0,76	-2,72	-2,92	-3,83	0,69	0,95
	a	0,38	0,39	0,33	0,00	0,00	0,57	0,56	0,46	0,00	0,00	1,11	1,01	0,84	0,00	0,00
	b	1,53	1,44	1,04	0,88	1,18	1,68	1,55	1,13	0,94	1,26	2,01	1,84	1,34	1,11	1,46
	rsq	**0,25**	**0,28**	**0,31**	**0,33**	**0,31**	**0,25**	**0,28**	**0,32**	**0,34**	**0,31**	**0,24**	**0,27**	**0,32**	**0,34**	**0,32**

Fit of a transport equation to model tests with pipeline covers
Sheet 5 Fit Critical scour method - Phi_q

		u = u0					u = uc					u = u_hc				
Test nr	ln(Phi)	ln(Psi_BK)	ln(Psi_GM)	ln(Psi_F)	ln(Theta)	ln(Mor)	ln(Psi_BK)	ln(Psi_GM)	ln(Psi_F)	ln(Theta)	ln(Mor)	ln(Psi_BK)	ln(Psi_GM)	ln(Psi_F)	ln(Theta)	ln(Mor)
W 1	-8,68	-4,49	-4,76	-6,54	-2,59	-1,21	-4,31	-4,64	-6,38	-2,41	-1,10	-3,79	-4,26	-5,88	-1,84	-0,73
W 2	-9,46	-4,49	-4,76	-6,54	-2,59	-1,21	-4,31	-4,64	-6,38	-2,41	-1,10	-3,79	-4,26	-5,88	-1,84	-0,73
W 3	-8,81	-3,68	-4,06	-5,51	-1,36	-0,51	-3,61	-3,98	-5,41	-1,26	-0,43	-3,34	-3,66	-5,00	-0,79	-0,09
W 4	-9,46	-3,68	-4,06	-5,51	-1,36	-0,51	-3,61	-3,98	-5,41	-1,26	-0,43	-3,34	-3,66	-5,00	-0,79	-0,09
W 5	-8,64	-3,32	-3,60	-4,86	-0,59	0,00	-3,28	-3,55	-4,80	-0,52	0,06	-3,02	-3,26	-4,44	-0,10	0,38
W 6	-9,58	-3,32	-3,60	-4,86	-0,59	0,00	-3,28	-3,55	-4,80	-0,52	0,06	-3,02	-3,26	-4,44	-0,10	0,38
W 7	-8,64	-3,33	-3,61	-4,87	-0,60	-0,01	-3,28	-3,56	-4,81	-0,53	0,05	-3,03	-3,27	-4,45	-0,12	0,37
W 8	-9,05	-3,33	-3,61	-4,87	-0,60	-0,01	-3,28	-3,56	-4,81	-0,53	0,05	-3,03	-3,27	-4,45	-0,12	0,37
W 9	-8,47	-3,13	-3,36	-4,52	-0,17	0,30	-3,09	-3,32	-4,47	-0,11	0,34	-2,84	-3,04	-4,13	0,28	0,66
W 10	-9,24	-3,13	-3,36	-4,52	-0,17	0,30	-3,09	-3,32	-4,47	-0,11	0,34	-2,84	-3,04	-4,13	0,28	0,66
W 11	-8,80	-3,14	-3,38	-4,54	-0,19	0,28	-3,10	-3,33	-4,48	-0,13	0,33	-2,85	-3,06	-4,15	0,26	0,65
W 12	-9,39	-3,14	-3,38	-4,54	-0,19	0,28	-3,10	-3,33	-4,48	-0,13	0,33	-2,85	-3,06	-4,15	0,26	0,65
W 13	-8,69	-3,87	-4,35	-6,00	-1,98	-0,81	-3,74	-4,21	-5,81	-1,77	-0,67	-3,40	-3,79	-5,28	-1,15	-0,25
W 14	-9,58	-3,41	-3,75	-5,12	-0,92	-0,18	-3,34	-3,66	-5,00	-0,79	-0,09	-3,01	-3,29	-4,54	-0,26	0,32
W 15	-9,68	-3,41	-3,75	-5,12	-0,92	-0,18	-3,34	-3,66	-5,00	-0,79	-0,09	-3,01	-3,29	-4,54	-0,26	0,32
W 18	-6,70	-4,11	-4,47	-5,90	-1,75	-0,92	-4,00	-4,35	-5,75	-1,57	-0,79	-3,66	-3,96	-5,25	-1,00	-0,37
W 19	-7,33	-4,11	-4,47	-5,90	-1,75	-0,92	-4,00	-4,35	-5,75	-1,57	-0,79	-3,66	-3,96	-5,25	-1,00	-0,37
W 20	-7,05	-3,49	-3,72	-4,88	-0,52	-0,06	-3,42	-3,65	-4,78	-0,41	0,03	-3,11	-3,31	-4,37	0,06	0,42
W 21	-7,37	-3,49	-3,72	-4,88	-0,52	-0,06	-3,42	-3,65	-4,78	-0,41	0,03	-3,11	-3,31	-4,37	0,06	0,42
W 22	-5,65	-3,06	-3,23	-4,22	0,27	0,56	-3,01	-3,23	-4,16	0,34	0,63	-2,73	-2,91	-3,80	0,75	0,99
W 23	-6,19	-3,06	-3,23	-4,22	0,27	0,56	-3,01	-3,23	-4,16	0,34	0,63	-2,73	-2,91	-3,80	0,75	0,99
W 26	-9,04	-3,24	-3,48	-4,65	-0,32	0,17	-3,23	-3,48	-4,65	-0,31	0,17	-3,15	-3,38	-4,53	-0,18	0,28
W 27		-3,38	-3,71	-5,07	-0,87	-0,14	-3,36	-3,69	-5,05	-0,84	-0,12	-3,21	-3,52	-4,83	-0,60	0,06
W 28	-11,38	-3,41	-3,74	-5,11	-0,91	-0,18	-3,39	-3,72	-5,09	-0,89	-0,16	-3,24	-3,56	-4,88	-0,65	0,02
W 29	-10,04	-3,42	-3,75	-5,13	-0,93	-0,19	-3,40	-3,74	-5,11	-0,91	-0,17	-3,26	-3,57	-4,90	-0,67	0,00
W 30	-11,09	-3,64	-4,04	-5,54	-1,42	-0,50	-3,57	-3,96	-5,43	-1,30	-0,42	-3,29	-3,63	-5,01	-0,82	-0,07
W 32	-8,64	-2,84	-3,01	-4,02	0,45	0,76	-2,84	-3,01	-4,02	0,46	0,77	-2,76	-2,93	-3,91	0,57	0,87
W 33	-9,84	-3,00	-3,24	-4,40	-0,05	0,42	-2,99	-3,22	-4,38	-0,03	0,43	-2,86	-3,08	-4,20	0,17	0,60
W 34	-10,04	-3,04	-3,27	-4,42	-0,06	0,39	-3,03	-3,26	-4,40	-0,04	0,41	-2,90	-3,12	-4,23	0,15	0,57
W 35	-9,71	-3,07	-3,31	-4,49	-0,16	0,33	-3,06	-3,30	-4,48	-0,14	0,34	-2,94	-3,17	-4,32	0,04	0,49
W 36		-3,28	-3,56	-4,82	-0,55	0,04	-3,24	-3,51	-4,76	-0,48	0,10	-2,98	-3,23	-4,41	-0,07	0,42
W 38	-8,13	-2,62	-2,79	-3,68	0,87	1,10	-2,61	-2,79	-3,68	0,87	1,11	-2,55	-2,72	-3,59	0,97	1,20
W 40	-10,01	-2,86	-3,06	-4,14	0,28	0,65	-2,85	-3,05	-4,12	0,29	0,67	-2,72	-2,91	-3,96	0,47	0,82
W 41	-8,46	-2,90	-3,11	-4,20	0,21	0,60	-2,89	-3,10	-4,18	0,22	0,61	-2,77	-2,96	-4,02	0,41	0,77
W 44	-9,32	-3,19	-3,40	-4,50	-0,10	0,30	-3,19	-3,40	-4,49	-0,10	0,30	-3,12	-3,32	-4,40	0,00	0,39
W 45	-10,00	-3,04	-3,23	-4,29	0,13	0,49	-3,02	-3,22	-4,28	0,15	0,51	-2,89	-3,07	-4,10	0,36	0,69
W 46	-7,93	-3,21	-3,41	-4,50	-0,10	0,29	-3,20	-3,40	-4,49	-0,09	0,30	-3,07	-3,26	-4,32	0,11	0,47
W 47	-10,67	-3,37	-3,65	-4,91	-0,64	-0,05	-3,36	-3,64	-4,90	-0,62	-0,04	-3,24	-3,51	-4,73	-0,43	0,11
W 48	-8,99	-3,42	-3,68	-4,90	-0,60	-0,06	-3,37	-3,63	-4,84	-0,53	0,00	-3,13	-3,36	-4,50	-0,14	0,31
W 49	-8,28	-3,72	-4,09	-5,52	-1,37	-0,54	-3,55	-3,89	-5,27	-1,09	-0,33	-3,14	-3,42	-4,68	-0,40	0,19
W 50	-9,82	-3,16	-3,37	-4,45	-0,04	0,35	-3,16	-3,36	-4,44	-0,03	0,35	-3,10	-3,29	-4,36	0,07	0,43
W 51	-9,78	-3,04	-3,23	-4,29	0,13	0,49	-3,02	-3,22	-4,28	0,15	0,51	-2,89	-3,07	-4,10	0,36	0,69
W 52	-8,39	-3,20	-3,41	-4,50	-0,10	0,29	-3,19	-3,40	-4,49	-0,09	0,30	-3,06	-3,26	-4,32	0,11	0,47
W 53	-10,56	-3,37	-3,66	-4,92	-0,65	-0,06	-3,37	-3,65	-4,91	-0,63	-0,04	-3,25	-3,51	-4,74	-0,44	0,10
W 54	-9,68	-3,41	-3,67	-4,89	-0,58	-0,05	-3,36	-3,62	-4,82	-0,51	0,01	-3,12	-3,35	-4,49	-0,12	0,32
W 55	-8,72	-3,71	-4,08	-5,52	-1,36	-0,53	-3,54	-3,89	-5,27	-1,08	-0,32	-3,13	-3,41	-4,67	-0,39	0,19
W 56	-7,23	-2,82	-3,02	-3,94	0,57	0,84	-2,82	-3,02	-3,93	0,58	0,85	-2,74	-2,94	-3,83	0,69	0,95
W 57	-7,22	-2,65	-2,84	-3,73	0,81	1,06	-2,65	-2,83	-3,72	0,82	1,07	-2,52	-2,69	-3,56	1,01	1,23
W 58	-6,74	-2,86	-3,06	-3,99	0,51	0,79	-2,85	-3,06	-3,98	0,52	0,80	-2,73	-2,92	-3,82	0,71	0,96
W 59	-7,68	-3,05	-3,26	-4,38	0,01	0,42	-3,04	-3,25	-4,36	0,02	0,44	-2,92	-3,12	-4,20	0,21	0,59
W 60	-8,12	-3,05	-3,24	-4,30	0,13	0,49	-3,02	-3,21	-4,26	0,18	0,53	-2,80	-2,97	-3,97	0,50	0,81
W 61	-7,06	-3,34	-3,59	-4,78	-0,45	0,05	-3,24	-3,48	-4,64	-0,30	0,17	-2,86	-3,06	-4,14	0,28	0,65
W 62	-7,80	-2,82	-3,02	-3,93	0,58	0,85	-2,81	-3,01	-3,93	0,58	0,85	-2,73	-2,93	-3,83	0,69	0,95
W 63	-7,22	-2,66	-2,84	-3,73	0,81	1,05	-2,65	-2,83	-3,72	0,82	1,06	-2,52	-2,69	-3,56	1,01	1,23
W 64	-7,05	-2,83	-3,04	-3,94	0,57	0,84	-2,83	-3,03	-3,93	0,58	0,85	-2,71	-2,90	-3,79	0,75	1,00
W 65	-8,31	-3,05	-3,27	-4,38	0,00	0,42	-3,04	-3,26	-4,37	0,01	0,43	-2,92	-3,13	-4,21	0,20	0,58
W 66	-8,58	-3,05	-3,25	-4,30	0,13	0,49	-3,02	-3,21	-4,26	0,18	0,53	-2,80	-2,98	-3,98	0,50	0,80
W 67	-6,97	-3,33	-3,58	-4,77	-0,45	0,05	-3,24	-3,48	-4,64	-0,30	0,18	-2,86	-3,06	-4,13	0,28	0,66
W 68	-7,71	-3,18	-3,37	-4,41	0,03	0,38	-3,18	-3,37	-4,40	0,04	0,38	-3,11	-3,29	-4,31	0,14	0,47
W 69	-7,41	-3,03	-3,20	-4,21	0,26	0,57	-3,02	-3,20	-4,20	0,27	0,58	-2,91	-3,12	-4,06	0,43	0,72
W 70	-7,34	-3,22	-3,41	-4,46	-0,02	0,33	-3,21	-3,40	-4,45	-0,01	0,34	-3,10	-3,28	-4,30	0,15	0,48
W 71	-8,18	-3,38	-3,64	-4,85	-0,54	-0,01	-3,37	-3,63	-4,84	-0,53	-0,01	-3,26	-3,51	-4,69	-0,35	0,14
W 72		-3,41	-3,64	-4,79	-0,44	0,02	-3,38	-3,61	-4,75	-0,40	0,06	-3,18	-3,39	-4,48	-0,08	0,31
W 73	-8,43	-3,65	-3,97	-5,31	-1,09	-0,40	-3,54	-3,85	-5,16	-0,92	-0,27	-3,20	-3,45	-4,66	-0,35	0,17
W 74	-8,41	-3,17	-3,36	-4,40	0,05	0,39	-3,17	-3,36	-4,39	0,05	0,39	-3,10	-3,28	-4,30	0,15	0,48
W 75	-8,00	-3,03	-3,20	-4,20	0,27	0,58	-3,02	-3,19	-4,20	0,28	0,59	-2,91	-3,11	-4,05	0,44	0,73
W 76	-7,97	-3,22	-3,41	-4,46	-0,02	0,33	-3,21	-3,40	-4,45	-0,01	0,34	-3,10	-3,28	-4,30	0,15	0,48
W 77	-8,62	-3,39	-3,65	-4,87	-0,56	-0,03	-3,38	-3,64	-4,86	-0,55	-0,02	-3,27	-3,52	-4,70	-0,37	0,12
W 78	-9,82	-3,40	-3,63	-4,78	-0,43	0,03	-3,37	-3,60	-4,74	-0,38	0,07	-3,17	-3,37	-4,47	-0,07	0,33
W 79	-9,12	-3,63	-3,95	-5,29	-1,06	-0,38	-3,53	-3,83	-5,14	-0,89	-0,25	-3,18	-3,44	-4,64	-0,33	0,19
W 80	-7,15	-2,63	-2,77	-3,58	1,04	1,22	-2,62	-2,77	-3,58	1,05	1,23	-2,55	-2,69	-3,48	1,15	1,32
W 82	-6,52	-2,69	-2,84	-3,65	0,96	1,15	-2,68	-2,82	-3,65	0,97	1,15	-2,56	-2,70	-3,50	1,14	1,31
W 83	-6,91	-2,67	-2,81	-3,62	1,01	1,19	-2,66	-2,80	-3,61	1,02	1,19	-2,55	-2,69	-3,47	1,18	1,34
W 86	-7,48	-2,67	-2,84	-3,68	0,90	1,11	-2,67	-2,84	-3,68	0,90	1,11	-2,62	-2,78	-3,62	0,98	1,18

Fit of a transport equation to model tests with pipeline covers
Sheet 5 Fit Critical scour method - Phi_q (continued)

		u = u0					u = uc					u = u_hc				
Test nr	ln(Phi)	ln(Psi_BK)	ln(Psi_GM)	ln(Psi_F)	ln(Theta)	ln(Mor)	ln(Psi_BK)	ln(Psi_GM)	ln(Psi_F)	ln(Theta)	ln(Mor)	ln(Psi_BK)	ln(Psi_GM)	ln(Psi_F)	ln(Theta)	ln(Mor)
W 87	-6,19	-2,52	-2,67	-3,49	1,12	1,31	-2,51	-2,66	-3,48	1,13	1,32	-2,40	-2,55	-3,35	1,28	1,46
W 88	-6,44	-2,73	-2,89	-3,75	0,83	1,04	-2,72	-2,89	-3,74	0,83	1,05	-2,62	-2,78	-3,62	0,98	1,18
W 89	-6,53	-2,70	-2,87	-3,72	0,86	1,07	-2,70	-2,86	-3,71	0,86	1,08	-2,60	-2,76	-3,59	1,01	1,20
W 90	-7,17	-2,91	-3,11	-4,02	0,49	0,76	-2,89	-3,09	-3,99	0,52	0,79	-2,69	-2,87	-3,74	0,81	1,04
W 92	-7,86	-2,60	-2,79	-3,66	0,88	1,12	-2,60	-2,79	-3,66	0,89	1,12	-2,53	-2,71	-3,57	0,99	1,21
W 94	-6,81	-2,66	-2,86	-3,74	0,80	1,04	-2,66	-2,84	-3,73	0,81	1,05	-2,53	-2,71	-3,57	0,99	1,22
W 95	-6,63	-2,68	-2,87	-3,77	0,77	1,02	-2,68	-2,87	-3,75	0,78	1,03	-2,55	-2,73	-3,59	0,97	1,20
W 96	-7,16	-2,76	-2,94	-3,84	0,70	0,95	-2,75	-2,94	-3,82	0,71	0,96	-2,63	-2,80	-3,67	0,89	1,11
W 97	-8,15	-2,76	-2,94	-3,84	0,70	0,95	-2,75	-2,94	-3,82	0,71	0,96	-2,63	-2,80	-3,67	0,89	1,11
W 100	-7,26	-2,64	-2,81	-3,69	0,86	1,10	-2,64	-2,81	-3,68	0,87	1,10	-2,54	-2,71	-3,56	1,01	1,23
W 101	-8,24	-2,64	-2,81	-3,69	0,86	1,10	-2,64	-2,81	-3,68	0,87	1,10	-2,54	-2,71	-3,56	1,01	1,23
W 102	-8,87	-2,64	-2,81	-3,69	0,86	1,10	-2,64	-2,81	-3,68	0,87	1,10	-2,54	-2,71	-3,56	1,01	1,23
W 103	-6,71	-2,64	-2,81	-3,69	0,86	1,10	-2,64	-2,81	-3,68	0,87	1,10	-2,53	-2,70	-3,55	1,03	1,24
W 104	-7,59	-2,64	-2,81	-3,69	0,86	1,10	-2,64	-2,81	-3,68	0,87	1,10	-2,53	-2,70	-3,55	1,03	1,24
W 105	-8,30	-2,64	-2,81	-3,69	0,86	1,10	-2,64	-2,81	-3,68	0,87	1,10	-2,53	-2,70	-3,55	1,03	1,24
W 106	-6,18	-2,64	-2,81	-3,69	0,86	1,10	-2,63	-2,80	-3,68	0,88	1,11	-2,49	-2,67	-3,51	1,08	1,29
W 107	-7,18	-2,64	-2,81	-3,69	0,86	1,10	-2,63	-2,80	-3,68	0,88	1,11	-2,49	-2,67	-3,51	1,08	1,29
W 108	-7,83	-2,64	-2,81	-3,69	0,86	1,10	-2,63	-2,80	-3,68	0,88	1,11	-2,49	-2,67	-3,51	1,08	1,29
W 109	-6,27	-2,64	-2,81	-3,69	0,86	1,10	-2,63	-2,81	-3,68	0,88	1,11	-2,50	-2,68	-3,52	1,06	1,27
W 110	-7,32	-2,64	-2,81	-3,69	0,86	1,10	-2,63	-2,81	-3,68	0,88	1,11	-2,50	-2,68	-3,52	1,06	1,27
W 111	-7,94	-2,64	-2,81	-3,69	0,86	1,10	-2,63	-2,81	-3,68	0,88	1,11	-2,50	-2,68	-3,52	1,06	1,27
W 112	-7,45	-2,74	-2,94	-3,85	0,67	0,93	-2,74	-2,94	-3,84	0,67	0,94	-2,64	-2,83	-3,72	0,82	1,07
W 113	-8,41	-2,74	-2,94	-3,85	0,67	0,93	-2,74	-2,94	-3,84	0,67	0,94	-2,64	-2,83	-3,72	0,82	1,07
W 114	-8,99	-2,74	-2,94	-3,85	0,67	0,93	-2,74	-2,94	-3,84	0,67	0,94	-2,64	-2,83	-3,72	0,82	1,07
W 115	-6,73	-2,74	-2,94	-3,85	0,67	0,93	-2,73	-2,93	-3,84	0,68	0,94	-2,59	-2,77	-3,65	0,89	1,13
W 116	-7,58	-2,74	-2,94	-3,85	0,67	0,93	-2,73	-2,93	-3,84	0,68	0,94	-2,59	-2,77	-3,65	0,89	1,13
W 117	-8,12	-2,74	-2,94	-3,85	0,67	0,93	-2,73	-2,93	-3,84	0,68	0,94	-2,59	-2,77	-3,65	0,89	1,13
W 121	-7,62	-2,80	-3,00	-3,92	0,59	0,86	-2,79	-3,00	-3,91	0,59	0,87	-2,69	-2,89	-3,79	0,74	0,99
W 122	-8,60	-2,80	-3,00	-3,92	0,59	0,86	-2,79	-3,00	-3,91	0,59	0,87	-2,69	-2,89	-3,79	0,74	0,99
W 123	-9,24	-2,80	-3,00	-3,92	0,59	0,86	-2,79	-3,00	-3,91	0,59	0,87	-2,69	-2,89	-3,79	0,74	0,99
W 124	-6,95	-2,80	-3,00	-3,92	0,59	0,86	-2,79	-2,99	-3,91	0,60	0,87	-2,67	-2,86	-3,76	0,77	1,03
W 125	-7,98	-2,80	-3,00	-3,92	0,59	0,86	-2,79	-2,99	-3,91	0,60	0,87	-2,67	-2,86	-3,76	0,77	1,03
W 126	-8,59	-2,80	-3,00	-3,92	0,59	0,86	-2,79	-2,99	-3,91	0,60	0,87	-2,67	-2,86	-3,76	0,77	1,03
W 127	-6,78	-2,80	-3,00	-3,92	0,59	0,86	-2,79	-2,99	-3,91	0,60	0,87	-2,64	-2,83	-3,72	0,81	1,06
W 128	-7,79	-2,80	-3,00	-3,92	0,59	0,86	-2,79	-2,99	-3,91	0,60	0,87	-2,64	-2,83	-3,72	0,81	1,06
W 129	-8,31	-2,80	-3,00	-3,92	0,59	0,86	-2,79	-2,99	-3,91	0,60	0,87	-2,64	-2,83	-3,72	0,81	1,06
W 130	-7,65	-2,88	-3,10	-4,04	0,45	0,74	-2,88	-3,09	-4,03	0,46	0,75	-2,77	-2,97	-3,89	0,62	0,89
W 131	-8,74	-2,88	-3,10	-4,04	0,45	0,74	-2,88	-3,09	-4,03	0,46	0,75	-2,77	-2,97	-3,89	0,62	0,89
W 132	-9,36	-2,88	-3,10	-4,04	0,45	0,74	-2,88	-3,09	-4,03	0,46	0,75	-2,77	-2,97	-3,89	0,62	0,89
W 133	-9,55	-2,88	-3,10	-4,04	0,45	0,74	-2,87	-3,08	-4,02	0,47	0,76	-2,74	-2,95	-3,86	0,66	0,93
W 134	-7,96	-2,88	-3,10	-4,04	0,45	0,74	-2,87	-3,08	-4,02	0,47	0,76	-2,74	-2,95	-3,86	0,66	0,93
W 135	-8,65	-2,88	-3,10	-4,04	0,45	0,74	-2,87	-3,08	-4,02	0,47	0,76	-2,74	-2,95	-3,86	0,66	0,93
W 136	-6,77	-2,88	-3,10	-4,04	0,45	0,74	-2,87	-3,08	-4,02	0,47	0,76	-2,72	-2,92	-3,83	0,69	0,95
W 137	-7,81	-2,88	-3,10	-4,04	0,45	0,74	-2,87	-3,08	-4,02	0,47	0,76	-2,72	-2,92	-3,83	0,69	0,95
W 138	-8,52	-2,88	-3,10	-4,04	0,45	0,74	-2,87	-3,08	-4,02	0,47	0,76	-2,72	-2,92	-3,83	0,69	0,95
	a	0,01	0,01	0,01	0,00	0,00	0,02	0,01	0,01	0,00	0,00	0,06	0,04	0,04	0,00	0,00
	b	1,17	1,09	0,82	0,70	0,95	1,34	1,23	0,91	0,77	1,05	1,87	1,65	1,19	0,99	1,33
	rsq	**0,16**	**0,18**	**0,21**	**0,23**	**0,22**	**0,18**	**0,19**	**0,23**	**0,25**	**0,24**	**0,23**	**0,24**	**0,28**	**0,30**	**0,29**

Fit of a transport equation to model tests with pipeline covers
Sheet 6 Fit Critical scour method - Hallermeijer

		u = u0					u = uc					u = u_hc				
Test nr	ln(Phi)	ln(Psi_BK)	ln(Psi_GM)	ln(Psi_F)	ln(Theta)	ln(Mor)	ln(Psi_BK)	ln(Psi_GM)	ln(Psi_F)	ln(Theta)	ln(Mor)	ln(Psi_BK)	ln(Psi_GM)	ln(Psi_F)	ln(Theta)	ln(Mor)
W 1	-6,55	-4,49	-4,76	-6,54	-2,59	-1,21	-4,31	-4,64	-6,38	-2,41	-1,10	-3,79	-4,26	-5,88	-1,84	-0,73
W 2	-7,34	-4,49	-4,76	-6,54	-2,59	-1,21	-4,31	-4,64	-6,38	-2,41	-1,10	-3,79	-4,26	-5,88	-1,84	-0,73
W 3	-6,51	-3,68	-4,06	-5,51	-1,36	-0,51	-3,61	-3,98	-5,41	-1,26	-0,43	-3,34	-3,66	-5,00	-0,79	-0,09
W 4	-7,16	-3,68	-4,06	-5,51	-1,36	-0,51	-3,61	-3,98	-5,41	-1,26	-0,43	-3,34	-3,66	-5,00	-0,79	-0,09
W 5	-6,21	-3,32	-3,60	-4,86	-0,59	0,00	-3,28	-3,55	-4,80	-0,52	0,06	-3,02	-3,26	-4,44	-0,10	0,38
W 6	-7,15	-3,32	-3,60	-4,86	-0,59	0,00	-3,28	-3,55	-4,80	-0,52	0,06	-3,02	-3,26	-4,44	-0,10	0,38
W 7	-6,21	-3,33	-3,61	-4,87	-0,60	-0,01	-3,28	-3,56	-4,81	-0,53	0,05	-3,03	-3,27	-4,45	-0,12	0,37
W 8	-6,62	-3,33	-3,61	-4,87	-0,60	-0,01	-3,28	-3,56	-4,81	-0,53	0,05	-3,03	-3,27	-4,45	-0,12	0,37
W 9	-5,94	-3,13	-3,36	-4,52	-0,17	0,30	-3,09	-3,32	-4,47	-0,11	0,34	-2,84	-3,04	-4,13	0,28	0,66
W 10	-6,71	-3,13	-3,36	-4,52	-0,17	0,30	-3,09	-3,32	-4,47	-0,11	0,34	-2,84	-3,04	-4,13	0,28	0,66
W 11	-6,27	-3,14	-3,38	-4,54	-0,19	0,28	-3,10	-3,33	-4,48	-0,13	0,33	-2,85	-3,06	-4,15	0,26	0,65
W 12	-6,86	-3,14	-3,38	-4,54	-0,19	0,28	-3,10	-3,33	-4,48	-0,13	0,33	-2,85	-3,06	-4,15	0,26	0,65
W 13	-6,57	-3,87	-4,35	-6,00	-1,98	-0,81	-3,74	-4,21	-5,81	-1,77	-0,67	-3,40	-3,79	-5,28	-1,15	-0,25
W 14	-7,28	-3,41	-3,75	-5,12	-0,92	-0,18	-3,34	-3,66	-5,00	-0,79	-0,09	-3,01	-3,29	-4,54	-0,26	0,32
W 15	-7,38	-3,41	-3,75	-5,12	-0,92	-0,18	-3,34	-3,66	-5,00	-0,79	-0,09	-3,01	-3,29	-4,54	-0,26	0,32
W 18	-4,15	-4,11	-4,47	-5,90	-1,75	-0,92	-4,00	-4,35	-5,75	-1,57	-0,79	-3,66	-3,96	-5,25	-1,00	-0,37
W 19	-4,78	-4,11	-4,47	-5,90	-1,75	-0,92	-4,00	-4,35	-5,75	-1,57	-0,79	-3,66	-3,96	-5,25	-1,00	-0,37
W 20	-4,33	-3,49	-3,72	-4,88	-0,52	-0,06	-3,42	-3,65	-4,78	-0,41	0,03	-3,11	-3,31	-4,37	0,06	0,42
W 21	-4,65	-3,49	-3,72	-4,88	-0,52	-0,06	-3,42	-3,65	-4,78	-0,41	0,03	-3,11	-3,31	-4,37	0,06	0,42
W 22	-2,79	-3,06	-3,23	-4,22	0,27	0,56	-3,01	-3,23	-4,16	0,34	0,63	-2,73	-2,91	-3,80	0,75	0,99
W 23	-3,34	-3,06	-3,23	-4,22	0,27	0,56	-3,01	-3,23	-4,16	0,34	0,63	-2,73	-2,91	-3,80	0,75	0,99
W 26	-6,48	-3,24	-3,48	-4,65	-0,32	0,17	-3,23	-3,48	-4,65	-0,31	0,17	-3,15	-3,38	-4,53	-0,18	0,28
W 27		-3,38	-3,71	-5,07	-0,87	-0,14	-3,36	-3,69	-5,05	-0,84	-0,12	-3,21	-3,52	-4,83	-0,60	0,06
W 28	-9,09	-3,41	-3,74	-5,11	-0,91	-0,18	-3,39	-3,72	-5,09	-0,89	-0,16	-3,24	-3,56	-4,88	-0,65	0,02
W 29	-7,75	-3,42	-3,75	-5,13	-0,93	-0,19	-3,40	-3,74	-5,11	-0,91	-0,17	-3,26	-3,57	-4,90	-0,67	0,00
W 30	-8,87	-3,64	-4,04	-5,54	-1,42	-0,50	-3,57	-3,96	-5,43	-1,30	-0,42	-3,29	-3,63	-5,01	-0,82	-0,07
W 32	-5,94	-2,84	-3,01	-4,02	0,45	0,76	-2,84	-3,01	-4,02	0,46	0,77	-2,76	-2,93	-3,91	0,57	0,87
W 33	-7,38	-3,00	-3,24	-4,40	-0,05	0,42	-2,99	-3,22	-4,38	-0,03	0,43	-2,86	-3,08	-4,20	0,17	0,60
W 34	-7,54	-3,04	-3,27	-4,42	-0,06	0,39	-3,03	-3,26	-4,40	-0,04	0,41	-2,90	-3,12	-4,23	0,15	0,57
W 35	-7,26	-3,07	-3,31	-4,49	-0,16	0,33	-3,06	-3,30	-4,48	-0,14	0,34	-2,94	-3,17	-4,32	0,04	0,49
W 36		-3,28	-3,56	-4,82	-0,55	0,04	-3,24	-3,51	-4,76	-0,48	0,10	-2,98	-3,23	-4,41	-0,07	0,42
W 38	-5,34	-2,62	-2,79	-3,68	0,87	1,10	-2,61	-2,79	-3,68	0,87	1,11	-2,55	-2,72	-3,59	0,97	1,20
W 40	-7,46	-2,86	-3,06	-4,14	0,28	0,65	-2,85	-3,05	-4,12	0,29	0,67	-2,72	-2,91	-3,96	0,47	0,82
W 41	-5,91	-2,90	-3,11	-4,20	0,21	0,60	-2,89	-3,10	-4,18	0,22	0,61	-2,77	-2,96	-4,02	0,41	0,77
W 44	-6,64	-3,19	-3,40	-4,50	-0,10	0,30	-3,19	-3,40	-4,49	-0,10	0,30	-3,12	-3,32	-4,40	0,00	0,39
W 45	-7,32	-3,04	-3,23	-4,29	0,13	0,49	-3,02	-3,22	-4,28	0,15	0,51	-2,89	-3,07	-4,10	0,36	0,69
W 46	-5,23	-3,21	-3,41	-4,50	-0,10	0,29	-3,20	-3,40	-4,49	-0,09	0,30	-3,07	-3,26	-4,32	0,11	0,47
W 47	-8,22	-3,37	-3,65	-4,91	-0,64	-0,05	-3,36	-3,64	-4,90	-0,62	-0,04	-3,24	-3,51	-4,73	-0,43	0,11
W 48	-6,43	-3,42	-3,68	-4,90	-0,60	-0,06	-3,37	-3,63	-4,84	-0,53	0,00	-3,13	-3,36	-4,50	-0,14	0,31
W 49	-5,94	-3,72	-4,09	-5,52	-1,37	-0,54	-3,55	-3,89	-5,27	-1,09	-0,33	-3,14	-3,42	-4,68	-0,40	0,19
W 50	-7,12	-3,16	-3,37	-4,45	-0,04	0,35	-3,16	-3,36	-4,44	-0,03	0,35	-3,10	-3,29	-4,36	0,07	0,43
W 51	-7,10	-3,04	-3,23	-4,29	0,13	0,49	-3,02	-3,22	-4,28	0,15	0,51	-2,89	-3,07	-4,10	0,36	0,69
W 52	-5,69	-3,20	-3,41	-4,50	-0,10	0,29	-3,19	-3,40	-4,49	-0,09	0,30	-3,06	-3,26	-4,32	0,11	0,47
W 53	-8,10	-3,37	-3,66	-4,92	-0,65	-0,06	-3,37	-3,65	-4,91	-0,63	-0,04	-3,25	-3,51	-4,74	-0,44	0,10
W 54	-7,12	-3,41	-3,67	-4,89	-0,58	-0,05	-3,36	-3,62	-4,82	-0,51	0,01	-3,12	-3,35	-4,49	-0,12	0,32
W 55	-6,37	-3,71	-4,08	-5,52	-1,36	-0,53	-3,54	-3,89	-5,27	-1,08	-0,32	-3,13	-3,41	-4,67	-0,39	0,19
W 56	-4,43	-2,82	-3,02	-3,94	0,57	0,84	-2,82	-3,02	-3,93	0,58	0,85	-2,74	-2,94	-3,83	0,69	0,95
W 57	-4,43	-2,65	-2,84	-3,73	0,81	1,06	-2,65	-2,83	-3,72	0,82	1,07	-2,52	-2,69	-3,56	1,01	1,23
W 58	-3,94	-2,86	-3,06	-3,99	0,51	0,79	-2,85	-3,06	-3,98	0,52	0,80	-2,73	-2,92	-3,82	0,71	0,96
W 59	-5,11	-3,05	-3,26	-4,38	0,01	0,42	-3,04	-3,25	-4,36	0,02	0,44	-2,92	-3,12	-4,20	0,21	0,59
W 60	-5,42	-3,05	-3,24	-4,30	0,13	0,49	-3,02	-3,21	-4,26	0,18	0,53	-2,80	-2,97	-3,97	0,50	0,81
W 61	-4,50	-3,34	-3,59	-4,78	-0,45	0,05	-3,24	-3,48	-4,64	-0,30	0,17	-2,86	-3,06	-4,14	0,28	0,65
W 62	-5,00	-2,82	-3,02	-3,93	0,58	0,85	-2,81	-3,01	-3,93	0,58	0,85	-2,73	-2,93	-3,83	0,69	0,95
W 63	-4,43	-2,66	-2,84	-3,73	0,81	1,05	-2,65	-2,83	-3,72	0,82	1,06	-2,52	-2,69	-3,56	1,01	1,23
W 64	-4,23	-2,83	-3,04	-3,94	0,57	0,84	-2,83	-3,03	-3,93	0,58	0,85	-2,71	-2,90	-3,79	0,75	1,00
W 65	-5,73	-3,05	-3,27	-4,38	0,00	0,42	-3,04	-3,26	-4,37	0,01	0,43	-2,92	-3,13	-4,21	0,20	0,58
W 66	-5,88	-3,05	-3,25	-4,30	0,13	0,49	-3,02	-3,21	-4,26	0,18	0,53	-2,80	-2,98	-3,98	0,50	0,80
W 67	-4,41	-3,33	-3,58	-4,77	-0,45	0,05	-3,24	-3,48	-4,64	-0,30	0,18	-2,86	-3,06	-4,13	0,28	0,66
W 68	-4,92	-3,18	-3,37	-4,41	0,03	0,38	-3,18	-3,37	-4,40	0,04	0,38	-3,11	-3,29	-4,31	0,14	0,47
W 69	-4,61	-3,03	-3,20	-4,21	0,26	0,57	-3,02	-3,20	-4,20	0,27	0,58	-2,91	-3,12	-4,06	0,43	0,72
W 70	-4,54	-3,22	-3,41	-4,46	-0,02	0,33	-3,21	-3,40	-4,45	-0,01	0,34	-3,10	-3,28	-4,30	0,15	0,48
W 71	-5,63	-3,38	-3,64	-4,85	-0,54	-0,01	-3,37	-3,63	-4,84	-0,53	-0,01	-3,26	-3,51	-4,69	-0,35	0,14
W 72		-3,41	-3,64	-4,79	-0,44	0,02	-3,38	-3,61	-4,75	-0,40	0,06	-3,18	-3,39	-4,48	-0,08	0,31
W 73	-5,97	-3,65	-3,97	-5,31	-1,09	-0,40	-3,54	-3,85	-5,16	-0,92	-0,27	-3,20	-3,45	-4,66	-0,35	0,17
W 74	-5,61	-3,17	-3,36	-4,40	0,05	0,39	-3,17	-3,36	-4,39	0,05	0,39	-3,10	-3,28	-4,30	0,15	0,48
W 75	-5,20	-3,03	-3,20	-4,20	0,27	0,58	-3,02	-3,19	-4,20	0,28	0,59	-2,91	-3,11	-4,05	0,44	0,73
W 76	-5,18	-3,22	-3,41	-4,46	-0,02	0,33	-3,21	-3,40	-4,45	-0,01	0,34	-3,10	-3,28	-4,30	0,15	0,48
W 77	-6,07	-3,39	-3,65	-4,87	-0,56	-0,03	-3,38	-3,64	-4,86	-0,55	-0,02	-3,27	-3,52	-4,70	-0,37	0,12
W 78	-7,15	-3,40	-3,63	-4,78	-0,43	0,03	-3,37	-3,60	-4,74	-0,38	0,07	-3,17	-3,37	-4,47	-0,07	0,33
W 79	-6,66	-3,63	-3,95	-5,29	-1,06	-0,38	-3,53	-3,83	-5,14	-0,89	-0,25	-3,18	-3,44	-4,64	-0,33	0,19
W 80	-4,13	-2,63	-2,77	-3,58	1,04	1,22	-2,62	-2,77	-3,58	1,05	1,23	-2,55	-2,69	-3,48	1,15	1,32
W 82	-3,51	-2,69	-2,84	-3,65	0,96	1,15	-2,68	-2,82	-3,65	0,97	1,15	-2,56	-2,70	-3,50	1,14	1,31
W 83	-3,86	-2,67	-2,81	-3,62	1,01	1,19	-2,66	-2,80	-3,61	1,02	1,19	-2,55	-2,69	-3,47	1,18	1,34
W 86	-4,55	-2,67	-2,84	-3,68	0,90	1,11	-2,67	-2,84	-3,68	0,90	1,11	-2,62	-2,78	-3,62	0,98	1,18

Fit of a transport equation to model tests with pipeline covers
Sheet 6 Fit Critical scour method - Hallermeijer (continued)

		u = u0					u = uc					u = u_hc				
Test nr	ln(Phi)	ln(Psi_BK)	ln(Psi_GM)	ln(Psi_F)	ln(Theta)	ln(Mor)	ln(Psi_BK)	ln(Psi_GM)	ln(Psi_F)	ln(Theta)	ln(Mor)	ln(Psi_BK)	ln(Psi_GM)	ln(Psi_F)	ln(Theta)	ln(Mor)
W 87	-3,26	-2,52	-2,67	-3,49	1,12	1,31	-2,51	-2,66	-3,48	1,13	1,32	-2,40	-2,55	-3,35	1,28	1,46
W 88	-3,51	-2,73	-2,89	-3,75	0,83	1,04	-2,72	-2,89	-3,74	0,83	1,05	-2,62	-2,78	-3,62	0,98	1,18
W 89	-3,60	-2,70	-2,87	-3,72	0,86	1,07	-2,70	-2,86	-3,71	0,86	1,08	-2,60	-2,76	-3,59	1,01	1,20
W 90	-4,31	-2,91	-3,11	-4,02	0,49	0,76	-2,89	-3,09	-3,99	0,52	0,79	-2,69	-2,87	-3,74	0,81	1,04
W 92	-5,07	-2,60	-2,79	-3,66	0,88	1,12	-2,60	-2,79	-3,66	0,89	1,12	-2,53	-2,71	-3,57	0,99	1,21
W 94	-4,02	-2,66	-2,86	-3,74	0,80	1,04	-2,66	-2,84	-3,73	0,81	1,05	-2,53	-2,71	-3,57	0,99	1,22
W 95	-3,83	-2,68	-2,87	-3,77	0,77	1,02	-2,68	-2,87	-3,75	0,78	1,03	-2,55	-2,73	-3,59	0,97	1,20
W 96	-4,32	-2,76	-2,94	-3,84	0,70	0,95	-2,75	-2,94	-3,82	0,71	0,96	-2,63	-2,80	-3,67	0,89	1,11
W 97	-5,32	-2,76	-2,94	-3,84	0,70	0,95	-2,75	-2,94	-3,82	0,71	0,96	-2,63	-2,80	-3,67	0,89	1,11
W 100	-4,42	-2,64	-2,81	-3,69	0,86	1,10	-2,64	-2,81	-3,68	0,87	1,10	-2,54	-2,71	-3,56	1,01	1,23
W 101	-5,40	-2,64	-2,81	-3,69	0,86	1,10	-2,64	-2,81	-3,68	0,87	1,10	-2,54	-2,71	-3,56	1,01	1,23
W 102	-6,04	-2,64	-2,81	-3,69	0,86	1,10	-2,64	-2,81	-3,68	0,87	1,10	-2,54	-2,71	-3,56	1,01	1,23
W 103	-3,88	-2,64	-2,81	-3,69	0,86	1,10	-2,64	-2,81	-3,68	0,87	1,10	-2,53	-2,70	-3,55	1,03	1,24
W 104	-4,76	-2,64	-2,81	-3,69	0,86	1,10	-2,64	-2,81	-3,68	0,87	1,10	-2,53	-2,70	-3,55	1,03	1,24
W 105	-5,47	-2,64	-2,81	-3,69	0,86	1,10	-2,64	-2,81	-3,68	0,87	1,10	-2,53	-2,70	-3,55	1,03	1,24
W 106	-3,35	-2,64	-2,81	-3,69	0,86	1,10	-2,63	-2,80	-3,68	0,88	1,11	-2,49	-2,67	-3,51	1,08	1,29
W 107	-4,34	-2,64	-2,81	-3,69	0,86	1,10	-2,63	-2,80	-3,68	0,88	1,11	-2,49	-2,67	-3,51	1,08	1,29
W 108	-5,00	-2,64	-2,81	-3,69	0,86	1,10	-2,63	-2,80	-3,68	0,88	1,11	-2,49	-2,67	-3,51	1,08	1,29
W 109	-3,44	-2,64	-2,81	-3,69	0,86	1,10	-2,63	-2,81	-3,68	0,88	1,11	-2,50	-2,68	-3,52	1,06	1,27
W 110	-4,48	-2,64	-2,81	-3,69	0,86	1,10	-2,63	-2,81	-3,68	0,88	1,11	-2,50	-2,68	-3,52	1,06	1,27
W 111	-5,10	-2,64	-2,81	-3,69	0,86	1,10	-2,63	-2,81	-3,68	0,88	1,11	-2,50	-2,68	-3,52	1,06	1,27
W 112	-4,67	-2,74	-2,94	-3,85	0,67	0,93	-2,74	-2,94	-3,84	0,67	0,94	-2,64	-2,83	-3,72	0,82	1,07
W 113	-5,63	-2,74	-2,94	-3,85	0,67	0,93	-2,74	-2,94	-3,84	0,67	0,94	-2,64	-2,83	-3,72	0,82	1,07
W 114	-6,22	-2,74	-2,94	-3,85	0,67	0,93	-2,74	-2,94	-3,84	0,67	0,94	-2,64	-2,83	-3,72	0,82	1,07
W 115	-3,96	-2,74	-2,94	-3,85	0,67	0,93	-2,73	-2,93	-3,84	0,68	0,94	-2,59	-2,77	-3,65	0,89	1,13
W 116	-4,81	-2,74	-2,94	-3,85	0,67	0,93	-2,73	-2,93	-3,84	0,68	0,94	-2,59	-2,77	-3,65	0,89	1,13
W 117	-5,34	-2,74	-2,94	-3,85	0,67	0,93	-2,73	-2,93	-3,84	0,68	0,94	-2,59	-2,77	-3,65	0,89	1,13
W 121	-4,85	-2,80	-3,00	-3,92	0,59	0,86	-2,79	-3,00	-3,91	0,59	0,87	-2,69	-2,89	-3,79	0,74	0,99
W 122	-5,83	-2,80	-3,00	-3,92	0,59	0,86	-2,79	-3,00	-3,91	0,59	0,87	-2,69	-2,89	-3,79	0,74	0,99
W 123	-6,47	-2,80	-3,00	-3,92	0,59	0,86	-2,79	-3,00	-3,91	0,59	0,87	-2,69	-2,89	-3,79	0,74	0,99
W 124	-4,17	-2,80	-3,00	-3,92	0,59	0,86	-2,79	-2,99	-3,91	0,60	0,87	-2,67	-2,86	-3,76	0,77	1,03
W 125	-5,20	-2,80	-3,00	-3,92	0,59	0,86	-2,79	-2,99	-3,91	0,60	0,87	-2,67	-2,86	-3,76	0,77	1,03
W 126	-5,81	-2,80	-3,00	-3,92	0,59	0,86	-2,79	-2,99	-3,91	0,60	0,87	-2,67	-2,86	-3,76	0,77	1,03
W 127	-4,01	-2,80	-3,00	-3,92	0,59	0,86	-2,79	-2,99	-3,91	0,60	0,87	-2,64	-2,83	-3,72	0,81	1,06
W 128	-5,02	-2,80	-3,00	-3,92	0,59	0,86	-2,79	-2,99	-3,91	0,60	0,87	-2,64	-2,83	-3,72	0,81	1,06
W 129	-5,53	-2,80	-3,00	-3,92	0,59	0,86	-2,79	-2,99	-3,91	0,60	0,87	-2,64	-2,83	-3,72	0,81	1,06
W 130	-4,87	-2,88	-3,10	-4,04	0,45	0,74	-2,88	-3,09	-4,03	0,46	0,75	-2,77	-2,97	-3,89	0,62	0,89
W 131	-5,97	-2,88	-3,10	-4,04	0,45	0,74	-2,88	-3,09	-4,03	0,46	0,75	-2,77	-2,97	-3,89	0,62	0,89
W 132	-6,58	-2,88	-3,10	-4,04	0,45	0,74	-2,88	-3,09	-4,03	0,46	0,75	-2,77	-2,97	-3,89	0,62	0,89
W 133	-6,78	-2,88	-3,10	-4,04	0,45	0,74	-2,87	-3,08	-4,02	0,47	0,76	-2,74	-2,95	-3,86	0,66	0,93
W 134	-5,19	-2,88	-3,10	-4,04	0,45	0,74	-2,87	-3,08	-4,02	0,47	0,76	-2,74	-2,95	-3,86	0,66	0,93
W 135	-5,88	-2,88	-3,10	-4,04	0,45	0,74	-2,87	-3,08	-4,02	0,47	0,76	-2,74	-2,95	-3,86	0,66	0,93
W 136	-4,00	-2,88	-3,10	-4,04	0,45	0,74	-2,87	-3,08	-4,02	0,47	0,76	-2,72	-2,92	-3,83	0,69	0,95
W 137	-5,04	-2,88	-3,10	-4,04	0,45	0,74	-2,87	-3,08	-4,02	0,47	0,76	-2,72	-2,92	-3,83	0,69	0,95
W 138	-5,74	-2,88	-3,10	-4,04	0,45	0,74	-2,87	-3,08	-4,02	0,47	0,76	-2,72	-2,92	-3,83	0,69	0,95
	a	0,51	0,50	0,45	0,00	0,00	0,90	0,80	0,71	0,00	0,00	3,76	2,65	2,08	0,00	0,00
	b	1,59	1,47	1,09	0,92	1,26	1,79	1,63	1,20	1,01	1,37	2,40	2,12	1,53	1,27	1,70
	rsq	**0,23**	**0,26**	**0,30**	**0,32**	**0,31**	**0,25**	**0,27**	**0,32**	**0,34**	**0,33**	**0,30**	**0,32**	**0,37**	**0,39**	**0,38**

Categorisation of data Lomonaco (1994) on qualitative damage
Sheet 1

Test nr	Bc	dn50	S	S*	damage category
-	m	m	-	-	-
W 26	0,06	3,65E-03	60,44	3,67	2
W 27	0,12	6,12E-03	4,53	0,23	1
W 28	0,12	6,12E-03	20,01	1,02	1
W 29	0,12	6,12E-03	41,45	2,12	2
W 30	0,25	8,33E-03	4,05	0,13	1
W 32	0,06	3,65E-03	31,99	1,94	2
W 33	0,12	6,12E-03	8,93	0,46	1
W 34	0,12	6,12E-03	8,26	0,42	1
W 35	0,12	6,12E-03	28,77	1,47	2
W 36	0,25	8,33E-03	10,18	0,34	1
W 38	0,06	3,65E-03	39,13	2,38	2
W 40	0,12	6,12E-03	10,63	0,54	1
W 41	0,12	6,12E-03	48,28	2,46	3
W 44	0,06	3,65E-03	12,28	0,75	1
W 45	0,12	3,65E-03	24,52	0,74	1
W 46	0,12	3,65E-03	46,17	1,40	2
W 47	0,12	6,12E-03	15,00	0,77	1
W 48	0,25	5,13E-03	21,35	0,44	1
W 49	0,25	8,33E-03	14,52	0,48	1
W 50	0,06	3,65E-03	16,79	1,02	1
W 51	0,12	3,65E-03	37,64	1,14	1
W 52	0,12	3,65E-03	62,08	1,89	2
W 53	0,12	6,12E-03	21,23	1,08	1
W 54	0,25	5,13E-03	33,45	0,69	1
W 55	0,25	8,33E-03	24,90	0,83	1
W 56	0,06	3,65E-03	75,04	4,56	3
W 57	0,12	3,65E-03	77,56	2,36	2
W 58	0,12	3,65E-03	140,38	4,26	3
W 59	0,12	6,12E-03	69,32	3,54	3
W 60	0,25	5,13E-03	46,02	0,94	2
W 61	0,25	8,33E-03	76,95	2,56	2
W 62	0,06	3,65E-03	97,71	5,94	2
W 63	0,12	3,65E-03	128,66	3,91	2
W 64	0,12	3,65E-03	215,94	6,56	2
W 65	0,12	6,12E-03	76,14	3,89	2
W 66	0,25	5,13E-03	73,74	1,51	2
W 67	0,25	8,33E-03	119,33	3,98	2
W 68	0,06	3,65E-03	47,96	2,91	2
W 69	0,12	3,65E-03	80,00	2,43	2
W 70	0,12	3,65E-03	85,88	2,61	2
W 71	0,12	6,12E-03	56,96	2,91	3
W 72	0,25	5,13E-03	50,64	1,04	1
W 73	0,25	8,33E-03	39,15	1,30	2
W 74	0,06	3,65E-03	54,52	3,31	2
W 75	0,12	3,65E-03	100,10	3,04	2
W 76	0,12	3,65E-03	104,96	3,19	2
W 77	0,12	6,12E-03	69,39	3,54	2
W 78	0,25	5,13E-03	66,16	1,36	1
W 79	0,25	8,33E-03	49,91	1,66	2
W 80	0,06	3,65E-03	92,11	5,60	3
W 82	0,12	3,65E-03	184,36	5,60	3
W 83	0,12	3,65E-03	209,44	6,36	3
W 86	0,06	3,65E-03	87,76	5,33	4
W 87	0,12	3,65E-03	199,30	6,05	3
W 88	0,12	3,65E-03	207,61	6,31	3
W 89	0,12	3,65E-03	227,15	6,90	4
W 90	0,25	5,13E-03	103,77	2,13	2
W 92	0,06	3,65E-03	51,64	3,14	2
W 94	0,12	3,65E-03	132,15	4,01	3
W 95	0,12	3,65E-03	203,95	6,19	3

Test nr	Bc	dn50	S	S*	damage category
-	m	m	-	-	-
WC 22	0,06	3,65E-03	56,03	3,40	2
WC 23	0,12	6,12E-03	6,28	0,32	1
WC 24	0,12	6,12E-03	5,44	0,28	1
WC 25	0,12	6,12E-03	34,99	1,79	2
WC 28	0,06	3,65E-03	83,81	5,09	4
WC 29	0,12	6,12E-03	10,10	0,52	1
WC 30	0,12	6,12E-03	9,64	0,49	1
WC 31	0,12	6,12E-03	38,32	1,96	2
WC 34	0,06	3,65E-03	37,96	2,31	2
WC 35	0,12	3,65E-03	73,47	2,23	2
WC 36	0,12	3,65E-03	53,52	1,63	2
WC 37	0,12	6,12E-03	40,30	2,06	2
WC 38	0,25	5,13E-03	49,72	1,02	1
WC 39	0,25	8,33E-03	37,53	1,25	1
WC 40	0,06	3,65E-03	81,62	4,96	4
WC 41	0,12	3,65E-03	137,69	4,18	2
WC 42	0,12	3,65E-03	116,58	3,54	2
WC 43	0,12	3,65E-03	178,40	5,42	4
WC 44	0,25	5,13E-03	60,15	1,23	2

Table A8.1 - Summary of fit results for S and $\hat{u}_0$, expressed as (adjusted) r^2 [in ‰].
Lomónaco – Van Gent and Wallast – Saers data set
Velocity at the bed in front of the structure ($\hat{u}_0$)

Model includes			Stability parameters				
			θ	Θ	Ψ_{BK}	Ψ_{GM}	Ψ_F
N, m_0			479	428	378	411	458
N, m_0	B_c/L		479	428	378	411	458
N, m_0	B_c/a_0		479	428	378	411	458
N, m_0	B/L		479	428	378	411	458
N, m_0	B/a_0		479	428	378	411	458
N, m_0		B_c/d_{n50}	***611***	***581***	***501***	***531***	***591***
N, m_0		h_c/h	479	428	378	411	458
N, m_0	other combinations		nt	nt	nt	nt	nt
N, Sa			479	428	378	411	458
N, Sa	B_c/L		479	428	378	411	458
N, Sa	B_c/a_0		479	428	378	411	458
N, Sa	B/L		479	428	378	411	458
N, Sa	B/a_0		479	428	378	411	458
N, Sa		B_c/d_{n50}	592	566	501	531	575
N, Sa		h_c/h	479	428	378	411	458
N, Sa	other combinations		nt	nt	nt	nt	nt

remarks nt: not tested
best fit per model in ***italics***

Table A8.2 - Summary of fit results for S, expressed as (adjusted) r^2 [in ‰].
Lomónaco – Van Gent and Wallast – Saers data set
Undisturbed velocity at the level of the crest of the structure ($\hat{u}_c$)

Model includes			Stability parameters				
			θ	Θ	Ψ_{BK}	Ψ_{GM}	Ψ_F
N, m_0			488	434	382	414	467
N, m_0	B_c/L		488	434	382	414	467
N, m_0	B_c/a_0		488	434	382	414	467
N, m_0	B/L		488	434	382	414	467
N, m_0	B/a_0		488	434	382	414	467
N, m_0		B_c/d_{n50}	***623***	***589***	***519***	***548***	***602***
N, m_0		h_c/h	488	434	382	414	467
N, m_0	other combinations		nt	nt	nt	nt	nt
N, Sa			488	434	382	414	467
N, Sa	B_c/L		488	434	382	414	467
N, Sa	B_c/a_0		488	434	382	414	467
N, Sa	B/L		488	434	382	414	467
N, Sa	B/a_0		488	434	382	414	467
N, Sa		B_c/d_{n50}	600	570	507	534	582
N, Sa		h_c/h	488	434	382	414	467
N, Sa	other combinations		nt	nt	nt	nt	nt

remarks nt: not tested
best fit per model in ***italics***

Table A8.3 - Summary of fit results for S, expressed as (adjusted) r^2 [in ‰].
Lomónaco – Van Gent and Wallast – Saers data set
Velocity at the crest of the structure ($\hat{u}_{hc}$)

Model includes				Stability parameters				
				θ	Θ	Ψ_{BK}	Ψ_{GM}	Ψ_F
N, m_0				488	427	360	395	462
N, m_0	B_c/L			488	427	360	395	462
N, m_0	B_c/a_0			488	427	360	395	462
N, m_0	B/L			488	427	360	395	462
N, m_0	B/a_0			488	427	360	395	462
N, m_0		B_c/d_{n50}		616	568	488	513	589
N, m_0			h_c/h	503	461	414	437	484
N, m_0		B_c/d_{n50}	h_c/h	***635***	***608***	***548***	***557***	***616***
N, m_0	other combinations			nt	nt	nt	nt	nt
N, Sa				488	427	360	395	462
N, Sa	B_c/L			488	427	360	395	462
N, Sa	B_c/a_0			488	427	360	395	462
N, Sa	B/L			488	427	360	395	462
N, Sa	B/a_0			488	427	360	395	462
N, Sa		B_c/d_{n50}		568	567	451	475	544
N, Sa			h_c/h	503	468	414	437	484
N, Sa		B_c/d_{n50}	h_c/h	613	592	548	557	598
N, Sa	other combinations			nt	nt	nt	nt	nt
remarks	nt: not tested							
	best fit per model in ***italics***							

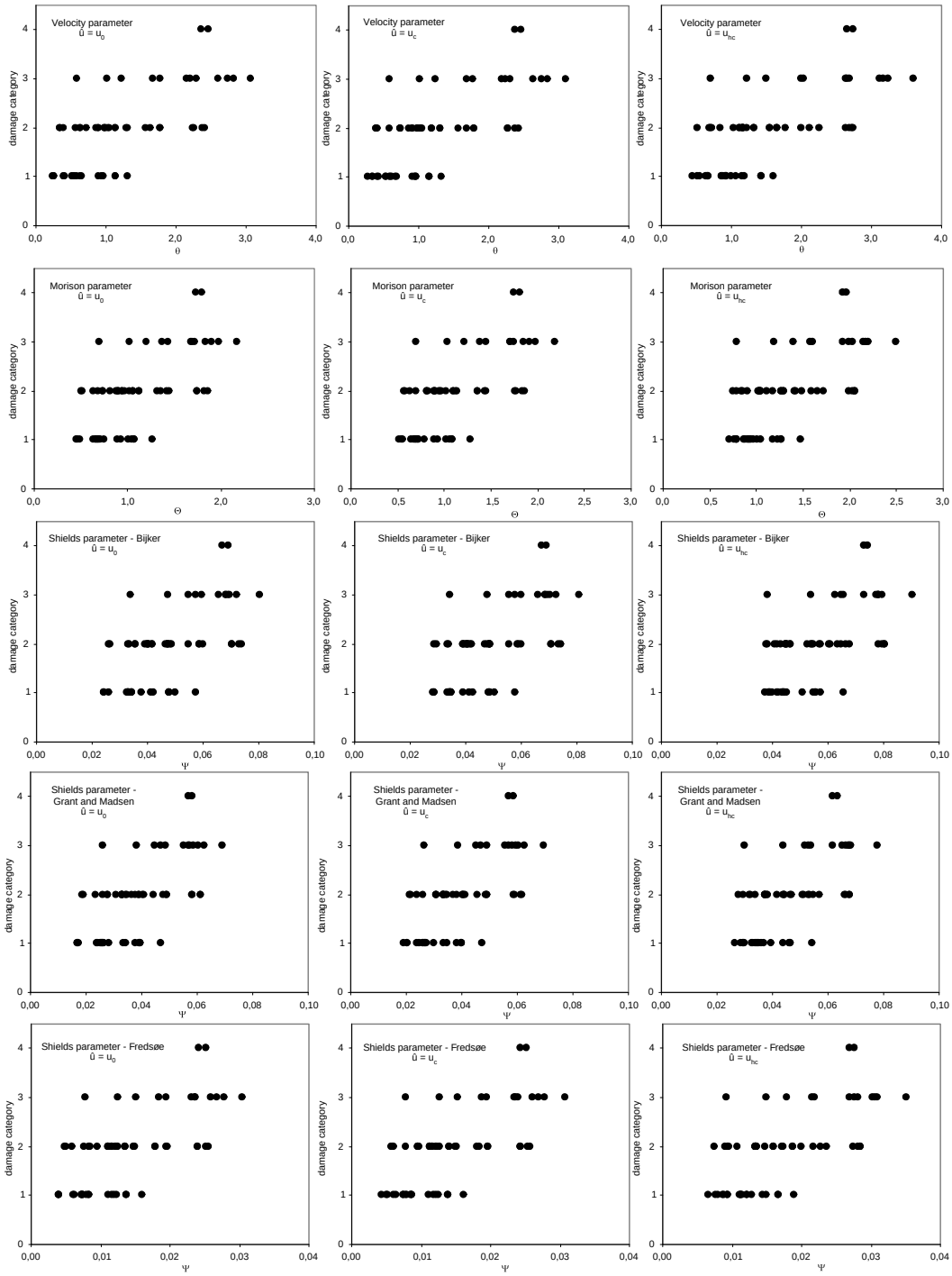

Figure A8.1 – Relationship between stability parameter and damage category for pipeline covers

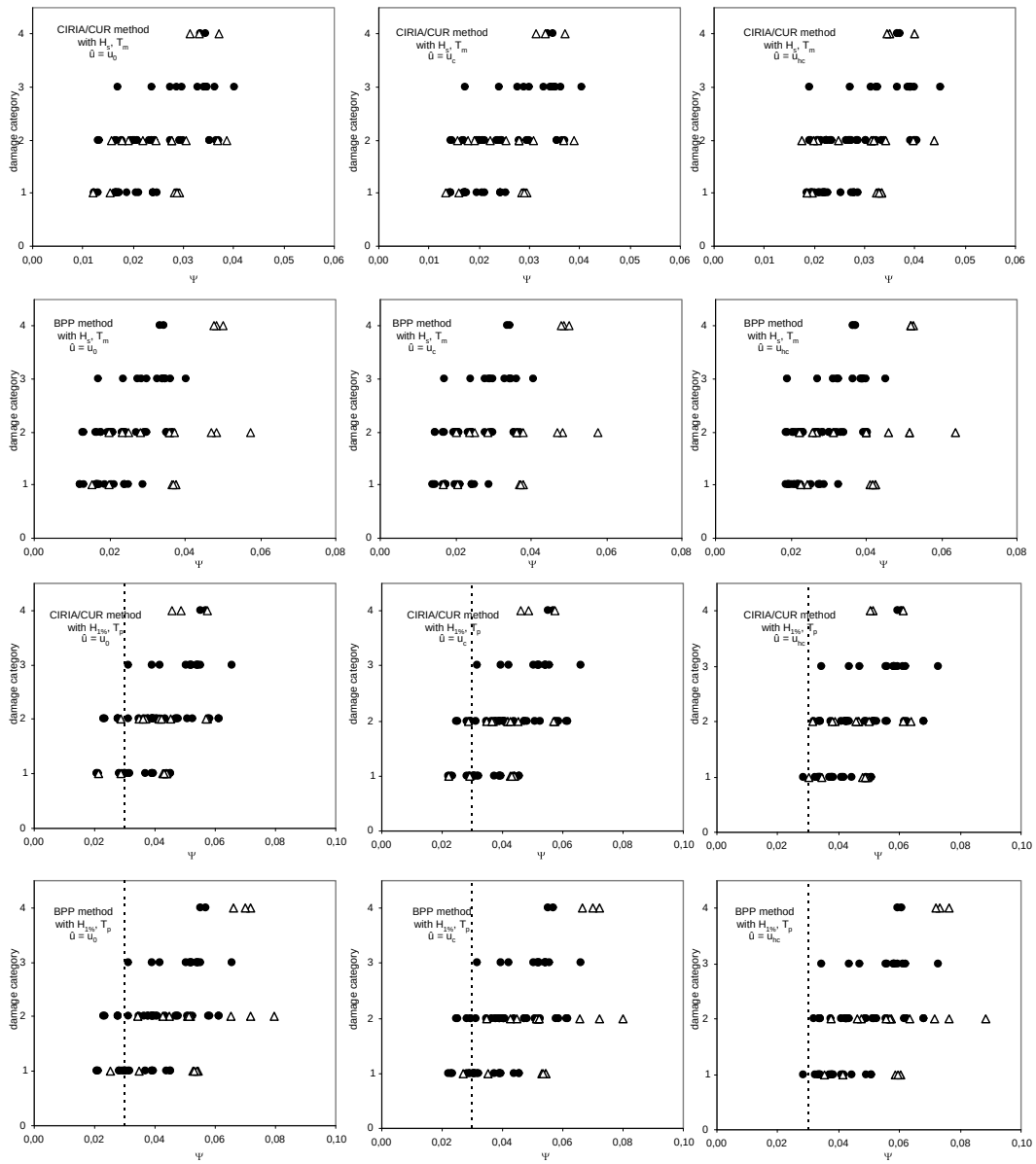

Figure A8.1 – Relationship between stability parameter and damage category for pipeline covers (continued)

Appendix 9 Case study: Santander outfall

A9.1 General data

After the construction of a sewer outfall off the North Spanish coast near Santander, the University of Cantabria took the opportunity to test the damage to this type of structure in prototype conditions. Three test sections were built on top of the original structure, using three different stone sizes (all smaller than the design stone size). The environmental conditions, in terms of wave height, period and flow velocities at the crest of the structure, were measured during a period of two years after the construction (September 1999 – August 2001), and the damage to the test sections was monitored with regular intervals. The results from these prototype tests, and an analysis of them, are reported by Vidal *et al* (2002) and Lomonaco *et al* (2005). In this appendix we will use their test

Figure A9.1 – Location of Santander outfall (British Admiralty Chart n^{o} 1105 – fragment)

data to validate the calculation methods used in this thesis; these calculations also serve as a calculation example.

The location of the test section is given in Figure A9.1. The original outfall consisted of a rubble mound with B_c = 3.0 m, m_0 = 2 and z_c = 4.0 m, with a 3 tonnes rock armour layer. The outfall is constructed on a gently sloping seabed with water depths ranging from h = 20 m to h = 21 m at the test sections. The test sections themselves are placed on top of the original structure, also with m_0 = 2, and the crest level was always placed at h_c = 15.0 m. This means that the layer thickness and consequently the crest width is different for each section; the principal dimensions of these sections are given in Figure A9.2.

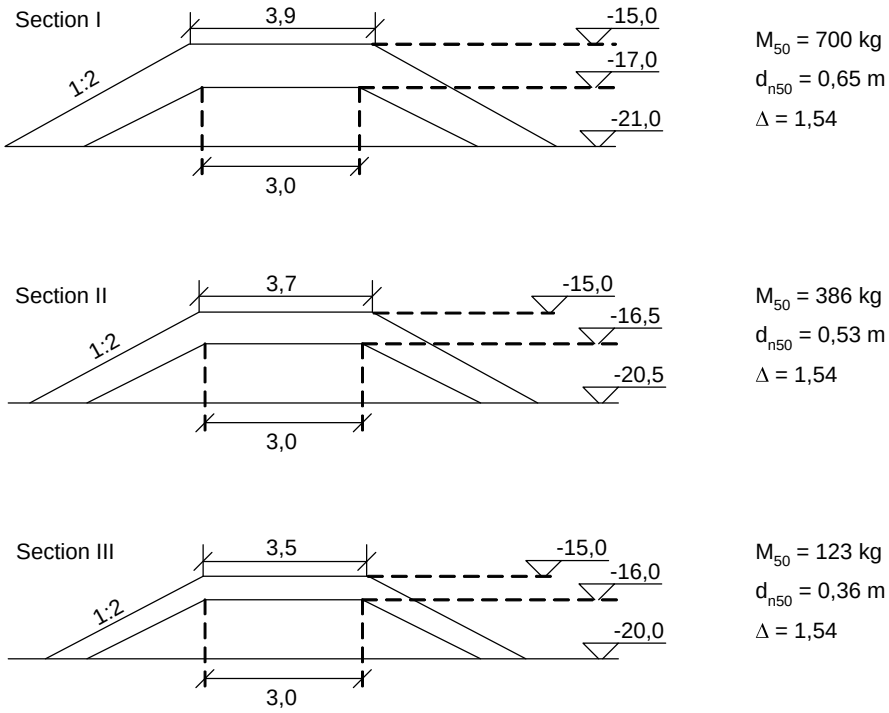

Figure A9.2 – Dimensions of test sections

Vidal *et al* (2002) describes the measured damage to the structure: section I suffered 'no appreciable damage' during the full test period; section II suffered 'important damage' ('wide areas in which the second layer of the armour was exposed') and section III was 'nearly destroyed'. The damage to sections II and III can be related to a single storm in November 2000. Also, section III suffered 'important damage' during an earlier period; the strongest storm during that period occurred in December 1999 – it will be assumed that this storm caused that damage. Vidal *et al* do not give very detailed quantitative

results, but from an accompanying graph in their article a rough estimate of the associated damage numbers S can be obtained. All required information is given in table A9.1.

Table A9.1 - Hydraulic conditions and damage for Santander outfall prototype measurements

Storm	H_s m	T_p s	Dur h	Damage to section I	Damage to section II	Damage to section III
November 2000	6.6	13.9	48	no damage	important damage S = 4 – 6	nearly destroyed S = 18 – 20
December 1999	5.9	14.2	27	(no damage)	(no damage)	important damage S = 3 – 5

In the following paragraphs we will test whether:

- the measured quantitative damage in terms of S can be predicted by the Van Gent and Wallast formula (eq 3.91) and by the new formula (eq 6.23);
- the damage predicted by these formulas can be related to the reported qualitative damage;
- the critical stability method could have been used to design this structure, using the storm of November 2000 as a design condition.
- the two damage-based design formulas could have been used to design this structure, using the storm of November 2000 as a design condition;

Using the observation that in the design conditions a stone with d_{n50} = 0.65 m was stable, and d_{n50} = 0.53 m was not, we will assume that a good design method should result in a stone diameter somewhere in that range (and probably closer to 0.65 m than to 0.53 m since this last stone size resulted in 'important damage'). This will be the basis for the last two tests.

Vidal *et al* only mention wave conditions in their article – they do not mention a current. For the sake of argument (and completeness of the calculation example) we will assume that there has been a current as well. This particular stretch of the north coast of Spain features strong tidal currents – according to the British Admiralty Pilot (n^o 22) up to 3 knots at spring tide. A tidal reconstruction (using the program TidePred and the harmonic constants for the port of Santander) shows that on 8 November 2001 (the day of the storm) the tide was halfway between neap and spring; we will therefore reduce the current velocity a little and assume u_{cur} = 2 kn = 1.0 m/s.

A9.2 Prediction of S

A9.2.1 Van Gent and Wallast formula

First we check the applicability of the formula in terms of current strength, so we need to check whether $X = \tau_c/(\tau_c + \tau_w) < 0.2$ (using $\rho_w = 1025$ kg/m^3, H_s, T_m, the average full water depth h = 20.5 m and a representative stone diameter $d_{n50} = 0.60$ m – the exact values do not really matter as this is only an order-of-magnitude estimate):

$\Rightarrow T_m = 0.8 \cdot T_p = 11.1$ s
$\Rightarrow \omega = 2\pi/T_m = 0.566$ rad/s
$\Rightarrow \omega^2 = gk \cdot \tanh(k \cdot h) \Rightarrow k = 0.0450$ rad/m (from iteration) $\Rightarrow L = 2\pi/k = 139.7$ m
$\Rightarrow \hat{u}_0 = \pi H_s/T_m \cdot (1/\sinh(k \cdot h)) = 1.77$ m/s (eq 2.29)
$\Rightarrow a_0 = \hat{u}_0/\omega = 3.12$ m
$\Rightarrow k_s = 2 \cdot d_{n50} = 1.20$ m
$\Rightarrow a_0/k_s = 2.60 \Rightarrow f_w = \exp(-6.0 + 5.2 \cdot (a_0/k_s)^{-0.19}) = 0.190 \Rightarrow \tau_w = \frac{1}{2} f_w \rho \hat{u}_0^2 = 304$ Pa
$\Rightarrow C = 18 \cdot \log(12 \cdot h/k_s) = 41.6$ m$^{1/2}$/s $\Rightarrow \tau_c = \rho(g/C^2) \cdot u_{cur}^2 = 5.8$ Pa
$\Rightarrow X = \tau_c/(\tau_c + \tau_w) = 0.02 << 0.2$ so the waves dominate (strongly) and the formula is valid.

The number of waves can be estimated as:

$\Rightarrow N = T_m \cdot$Duration = 15560 (this is quite large but simply follows from the extremely long duration of the storm – 48 hours!)

The Van Gent and Wallast formula uses $\hat{u}_{hc}$, H_s and T_m. Assuming a water depth equal to h_c everywhere gives (for section I):

$\Rightarrow \omega^2 = gk \cdot \tanh(k \cdot h_c) \Rightarrow k = 0.0509$ rad/m (from iteration) $\Rightarrow L = 2\pi/k = 123.6$ m
$\Rightarrow \hat{u}_{hc} = \pi H_s/T_m \cdot (1/\sinh(k \cdot h_c)) = 2.23$ m/s (eq 2.29)
$\Rightarrow \theta_{hc} = \hat{u}_{hc}^2/(g\Delta d_{n50}) = 0.51$ (eq 4.4)
$\Rightarrow S = 0.2 \cdot (\theta_{hc})^3 \cdot \sqrt{N} = 3.33$ (eq 3.91)
$\Rightarrow S^* = S \cdot (d_{n50}/B_c) = 0.55$ (eq 6.18)
$\Rightarrow A_e = S \cdot d_{n50}^2 = 1.39$ m^2 (eq 3.87)
$\Rightarrow \Delta z = (-B_c + \sqrt{(B_c^2 + 4 \cdot m_0 \cdot A_e)})/2m_0 = 0.31$ m (eq 6.6)
$\Rightarrow \Delta z/d_{n50} = 0.48$

Results for the other sections follow from similar calculations; these are given in table A9.2

Table A9.2 – Calculation results for Santander outfall
Van Gent and Wallast formula

Section	H_s	T_m	h_c	$\hat{u}_{hc}$	θ_{hc}	S	S*	$\Delta z/d_{n50}$
	m	s	m	m/s	-	-	-	-
I	6.6	11.1	15	2.23	0.51	3.33	0.55	0.48
II	6.6	11.1	15	2.23	0.62	6.03	0.86	0.72
III	6.6	11.1	15	2.23	0.91	18.9	1.96	1.49

A9.2.2 New design formula

The new formula uses $\hat{u}_{hc,}$ $H_{1\%}$ and T_p. We calculate $H_{1\%}$ using the full water depth h. Here, too, X = 0.02 << 0.2 so the formula is valid.

For section I, h = 21.0 m so we get:

$\Rightarrow H_{1\%} = H_s \cdot 1.52/(1+H_s/h)^{1/3} = 9.16$ m
$\Rightarrow \omega = 2\pi/T_p = 0.452$ rad/s
$\Rightarrow \omega^2 = gk\cdot\tanh(k\cdot h_c) \Rightarrow k = 0.0393$ rad/m (from iteration) $\Rightarrow L = 2\pi/k = 159.7$ m
$\Rightarrow \hat{u}_{hc\ 1\%} = \pi H_{1\%}/T_p \cdot (1/\sinh(k\cdot h_c)) = 3.31$ m/s
$\Rightarrow \theta_{hc\ 1\%} = (\hat{u}_{hc\ 1\%})^2/(g\Delta d_{n50}) = 1.13$
$\Rightarrow S^* = 0.048\cdot(\theta_{hc\ 1\%})^{1.6}\cdot N^{0.3}\cdot m_0^{-0.6} = 0.69$ (eq 6.23)
$\Rightarrow S = S^*\cdot(B_c/d_{n50}) = 4.18$
$\Rightarrow A_e = S\cdot d_{n50}^2 = 1.74$ m^2
$\Rightarrow \Delta z = (-B_c + \sqrt{(B_c^2+4\cdot m_0\cdot A_e)})/2m_0 = 0.38$ m
$\Rightarrow \Delta z/d_{n50} = 0.58$

Results for the other sections follow from similar calculations and are given in table A9.3

Table A9.3 – Calculation results for Santander outfall
New design formula

Section	$H_{1\%}$	T_p	h_c	$\hat{u}_{hc\ 1\%}$	$\theta_{hc\ 1\%}$	S*	S	$\Delta z/d_{n50}$
	m	s	m	m/s	-	-	-	-
I	9.16	13.9	15	3.31	1.13	0.69	4.18	0.58
II	9.14	13.9	15	3.31	1.37	0.95	6.65	0.78
III	9.12	13.9	15	3.30	2.00	1.73	16.8	1.35

A9.2.3 Relation with reported damage

In quantitative terms, we see that both the Van Gent and Wallast formula and the new formula predict values of S for section II and III that are close to the reported damages. Other quantitative results, for instance in terms of $\Delta z/d_{n50}$ can not be compared as these values are not given by Vidal *et al* However, if we try to relate the values of S* for these sections to the reported qualitative damage we see that the values are too low: according to table 6.4 we should have had S* > 2.5 for section II ('important damage') and S* > 4.5 for section III ('destroyed'). Perhaps the values given in table 6.4 are too low – we must keep in mind that they originate from a visual assessment of *drawings of* damaged structures, not from a direct assessment of the structures themselves.

We can also try to relate the calculated crest reductions ($\Delta z/d_{n50}$) to the reported damage. From Figure A9.2 we see that all test sections have a thickness of roughly 3 times d_{n50}. The maximum calculated crest reduction is roughly 1.5 times d_{n50}, so only half the layer thickness; though it is reported that this layer was 'nearly destroyed'. Of course the calculated crest reduction is only an average value, and the real damage could well be much higher locally. Still, a difference of a factor 2 is quite large and makes this method not very reliable to use in practice. In general, we conclude that perhaps there is room for improvement (by means of a separate research) of the relation between S* (or $\Delta z/d_{n50}$) and damage.

A9.3 Design with critical stability approach

As discussed before, it seems that the required stone diameter for this structure is in the order d_{n50} = 0.60 m. It is interesting to see whether we would have found this diameter with the critical stability approach. First we study the situation without a current, then we study the situation with the (assumed) current u_{cur} = 1 m/s.

We use the CIRIA/CUR method with $H_{1\%}$, T_p and $\hat{u}_{hc}$, in combination with Ψ_{cr} = 0.030, as recommended in section 6.4.2. The calculation requires iteration, we start with d_{n50} = 0.60 m.

For section I we get:

$\Rightarrow \omega$ = 0.452 rad/s, $H_{1\%}$ = 9.16 m and $\hat{u}_{hc\,1\%}$ = 3.31 m/s as before
$\Rightarrow a_0 = \hat{u}/\omega$ = 7.33 m/s
$\Rightarrow k_s = 2 \cdot d_{n50}$ = 1.20 m
$\Rightarrow a_0/k_s = 6.11 \Rightarrow f_w = \exp(-6.0 + 5.2 \cdot (a_0/k_s)^{-0.19}) = 0.099 \Rightarrow \tau_w = \frac{1}{2} f_w \rho \hat{u}_0^2$ = 556 Pa
$\Rightarrow \tau_{w,av} = \frac{1}{2}\tau_w$ = 278 Pa

$\Rightarrow d_{n50} = \tau_{w,av}/(\rho g \Delta \Psi_{cr}) = 0.60$ m so the calculation converges after the first iteration.

For sections II and III we get $d_{n50} = 0.59$ m (because $H_{1\%}$ is slightly lower there).

If we use the computer programme BPP we get $d_{n50} = 0.50$ m. This is because, by default, BPP calculates $H_{1\%}$ with $h = h_c = 15.0$ m instead of $h = 21$ m, giving $H_{1\%} = 8.88$ m. If we force the programme to use $H_{1\%} = 9.17$ m (by feeding it with a higher value for H_s until the calculated bed orbital velocity equals the value that corresponds with $H_{1\%} = 9.17$ m, so $\hat{u}_{hc} = 3.31$ m/s) we get $d_{n50} = 0.57$ m. So, now we see that the values from the CIRIA/CUR calculation and BPP are almost the same (in theory, in the absence of a current, they should be exactly the same – the difference is probably due to rounding errors).

When we add the current velocity we get (again iterating with CIRIA/CUR and $d_{n50} = 0.60$ as a start value, and using $h = h_c$):

$\Rightarrow \tau_w = \frac{1}{2} f_w \rho \hat{u}_0^2 = 556$ Pa as before
$\Rightarrow C = 18 \cdot \log(12 \cdot h_c/k_s) = 39.2$ m$^{1/2}$/s $\Rightarrow \tau_c = \rho(g/C^2) \cdot u_{cur}^2 = 12.8$ Pa
$\Rightarrow \tau_{wc} = \tau_c + \frac{1}{2}\tau_w = 403$ Pa
$\Rightarrow d_{n50} = \tau_{wc}/(\rho g \Delta \Psi_{cr}) = 0.61$ m $\Rightarrow$ repeat iteration. The values converge to $d_{n50} = 0.65$ m.

For sections II and III we get $d_{n50} = 0.65$ m and $d_{n50} = 0.64$ m, respectively. This is only a little larger than the values without a current, which seems logical considering our earlier conclusion that the wave are dominant. Interestingly, if we use BPP with $u_{cur} = 1.0$ m, we get $d_{n50} = 1.78$ m (!), which is obviously way too large. This is a conformation of our conclusion of section 6.1 that $\Psi_{cr} = 0.030$ is too conservative for this method. Some trial-and-error shows that, if we want to get the same order of magnitude results as with the CIRIA/CUR method, we need to use $\Psi_{cr} = 0.038$. This does not correspond with the values found earlier in this thesis: $\Psi_{cr} = 0.05$ in paragraph 6.4.1, $\Psi_{cr} = 0.03$ in paragraph 6.4.2.

Again, we conclude that the CIRIA/CUR method gives reasonable results, and the BPP method may better not be used because it is not clear what Ψ_{cr} should be (especially in the case of a combination of waves and a current)

A9.4 Damage-based design

We can also try to use the Van Gent and Wallast formula, or the new design formula, to calculate a stone size that results in a reasonable amount of damage. As a starting point, we will use $S^* = 1$ as a design criterion (see table 6.4). Again, we would expect an

outcome in the order d_{n50} = 0.60 m.

A9.4.1 Design with the Van Gent and Wallast formula

Since our starting point is S* we have to translate this to S first, which requires an estimate of d_{n50} – therefore the calculation is iterative. We start with d_{n50} = 0.60 m.

For section I we get:

$S^* = 1$
$\Rightarrow S = S^* \cdot (B_c/d_{n50}) = 6.50$
$\Rightarrow \theta_{hc} = ((1/0.2) \cdot S/\sqrt{N})^{1/3} = 0.64$
$\Rightarrow d_{n50} = \hat{u}_{hc}^2/(g\Delta\theta) = 0.52$ m $\Rightarrow$ the iteration must be repeated. The values converge to d_{n50} = 0.48 m.

For section II we get d_{n50} = 0.49 m, for section III d_{n50} = 0.50 m (the values are slightly different because B_c is different for each section and so the requirement S* = 1 leads to different required values for S)

We see that the calculated stones are too small – apparently we need to use a lower design value of S*. This again confirms our earlier observation that the S* values in table 6.4 are probably too high. Some trial-and-error shows that if we start with S* = 0.7 we end up with d_{n50} = 0.57 m (section I), d_{n50} = 0.58 m (section II) and d_{n50} = 0.60 m (section III), which is more in the range that we expected, and equal to the values obtained with the critical stability method.

A9.4.2 Design with the new design formula

The new formula uses S* instead of S so iteration is not necessary. For section I we get:

$S^* = 1$
$\Rightarrow \theta_{hc\,1\%} = ((1/0.048) \cdot S \cdot N^{-0.3} \cdot m_0^{0.6})^{1/1.6} = 1.42$
$\Rightarrow d_{n50} = (\hat{u}_{hc\,1\%})^2/(g\Delta\theta) = 0.51$ m

For section II and III we get d_{n50} = 0.51 m as well (the only difference between the sections is a very small difference in $\hat{u}_{hc\,1\%}$ which does not influence the outcome). Again we see that these stones are too small. If we want to get results comparable to those obtained with the critical stability method we need to use S* = 0.75, as found by trial-and-error. This gives d_{n50} = 0.61 m for all sections.

We see that both the Van Gent and Wallast formula and the new design formula can be

used for damage-based design of pipeline covers; however, the design criterion in terms of S* must be set lower than the value suggested by Table 6.4 (S* = 1). For the Van Gent and Wallast formula S* = 0.7 seems more appropriate, for the new design formula the corresponding value is S* = 0.75. These values give results in terms of required d_{n50} that are comparable to the results from the critical stability method.

A9.5 Conclusions

This case study has shown the following:

- Both the Van Gent and Wallast formula and the new design formula predicted the actually measured damage to the outfall cover well, in quantitative terms (S).
- In qualitative terms it is suggested that the values of S* as mentioned in table 6.4 are too high. It is recommended to study the relationship between S* (and/or $\Delta z/d_{n50}$) and (qualitative) damage in more detail in a separate study. A clue can be obtained from the prototype measurements: S* ˜ 0.6 – 0.7 means 'no damage', S* ˜ 0.9 – 1.0 means 'important damage' and S* ˜ 1.7 – 2.0 means 'almost destroyed'.
- Given the damage to the structure, it is expected that a stone size in the range d_{n50} = 0.60 – 0.65 m would have been the 'correct' outcome of a design formula. The critical stability method (CIRIA/CUR method with $H_{1\%}$, T_p, $\hat{u}_{hc}$ and Ψ_{cr} = 0.030) predicts these values quite well. The BPP method also works well in the absence of a current, but as soon as a (small) current is assumed the predicted d_{n50}-values get (way) too large. The CIRIA/CUR method still gives reasonable answers when the current is added.
- Both the Van Gent and Wallast formula and the new design formula can be used for damage-based design of pipeline covers, but again the design requirement (in terms of S*) must be lower than the values suggested by table 6.4. For the Van Gent and Wallast method S* = 0.7 is suggested, and for the new design formula S* = 0.75, in order to obtain the same results as with the critical stability formula.